

**Design of High-Capacitance Polymers: Side Chain Length and Polarity Effects on Permittivity**

by

**Anneliese Schmidt**

B.S. Chemistry, University of South Carolina Upstate, 2009

Submitted to the Graduate Faculty of the  
Dietrich School of Arts and Sciences in partial fulfillment  
of the requirements for the degree of  
Doctor of Philosophy

University of Pittsburgh

2024

UNIVERSITY OF PITTSBURGH

DIETRICH SCHOOL OF ARTS AND SCIENCES

This dissertation was presented

by

**Anneliese Schmidt**

It was defended on

December 8, 2023

and approved by

Geoff Hutchison, Associate Professor, Department of Chemistry

Peng Liu, Associate Professor, Department of Chemistry, Department of Chemical and  
Petroleum Engineering

Kevin Noonan, Department of Chemistry, Carnegie Mellon University

Tara Meyer, Professor, Department of Chemistry and The McGowan Institute for Regenerative  
Medicine

Copyright © by Anneliese Schmidt

2024

# **Design of High-Capacitance Polymers: Side Chain Length and Polarity Effects on Permittivity**

Anneliese Schmidt, PhD

University of Pittsburgh, 2024

Dielectric polymers (DPs) are attracting attention for applications in energy storage devices and potential as greener materials. This work serves to expand and explore a variation of side chain (SC) DPs, which addresses one major challenge, inherently low permittivity. This design of SCDPs combines a long aliphatic backbone, having low permittivity and loss, with conjugated SCs, having high permittivity and loss, and is expected to demonstrate these characteristics. Cast films, subjected to a dipole-aligning external field, achieved high permittivities. Effective dipole orientation, facilitated by backbone flexibility and SC conjugation for electron mobility, increased the induced dipole.

A series of polymers with an alkyl backbone and variable length phenylene ethynylene (PhE) SCs were prepared. Diolfin macromonomers, containing a halogenated phenyl, were polymerized via ADMET. Sonogashira coupling of PhE units gave SCs that were 1, 2, and 3 units long, and post-polymerization coupling gave polymers termed: poly-dimer, with two phenyls; poly-trimer, with three phenyls; poly-tetramer, with four phenyls. PhE units were of 2 types: a 2,5-alkoxy functionalized phenyl, for improved solubility, and a 4-nitrile functionalized phenyl, to enhance polarity.

The effects of conjugation length, polarity, and poling the polymers' permittivities were studied. Sample films, prepared by solution deposition between brass electrodes, were characterized by broadband dielectric spectroscopy at 20 °C and 1 kHz. The type of solvent used



showed little effect, whereas the amount of solvent present changed the materials' response significantly. All unpoled polymers exhibited high permittivities: backbone and poly-tetramer  $\sim 4.3$ ; poly-dimer  $\sim 4.6$ ; poly-trimer  $\sim 4.9$ . Poling at a 15-volt potential increased their permittivities: backbone  $\sim 4.9$ ; poly-dimer  $\sim 12.4$ ; poly-trimer  $\sim 7.1$ ; poly-tetramer  $\sim 5.9$ . This increase over the unpoled samples demonstrated their potential as high-performance DPs. After poling, the backbone's small increase,  $\Delta\epsilon' = 0.6$ , was expected. Surprisingly, as the SC length increased, the  $\Delta\epsilon'$  decreased, showing a maximum of: poly-dimer  $\Delta\epsilon' = 7.8$ ; poly-trimer  $\Delta\epsilon' = 2.2$ ; poly-tetramer  $\Delta\epsilon' = 1.6$ . Alignment of increasingly longer SCs was expected to yield incrementally higher permittivities. One explanation, since permittivities were highly dependent on mobility, longer SCs may remain partially hindered to rotation, despite plasticization. The correlation between SC length and poled permittivity indicates hinderance may increase with SC length and prevent maximum alignment.

# Table of Contents

<b>Dedication .....</b>	<b>xix</b>
<b>Acknowledgements .....</b>	<b>xx</b>
<b>1.0 Introduction.....</b>	<b>1</b>
<b>1.1 Significance .....</b>	<b>1</b>
<b>1.1.1 Project Overview.....</b>	<b>2</b>
<b>1.2 Theory of Dielectric Materials .....</b>	<b>3</b>
<b>1.2.1 Capacitors .....</b>	<b>8</b>
<b>1.2.2 Dipolar Glass Polymers .....</b>	<b>13</b>
<b>1.3 Approaches to Improve Dielectric Polymers .....</b>	<b>15</b>
<b>1.4 Design of Side Chain Dielectric Polymers (SDPs) .....</b>	<b>18</b>
<b>1.5 Broadband Dielectric Spectroscopy.....</b>	<b>22</b>
<b>1.5.1 Instrument Basics.....</b>	<b>23</b>
<b>1.5.2 Polymeric Response .....</b>	<b>25</b>
<b>1.6 Project Goals.....</b>	<b>27</b>
<b>2.0 Phenylene Ethynylene Based Polymers .....</b>	<b>30</b>
<b>2.1 Summary .....</b>	<b>30</b>
<b>2.2 Introduction .....</b>	<b>30</b>
<b>2.3 Experimental.....</b>	<b>32</b>
<b>2.3.1 Materials. ....</b>	<b>32</b>
<b>2.3.2 Characterizations .....</b>	<b>32</b>
<b>2.3.3 Synthesis.....</b>	<b>33</b>

2.3.4 Film Preparation and Dielectric Experiments .....	33
2.4 Results.....	35
2.4.1 Synthesis.....	35
2.4.2 Polymer Properties.....	42
2.4.3 Broadband Dielectric Spectroscopy .....	46
2.5 Discussion .....	61
2.5.1 Synthesis.....	61
2.5.2 Polymer Properties.....	65
2.5.3 Broadband Dielectric Spectroscopy .....	67
3.0 Phenylene Vinylene Based Polymers.....	71
3.1 Introduction .....	71
3.2 Project Goals .....	72
3.3 Results.....	75
3.3.1 Naming Convention .....	75
3.3.2 Synthesis of Monomers and Their Building Blocks .....	76
3.3.3 Metathesis of Polymers and Ring-Closed Monomers .....	82
4.0 Future directions .....	87
Appendix A Supporting Data and Spectra for Chapter 2.....	90
Appendix A.1 Synthesis and Characterization Data.....	90
Appendix A.1.1 General Procedures .....	90
Appendix A.1.2 Synthesis of Side Chain Moieties.....	92
Appendix A.1.3 Polymerizations and Side Chain Couplings .....	101
Appendix A.1.4 NMR.....	111

Appendix A.2 Broadband Dielectric Spectroscopic Data .....	129
Appendix B Supporting Data and Spectra for Chapter 3.....	141
Appendix B.1 Synthesis and Characterization Data .....	141
Appendix B.1.1 Synthesis of Monomer Building Blocks .....	141
Appendix B.1.2 Synthesis of Monomers.....	148
Appendix B.1.3 Polymerizations .....	156
Appendix B.1.4 NMR.....	163
Bibliography .....	183

## List of Tables

<b>Table 1: Dielectric constants of commonly used materials.<sup>35, 36</sup> .....</b>	<b>16</b>
<b>Table 2: Abbreviations used in naming prepared compounds.....</b>	<b>36</b>
<b>Table 3: Properties of Side Chain Dielectric Polymers. ....</b>	<b>38</b>
<b>Table 4: Permittivities for the cumulative poling of sample p-BSU-CN at 20 °C.....</b>	<b>61</b>
<b>Table 5: Abbreviations used in naming prepared phenylene vinylene compounds .....</b>	<b>75</b>
<b>Table 6: Polymerization results for phenylene vinylene substrates .....</b>	<b>86</b>
<b>Appendix Table 1: Average permittivities for all of the poled and unpoled polymers at 1 kHz and 20 °C.....</b>	<b>129</b>
<b>Appendix Table 2: Average dielectric loss for all of the poled and unpoled polymers at 1 kHz and 20 °C.....</b>	<b>130</b>

## List of Figures

<b>Figure 1: Side chain dielectric polymers with varying side chains lengths and a polar end group. ....</b>	<b>3</b>
<b>Figure 2: Dipoles a) natural state b) in the presence of a static applied field. ....</b>	<b>4</b>
<b>Figure 3: Frequency dependence of polarization modes and losses, reproduced from ref.<sup>9, 17</sup> .....</b>	<b>5</b>
<b>Figure 4: Diagram of the different modes of polarization. Figure reproduced from ref. <sup>18</sup> ..</b>	<b>6</b>
<b>Figure 5: Treelike pattern showing dielectric breakdown in a block of plexiglas, which stems from the root of the breakdown. Figure reporduced from ref.<sup>21</sup> .....</b>	<b>8</b>
<b>Figure 6: Diagram of a capacitor connected to a voltage source. Figure reporduced from ref<sup>22</sup> .....</b>	<b>9</b>
<b>Figure 7: Relationship between an applied electric field and the response of a material. (a) Phase shift between the applied electric field and the displacement field. (b) relationship between the complex dielectric function and the phase angle. Figure reproduced from reference.<sup>23</sup> .....</b>	<b>10</b>
<b>Figure 8: Diagram of a capacitor showing the effect an electric field has on the dipoles within a dielectric material. (a) parallel plate capacitor in a circuit; (b) before application of an electric field (E) the dipoles are randomly oriented; (c) after application of E the dipoles are aligned. Figure adapted from.<sup>24</sup> .....</b>	<b>12</b>
<b>Figure 9: Dipole and domain structures with increasing interactions from left to right (blue arrows indicate individual atomic/molecular dipoles). Reproduced from reference.<sup>1</sup> .....</b>	<b>13</b>

<b>Figure 10: Schematic of the structural design of dipolar glass polymers. Reproduced from reference.<sup>25</sup> .....</b>	<b>14</b>
<b>Figure 11: Diagram of interfacial polarization from impurity ions and free electrons in a multilayer PVDF/polysulfone (PSF) film. Reproduced from ref.<sup>5</sup> .....</b>	<b>17</b>
<b>Figure 12: Multilayered self-assembled nanodielectric (SAND) developed by the Marks' group using a phosphonic acid-based <math>\pi</math>-electron, PAE, layer. (a) fabrication procedure for zirconium-SANDs (b) SANDs incorporating aliphatic and aromatic layers. Figure reproduced from ref<sup>47, 50</sup> .....</b>	<b>18</b>
<b>Figure 13: Conjugated substrates for self-assembled nanodielectrics (SANDs) designed by the Marks' group. Figure adapted from ref <sup>50, 53</sup> .....</b>	<b>19</b>
<b>Figure 14: Alignment of polymer chains and side chains and the effect of poling on their orientation. After deposition onto an electrode, the polymer side chains are in random orientations (left) and the total dipole moment of the material is reduced. After poling for an extended period of time the polymer side chains are partially aligned (right) and the total dipole moment of the material is increased.....</b>	<b>20</b>
<b>Figure 15: Correlation between the frequencies, analytical techniques and molecular responses across the electromagnetic spectrum. <sup>64</sup> .....</b>	<b>22</b>
<b>Figure 16: Schematic of Frequency Response Analyzer Circuit. Figure reproduced from ref <sup>65</sup> .....</b>	<b>23</b>
<b>Figure 17: Voltage and current response of a hypothetical polymer material. Figure reproduced from <sup>66</sup>.....</b>	<b>24</b>

<b>Figure 18: A fragment of a hypothetical polymer chain that contains polar bonds. The molecular dipole moments are indicated by the black arrows and one bond that would rotate in the presence of an electric field is indicated by the blue curved arrow.....</b>	<b>25</b>
<b>Figure 19: Proposed polymer series. Starting from the top left is the base structure, the polymer backbone, continuing with the poly-dimer, poly-trimer and poly-tetramer. (note on nomenclature, a dimer, trimer, etc. refers to the number of phenyl groups in the monomer). .....</b>	<b>28</b>
<b>Figure 20: Illustration depicting the naming conventions applied here. ....</b>	<b>35</b>
<b>Figure 21: Synthesis of H-U-CN, the terminal PhE segment for all side chains. ....</b>	<b>36</b>
<b>Figure 22: Synthesis of substituted PhE segment 5. ....</b>	<b>37</b>
<b>Figure 23: Synthesis of side chain moieties.....</b>	<b>38</b>
<b>Figure 24: Synthesis of the unsubstituted polymer, p-B-Br, and the polymer backbone, coupling partner, p-B-I.....</b>	<b>39</b>
<b>Figure 25: Synthesis of side chain dielectric polymers. ....</b>	<b>40</b>
<b>Figure 26: <sup>1</sup>H NMR for the synthesis of p-BSSU-CN, from the polymer backbone, p-B-I, and the side chain moiety, H-SSU-CN. Residuals from the deuterated solvent and dichloromethane are noted.....</b>	<b>42</b>
<b>Figure 27: SEC showing the increase in molecular weight of the three substituted polymers as compared to the unsubstituted polymer.....</b>	<b>43</b>
<b>Figure 28: The DSC thermograms for the second heating (solid curves) and cooling (dashed curves) scans for all polymers, at a heating rate of 10 °C/min under nitrogen.....</b>	<b>44</b>



**Figure 29: The DSC thermograms of the  $T_g$  for p-BU-CN when a sample is vacuum dried (dashed curve) compared to when a sample has toluene added (solid curve) to induce plasticization, at a heating rate of  $10\text{ }^\circ\text{C}/\text{min}$  under nitrogen..... 45**

**Figure 30: Frequency dependent permittivity for each of the unpoled and poled polymers, (a) spectral overlay of the average permittivity for the unpoled and poled samples measured at  $20\text{ }^\circ\text{C}$ . The vertical lines on the spectra are placed at  $1\text{ kHz}$  and correspond to the boxes in the chart in b. (b) the average and range for the unpoled and poled polymers extracted from the spectra in a, measured at  $1\text{ kHz}$  and  $20\text{ }^\circ\text{C}$ . 47**

**Figure 31: Dielectric loss as a function of frequency for unpoled (right) and poled (left) polymers, measured at  $20\text{ }^\circ\text{C}$ . ..... 49**

**Figure 32: The effect of plasticization on the permittivity of p-BU-CN as a function of temperature at different frequencies, ranging from  $1\text{ Hz}$  (lightest blue) to  $1\text{ MHz}$  (darkest blue), when a sample is vacuum dried (left) compared to when a sample has toluene added (right)..... 50**

**Figure 33: Average permittivity (top) and dielectric loss (bottom) as a function of frequency, measured at  $20\text{ }^\circ\text{C}$ , for p-BU-CN (left) and p-BSU-CN (right). ..... 51**

**Figure 34: Permittivity (top) and dielectric loss (bottom) of unpoled (left) and poled (right) p-BU-CN as a function of temperature at frequencies from  $1\text{ Hz}$  to  $1\text{ MHz}$ ..... 52**

**Figure 35: Permittivity and dielectric loss as a function of temperature for all of the unpoled and poled polymers at  $1\text{ kHz}$ ..... 54**

**Figure 36: Diagram depicting sample capacitor. .... 55**

**Figure 37: Permittivity of vacuum dried p-BU-CN for the average of the unpoled (solid curves) and poled (dashed curves) samples measured at  $20\text{ }^\circ\text{C}$ . ..... 56**

**Figure 38: Diagram depicting the film casting and capacitor preparation procedure. .... 57**

**Figure 39: Permittivity, as a function of frequency, of p-BU-CN samples with varied initial drying times (time before placing the top electrode), measured at 20 °C. Samples represented by solid curves received additional drying time after placing the top electrode ( $t \geq 12$  h) before measuring permittivity. The samples represented by dashed curves were measured within an hour of placing the top electrode. .... 58**

**Figure 40: Permittivity, as a function of frequency, of p-BU-CN samples with either toluene (solid curves) or chlorobenzene (dashed curves), measured at 20 °C. The samples prepared with toluene are labeled T1-T4 and the samples prepared with chlorobenzene are labeled CB1-CB3..... 59**

**Figure 41: Cumulative poling of one p-BSU-CN sample, measured at 20 °C..... 60**

**Figure 42: Proposed polymer sequences. Starting from the top left is the base structure, i.e. the backbone or mono-phenylene, continuing with dimers, trimers, and tetramers. The trimers and tetramers have one unsequenced chain and two sequenced chains with the same composition. (note on nomenclature, a dimer, trimer, etc. refers to the number of phenyl groups in the monomer)..... 73**

**Figure 43: Proposed pentamer sequences have one unsequenced chain and three sequenced chains with the same composition. (note on nomenclature, pentamer refers to the number of phenyl groups in the monomer)..... 74**

**Figure 44: Alternative monomers for increased polarizability of the polymer side chains. (a) and (b) are polarizable end groups; (c) and (d) are electron deficient moieties. .... 75**

**Figure 45: Synthesis of mono-B-A..... 76**

**Figure 46: Synthesis of phosphonate 4..... 77**

<b>Figure 47: Synthesis of phosphonate 9.....</b>	<b>78</b>
<b>Figure 48: <sup>1</sup>H NMR for the transformation of nitrile-derivative 8 to phosphonate-derivative 9. (a) nitrile 8; (b) intermediate; (c) phosphonate 9. The arrow colors correspond product spectrum color and indicate the peak changes that occur from the starting material to the product.....</b>	<b>79</b>
<b>Figure 49: Representative iterative HWE coupling sequence. ....</b>	<b>80</b>
<b>Figure 50: <sup>1</sup>H NMR for the synthesis of mono-BP-N. (a) mono-B-A; (b) phosphonate 4; (c) mono-BP-N. The arrow colors correspond to the respective spectrum color and indicate the peak changes that occur from the starting materials to the product. ...</b>	<b>81</b>
<b>Figure 51: ADMET proved a more viable route for polymerization than RCM.....</b>	<b>82</b>
<b>Figure 52: Left- RCM of mono-B-N; (a) dimer; (b) monomer; (c) starting material. Right - ADMET of mono-B-N; (a) polymer; (b) starting material. Red arrows - terminal olefin; teal arrow - internal olefin; purple arrows – broadened peaks.....</b>	<b>83</b>
<b>Figure 53: SEC curves for poly(nitriles). <sup>a</sup>Trial one for poly-B-N was precipitated. ....</b>	<b>84</b>
<b>Figure 54: SEC curves for poly(aldehydes). <sup>a</sup>Trial one for poly-B-A was precipitated. <sup>b</sup>Trial one ran for 19 h. <sup>c</sup>Trial two ran for 35 h.....</b>	<b>85</b>

## List of Abbreviations

A	area
AC	alternating current
ADMET	acyclic diene metathesis polymerization
BDS	broadband dielectric spectroscopy
BOPP	biaxially oriented polypropylene
BPO	benzoyl-peroxide
<sup>n</sup> BuLi	n-butyl lithium
C	capacitance
CDCl <sub>3</sub>	deuterated chloroform
CuI	copper iodide
d	sample thickness
D	displacement field
Đ	dispersity
Da	dalton
DC	direct current
DCE	dichloroethane
DCM	dichloromethane
DGP	dipolar glass polymer
DIBAL-H	diisobutylaluminum hydride
DMF	dimethylformamide
DMSO	deuterated dimethyl sulfoxide
DP	degree of polymerization
DSC	differential scanning calorimetry
E	applied/external electric field
E <sub>b</sub>	dielectric breakdown strength
ED-ROMP	Entropy-driven ring-opening metathesis polymerization
EDL	electric double layer
EDU	electron donating unit
EM	electromagnetic spectrum
FE	ferroelectric
FIR	far infrared frequency
FRA	frequency response analyzer
GII	Grubbs 2 <sup>nd</sup> generation catalyst
GCMS	Gas chromatography–mass spectrometry
H <sub>2</sub> SO <sub>4</sub>	sulfuric acid
HBr	hydrobromic acid
HI	hydroiodic acid
Hz	hertz
I	current
IR	infrared frequency
KIO <sub>3</sub>	potassium iodate

KO <sup>t</sup> Bu	potassium tert-butoxide
MeOH	methanol
MLF	multilayer films
M <sub>n</sub>	number average molecular weight
M <sub>RU</sub>	repeat unit molecular weight
MgSO <sub>4</sub>	magnesium sulfate
n	degree of polymerization
N <sub>2</sub>	nitrogen
NaHCO <sub>3</sub>	sodium bicarbonate
Na <sub>2</sub> S <sub>2</sub> O <sub>3</sub>	sodium thiosulfate
NBS	N-bromosuccinimide
NIR	near infrared frequency
NMR	nuclear magnetic resonance spectroscopy
P	polarization
P <sub>dip</sub>	orientational/dipolar polarization
P <sub>elect</sub>	electronic polarization
P <sub>ion</sub>	ionic polarization
P <sub>int</sub>	interfacial polarization
P <sub>max</sub>	maximum polarization
P <sub>vib</sub>	atomic/vibrational polarization
PdCl <sub>2</sub> (PPh <sub>3</sub> ) <sub>2</sub>	Bis(triphenylphosphine)palladium(II) dichloride
Pd(dba) <sub>2</sub>	Bis(dibenzylideneacetone)palladium(0)
PE	paraelectric
PhE	phenylene ethynylene
PhMe	toluene
ppm	parts per million
PS	polystyrene
PV	phenylene vinylene
PVDF	polyvinylidene fluoride
q	charge
r	vector distance
R	resistance
RT	room temperature
R <sub>x</sub>	resistor
RCM	ring closing metathesis
RFE	relaxorferroelectric
ROMP	ring opening metathesis polymerization
SAND	self-assembled nanodielectrics
SAM	self-assembled monolayers
SCM	side chain moieties
SEC	size exclusion chromatography
SDP	side chain dielectric polymers
tan (δ)	dielectric loss
TEA	triethylamine
T <sub>g</sub>	glass transition temperature
THF	tetrahydrofuran

TMS	trimethylsilyl
TMSA	trimethylsilyl acetylene
$U_e$	energy density
$U_1, U_2$	voltage
UV	ultraviolet frequency
$v$	volume
V	potential
VIS	visible frequency
WES	Williamson ether synthesis
Z	impedance
$\varepsilon$	permittivity
$\varepsilon_r$	relative permittivity or permittivity
$\kappa$	dielectric constant
$\mu$	dipole moment

## **Dedication**

To my father,

Kenneth William Schmidt, Sr.

Thank you for your endless love and support and for instilling in me the discipline  
and dedication that allowed me to persevere in this pursuit.

## Acknowledgements

I would like to express my deepest appreciation to my advisors Dr. Tara Y. Meyer and Dr. Geoffrey R. Hutchison. Thank you for your mentorship, guidance, and support. Thank you for reminding me that I am capable and providing encouragement when the project was tough.

Many thanks to all my current and former group members, especially Megan E. Clark, Michael T. Cole, Sarah M. Craig, Jordan A. Fitch, Dr. Jamie A. Nowalk, and Dr. Jordan H. Swisher. To all my friends and former colleagues in the department, especially Dr. Jean-Marc I. A. Lawrence, Dr. Kimberly A. Kowallis, Dr. Dylan T. Tomares, Dr. Kaitlyn Stepler, and Savannah Albright. Thank you for your inciteful suggestions and for all the laughter that helped me through the challenging moments.

Thank you to my grandmother, Rosemary Z. Schmidt, who encouraged me to attend graduate school long before I realized I wanted to. Thank you to my dad, Kenneth W. Schmidt, Sr., and my brother, Kenneth W. Schmidt, Jr., for the weekly Zoom chats which have meant so much to me. Thank you for helping me through some of the hardest times in this endeavor. Thank you to my mom, Margaret A. Schmidt, for all your love over the years and for the extra support when I first moved to Pittsburgh. Thank you to my sister-in-law, Jean-Anne H. Schmidt, my nephew, Henry W. Schmidt, and my niece, Chadley G. Schmidt. I am sincerely grateful to all of you for your support and for the comfort and happiness you have given me throughout my life.

Thank you to Kristin A. Davis and Megan J. Fresia, two of the best friends I could ever ask for. I also want to thank Beth W. Trenor and Robin E. Bayles-Wiik. Thank you, ladies, for all your support, for your confidence in my ability to succeed, and for the amazing weekend getaways that gave me a boost when I needed it most.



I am incredibly grateful for my sweet puppy, Watson, who greeted me with such love and enthusiasm every single day and made some of the toughest days more bearable.

## 1.0 Introduction

### 1.1 Significance

Dielectric materials are of great importance in a variety of electrical and energy storage applications, including film capacitors, renewable energy, artificial muscles, and electric/hybrid vehicles. Traditionally, ceramics are used as dielectrics due to their extremely high permittivities ( $\epsilon_r$ ) and excellent thermal stability<sup>1</sup>, however they tend to have high dielectric losses ( $\tan \delta$ ), low breakdown strengths ( $E_b$ ) and are inflexible.

As an alternative, polymers are being explored because they are light weight, easily processable, and have high breakdown strengths making them ideal candidates for many applications<sup>2-4</sup>. High permittivity and low energy loss polymers, an imperative for the continued miniaturization of electronic components, would enable high power density and energy density, while maintaining dielectric strength.<sup>5-8</sup> Typical polymers exhibit low permittivities ( $\epsilon_r = 2-4$ ) and, while aliphatic polymers have desirably low losses, they also have low glass transition temperatures ( $T_g$ ) which limits their range of applications. On the other hand, conjugated polymers, which have increased permittivities, have higher  $T_g$ s but also have higher losses due to a reduction in the band gap. The current industry standard, biaxially oriented polypropylene (BOPP), has very low dielectric losses ( $\tan \delta \approx 0.0002$ <sup>9, 10</sup>) at relatively high operating temperatures (up to 85 °C), however its low permittivity ( $\epsilon_r = 2.2$ ) imparts low energy density thereby limiting its energy storage capacity, and high losses above 85 °C, due to conduction, limits its range of applications.

Though there is a breadth of knowledge regarding the effect of backbone monomer composition on the bulk properties of polymers, the effect of side chain composition, length and spacing on a polymer's dielectric properties is limited. The work described herein, along with the founding work of Wei et al. and Ha et al., describes a method to prepare side chain dielectric polymers that are functionalized by a post-polymerization coupling procedure with high fidelity. This method provides a pathway to easily change the moiety utilized as the side chain. This work will contribute to the diversification of the classes of polymers suitable for dielectric applications.

### 1.1.1 Project Overview

The goal of this project is to establish a new class of tunable high-capacitance dielectric polymers, through implementation of rational design principles and varying side chain lengths. This project will investigate influential monomer parameters, through manipulations of the side chain lengths, to develop a process for rationally tuning the dielectric properties of this new class of polymers. The monomer design incorporates phenylene ethynylene (**PhE**) moieties for increased polarizability and a polar end group to increase the side chain's dipole (Figure 1). By utilizing the **PhEs** as substituents for side chains and employing an aliphatic backbone, a strategy that has not been fully explored, we hypothesize that the resulting flexibility of the polymer will allow the side chains to be aligned, thereby reinforcing the polymer's overall dipole moment.

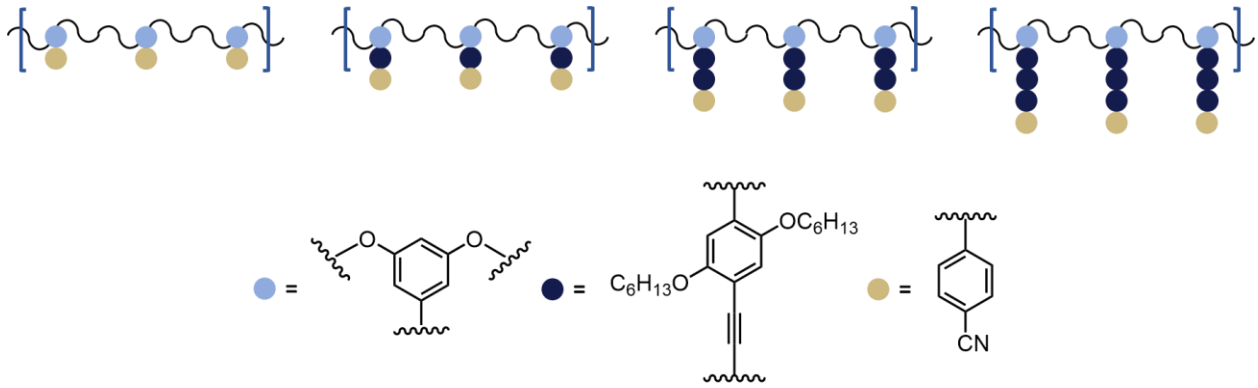


Figure 1: Side chain dielectric polymers with varying side chains lengths and a polar end group.

## 1.2 Theory of Dielectric Materials

A dielectric is a material that supports electric charge<sup>11</sup> by polarizing under the influence of an applied electric field ( $E$ ). Due to the lack of freely moving electrons, these materials generally cannot conduct charge hence they are commonly referred to as insulators.

A dipole, the basic element of electrical structures<sup>12-16</sup>, is formed when there is a separation of charges ( $q$ ) and is permanent or induced by an applied field. Dipoles are inherently directional, the positive charge is displaced by some distance ( $\mathbf{r}$ ), in the  $x$ ,  $y$ ,  $z$  direction, from the negative charge, and to fully encapsulate these parameters, a variable known as the dipole moment ( $\boldsymbol{\mu}$ ) is used (1.1).

$$\boldsymbol{\mu} = q\mathbf{r} \quad (1.1)$$

Polarizing, which can be thought of as the absorption of energy, is the alignment of a dipole with the field, and the sum of all of the dipole moments in a system per unit volume ( $v$ ), is the macroscopic property a material known as its polarization ( $\mathbf{P}$ ) (1.2).

$$P = \frac{1}{V} \sum \mu_i \quad (1.2)$$

The measure used for the amount of polarization occurring in a given material is termed its permittivity ( $\epsilon$ ), but a material's permittivity can be described by its dielectric constant ( $\kappa$  or  $\epsilon_r$ ), which is relative to the permittivity of a vacuum ( $\epsilon_0 = 8.8542 \times 10^{-12}$  F/m) (1.3). (Note that the relative permittivity of air is  $\sim 1$  and all other materials have permittivities  $> 1$ )

$$\kappa = \epsilon_r = \frac{\epsilon}{\epsilon_0} \quad (1.3)$$

When the permittivity of the material is increased, it becomes a more effective dielectric, therefore it can absorb more energy.

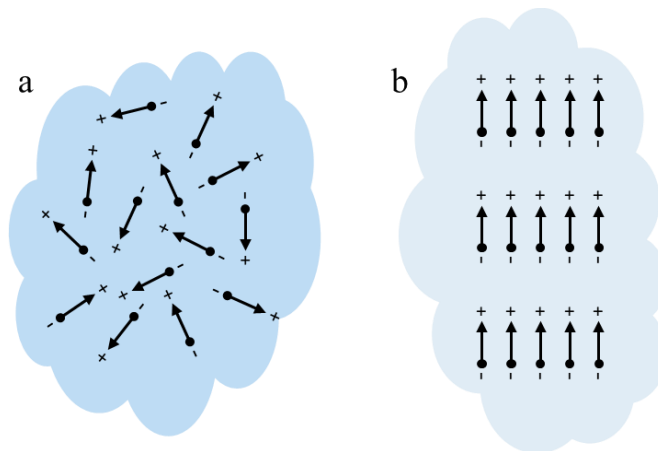


Figure 2: Dipoles a) natural state b) in the presence of a static applied field.

The natural state of a system of dipoles is to be randomly oriented and, as a result, the material's bulk polarization will generally be negligible. The application of an electric field will increase alignment and cause the dipoles to exhibit a bulk polarization that aligns with the field (Figure 2). In a direct current (DC) system, a static field is applied and there is 'infinite' time for the dipoles to align ( $\epsilon_{rs}$ : static/maximum permittivity). In this case, the maximum polarization

( $\mathbf{P}_{max}$ ) at a given field strength can be expressed in terms of the static permittivity and the field applied (1.4).

$$\mathbf{P}_{max} = \epsilon_0(\epsilon_{rs} - 1)\mathbf{E} \quad (1.4)$$

However, in an alternating current (AC) system, there is a finite amount of time before the field direction is switched, causing the dipoles to begin to align in the opposite direction. Due to the nature of dipoles, they may not fully align with the field before they begin to flip their alignment, and this results in a lower permittivity for the system.

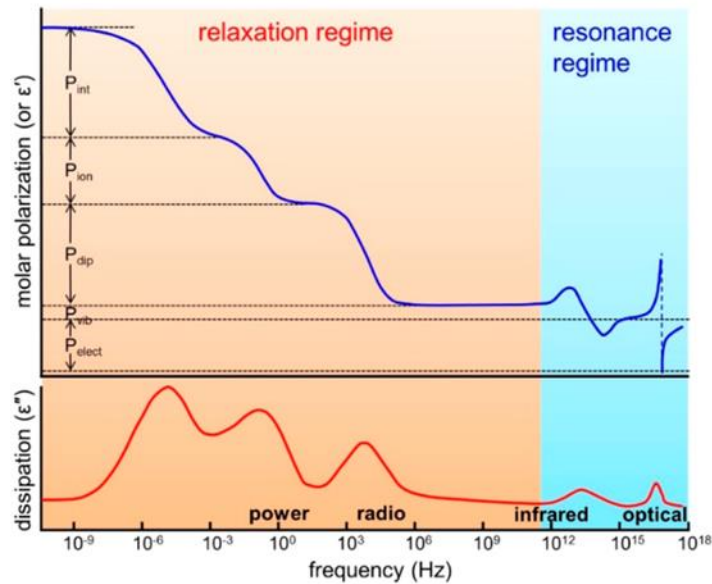


Figure 3: Frequency dependence of polarization modes and losses, reproduced from ref.<sup>9, 17</sup>

In order to design a polymeric system with an enhanced permittivity, it is important to understand the various mechanisms, also referred to as modes or types, of polarization through which induced dipoles act (Figure 3), namely: electronic ( $P_{elect}$ ), atomic/vibrational ( $P_{vib}$ ), orientational/dipolar ( $P_{dip}$ ), ionic ( $P_{ion}$ ), and interfacial ( $P_{int}$ ).

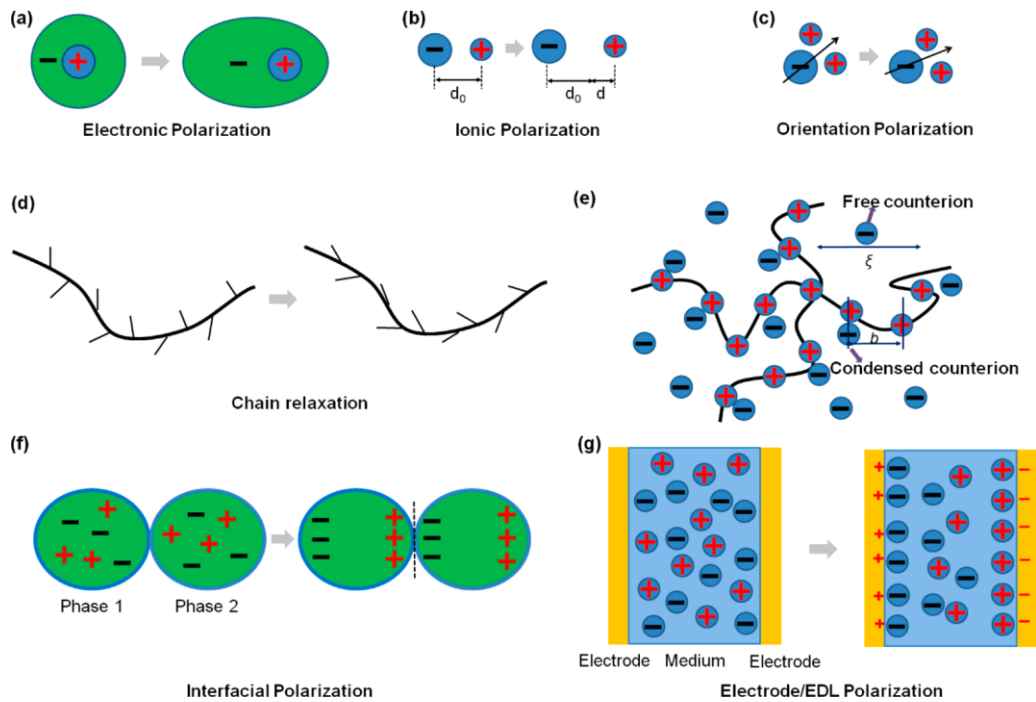


Figure 4: Diagram of the different modes of polarization. Figure reproduced from ref. <sup>18</sup>

As the frequency of an applied field increases various modes of polarization become inactive, whereas at the lowest frequencies all modes of polarization are active. Electronic, the displacement of the electron cloud with respect to the nucleus inducing a dipole (Figure 4), and vibrational polarization, the stretching of bonds between atoms increasing the inherent dipole created by those two atoms, are active in the ultraviolet (UV,  $7.5 \times 10^{14} - 3 \times 10^{16}$  Hz), optical (VIS,  $4 \times 10^{14} - 7.5 \times 10^{14}$  Hz) and near-infrared (NIR,  $2 \times 10^{14} - 4 \times 10^{14}$  Hz) frequencies.<sup>19</sup> Orientational/dipolar polarization is the reorientation, including rotation and translation, of small covalently bonded atoms and molecules or polar components of a larger system (e.g. dipoles within or on a polymer), in the presence of an electric field and is active over a broad range of frequencies, radio ( $< 3 \times 10^9$  Hz), microwave ( $3 \times 10^9 - 3 \times 10^{11}$  Hz), and far-infrared (FIR,  $3 \times 10^{11} - 2 \times 10^{13}$  Hz). Ionic polarization is the migration of positively and negatively charged atoms over long distances ( $>10 \text{ nm}^9$ ) through the material in opposing directions, and is active in the lower range

of power frequencies, below 1 Hz. Interfacial polarization is the buildup of charge at the interface of two materials, usually in heterogenous systems, often causing a secondary polarization at that interface (electric double layer, EDL), and occurs at such slow timescales as to make it not useful for applications.

While  $P_{\text{elect}}$  and  $P_{\text{vib}}$  are active throughout the frequencies of interest, they are fundamentally limited due to the nature of molecular bonding ( $\epsilon_r = 2-5^{20}$ ) and do not contribute much to the total polarization of a system nor to the losses (Figure 3).  $P_{\text{ion}}$  has a very limited useful frequency range and can lead to losses due to conduction. This leaves  $P_{\text{dip}}$  as the mode through which the largest increases in permittivity can be gained. However, by incorporating multiple modes of polarization into a system greater permittivities can be achieved.

When designing a system, it is usually a balancing act between various, frequently conflicting, properties. Real systems are not simple/ideal, but instead experience losses and their properties are expressed as complex quantities, where a single prime denotes the real part of the complex equation, and a double prime denotes the imaginary part. Dielectric materials inherently dissipate some of the EM energy applied as heat to the system and this loss often increases with increasing polarizability (1.5).

$$\epsilon^* = \epsilon' - j\epsilon'' \quad (1.5)$$

There are two main processes through which losses occur: 1. conduction occurs when some charge is able to flow through the system and 2. dielectric loss is due to the lag of dipole alignment above its active frequency range. Minimization of dielectric loss ( $\tan \delta$ ) is of the utmost importance, as heating a material can not only increase the rate of degradation, thereby reducing its useful lifetime, but also increase the probability of conduction through the material possibly leading to breakdown (1.6).



$$\tan \delta = \frac{\epsilon''}{\epsilon'} \quad (1.6)$$

Dielectric breakdown ( $E_b$ ) (Figure 5), also referred to as dielectric strength, is the voltage (V) at which the material conducts substantial current and becomes damaged and permanently conducting (1.7).

$$E_b = \frac{V}{d} \quad (1.7)$$



Figure 5: Treelike pattern showing dielectric breakdown in a block of plexiglas, which stems from the root of the breakdown. Figure reproduced from ref.<sup>21</sup>

### 1.2.1 Capacitors

A dielectric material's capacitance is a measure of its ability to store electric charge. The most used setup for measuring capacitance is a parallel plate capacitor, consisting of a dielectric material between two electrodes connected to a voltage source (Figure 6).

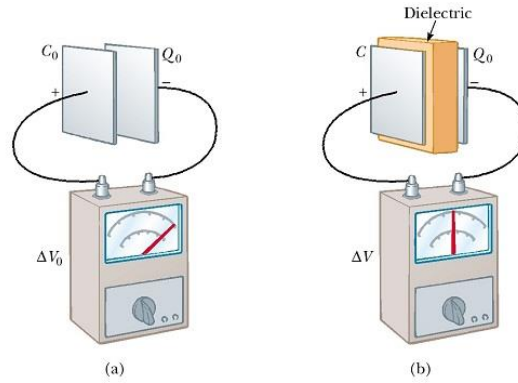


Figure 6: Diagram of a capacitor connected to a voltage source. Figure reproduced from ref<sup>22</sup>

The potential ( $V$ ) applied to a circuit is equivalent to the product of the flow of current ( $I$ ) through the circuit and the resistance ( $R$ ) the circuit presents to the current, which is also equivalent to the product of the applied electric field ( $E$ ) and the thickness of the sample ( $d$ ) (1.8).

$$V = IR = Ed \quad (1.8)$$

The capacitance ( $C$ ) of said capacitor is a ratio of the charge ( $q$ ) on the plates to the voltage applied (1.9).

$$C = \frac{q}{V} \quad (1.9)$$

This shows that if a larger potential is applied, there must be more charge stored for the inherent capacitance of the material of interest, which in turn means the material is capable of a larger polarization.

When the dielectric is polarized it creates a field of its own, opposing that of the applied field. This local field is related to the displacement field ( $\mathbf{D}$ ) (1.10), which amounts to the magnitude of charge per area ( $A$ ), that of the plate.

$$\mathbf{D} = \frac{q}{A} = \frac{CV}{A} \quad (1.10)$$

Given that polarization is proportional to the applied field, it follows that the displacement field is as well, and both are governed by the dielectric's permittivity (1.11).

$$\mathbf{D} = \varepsilon_0 \varepsilon_r \mathbf{E} + \mathbf{P} \quad (1.11)$$

Therefore,  $\mathbf{D}$  can also be related to the complex dielectric function as the ratio of the imaginary permittivity to the real permittivity (Figure 7) (1.12).

$$\mathbf{D} = \tan \delta = \frac{\varepsilon''}{\varepsilon'} \quad (1.12)$$

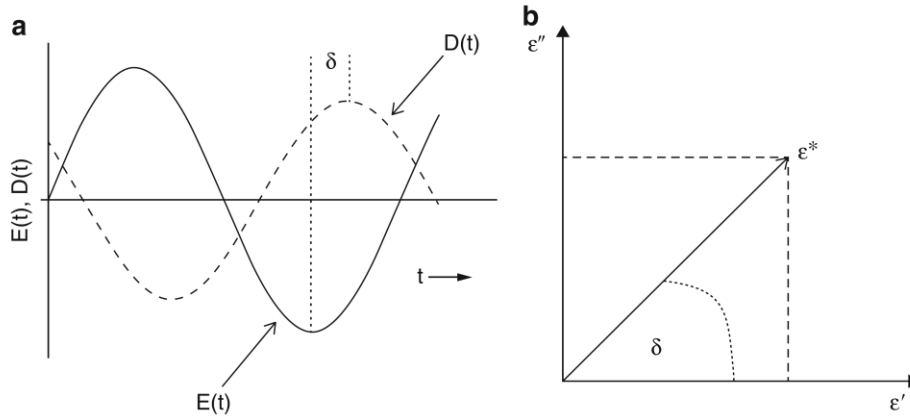


Figure 7: Relationship between an applied electric field and the response of a material. (a) Phase shift between the applied electric field and the displacement field. (b) relationship between the complex dielectric function and the phase angle. Figure reproduced from reference.<sup>23</sup>

Capacitance, being a function of the dielectric's response to an applied field, can also be calculated from the measured displacement field (1.13).

$$C = \frac{(\varepsilon_0 \varepsilon_r \mathbf{E} + \mathbf{P})A}{V} \quad (1.13)$$

This relationship can be simplified to

$$C = \kappa \frac{\varepsilon_0 A}{d} \quad (1.14)$$

In the case where there is no dielectric present, meaning there is an air gap between the plates with an equivalent separation to that of the sample/dielectric thickness ( $d$ ), the capacitance ( $C_0$ ) is quite small (1.15).

$$C_0 = \frac{\epsilon_0 A}{d} \quad (1.15)$$

When a dielectric material is inserted between the plates the capacitance ( $C$ ) is increased by the factor of its dielectric constant. For a given volume ( $v$ ), when this space is occupied by air, there is a small number of molecules present that can align with the field. However, when a dielectric material is placed in that same volume, with the same applied potential, there is a significantly larger number of molecules that can polarize. When the polarization in the capacitor is increased, so is the displacement field, and since the potential and area are constant, the capacitance must also increase. From equations 1.14 and 1.15 we can see that the dielectric constant is also equivalent to the ratio of the capacitance of the capacitor with the dielectric present to the capacitor without the dielectric (1.16).

$$\kappa = \frac{C}{C_0} \quad (1.16)$$

How does a capacitor store energy? When the source is turned on, the circuit is closed, a potential difference is applied across the electrodes and electrons flow from the source to one of the two electrodes causing an accumulation of negative charge on the outside of that electrode. The charge on that plate causes (electrons to migrate) dipoles within the dielectric material to rotate such that the positive charge is oriented toward the negatively charged plate (Figure 8), which in turn causes charge to accumulate on the inside of the second electrode.

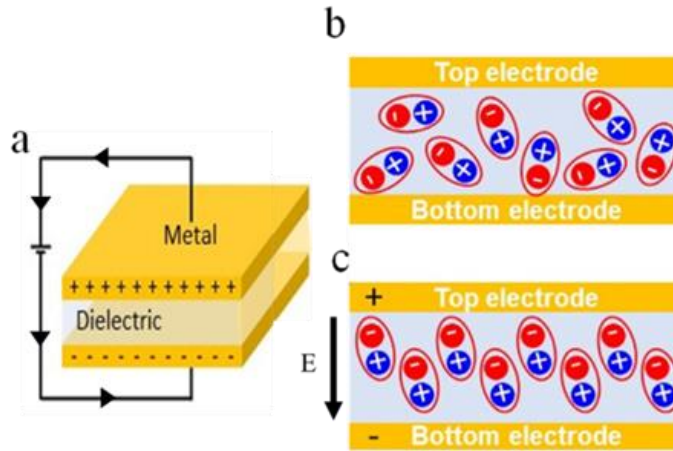


Figure 8: Diagram of a capacitor showing the effect an electric field has on the dipoles within a dielectric material. (a) parallel plate capacitor in a circuit; (b) before application of an electric field (E) the dipoles are randomly oriented; (c) after application of E the dipoles are aligned. Figure adapted from.<sup>24</sup>

As negative charge builds up on the inside of this second electrode, it begins to repel electrons on the outside of the second plate, giving an apparent ‘flow of electrons through’ the capacitor back to the source. Once the charge on the electrodes matches that of the source, the flow of electrons stops and the displacement field produced by the dielectric material exactly matches that of the applied field but is oppositely directed therefore the field within the capacitor becomes zero (1.17).

$$\mathbf{D} - \frac{CEd}{A} = 0 \quad (1.17)$$

At this point the maximum capacitance of the dielectric material is obtained. By disconnecting the capacitor from the circuit before turning off the source, the polarization of the dielectric is maintained thereby storing the energy consumed in producing the polarization.

## 1.2.2 Dipolar Glass Polymers

Material Type	Linear Dielectric	Dipolar Glass	Parraelectric	Relaxor-ferroelectric	Ferroelectric	Antiferroelectric
Dipole Structure						
Dipoles and Domains	No net dipole No FE domains	Isolated dipoles No FE domains	Interacting dipoles No FE domains	Nano-domain Few dipoles	Large domain Many dipoles	Large domain antiphase dipoles
D-E Loops						

Figure 9: Dipole and domain structures with increasing interactions from left to right (blue arrows indicate individual atomic/molecular dipoles). Reproduced from reference.<sup>1</sup>

Polymers can be organized into two main categories, ferroelectric and nonferroelectric (Figure 9), based on their dielectric response<sup>20</sup>. Ferroelectric materials contain regions of permanent (natural) polarization, known as ferroelectric domains (FE), in which there are large numbers of aligned dipoles. These regions spontaneously polarize in the presence of an applied electric field, and the interactions of these domains result in remnant polarization when the field is removed thereby causing dielectric losses. Relaxor-ferroelectric (RFE) materials contain smaller ferroelectric regions, i.e., nanodomains, which results in lower losses when the field is removed. Antiferroelectric, not to be confused with nonferroelectric, materials contain large FE domains, but they are oriented in opposing directions effectively cancelling out and the systems total polarization is zero.

In contrast, nonferroelectrics contain isolated and weakly interacting dipoles, but no domains. A linear dielectric, as the name implies, is a nonferroelectric in which the dielectric response has a linear relationship with, and is proportional to the strength of, the applied field ( $E$ ). Paraelectric polymers (PE) tend to have an increased number of dipoles that respond quickly, but

are often molten polymers, used above  $T_g$ , and plagued by high electronic conduction which translates into higher losses.

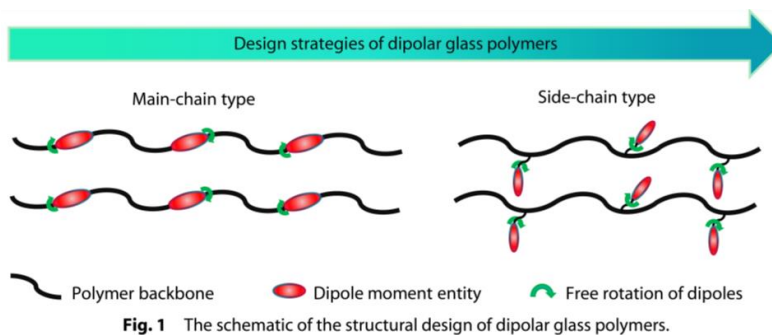


Figure 10: Schematic of the structural design of dipolar glass polymers. Reproduced from reference.<sup>25</sup>

One of the more recently studied dielectrics is dipolar glass polymers (DGP), in which there are fewer dipoles present allowing them to be isolated and have weak dipolar interactions, thereby reducing the losses from the system.<sup>5, 25-27</sup> DGPs incorporate small molecules and functional groups with large dipoles into the backbone or the sidechain of the polymers (Figure 10) because they are not subject to significant steric hindrance.

Lie Zhu defined DGPs as amorphous polymers having a high  $T_g$ , substantial orientational polarization, sub- $T_g$  transition and a broad range between the temperatures for sub- $T_g$  and  $T_g$ .<sup>9, 28</sup> A large difference between sub- $T_g$  and  $T_g$  increases the range of applications for the polymer, since the polymer will exhibit the desired properties at higher operating temperatures. Because DGPs are utilized below  $T_g$  chain dynamics are essentially frozen, reducing translational and frictional losses, and a kind of trap is formed that prevents conduction therefore reduces ionic losses.<sup>20, 29 30</sup>

Ideally frequency independent polarizability is desired and would increase the suitability of the polymer to a wider range of applications. Frequency independence also endows the polymer with a very broad loss peak, ensuring that loss is not a restricting factor for its applications. DGPs

are proving to be a step toward materials with high permittivity and frequency independent polarization.

### 1.3 Approaches to Improve Dielectric Polymers

The greatest improvements in the bulk dielectric constant can be achieved by enhancing the material's polarizability, increasing its packing density and dielectric strength, while reducing its energy losses.<sup>2, 9, 31, 32</sup> The magnitude of energy stored is proportional to the degree of polarization and can be ascertained by measuring the materials capacitance. However, when the force of the applied field becomes too large the dielectric will break down and begin to conduct electricity. The strength of the field just before breakdown occurs is defined as the dielectric strength ( $E_b$ ) of the material, for example biaxially oriented polypropylene (BOPP) has a breakdown strength of  $730 \text{ MV m}^{-1}$ .<sup>28, 33</sup>

Polarization is dependent not only on the strength of the applied field, but also if the field's source is a direct current (DC), creating a static field, or an alternating current (AC), generating an oscillating field. A static field induces electronic polarization ( $P_{\text{elect}}$ ) resulting in a redistribution of the dielectric's electron density, opposite the direction of the applied field, and over time, charge accumulation reaches saturation. In contrast, an oscillating field induces regular inversions of polarization corresponding to the frequency (Figure 3).<sup>34</sup> As the response may lag behind the switching rate, however, dielectric losses can result in dissipation of energy in the form of heat (Figure 7).<sup>34</sup> At lower frequencies molecular dipoles can be aligned, and for effective increases in orientational polarization ( $P_{\text{dip}}$ ), it is necessary to orient the polar constituents within the electric field, as well as the constituents' alignment with respect to each other.<sup>11</sup>



Commonly used inorganic dielectric materials suffer from a variety of limitations, such as failure at high frequencies, poor processability, and limited applicability. Ceramic materials tend to exhibit high energy densities and high dielectric constants at low frequencies, due to strong ionic polarizability ( $P_{ion}$ ). In contrast, exposure to higher frequencies can induce conduction, resulting in lower dielectric strengths and greater dielectric losses.<sup>3</sup> Despite having a low dielectric constant, silicon dioxide has increased capacitance as its thickness is decreased (Table 1). However, it is reaching its theoretical limit, approximately 2 nm, for small scale applications, due to exponential increases in leakage current.<sup>11</sup>

Table 1: Dielectric constants of commonly used materials.<sup>35, 36</sup>

Material	k	Material	k
Inert Gasses	1	Biaxially Oriented Polypropylene (BOPP)	2.2
Oils	2 - 5	Polyphenylene Sulfide (PPS)	3.5
Water	~80	Polycarbonate (PC)	3
Kraft Paper	4 - 7.5	Polyvinylidene Fluoride (PVDF)	10 - 12
Silicon Dioxide	3.9	Ceramics (e.g. BaTiO <sub>3</sub> )	4 - 1235

Since polymers perform reliably over their intended lifetime, exhibit high breakdown strength, and are easily processable, scalable, and lightweight, they have great potential as dielectrics.<sup>6, 34, 37</sup> However, current organic polymer dielectrics have their own limitations, namely relatively low dielectric constants, 2-4, a value that provides insufficient energy density for most capacitance applications.<sup>3, 4, 38</sup> For instance, biaxially oriented polypropylene (BOPP) has improved strength and optical clarity however, due to its low dielectric constant,  $\epsilon = 2.2$ , it has a low energy density,  $U_e = 1-3 \text{ J/cm}^3$ ,<sup>3, 34, 37, 39, 40</sup> and a high dielectric loss at  $T > 85 \text{ }^\circ\text{C}$ .<sup>9</sup>

Polyvinylidene fluoride (PVDF), a semicrystalline polymer that has been widely studied as a dielectric material, can achieve a large permittivity,  $\epsilon = 12$ ,<sup>9</sup> and a high energy density,  $U_e = 13.1 \text{ J/cm}^3$ .<sup>40</sup> However, due to its ferroelectric nature it is susceptible to high dielectric loss, and its dielectric constant is highly dependent upon the crystalline structure, which requires mechanical stretching to induce.<sup>12, 21, 22</sup>

Many approaches to improving key figures of merit for dielectric polymers have been investigated. One of the most common and highly investigated areas is the layering of polymers with differing permittivities, referred to as multilayer films (Figure 11).<sup>41</sup> This method utilizes the interfacial polarization mechanism to increase permittivity by alternating layers of low  $k$ /high  $E_b$  and high  $k$ /low  $E_b$ , but requires that the distance between interfaces be large enough.<sup>9</sup> Multilayer films effectively reduce migration of impurity ions.<sup>42, 43</sup>

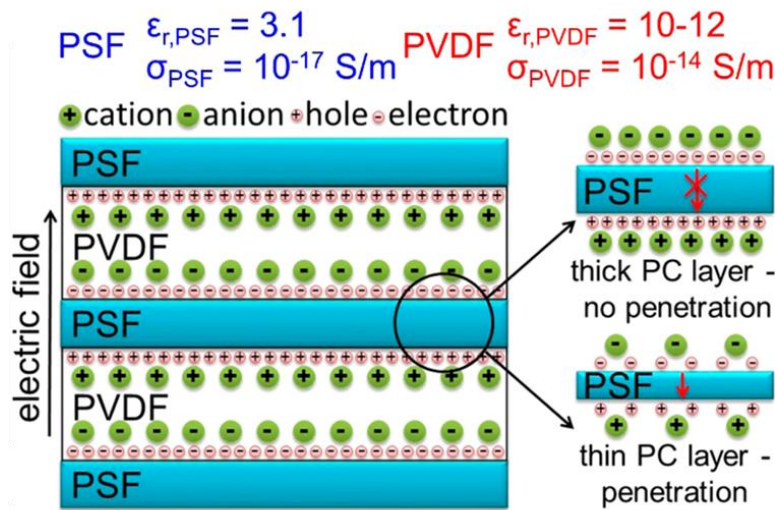


Figure 11: Diagram of interfacial polarization from impurity ions and free electrons in a multilayer PVDF/polysulfone (PSF) film. Reproduced from ref.<sup>5</sup>

Another well-established method is the doping of low  $\epsilon$  polymers with high  $\epsilon$  small molecules or inorganic nanomaterials, creating composites or nanodielectrics.<sup>1, 10, 44</sup> Small molecules tend to want to aggregate creating microphase separated regions that can begin to act as

ferroelectric materials, which increases the dielectric loss. Inorganic materials also suffer from non-uniform dispersion and require high loadings to achieve meaningful increases in permittivity, which makes processing difficult. However, at high loadings the percolation threshold, which is when particles essentially behave as if they are connected, provides a pathway for conduction. When there is a large  $\Delta\epsilon$  the  $E_b$  decreases, because the field between highly conductive particles increases the local field in the polymer which allows for tunneling.

#### 1.4 Design of Side Chain Dielectric Polymers (SDPs)

Our proposed use of polymers with varying length side chains builds on the extensive knowledge the Marks' group has contributed to the field, which has centered largely on the development of self-assembled nanodielectrics (SANDs), a class of self-assembled monolayers (SAMs) that employ inorganic and organic materials into a hybrid (multi)layered system.<sup>11, 38, 44-49</sup> More recent designs have explored the incorporation of an alkyl layer, resulting in similar capacitances, but aromatic layers have large impact on breakdown strength (Figure 12, right).

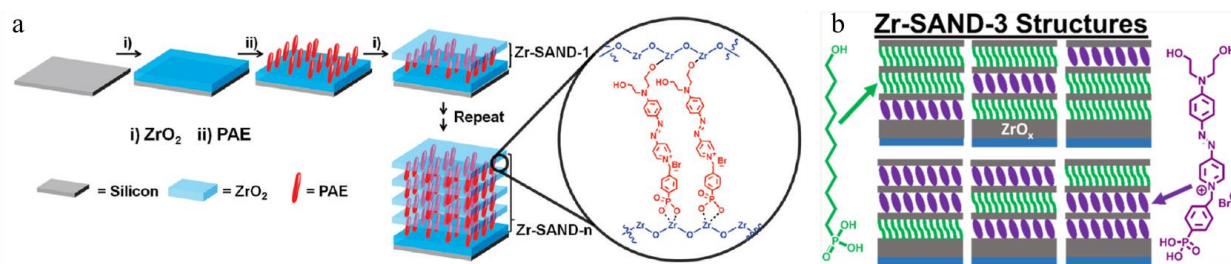


Figure 12: Multilayered self-assembled nanodielectric (SAND) developed by the Marks' group using a phosphonic acid-based  $\pi$ -electron, PAE, layer. (a) fabrication procedure for zirconium-SANDs (b) SANDs incorporating aliphatic and aromatic layers. Figure reproduced from ref<sup>47, 50</sup>

In an integral effort with the Ratner group, key components to enhance the dielectric constant of any rationally designed dielectric material were elucidated through computational

analysis.<sup>11, 38, 45, 46, 48, 51</sup> They report the maximum dielectric constant can be achieved when: 1) molecular geometry is controlled, and planarity is maintained, i.e. the  $\pi$ -orbitals remain oriented such that the greatest orbital overlap can occur; 2) the  $\pi$ -system is aligned parallel to the electric field; 3) the substrates can achieve high packing density; and 4) polarizable substituents are incorporated. Implementation of these design aspects have resulted in several effective organic macromolecules (Figure 13), whose dielectric constants range from  $k = 9$ -13.<sup>7, 8, 52</sup>

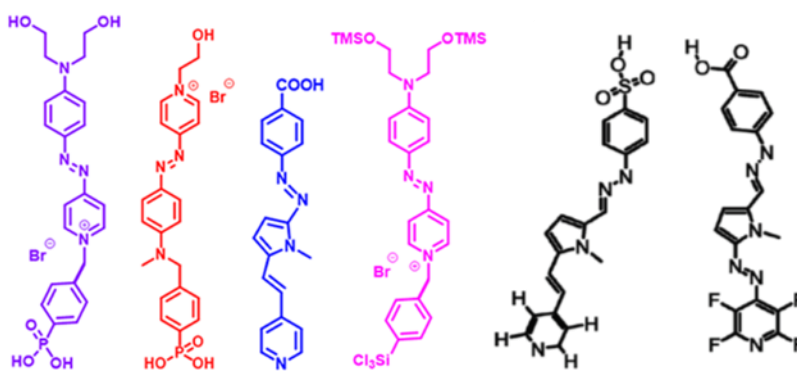


Figure 13: Conjugated substrates for self-assembled nanodielectrics (SANDs) designed by the Marks' group. Figure adapted from ref <sup>50, 53</sup>

Although much has been learned through these studies, this surface-based approach is not practical for most applications. SAM deposition can take up to 18 h, for a single layer, due to the slow reorganization process during film growth, rendering SAMs and SANDs impractical for mass production of electrical components.<sup>52</sup> Moreover, in the case of *in situ* siloxane formation, the packing and ordering of the chemisorbed substrates, determined by the amorphous structure of the siloxane network, affords inconsistent mediation of the dielectric constant. Finally, for layered nanodielectrics, the combined dielectric constant is dominated by the behavior of the material with the lowest dielectric constant, therefore introducing a low  $k$  layer significantly reduces the overall dielectric constant.<sup>11</sup>

This work integrates the foundation laid by the Marks' group into a more practical polymeric design. A polymer's polar nature is largely determined by the chain geometry, thus an inherently flexible aliphatic backbone has been chosen to allow the polymer's conformation to be optimized.<sup>11, 34</sup> Unlike fully conjugated polymers, an aliphatic backbone only requires small segmental motion to adjust its arrangement, due to free rotation about the single bonds.<sup>9</sup> This mobility should allow for orientation of the side chains by an applied electric field while casting the film, a process known as poling, thereby increasing the overall dipole moment of the polymer. After deposition, a polymer sample's chains will inherently be tangled, its side chains will be randomly aligned, and the total dipole moment of a film is reduced by the misalignment of the individual dipoles (Figure 14, left). Once the film has been exposed to a static electric field for an extended period of time, it is expected that the side chains will have reorganized and aligned, to some extent, with the field effectively increasing the samples total polarization (right).

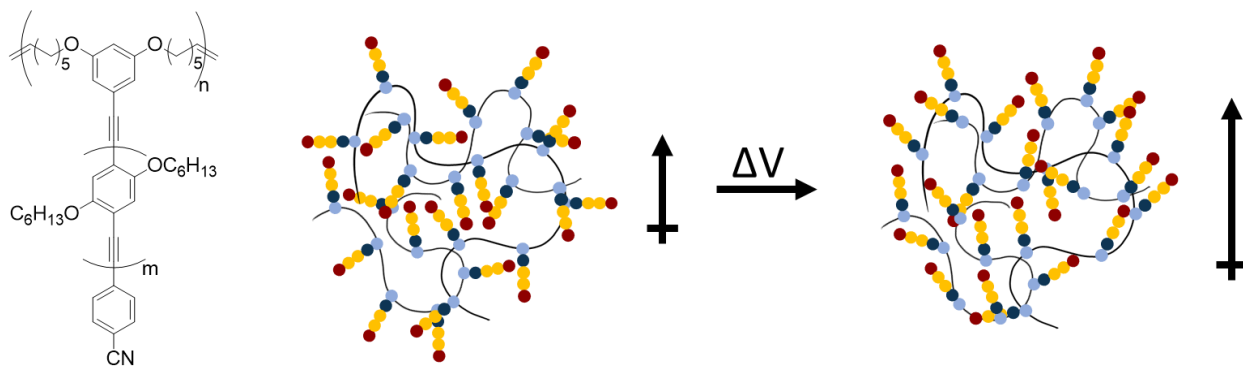


Figure 14: Alignment of polymer chains and side chains and the effect of poling on their orientation. After deposition onto an electrode, the polymer side chains are in random orientations (left) and the total dipole moment of the material is reduced. After poling for an extended period of time the polymer side chains are partially aligned (right) and the total dipole moment of the material is increased.

Conjugation is known to increase a substrate's electronic polarizability, but as the conjugation length increases the band gap decreases, leading to low-breakdown voltages and conduction.<sup>9, 54, 55</sup> By employing conjugation in the side chains, the conjugation length is restricted while still increasing the electronic polarization of the monomers. Since phenylene vinylene

systems have been studied extensively and are well characterized, the unsubstituted and dialkoxy-substituted phenylenes, previously synthesized in the Meyer group, have been targeted as components of the side chain, but instead of a vinylene linkage between aromatics, an ethynylene unit is employed.<sup>56</sup> Zhang, et.al. reported that an electron withdrawing end group has a significant effect on the optoelectronic properties of conjugated oligomers, hence the highly polarizable nitrile has been chosen to further enhance the side chain's dipole.<sup>55, 57</sup>

While experimentation has provided many successes, it is time intensive and is often not generalizable, whereas computationally driven design is more efficient, faster, and uniform.<sup>38, 48, 58, 59</sup> Our strategy in this project combines current understanding of material and molecular properties with quantum chemical calculations, to screen and identify suitable synthetic targets.<sup>48, 58, 59</sup> A method for rapid screening of molecules based on the polarizability and the dipole is being developed, utilizing machine learning techniques, by the Hutchison group.<sup>60-63</sup> In a joint effort to develop high permittivity side chain dielectric polymers, more effective **PhE** constituents will be ascertained and integrated into the monomer design.

## 1.5 Broadband Dielectric Spectroscopy

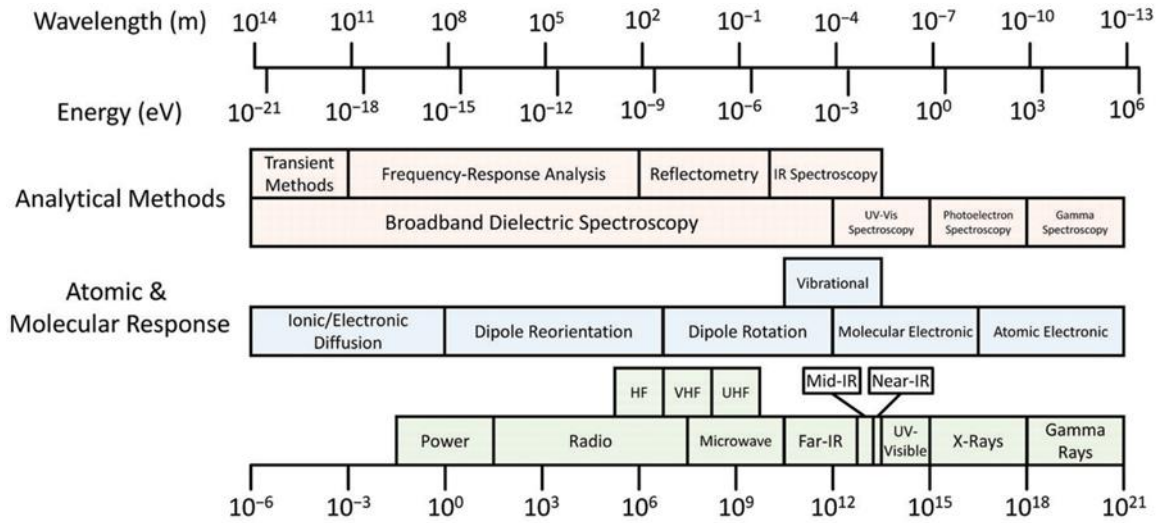


Figure 15: Correlation between the frequencies, analytical techniques and molecular responses across the electromagnetic spectrum.<sup>64</sup>

Broadband dielectric spectroscopy (BDS) is the study of interactions of EM radiation with matter and covers a wide range of the electromagnetic spectrum (Figure 15). Whereas more well known spectroscopic techniques, for example IR or NMR, measure at frequencies above those used in BDS and only cover 1-2 decades of frequency ranges. BDS, more specifically, is the study of the dielectric properties, also referred to as the dielectric response, of a material which is the movement of dipoles in the presence of an electric field. A range of molecular dynamic processes can be studied for a given material, including but not limited to polymerization rates, thermal transitions (e.g.  $T_g$ ), activation energies, and molecular relaxations. BDS is an indispensable technique in the fundamental understanding of these processes.

### 1.5.1 Instrument Basics

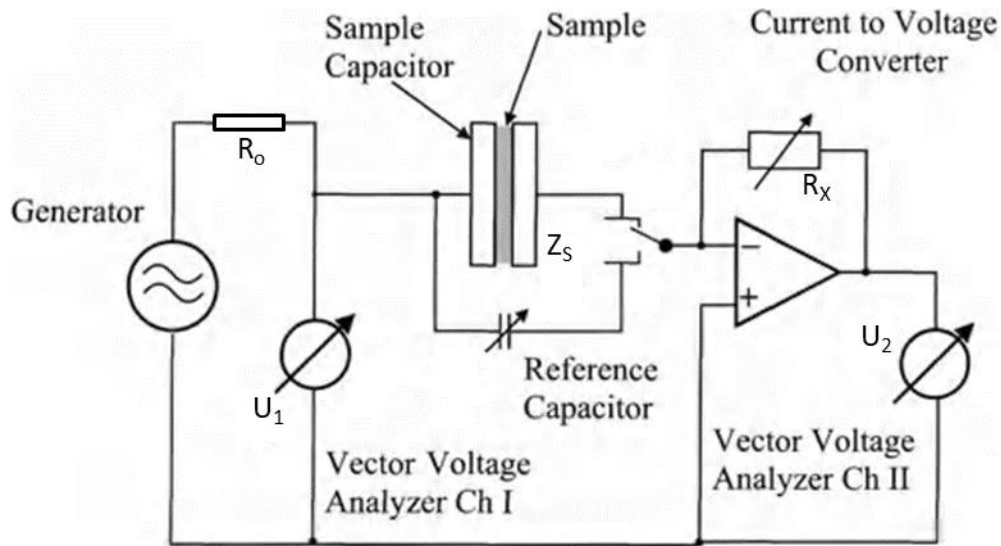


Figure 16: Schematic of Frequency Response Analyzer Circuit. Figure reproduced from ref <sup>65</sup>

Different measurement systems are required to cover the entire range of frequencies, but the only one discussed here is based on the turnkey system designed by Novocontrol Technologies, as the others are beyond the scope of this work. (Note: the Novocontrol system is designed and optimized so the user can ignore effects due to the various connecting cables and sample cell.) This system utilizes a frequency response analyzer (FRA) (Figure 16) with two phase sensitive voltmeters that measure voltage and current response and a lock-in amplifier that ensures the output is in a reliably measurable range.



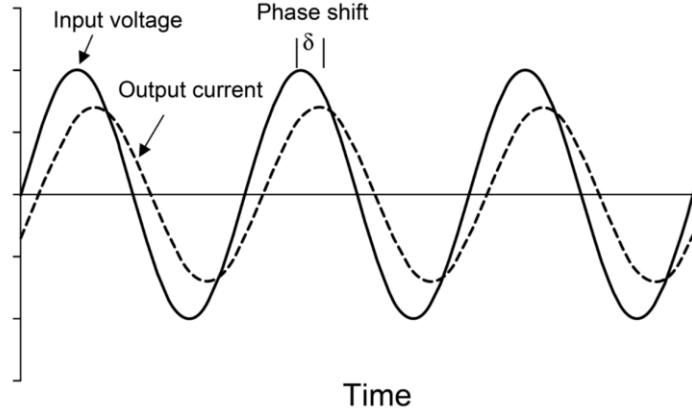


Figure 17: Voltage and current response of a hypothetical polymer material. Figure reproduced from <sup>66</sup>

A sample capacitor is placed in a sample cell and this sample cell is isolated in a cryostat, which is capable of precisely controlling the temperature of the sample via a liquid nitrogen supply and heaters. Once the experimental details, e.g.  $T$  and  $\nu$  ranges, have been entered and the experiment started, the generator applies a sinusoidal voltage to the sample. The response of the sample to the applied voltage, not being an instantaneous process, causes a phase shift in the output current ( $I_S$ ) (Figure 17) (the result of an applied voltage is the flow of current). A variable in line resistor ( $R_x$ ) then converts the current ( $I_S$ ) to a voltage ( $U_2$ ), using a feedback loop and the lock-in amplifier (1.18).

$$I_S = \frac{U_2}{R_x} \quad (1.18)$$

Two phase sensitive voltmeters (vector voltage analyzer Ch I and Ch II) measure the amplitude and phase of the applied voltage ( $U_1$ ) and sample voltage ( $U_2$ ). After each sample measurement the system switches to a variable reference capacitor and a second measurement is obtained as an online calibration to improve the accuracy of the measurements. From these measurements the sample impedance ( $Z_S$ ) can be calculated (1.19).

$$Z_S = \frac{U_1}{I_S} = -\frac{U_1}{U_2} R_x \quad (1.19)$$

The complex permittivity  $\epsilon^*$ , as a function of the angular frequency ( $\omega$ ) of the applied sinusoidal waveform, can be derived from the sample impedance ( $Z_S = Z^*(\omega)$ , 1.20).

$$\epsilon^*(\omega) = \frac{1}{i\omega Z^*(\omega)C_0} \quad (1.20)$$

### 1.5.2 Polymeric Response

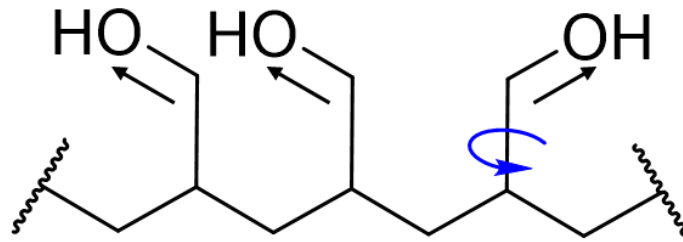


Figure 18: A fragment of a hypothetical polymer chain that contains polar bonds. The molecular dipole moments are indicated by the black arrows and one bond that would rotate in the presence of an electric field is indicated by the blue curved arrow.

As described in section 1.2, there are several modes of polarization that are each activated by an applied electric field at a particular frequency. While there is a 'typical' range of frequencies at which a particular polarization will activate, the overall movement depends on the state of the sample and the influence of neighboring bonds and functional groups. In the case of a polymer, its chain entanglement, the amount of free volume available, and the glass transition temperature have a significant impact on dipolar rearrangements.

For small dipolar groups attached as side chains, such as those in the hypothetical polymer segment depicted in Figure 18, there is typically enough free volume in the polymer sample to allow the dipoles to align easily with the field. In this case, the bond between the methine in the

backbone and methylene in the side chain would rotate with the field (curved blue arrow). In a static field, given enough time, all of the C-OH dipoles would rotate to orient in the same direction and the maximum possible polarization would be achieved. When the sample is subjected to an oscillating field, such as in a BDS experiment, the dipoles within the sample will rotate and change direction with the field. At low frequencies the time scales are long and a higher permittivity is observed. However, as the frequency of the field increases, the dipoles will not fully align with the field before the force of the field causes the dipoles to reverse their movement. Because the dipole vectors do not fully align before reversing their movement, the permittivity obtained for the sample is reduced.

For a polymer with a rigid side chain structure, the amount of free volume available becomes a more influential factor. When the side chain is relatively short, it can behave similarly to that observed with the small dipolar group side chain described above. As the length of the side chain increases, the free volume in the sample also increases. However, as the length increases the side chain requires more room to rotate and the increase in free volume may not be proportional to what is required. In other words, at moderate lengths the side chains may be able to move and align with an applied field, but this may require an even longer exposure to a static field. Long side chains may be significantly more hindered and some may rotate, but most will likely only rotate to a small degree. When these polymers are subjected to an oscillating field, instead of a rotational motion with the oscillating field, the side chains may exhibit a vibrational motion or a wag of the dipole with the reversing field direction.

The glass transition temperature of the polymer can have a substantial impact on its response to an applied field. When a sample is below its  $T_g$ , referred to as being in a glassy state, its chain dynamics are frozen. If the dipoles are small enough, as in the example polymer above

(Figure 18), they may still be capable of rotating in the glassy state. However, with larger and more rigid dipoles, it has been found that there is no 'give' when the side chain movement interacts with an adjacent polymer chain or side chain. In some instances there appears to be no movement, and the permittivity obtained is attributable to electronic polarization only.

For dielectric materials, the spectrum acquired for the frequency dependent motion will display a gradual increase in the permittivity of the sample as the frequency decreases. Note that when the dipoles are activated, it is not a binary event, there is a transition through which more dipoles are gradually activated. This is observed as a distinct change in the slope of the spectrum, often before the slope reverts back to a more shallow angle.

## **1.6 Project Goals**

The goal of this project is to design a method for synthesizing and testing a side chain dielectric polymer that is easily tunable and maintains high monomer fidelity. Influential monomer parameters will also be identified, through side chain engineering, for rationally tuning the dielectric properties of this new class of polymers. These studies will address factors hypothesized to influence the dielectric behavior of the polymers. Specifically, what length of the side chain is required to induce a measurable effect on the dielectric constant? Will a poling field impact the side chain alignment, and which length produces the greatest response?

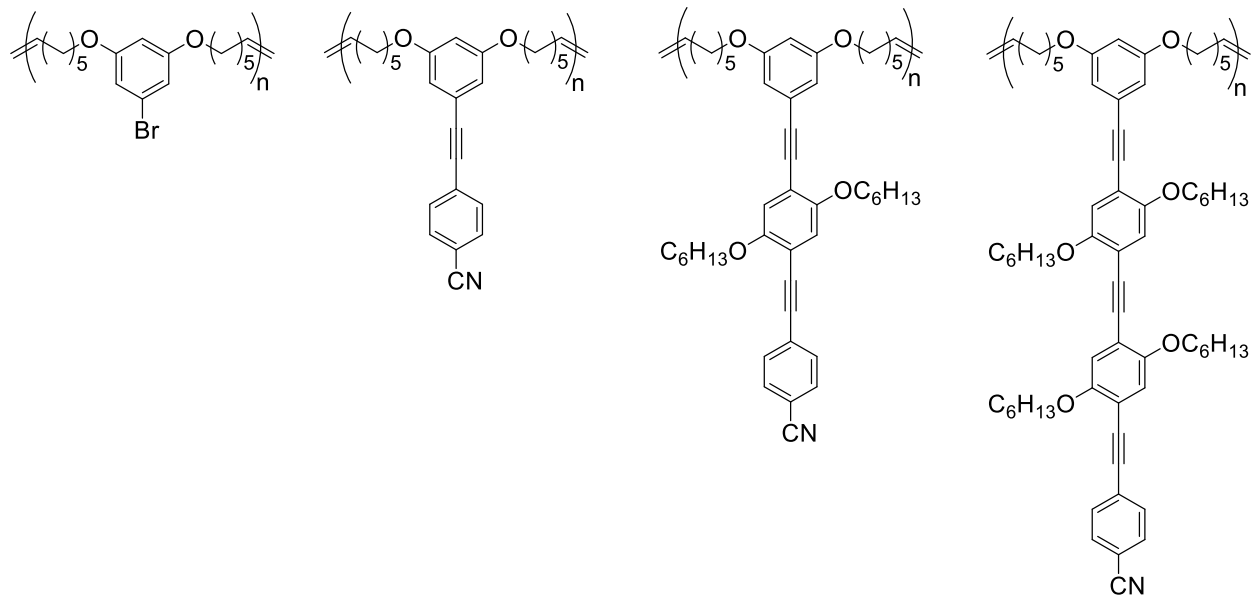


Figure 19: Proposed polymer series. Starting from the top left is the base structure, the polymer backbone, continuing with the poly-dimer, poly-trimer and poly-tetramer. (note on nomenclature, a dimer, trimer, etc. refers to the number of phenyl groups in the monomer).

A series of polymers with systematically increasing side chain length will be synthesized and polymerized based on the well-established phenylene ethynylene system (Figure 19). Each of these polymers will also bear a terminal nitrile functional group, or other polarizable end group, to increase the side chain's dipole moment. The development of this synthetic route will establish a procedure that provides a means to readily modify the monomer for ease of tuning the system.

These polymers will be studied by broadband dielectric spectroscopy to determine their merit as dielectric materials. The polymers will be evaluated through a series of frequency and temperature dependent experiments, that will establish what length side chain is required to produce a measurable effect on the permittivity.

These materials will subsequently be subjected to a static electric field to force orientation of the side chains, and these polymers will again be evaluated with broadband dielectric spectroscopy. Their behavior will establish whether a poling field will have an impact on the

alignment of the polymer side chains and what parameters are required to obtain the greatest impact.

## 2.0 Phenylene Ethynylene Based Polymers

### 2.1 Summary

In this work, a new class of side chain dielectric polymers based on a phenylene ethynylene (**PhE**) structure and their characterization is presented. The effects of conjugation length, polarity, and poling on the permittivity of the system were studied. The polymers were synthesized via acyclic diene metathesis (ADMET) and post-polymerization functionalization, and their molecular weights ( $M_n$ ) ranged from 13 to 26 kDa with dispersities around 1.6. Sample films were prepared by solution deposition between a pair of brass electrodes and characterized by broadband dielectric spectroscopy. All unpoled polymers exhibited high permittivities of  $\epsilon' \geq 4.3$  (at 20 °C and 1kHz). Poling at a 15-volt potential resulted in a measurable increase in the permittivities, up to  $\epsilon' = 12.4$ , demonstrating their potential as high-performance dielectric polymers.

### 2.2 Introduction

The advancement of all-polymer dielectrics with high permittivity and low dielectric loss has been the focus of much research for their potential as capacitor materials. Practical applications such as energy storage systems, signal processing, and electric vehicles require high energy density and high efficiency. Polymeric systems are attractive because, unlike traditional ceramic materials,

they are easily processable, light weight, and have high breakdown strengths ( $E_b$ ) making them particularly suitable as capacitor materials. The major disadvantage to polymeric materials is that they tend to have low permittivities, 2-5, and therefore have low capacitances.

Many strategies for improving polymer permittivities have been explored. Multilayered films with alternating high permittivity, often PVDF, and high  $E_b$ /low loss polymers that resulted with either good permittivities,  $\epsilon'$  4.9-5.8, but exhibited high losses<sup>67</sup>, or typical permittivities,  $\epsilon'$  3.1-3.7 with good losses<sup>68</sup>.

Conjugation is one component often employed to improve the permittivity of a material. However, polymers with fully conjugated backbones are rigid in nature, which restricts the movement of the randomly aligned dipoles. This inherent misalignment of the dipoles, some of which completely cancel each other out, reduces the maximum possible permittivity of the material.<sup>69</sup>

The Marks' group designed a system of self-assembled nanodielectrics (SANDs), in which they utilized alternating layers of inorganic metal oxide and short conjugated chromophores to build thin film transistors.<sup>8, 49, 50, 70-72</sup> Similarly, this work designed short segments of conjugated species that, instead of self-assembled, are tied together with long flexible aliphatic chains between the aromatic junctions. This configuration will deliver a simpler and faster film fabrication process.

The  $sp^3$  hybridized bonds in the backbone offer freedom of movement through rotation and the side chains provide added free volume to the system. Combined, these factors will ultimately aid in the alignment of the side chains' dipoles. Similar to the polymers presented in Xu, et al.'s work published in 2021<sup>73</sup>, it is hypothesized that the phenyl groups in the side chain may also aid in the alignment through  $\pi$ - $\pi$  interactions.



## 2.3 Experimental

### 2.3.1 Materials.

Reagents were purchased from Sigma Aldrich and Fisher Scientific. Bromohydroquinone (TCI & Sigma), Grubbs II, Copper(I) Iodide, triphenylphosphine, piperidine, Dichlorobis(triphenylphosphine)palladium(II), boron tribromide, diphenyl ether, n-Butyllithium,

Fisher Scientific: 4-bromobenzonitrile (TCI and Fisher), boron tribromide (1 M in DCM; Acros), trimethylsilyl acetylene (TCI), 1-bromo-3,5-dimethoxybenzene (TCI), 7-bromo-1-heptene, Grubbs II, Palladium(0) bis(dibenzylideneacetone) (TCI), Bis(triphenylphosphine)palladium(II) chloride (Acros),

All solvents were purchased from Fisher Scientific and Sigma-Aldrich and used as purchased, unless otherwise indicated.

### 2.3.2 Characterizations

$^1\text{H}$  and  $^{13}\text{C}$  NMR spectra were acquired from Bruker spectrometers (300, 400, and 500 MHz) in deuterated chloroform ( $\text{CDCl}_3$ ) or dimethyl sulfoxide (DMSO) and calibrated to the residual solvent peaks ( $\delta$  7.26 and  $\delta$  77.1,  $\delta$  2.50 and  $\delta$  39.52 respectively).

Thermal properties were obtained from Perkin Elmer DSC 6000, under an inert  $\text{N}_2$  atmosphere, in a 4 step cycle, repeated once, (i) hold for 1 min at  $-50\text{ }^\circ\text{C}$ ; (ii) heat to  $150\text{ }^\circ\text{C}$  at  $10\text{ }^\circ\text{C}/\text{min}$ ; (iii) hold for 1 min at  $150\text{ }^\circ\text{C}$  (iv) cool to  $-50\text{ }^\circ\text{C}$  at  $10\text{ }^\circ\text{C}/\text{min}$ . Glass transition temperatures were calculated from the inflection point in the second heating cycle. Molecular weights and

dispersities were acquired using a TOSOH EcoSEC HLC-8320GPC relative to polystyrene standards of 2.5, 9, 30 and 50 kDa.

### **2.3.3 Synthesis**

The experimental and characterization details for the compounds and polymers synthesized can be found in Appendix A.1.

### **2.3.4 Film Preparation and Dielectric Experiments**

The films were prepared by solution deposition between a pair of brass electrodes, bottom and top electrode dimensions are 32 and 15 mm in diameter, respectively, by 3 mm thick, which were cut by the machine shop. Before deposition, the electrodes were initially sanded to a fine finish with sandpaper grits: 400, 800, 1200, 1500, 2000, and 2500 in sequence, then polished and sonicated for ten minutes each in methanol, acetone, and isopropyl alcohol. For subsequent uses, only the 2500 grit followed by polishing and sonication were performed.

The polymers were dissolved in toluene, or chlorobenzene, at 3  $\mu\text{L}/\text{mg}$ . An 85  $\mu\text{L}$  aliquot of solution was deposited onto the bottom electrode by first tracing an outer ring slightly larger than the diameter of the top electrode and then filling in the circle (Figure 36). The films were generally allowed to dry for approximately one hour (longer times were also investigated but 1 hour proved optimal) before the top electrode was centered and placed on top of the film. The ‘capacitor’ was allowed to continue drying for a minimum of 12 hours before BDS measurements or poling of the films were conducted. It is important to note that the polymer between the

electrodes did not fully dry during this period, which is important since the solvent-induced plasticization was key to subsequent poling.

BDS experiments were performed using a Novocontrol Alpha High-resolution analyzer. Frequency scans were generally measured from  $10^{-1}$  to  $10^6$  Hz at 20 °C, and temperature scans were measured from -120 to 100 °C at frequencies between  $10^{-1}$  to  $10^6$  Hz, with an applied voltage of 1.0 V for all measurements. Films were measured before and/or immediately after each poling period.

To ‘pole’ the polymer samples, they were placed in a static electric field. Specifically, a completed ‘capacitor,’ as described above, was placed on a heat-controlled conductive stage in a Micromanipulator. The circuit was formed when a probe was placed in contact with outer surface of the top electrode, and a Keithley Series 2614B Source Meter was used to apply a static electric field across the film with an applied potential that ranged from 5 V to 15 V. The samples were poled at temperatures ranging from room temperature to 50 °C for periods of time ranging from 15 minutes to approximately 20 hours. In the optimized procedure samples were poled at room temperature, at a 15 V potential and for approximately 20 hours.



substituted **PhE** and one unsubstituted **PhE** with a terminal nitrile. Before coupling, **H-SU-CN** describes this polymer's side chain. Since all arenes are connected with alkynes, their presence is assumed in the **B**, **S**, and **U** terms.

Table 2: Abbreviations used in naming prepared compounds

Symbol	Definition
<b>B</b>	Polymer backbone phenyl ether
<b>S</b>	Substituted phenylene ethynylene
<b>U</b>	Unsubstituted phenylene ethynylene
<b>H</b>	Deprotected terminal alkyne
<b>TMS</b>	Trimethylsilyl protected alkyne
<b>CN</b>	Terminal nitrile
<b>Br/I</b>	Terminal bromine or iodine, respectively
<b>p-</b>	Polymer

The shortest side chain, the terminal **PhE** segment **H-U-CN** (Figure 21), was synthesized and used without further purification. Following the Sonogashira conditions reported by Shirai, et.al.<sup>74</sup> the coupling of TMSA with, as purchased, *p*-bromobenzonitrile, produced alkynylated arene **1**. TMS deprotection of **PhE 1** with potassium carbonate resulted in near-quantitative yields of terminal alkyne **H-U-CN**.

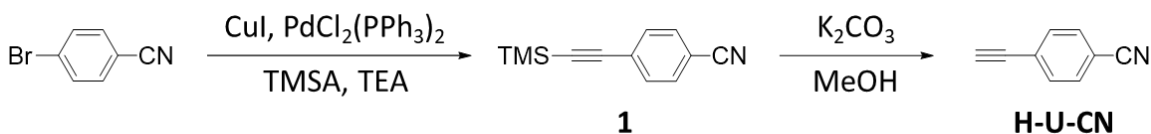


Figure 21: Synthesis of **H-U-CN**, the terminal **PhE** segment for all side chains.

To synthesize the substituted **PhE** segment (Figure 22), first bromohydroquinone was subjected to a biphasic ether synthesis<sup>54</sup> with 1-bromohexane to obtain the alkylated intermediate **2**. Iodine was successfully substituted *para* to the bromine on arene **2** with molecular iodine and potassium iodate<sup>75, 76</sup> to produce bromo/iodo-arene **3**. Sonogashira conditions were applied to couple trimethylsilyl acetylene (TMSA) with arene **3**, almost exclusively replacing the iodine, to

form monoalkynylated arene **4**. Initially, TMS protected bromo-arene **4** was coupled with **H-U-CN**, but these reactions required excessive heat and very long reaction times and resulted in yields less than 40%. Consequently, a bromo-iodo exchange was carried out to transform arene **4** into TMS protected iodo-arene **5**. Subsequent coupling of iodo-arene **5** to **H-U-CN** dramatically improved yields to around 85-95%.

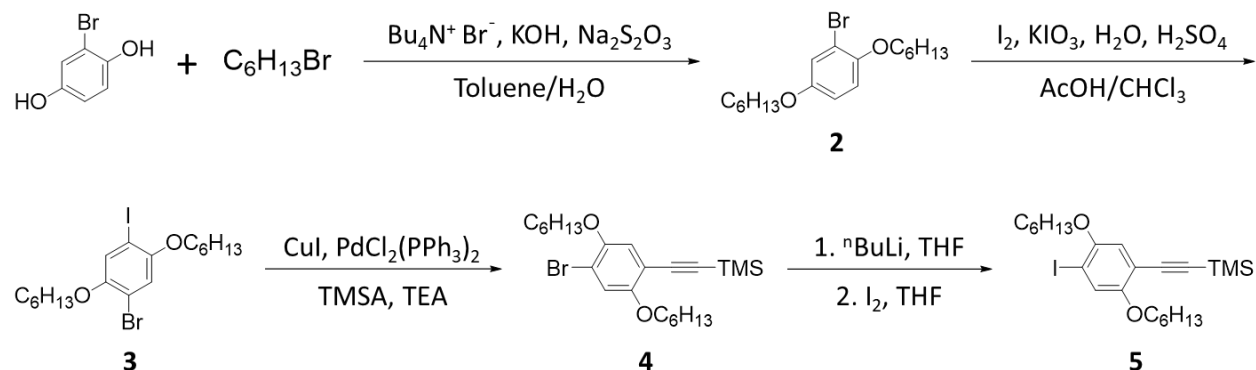


Figure 22: Synthesis of substituted **PhE** segment **5**.

Preparation of the remaining side chains, to complete the series of polymers studied in this work, was achieved through a series of palladium couplings and carbonate deprotections (Figure 23). Terminal alkyne **H-U-CN** was coupled with iodo-arene **5** to produce the TMS-protected side chain dimer, **TMS-SU-CN**. After deprotection, terminal alkyne **H-SU-CN** was obtained in near-quantitative yields. Without further purification, **H-SU-CN** was coupled to a second iodo-arene **5** to give the final side chain segment, the TMS-protected side chain trimer, **TMS-SSU-CN**. As with the other side chains, once terminal alkyne **H-SSU-CN** was obtained, the following couplings were performed without further purification.

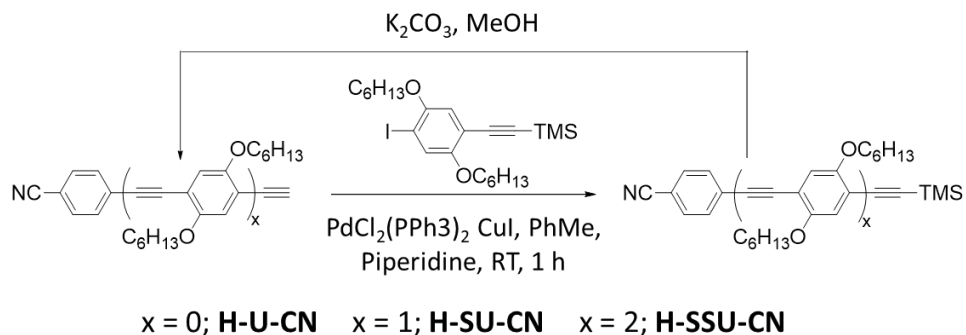


Figure 23: Synthesis of side chain moieties.

Table 3: Properties of Side Chain Dielectric Polymers.

	$M_{\text{repeat unit}}$ (g/mol) <sup>a</sup>	$M_n$ (kDa) <sup>b</sup>	$\bar{D}$	% substitution	DP <sup>c</sup>	$T_g$ (°C) <sup>d</sup>
<b>p-B-Br</b>	353	18.7	1.56	NA	56	-20
<b>p-B-I</b>	400	21.6	1.56	NA	54	-11 <sup>e</sup>
<b>p-BU-CN</b>	400	19.1	1.76	94-100	48	35 <sup>f</sup>
<b>p-BSU-CN</b>	700	24.4	1.67	96-100	35	23 <sup>g</sup>
<b>p-BSSU-CN</b>	1000	31.3	1.39	98-100	31	24

<sup>a</sup>Calculated; <sup>b</sup>Number average molecular weight measured by SEC in THF relative to polystyrene standards; <sup>c</sup>DP calculated from  $M_n$ ; <sup>d</sup> $T_g$  measured by DSC; <sup>e</sup> $M_n = 20.3$  kDa and  $\bar{D} = 1.68$  for the sample used to obtain  $T_g$ ; <sup>f</sup> $M_n = 21.1$  kDa and  $\bar{D} = 1.57$  for the sample used to obtain  $T_g$ ; <sup>g</sup> $M_n = 21.2$  kDa and  $\bar{D} = 2.00$  for the sample used to obtain  $T_g$ ;

The unsubstituted polymers **p-B-Br** and **p-B-I** (Figure 24) were synthesized in three or four steps, respectively, starting with the demethylation of commercially available 1-bromo-3,5-dimethoxybenzene with boron tribromide<sup>77-80</sup> to give diol **6**, after crystallization from chloroform. Installation of the alkene functional groups required for metathesis polymerization was accomplished by reaction of diol **6** with 7-bromo-1-heptene under biphasic ether synthesis conditions to produce monomer **7**. Polymerization of bromo-monomer **7** was performed by acyclic diene metathesis (ADMET), using Grubbs 2<sup>nd</sup> generation catalyst (Grubbs II), to obtain **p-B-Br**. The ADMET polymerization required several days at mild temperatures to achieve high  $M_n$ . At a concentration of 2 M and a catalyst loading of 3 mol%, the  $M_n$  of the polymers ranged from 16.8

to 19.7 kDa with dispersities averaging around 2.1; the characterization for an example polymer shown in Table 3, first row. It is important to note that the substituted variants were not all prepared from the same backbone batch. Alternately, bromo-monomer **7** was subjected to two lithium-halogen exchanges<sup>81</sup>; first, **7** was reacted with n-butyllithium to displace bromine, then with elemental iodine to form iodo-monomer **8**. Polymerization of monomer **8** under the same ADMET conditions resulted in **p-B-I** with  $M_n$ s in a similar range, 16.6-24.9 kDa, while dispersities improved, averaging around 1.7.

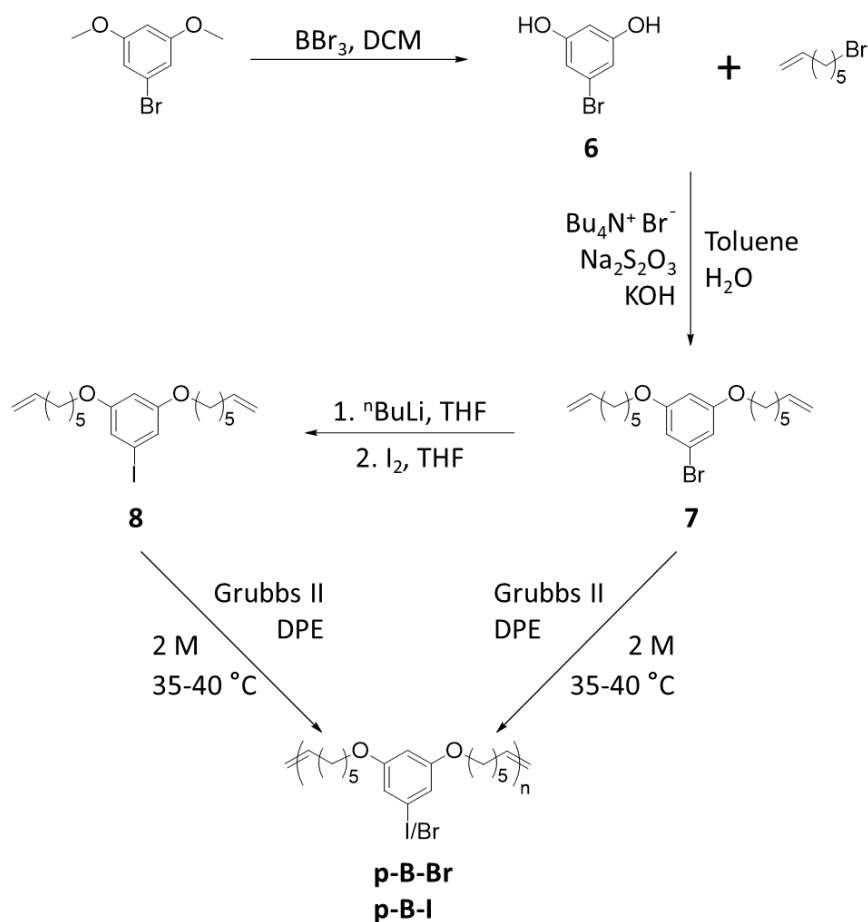


Figure 24: Synthesis of the unsubstituted polymer, **p-B-Br**, and the polymer backbone, coupling partner, **p-B-I**.

Post polymerization functionalization of the polymer backbone, under Sonogashira conditions, was implemented to prepare the substituted polymers (Figure 25). When side chain



coupling was performed with **p-B-Br**, these reactions required high temperatures and very long reaction times, often 8 or more days. These **p-B-Br** couplings generated polymers with appreciably reduced molecular weights, as much as half the  $M_n$  of the starting **p-B-Br**, modest substitution rates, and large dispersities. Whereas upon switching to iodine, the reactions worked at room temperature, and the percent substitution was near quantitative. Nevertheless, reaction times were still at least 8 days and molecular weights were reduced relative to the bromo-couplings. Once the base was changed to piperidine, the reactions were complete within 30 minutes after adding the alkyne and the  $M_n$ s were only slightly reduced. The polymers obtained were of moderate length, with degrees of polymerization (DP) between 31 and 48 repeat units, and their dispersities ranged from 1.4 to 1.8 (Table 3).

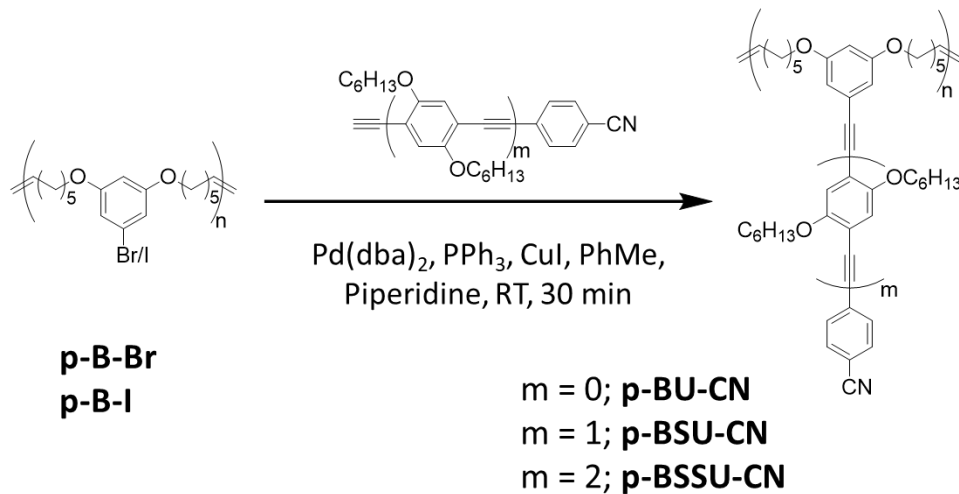


Figure 25: Synthesis of side chain dielectric polymers.

$^1\text{H}$  NMR spectral analysis of the purified polymers confirmed the successful synthesis and molecular structure of all the substituted polymers. For example, the  $^1\text{H}$  NMR spectrum for **p-BSSU-CN** and its precursors is shown in

Figure 26. The near complete disappearance of the aromatic peaks at 6.82 and 6.38 ppm present in **p-B-I**, along with the emergence of peaks at 6.67 and 6.44 ppm, respectively, in **p-**

**BSSU-CN** indicate effective coupling of the side chain, approaching quantitative substitution. The broadened peaks in the spectra of **p-B-I** and **p-BSSU-CN** are consistent with a polymeric structure. Another indication of successful coupling can be seen in the aromatic peaks that are associated with the two substituted **PhE** segments in the side chain **H-SSU-CN**. In the  $^1\text{H}$  NMR spectrum of **H-SSU-CN** there are clearly four overlapping peaks at  $\sim 7$  ppm. Once coupled with the backbone, subtle shifts due to the change in the electronic environment are observed.

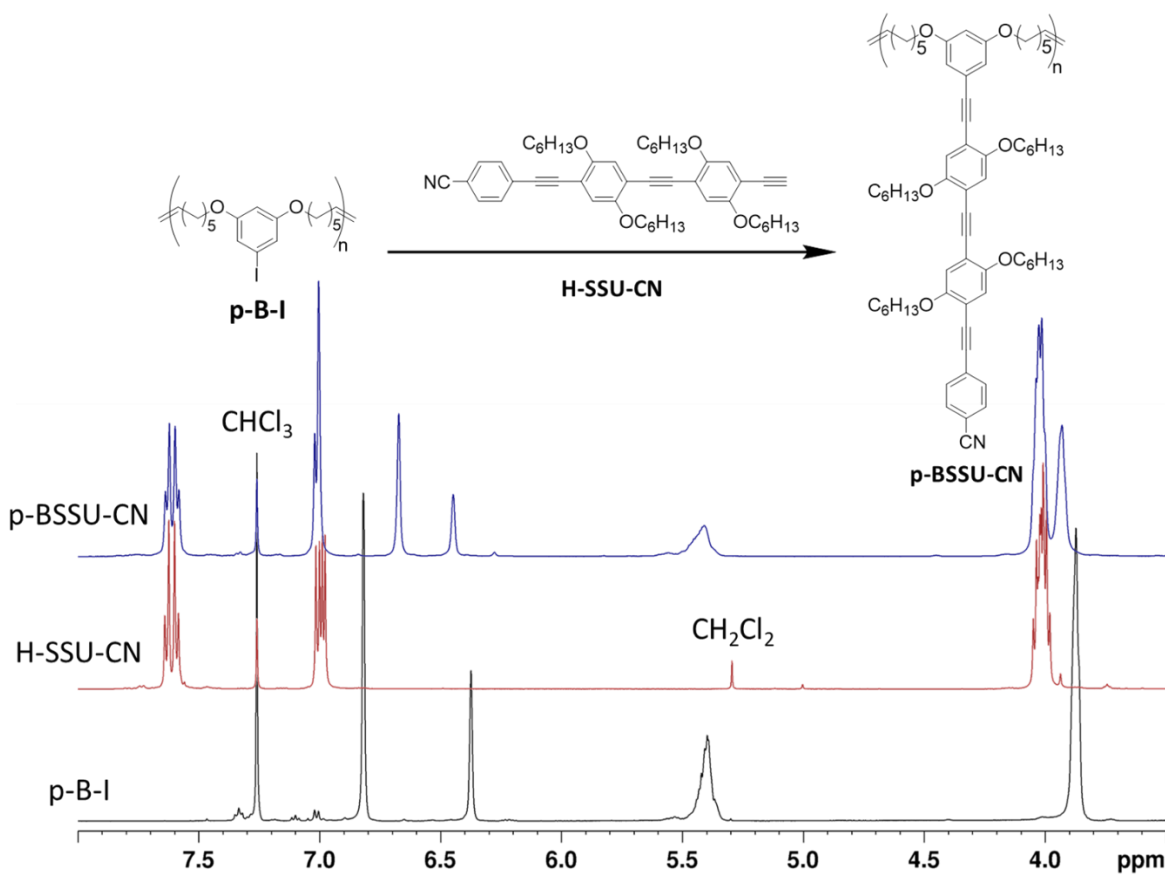


Figure 26:  $^1\text{H NMR}$  for the synthesis of **p-BSSU-CN**, from the polymer backbone, **p-B-I**, and the side chain moiety, **H-SSU-CN**. Residuals from the deuterated solvent and dichloromethane are noted.

## 2.4.2 Polymer Properties

To further characterize the polymers, the number average molecular weights ( $M_n$ ) and molecular weight distributions, or dispersities ( $\mathcal{D}$ ), were measured by size exclusion chromatography (SEC) using THF as the eluent and polystyrene standards (Table 3). An additional characteristic of a polymer is its degree of polymerization (DP), which describes the number of repeat units present in a polymer and is frequently calculated from a  $^1\text{H NMR}$  spectrum. The molecular weights of the polymers synthesized here are high enough that the end groups are not

visible in the NMR spectra; therefore, it was necessary to calculate the DP from the  $M_n$  obtained by SEC despite the fact that these values are not absolute.

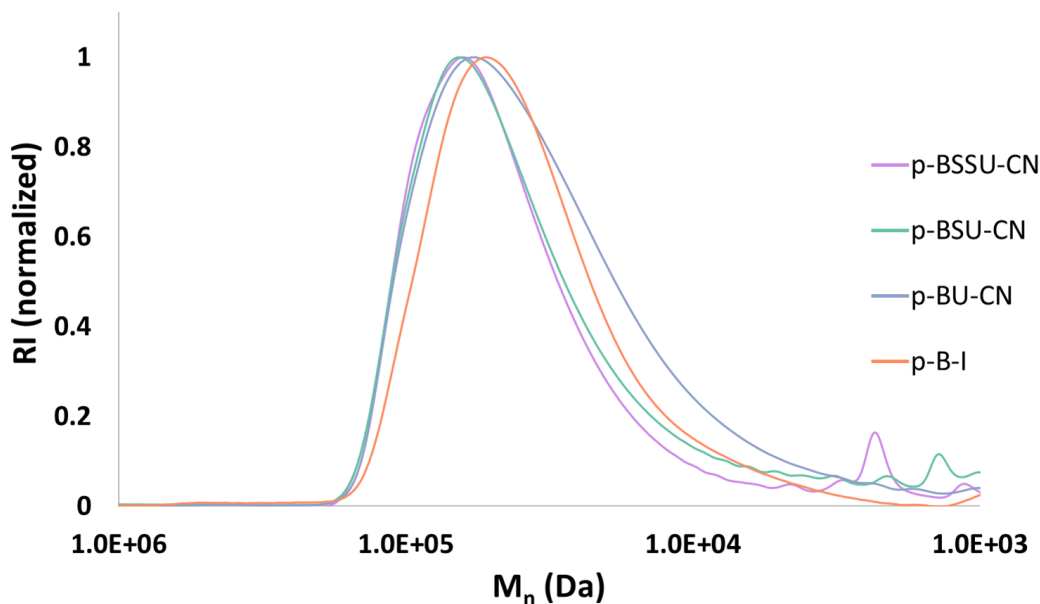


Figure 27: SEC showing the increase in molecular weight of the three substituted polymers as compared to the unsubstituted polymer.

The SEC measurements provided additional evidence that coupling of the side chains to the polymer backbone was successful. An SEC measurement provides an estimate of the molecular weight of the sample measured, because it measures the hydrodynamic volume of the sample, the amount of space occupied by the polymer in a solution. Every polymer exhibits its own hydrodynamic volume and often, as it was here, the reference used for calibration is polystyrene (PS). The chromatogram revealed that the unsubstituted polymer, **p-B-I**, which had a repeat unit molecular weight ( $M_{RU}$ ) of 400 g/mol, had an average molecular weight of 22 kDa with a dispersity of 1.6 and a calculated DP of 54 (Figure 27). After coupling, it was expected that the  $M_n$ s for polymers **p-BSU-CN** and **p-BSSU-CN**, whose  $M_{RUS}$  were 700 g/mol and 1000 g/mol, would increase significantly to 38 kDa and 54 kDa, respectively, while that for **p-BU-CN**, whose  $M_{RU}$  is identical to that of **p-B-I**, should not change. However, the  $M_n$  only increased to 24 kDa for **p-**

**BSU-CN** and to 31 kDa for **p-BSSU-CN**, whereas it decreased for **p-BU-CN** to 19 kDa. The difference in the  $M_n$  obtained for these coupled polymers from those expected may be partly due to changes in hydrodynamic radii and partly due to chain cleavage (see section 2.5.1).

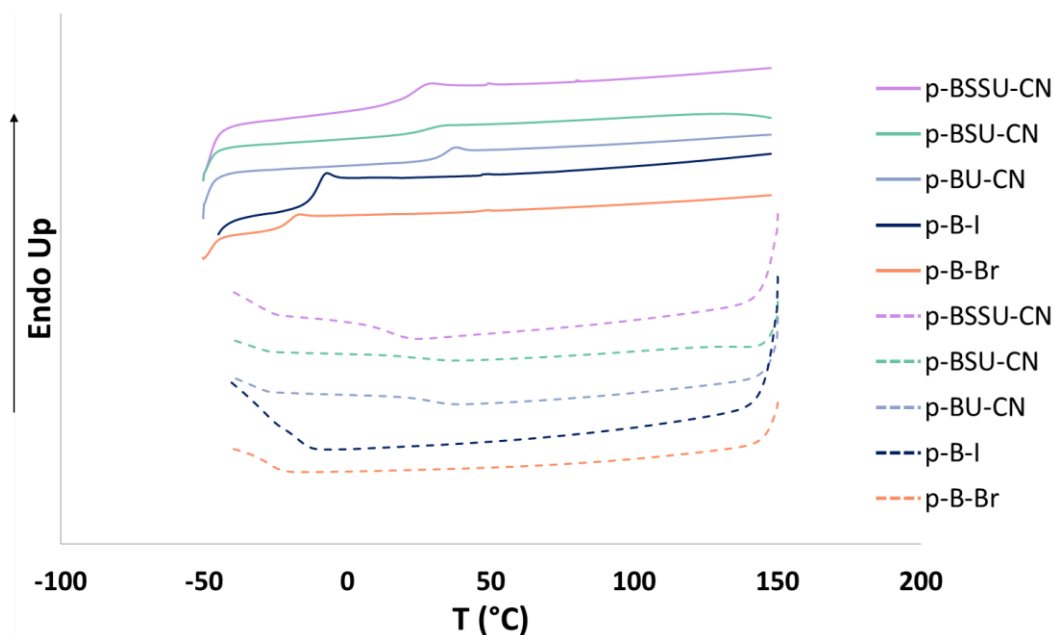


Figure 28: The DSC thermograms for the second heating (solid curves) and cooling (dashed curves) scans for all polymers, at a heating rate of 10 °C/min under nitrogen.

The thermal properties of each of the polymers synthesized herein were obtained by differential scanning calorimetry (DSC) at a heating rate of 10 °C/min and the second heating and cooling scans are depicted in Figure 28. The glass transition temperature ( $T_g$ ) is the region in which polymers transition from a more rigid glassy state to an amorphous structure. The unsubstituted polymers, **p-B-Br** and **p-B-I**, exhibit low glass transitions, -20 °C and -11 °C, respectively (Table 3), whereas all substituted polymers displayed increased  $T_g$ s. The transition of **p-BU-CN** was around 35 °C, while **p-BSU-CN** and **p-BSSU-CN** presented transitions near room temperature.

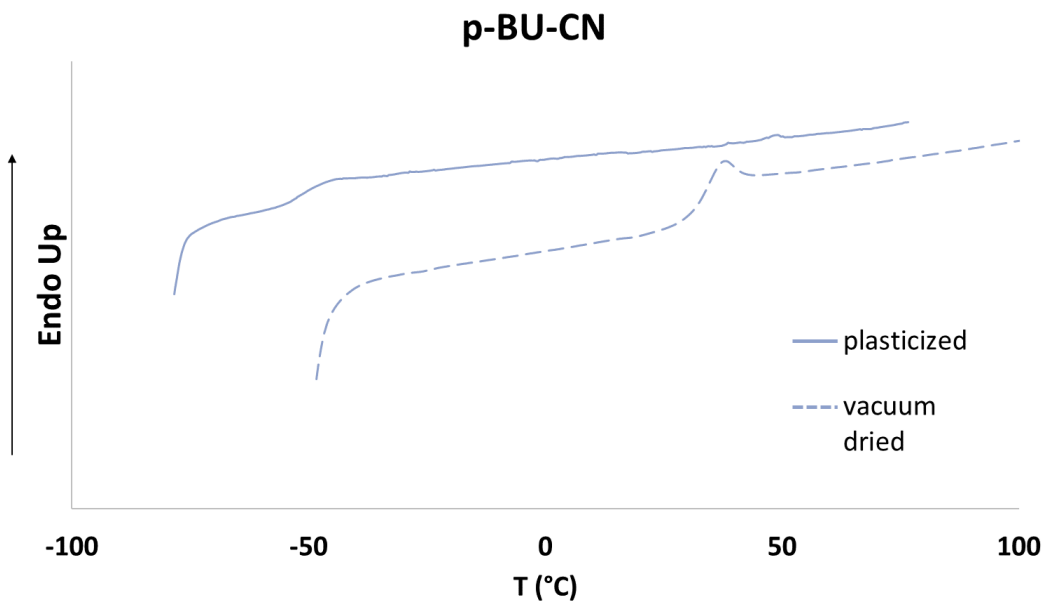


Figure 29: The DSC thermograms of the  $T_g$  for **p-BU-CN** when a sample is vacuum dried (dashed curve) compared to when a sample has toluene added (solid curve) to induce plasticization, at a heating rate of 10 °C/min under nitrogen.

As they are relevant to samples used for poling (*vide infra*), the thermal properties of **p-BU-CN** plasticized by toluene were also measured by DSC (Figure 29). Plasticization was accomplished by ensuring that some residual solvent (not quantified but similar to films used later) was present in the films made. As expected, the presence of the toluene decreased the  $T_g$  significantly, from 35 °C for a vacuum dried sample of **p-BU-CN** to -50 °C when toluene was added.

### 2.4.3 Broadband Dielectric Spectroscopy

Relative permittivity, which is a measure of the ability of a material to polarize in response to an applied field<sup>2</sup>, is related to the total polarization in a system. While there are several modes of polarization, much of the work reported is focused on improving orientational polarization. This mode can have the greatest impact on permittivity because it is the most responsive to an applied field, aside from electronic polarization. Electronic polarization is limited<sup>82</sup> in how much it can be improved because as the band gap decreases, it becomes more likely that a material will conduct electricity. Orientational polarization is relatively easily manipulated through inclusion of components with high dipole moments, increasing the number of these dipoles present, or influencing their ability to align with an applied field.

The dielectric polymers designed here are an attempt to improve on polymeric systems reported in the literature, the vast majority of which exhibit low relative permittivities, between 2-5<sup>33, 83-86</sup>. There are some examples of higher permittivities ranging from 7.1-21.3<sup>73, 83, 87-90</sup> that have been reported, although they are relatively rare. To understand how well our design compares with previously prepared polymers, the frequency and temperature dependent dielectric properties of our materials were evaluated through broadband spectroscopy.

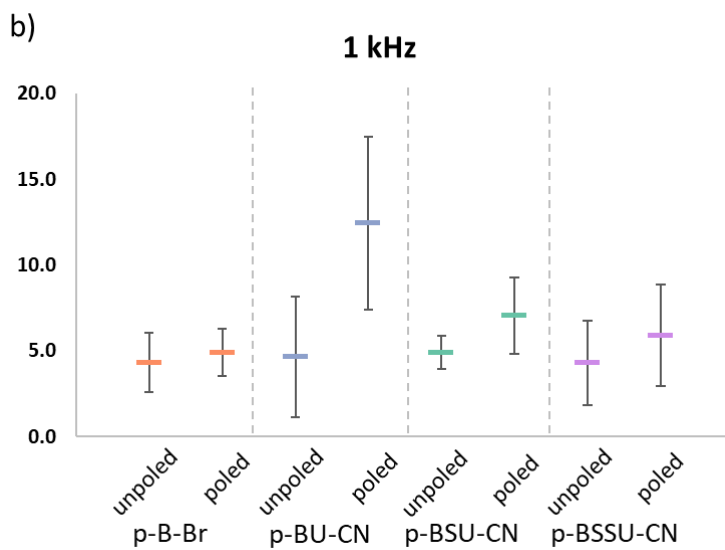
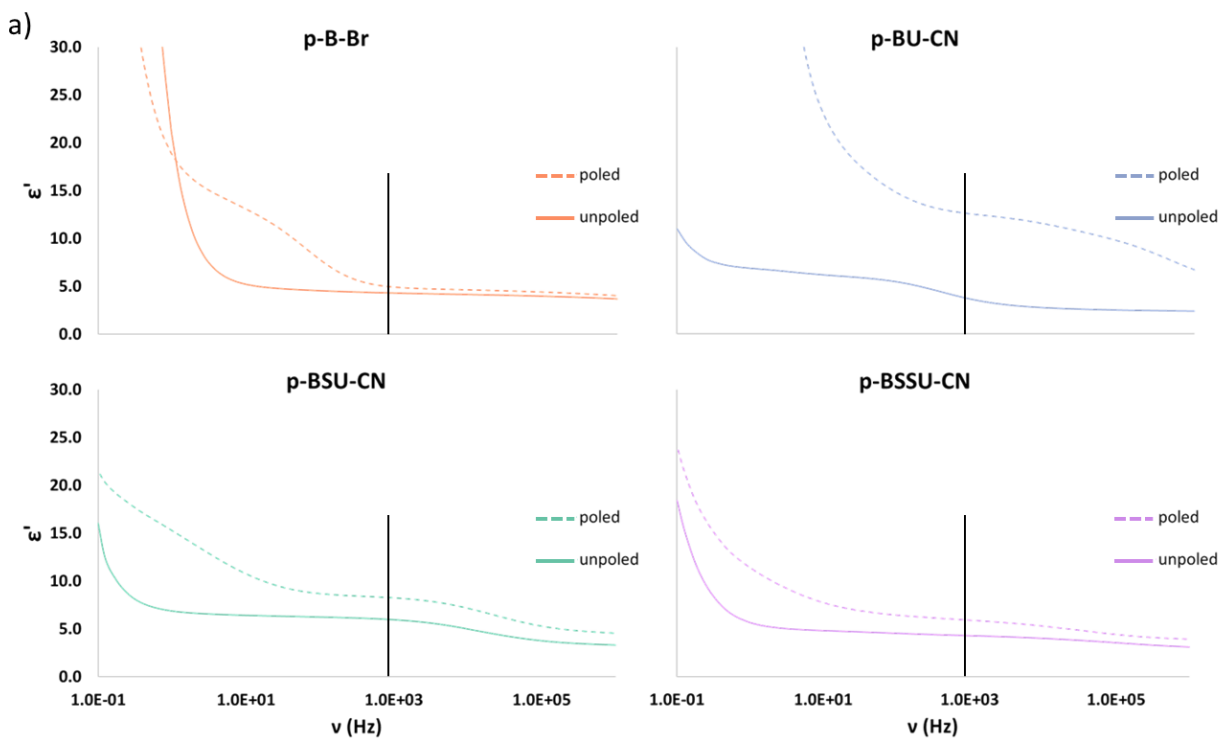


Figure 30: Frequency dependent permittivity for each of the unpoled and poled polymers, (a) spectral overlay of the average permittivity for the unpoled and poled samples measured at 20 °C. The vertical lines on the spectra are placed at 1 kHz and correspond to the boxes in the chart in b. (b) the average and range for the unpoled and poled polymers extracted from the spectra in a, measured at 1 kHz and 20 °C.

Films plasticized by included solvent exhibited sufficient mobility for the polarization processes to respond to an applied oscillating field, at a 1 V potential (Figure 30 and Appendix



Figure 2). The unpoled polymers (solid curves) exhibited permittivities ranging between 4.3 and 4.9 at 1 kHz and 20 °C (Figure 30b and Appendix Table 1), which is around the maximum reported for the typical aliphatic polymer, but there was no apparent trend in the  $\epsilon'$  among the four different materials.<sup>28, 83, 87</sup> The poled samples (dashed curves), however, exhibited a range of behaviors. The backbone polymer **p-B-Br** (orange spectra), which did not have a side chain, exhibited the smallest increase in permittivity to about from 4.3 to 4.9. The poly-dimer, **p-BU-CN**, with the shortest side chain, demonstrated the greatest increase to approximately 12.4 from 4.6. Interestingly, the materials with longer side chains did not exhibit the same degree of enhanced permittivity: **p-BSU-CN**  $\epsilon'$  increased from 4.9 to 7.1 and **p-BSSU-CN**  $\epsilon'$  from 4.3 to 5.9. It can be clearly seen in Figure 30b that poling was most effective for **p-BU-CN** (blue). For all samples there was a gradual increase in permittivity as the frequency of the applied field decreased.

As the most extensively tested system, **p-BU-CN** exhibited more variability in its results than all others synthesized here (Appendix Figure 3). Disparities between batches, such as a difference in molecular weight that would alter the amount of free volume present, are likely major contributing factors in its variability. Although there was a consistent amount of solvent added to make the deposition solution, minor discrepancies in viscosity (not visible by the naked eye) also contributed to the variability. A change in viscosity would have altered the rate of diffusion and evaporation during the initial drying step causing some films to be more plasticized than others.

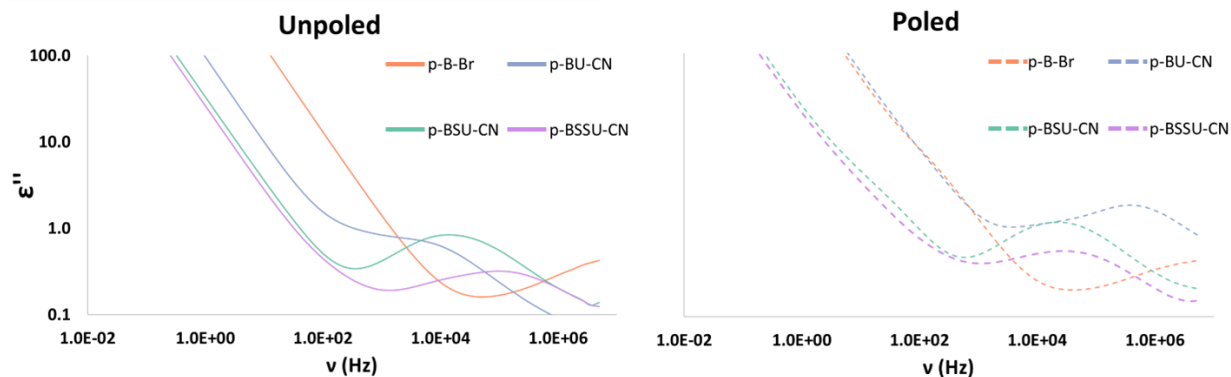


Figure 31: Dielectric loss as a function of frequency for unpoled (right) and poled (left) polymers, measured at 20 °C.

The frequency dependent relaxation process were the same for all the polymers, as evidenced by the similar shape of the spectra (Figure 31, Appendix Figure 6, Appendix Figure 7, Appendix Figure 12, and Appendix Table 2), and the slope of these spectra at frequencies below this relaxation was an indication of contributions from conduction processes. Poling does not fundamentally change this relaxation but does shift the relaxation frequency and intensity. For the unpoled polymers (left), this relaxation shifted to higher frequencies as the side chain length increased (Appendix Figure 4). Polymers **p-BSU-CN** and **p-BSSU-CN** displayed a maximum energy dissipation of around 15 kHz and 100 kHz, respectively, while the dissipation for **p-B-Br** approached a maximum at the end of the measurement regime, 1 MHz and **p-BU-CN** exhibited more of a transition in its dissipation near 10 kHz. Poling increased the dielectric loss for all polymers (right) and here **p-BU-CN** did display a maximum. Interestingly, the overall trend was the reverse of that for the unpoled samples; that is, the maximum loss shifted toward lower frequencies as the side chain length increased.

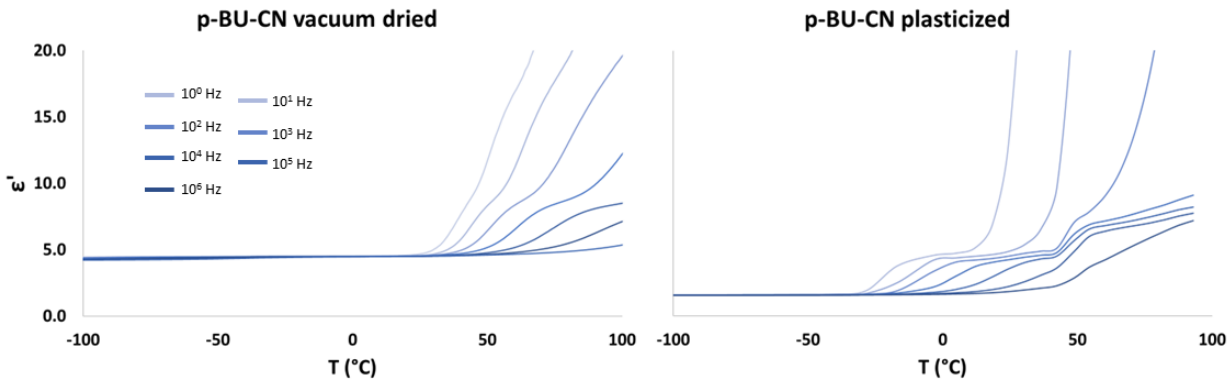


Figure 32: The effect of plasticization on the permittivity of **p-BU-CN** as a function of temperature at different frequencies, ranging from 1 Hz (lightest blue) to 1 MHz (darkest blue), when a sample is vacuum dried (left) compared to when a sample has toluene added (right).

Plasticization in the form of a small amount of toluene (~28 wt%), clearly had a significant effect on the temperature dependence of the polarization processes in these polymers. The glass transition temperature, which is correlated with the beginning of large-scale segmental motion in a sample, is evidenced by an increase in the measured permittivity as the temperature increases. For dried **p-BU-CN**, this increase in motion was observed at about 30 °C (Figure 32, left), slightly below the  $T_g$  found by DSC (Figure 29 and Table 3). A substantial shift in the  $T_g$ , of nearly -60 °C, was seen when toluene was added (Figure 32, right), to around -30 °C. The observed  $T_g$  was 20 °C warmer than that observed on a similarly prepared sample of **p-BU-CN** by DSC. The disparity is likely due to small deviations in the toluene content of the samples.

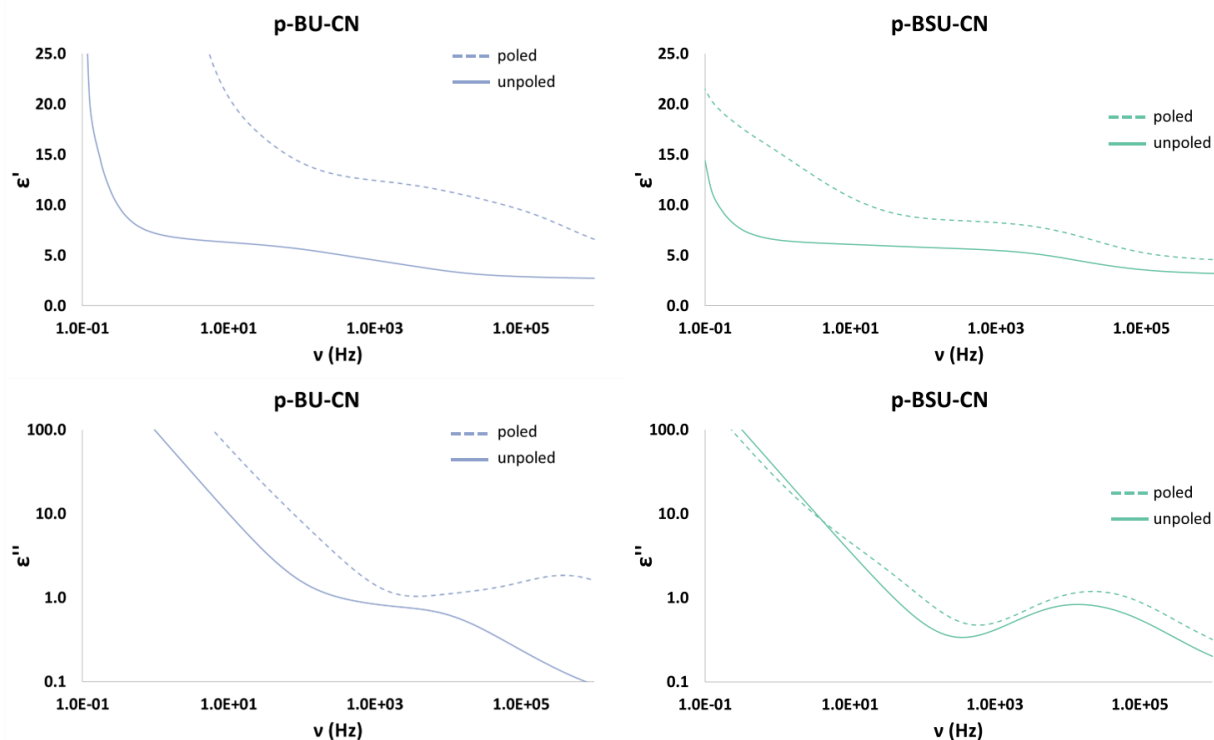


Figure 33: Average permittivity (top) and dielectric loss (bottom) as a function of frequency, measured at 20 °C, for **p-BU-CN** (left) and **p-BSU-CN** (right).

The frequency dependent dielectric data was obtained well above the effective  $T_g$ , yet the rigid nature and size of the dipoles in these polymers limited their motions considerably. In all the  $\epsilon'$  spectra there was a noticeable transition that suggested the presence of a polarization process that became active as the frequency decreased (Figure 33 and Appendix Figure 4). For the unpoled polymers, this process shifted toward higher frequencies as the side chain length increased. However, for the poled samples, there was no obvious trend for activation of this polarization response. For **p-BU-CN** (left), poling resulted in a sizeable shift in this process toward higher frequencies, whereas for **p-BSU-CN** (right), this process exhibited a modest shift toward higher frequencies. As expected, the dispersion peaks observed in  $\epsilon''$  revealed that the corresponding maximum losses for each polymer coincided with the polarization response in  $\epsilon'$ . It is well documented that an increase in permittivity is correlated with an increase in dielectric loss

(Appendix Figure 8), and this was observed for the substituted polymers; however, the loss observed for **p-B-Br** was relatively unchanged.<sup>87, 91</sup>

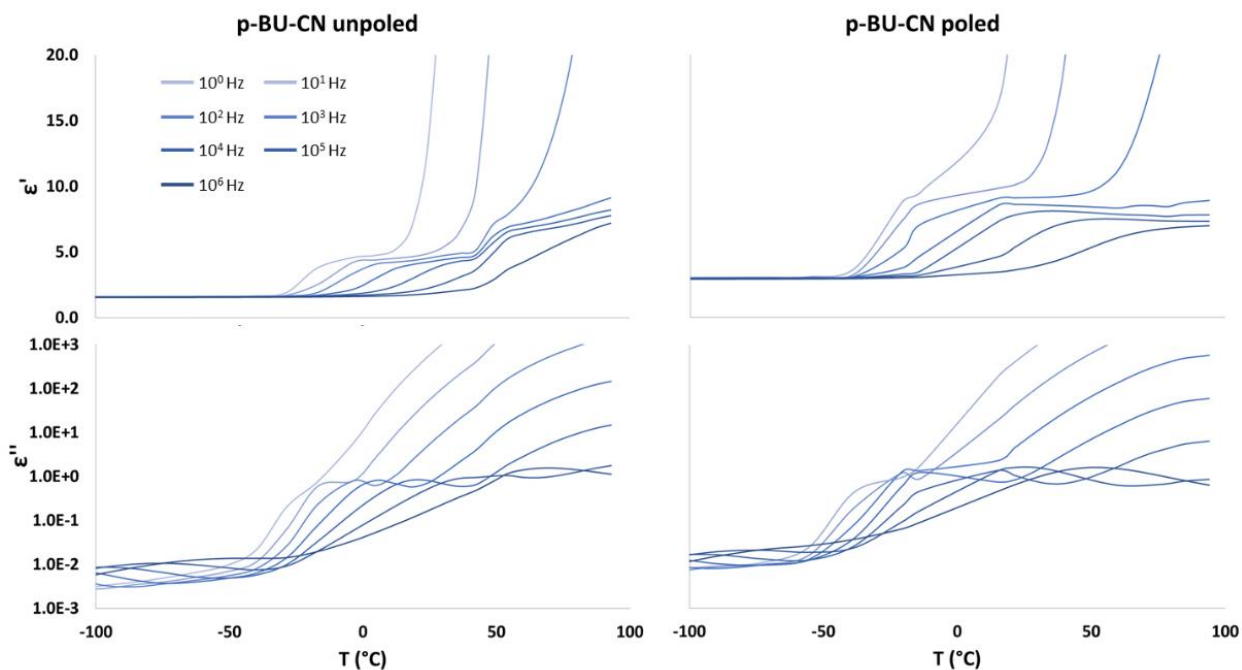


Figure 34: Permittivity (top) and dielectric loss (bottom) of unpoled (left) and poled (right) **p-BU-CN** as a function of temperature at frequencies from 1 Hz to 1 MHz.

The temperature dependence of the transitions for the unpoled and poled samples (Figure 34 and Appendix Figure 9) demonstrated the expected shift toward higher temperatures at higher frequencies.<sup>92</sup> Polymer **p-BU-CN** exhibited two main transitions in permittivity, and poling resulted in an increase in permittivity in the corresponding isochronal spectra as well as an overall shift of the transitions toward lower temperatures. While this trend was also seen for polymers **p-BSU-CN** and **p-BSSU-CN**, poling of **p-B-Br** resulted in a shift toward higher temperatures. It was observed that the polarization processes were activated at a much lower temperature for **p-B-Br** than for the substituted polymers. Polymer **p-BSSU-CN** required the highest temperature to activate these same processes, while activation for **p-BU-CN** and **p-BSU-CN** was approximately the same temperature. Although the activation temperature for **p-B-Br**, after poling, shifted

opposite to that observed for the substituted polymers, the overall trend in activation temperature from unsubstituted to the longest side chain holds.

All polymers exhibited three different relaxations (Figure 34 and Appendix Figure 10). The transition at the lowest temperatures, often referred to as a sub- $T_g$  transition or  $\gamma$ -transition, varied greatly between the samples and did not show an obvious trend within the measured temperature range. This is the region in which very small molecular motions can occur, and Wei et.al attributed these relaxations to rotations of the sulfonyl groups in side chains in a polymer they designed for high permittivities.<sup>28</sup> The main relaxation exhibited by all polymers shifted to higher temperatures and broadened with increasing frequency. These relaxations have been referred to as a  $\beta$  or  $\alpha'$  transition and were reported by Huang et.al as the region where precursor motions to the  $\alpha$  transition occur.<sup>91</sup> The relaxation at high temperatures was well above the effective  $T_g$ , and therefore, related to large-scale segmental motions.

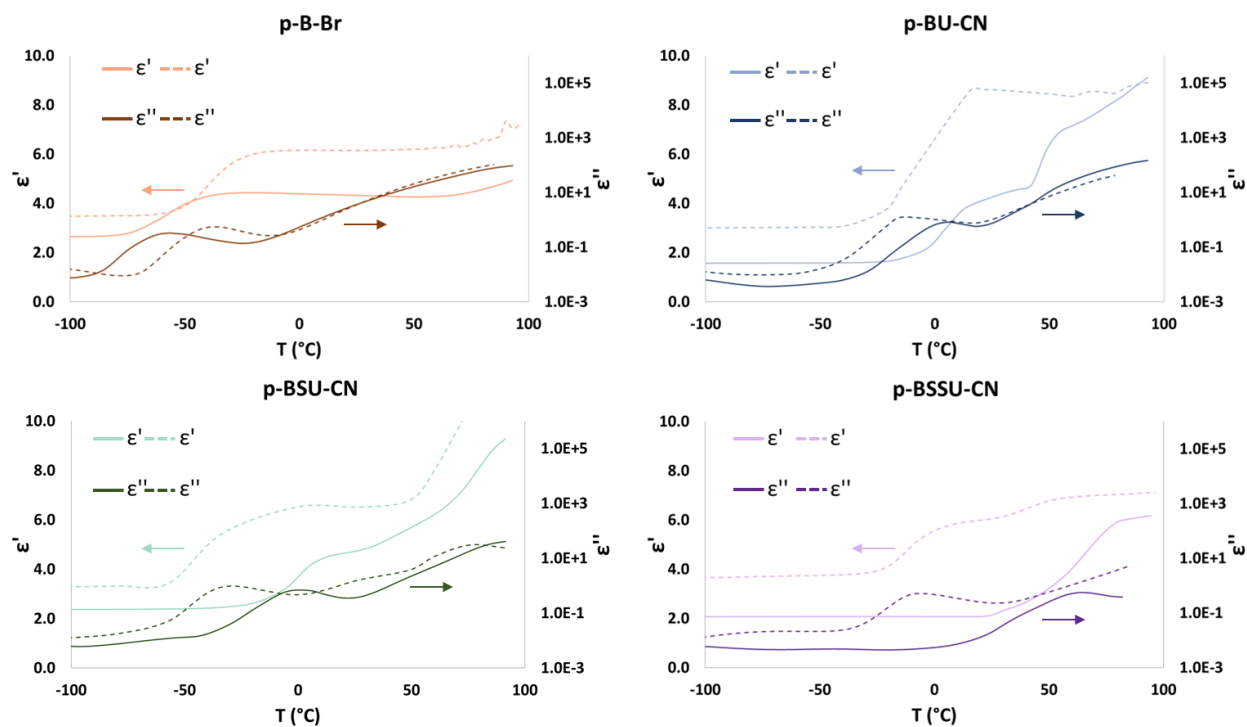


Figure 35: Permittivity and dielectric loss as a function of temperature for all of the unpoled and poled polymers at 1 kHz.

The temperature dependent permittivities of the poled samples were larger than their corresponding unpoled permittivities at 1 kHz (Figure 35 and Appendix Figure 11), but there was no clear trend in the permittivity of the polymers within the unpoled or poled populations. Unpoled and poled **p-B-Br** each exhibited one major transition at very low temperatures, and poling resulted in a shift of this transition to a slightly higher temperature. The unpoled substituted polymers showed one or more transitions that were shifted to significantly higher temperatures than those for **p-B-Br**, but there was no apparent correlation with the side chain length. As with the unpoled substituted polymers, the poled samples did not show a correlation of side chain length to the temperature at which polarization began. Interestingly, the onset of polarization for poled **p-BSU-CN** is at approximately the same temperature as that for poled **p-B-Br**. This transition for **p-BSU-CN** was uniquely broad, which indicated that there may be overlap of polarization processes.

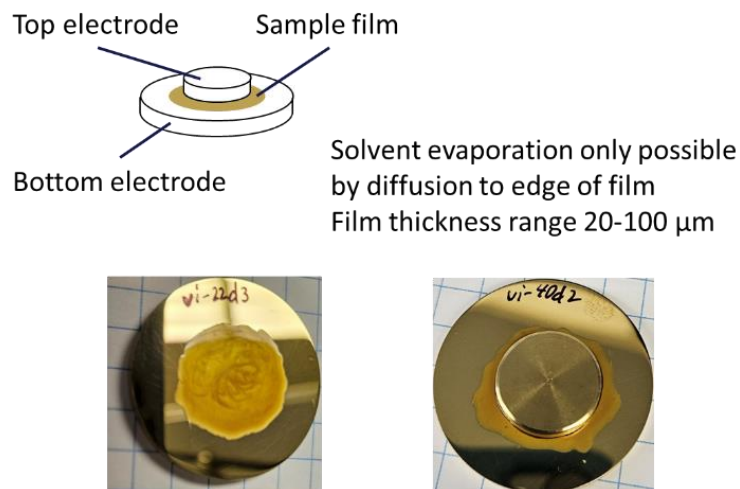


Figure 36: Diagram depicting sample capacitor.

As sample preparation was determined to be imperative to obtain good dielectric data, extensive experimentation was performed to develop the film preparation and poling procedure. Polymer **p-BU-CN**, which has the shortest side chain, was exploited as the model polymer, because it was expected that the side chain might significantly change the behavior of the system toward poling. To ensure that the dielectric spectroscopic results were due to the polymers and not an effect of residual solvent, the films were initially formed by deposition from chlorobenzene onto the large brass electrode (Figure 36). These films were allowed to dry overnight, followed by vacuum drying for 24 hours at room temperature. Once dried, a hot press was used to affix the small electrode, with minimal force at approximately 100 °C for 5 to 15 minutes, to complete the capacitor setup.



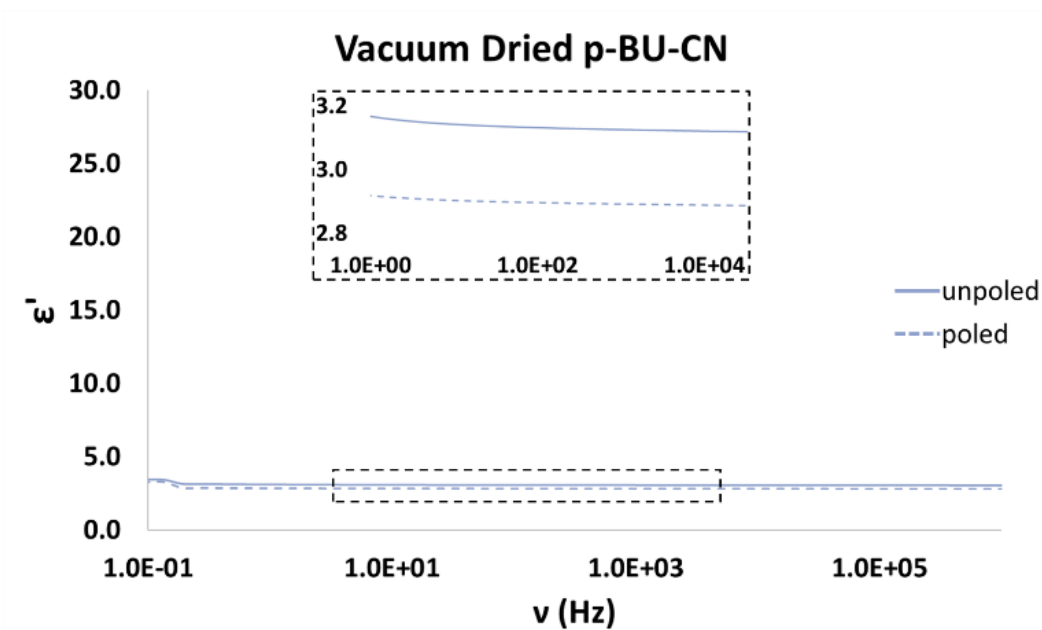


Figure 37: Permittivity of vacuum dried **p-BU-CN** for the average of the unpoled (solid curves) and poled (dashed curves) samples measured at 20 °C.

It is well-known that the force of an applied field causes dipoles to move and orient with that field and that BDS elucidates the frequencies at which these polarization and relaxation processes occur. These processes are seen as increases, or transitions, in the measured  $\epsilon'$  of a system as the frequency of the applied field decreased. Unpoled, vacuum dried **p-B-Br** revealed a distinct transition around 20 kHz and 0.2 Hz (Appendix Figure 1), whereas unpoled and poled, vacuum dried **p-BU-CN** both displayed flat, featureless spectra (Figure 37). Additionally, the permittivity for poled, vacuum dried **p-BU-CN** was below that found for the unpoled, vacuum dried films. The absence of polarization processes and lack of enhancement in  $\epsilon'$  after poling for vacuum dried **p-BU-CN** implied that once a side chain was introduced the mobility of the polymer's dipoles were severely hindered.

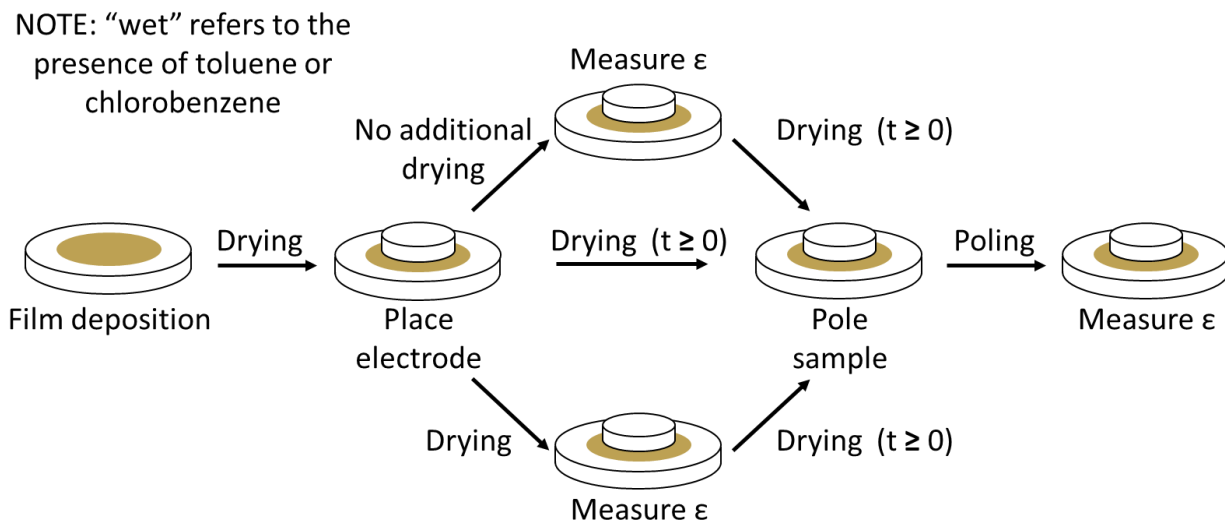


Figure 38: Diagram depicting the film casting and capacitor preparation procedure.

To increase the mobility of the polymers, the film preparation was altered to leave a small amount of solvent within the film, thus providing the required free volume (Figure 38). After deposition, the film was allowed to dry for twenty minutes to three hours before placing the small electrode on top of the film. Drying was continued overnight, a secondary drying step to ‘set’ the top electrode, before the dielectric response was measured, or the sample was introduced to the poling field. Despite this drying time, the samples between the electrodes retained solvent, thereby remaining plasticized, as was confirmed by  $^1\text{H}$  NMR of samples subjected to these conditions.

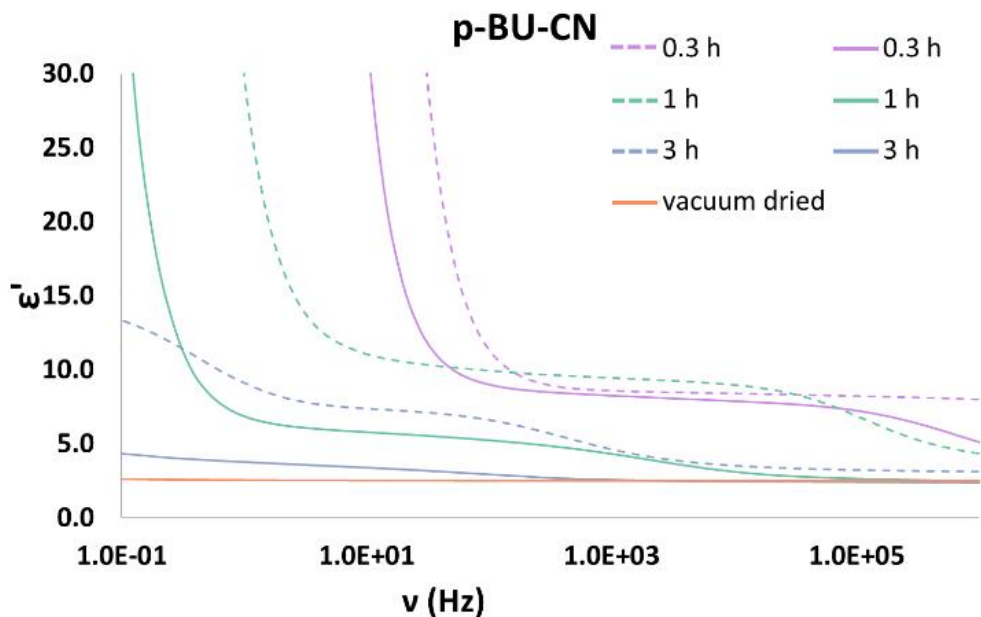


Figure 39: Permittivity, as a function of frequency, of **p-BU-CN** samples with varied initial drying times (time before placing the top electrode), measured at 20 °C. Samples represented by solid curves received additional drying time after placing the top electrode ( $t \geq 12$  h) before measuring permittivity. The samples represented by dashed curves were measured within an hour of placing the top electrode.

The permittivities of these ‘wet’ samples clearly increased with decreasing frequency (Figure 39) and demonstrated plasticization was undoubtedly necessary for the polarization mechanisms to respond to the applied field. Samples that were measured without additional drying time (dashed curves) showed increased permittivity compared to their drier counterparts (solid curves). The samples with the shortest initial drying time (purple curves), about 0.3 hours, overall showed greater polarization than the longer initial drying times. Although three hours of initial drying time indicated some effect on polarization response, due to the variation seen in the results from sample to sample, some three-hour samples showed no capacity for poling (Appendix Figure 5 and Appendix Figure 3). There was a tendency for the top electrode to slide when the film was too wet. Moreover, placement of the top electrode when the toluene content was too high compressed the samples to the point that the electrodes touched as evidenced by significant

conduction. Based on many trials, the optimal drying time for these samples was found to be 1 hour, and the second stage of drying was essential for optimum sample performance.

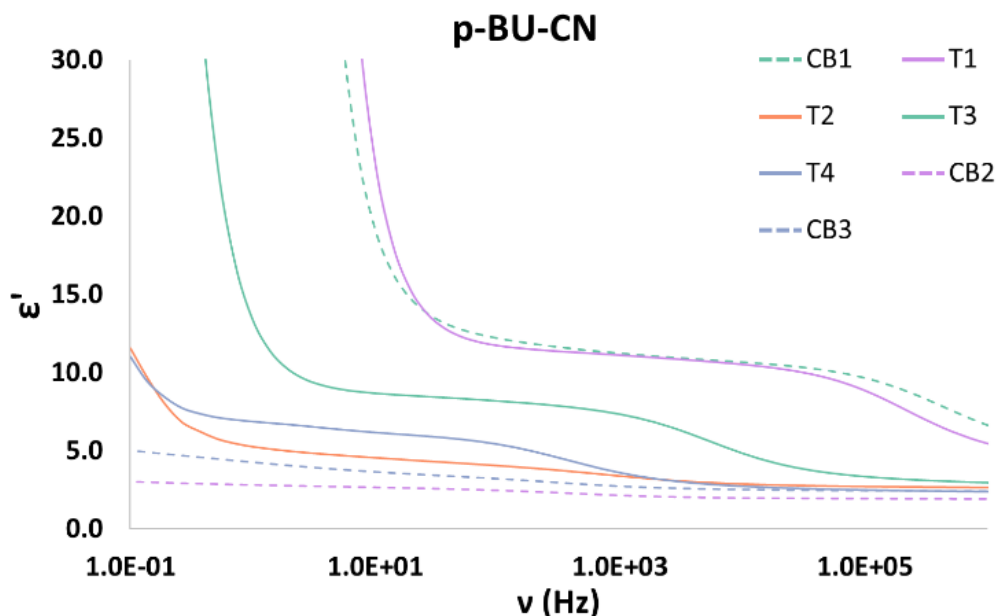


Figure 40: Permittivity, as a function of frequency, of **p-BU-CN** samples with either toluene (solid curves) or chlorobenzene (dashed curves), measured at 20 °C. The samples prepared with toluene are labeled **T1-T4** and the samples prepared with chlorobenzene are labeled **CB1-CB3**.

In addition to determining the minimum amount of solvent required for the polarization processes to be observed, the effect of the type of solvent on the response of unpoled **p-BU-CN** was investigated and revealed that there was not a meaningful difference between the solvents studied. The chlorobenzene samples (Figure 40 dashed curves, **CB1-CB3**) were allowed to dry for two hours before placement of the top electrode and were measured one day after film deposition. The toluene samples (solid curves, **T1-T4**) were permitted to dry for one or three hours before placement of the top electrode and these spectra were obtained between one and eight days after film deposition. If the solvent contributed significantly to the measured responses, it would be expected that the response for all chlorobenzene samples would be larger than that for the toluene samples. Samples **CB1-CB3** had the same preparation, but **CB2** and **CB3** showed a significantly

smaller response than **CB1**. Samples **T1** and **CB1** were each measured one day after deposition, but **T1** only dried for one hour, while **CB1** dried for two hours yet these samples displayed very similar responses. Samples **T1-T3** had the same preparation, but each exhibited a different response. Interestingly, **T3** dried an additional week after placing the top electrode compared to one day for both **T1** and **T2**, but its response was greater than **T2** and less than **T1**. Sample **T4** dried for three hours while **CB2** and **CB3** only dried for one hour, but **T4**, which was less plasticized, exhibited a greater response than **CB2** and **CB3**. These results demonstrated that there were no significant differences in the response of the polymers due to chlorobenzene or toluene; therefore, due to its ease of removal, toluene was utilized in the final procedure.

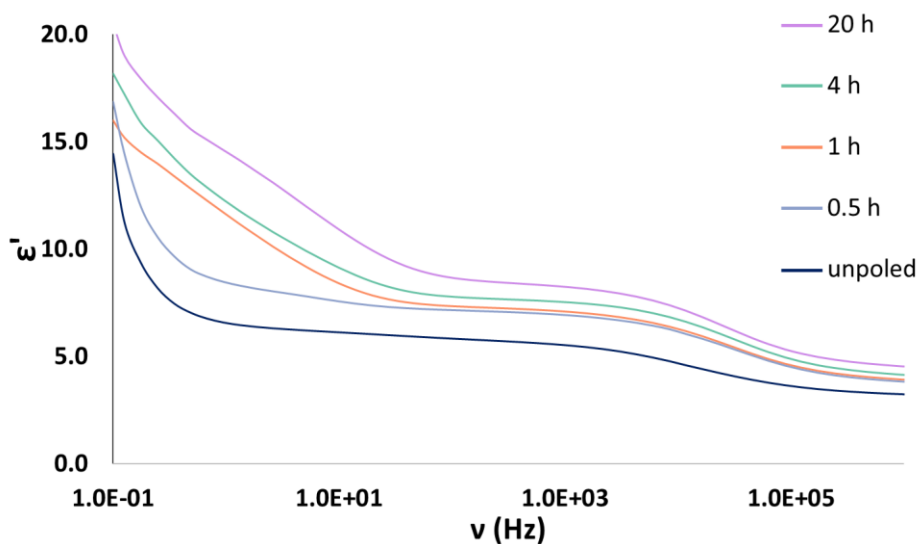


Figure 41: Cumulative poling of one **p-BSU-CN** sample, measured at 20 °C.

To better understand how poling affected a given film, to explore whether repeated exposure increased the polarization of the system, and to determine how much exposure was required to acquire the maximum potential polarization, consecutive incremental poling was performed (Figure 41). The average of the unpoled **p-BSU-CN** samples is used as the baseline (dark blue curve) which showed a permittivity of 3.21 at 1 MHz that increased, as the frequency

decreased, to 5.49 at 1 kHz and 6.57 at 1 Hz (Table 4). A new **p-BSU-CN** sample was placed under a static 15 V potential for a designated amount of time; upon removal from the poling field the dielectric spectrum was recorded and then the sample was quickly returned to the poling field. After 30 minutes of poling, there was an increase in permittivity to 6.9 at 1 kHz and 8.5 at 1 Hz. Each additional poling showed modest increases compared to the previous length of poling, such that after four hours the permittivity was 7.5 at 1 kHz and 12.3 at 1 Hz. Compared to the results at four hours, the moderate increase at 20 hours to 8.2 at 1 kHz and 14.6 at 1 Hz suggested that the sample had approached its maximum polarization.

Table 4: Permittivities for the cumulative poling of sample **p-BSU-CN** at 20 °C

<b>Poling time (h)</b>	<b>1 MHz</b>	<b>100 kHz</b>	<b>1 kHz</b>	<b>1 Hz</b>
<b>0<sup>a</sup></b>	3.21	3.54	5.49	6.57
<b>0.5</b>	3.81	4.38	6.90	8.46
<b>1</b>	3.90	4.47	7.06	11.7
<b>4</b>	4.12	4.75	7.51	12.3
<b>20</b>	4.51	5.11	8.21	14.6

<sup>a</sup>For the unpoled entry the average values from all samples measured were used

## 2.5 Discussion

### 2.5.1 Synthesis

There is much interest in precise polymers<sup>93</sup> for dielectric applications, as defects readily affect the resulting properties. The synthetic strategy applied here was based on a post-

polymerization functionalization method and successfully addressed the concern of exact features in repeat units, which are delineated in Figure 21 through Figure 25. The initial strategy for building the side chains was to exploit the orthogonal protection groups, diethyltriazene and trimethylsilyl, employed by the Moore<sup>94</sup> and Tour<sup>95-98</sup> groups. This convergent synthetic route would allow for differential<sup>99</sup> and incremental increases in the side chain length, and provide the potential to incorporate controlled sequences. The final strategy applied in this work exploited trimethylsilyl as the only protecting group.

Several lessons were learned in the course of developing the synthetic conditions used. The demethylation reaction, carried out at -78 °C, was prone to freezing at the concentrations reported in the literature, and it was found that at a 3-fold dilution the reaction mixture stirred freely<sup>77-80</sup>. These reported procedures used 4.5-6 equivalents of Br<sup>-</sup> per methoxy group, whereas this work established that 2.9 equivalents were sufficient for complete methyl removal. Despite this sizeable reduction in boron tribromide, residual bromine by-products persisted and were not readily removed by washing with sodium thiosulfate solution. Alkylation of diol **6** under the traditional Williamson ether conditions<sup>80, 100</sup>, and variations thereof, resulted in yields less than 50%. However, when the biphasic conditions reported by the Meyer group<sup>56</sup> were employed, the reactions gave yields ranging from 72-90%, with nearly quantitative di-substitution of diol **6**.

We also determined that stirring of an ADMET polymerization reaction was critical to achieve suitable molecular weights. The viscosity of the reaction mixture increased rapidly as  $M_n$  increased and formed a thick rubbery layer on top. This rubbery layer was insoluble, in chloroform or THF, suggesting very high molecular weights and possible crosslinking. The mixture below it was quite fluid indicating the presence of a mostly oligomeric species and implied that the rubbery layer impeded the removal of the ethylene formed. It was discovered that magnetic stirring was

ineffective after only one day, but the rubbery layer could be prevented by manual stirring once daily.

The substituted **PhE** segment **5**, outlined in Figure 22, was found to be essential for side chain extension. Long conjugated species are known to be difficult to solubilize and this was addressed through the alkylation of bromohydroquinone with bromohexane, a linear aliphatic chain, resulting in dialkoxy arene **2**. An alkyne is required to extend conjugation and for ease of linking the phenyl segments. Synthesis of monoalkynylated intermediate **4** was originally attempted from 1,4-dibromohydroquinone; however, a single addition of TMSA to alkylated dibromo species was difficult to achieve and separation of **4** from the di and unsubstituted species was only moderately successful. It was discovered that when palladium-catalyzed coupling of TMSA was performed with bromo-iodo arene **3**, the reaction yielded almost exclusively monoalkynylated bromo-arene **4**.

We learned that certain couplings required iodo arene substitution rather than bromo. The coupling of bromo-arene **4** with a terminal aryl-alkyne lead to exceedingly poor yields, but once a bromo-iodo exchange was carried out to transform arene **4** into TMS protected iodo-arene **5**, the yields of the coupling reactions improved dramatically. The success of the bromo-iodo exchange was highly dependent upon the order of addition. It was observed that when the iodine/THF solution was added to the lithiated solution, no iodo product was formed. However, when the addition was reversed, iodo-arene **5** was obtained. This reaction was also very sensitive to any exposure to air, and, despite employing good air-free techniques, the amount of reduced material formed could not be decreased below 10%.

Solvent choice was crucial in optimizing the yields of the couplings. When the orthogonal protecting group triazene was a main component of the synthetic route, methods employed by the



Moore group<sup>94</sup>, and frequently utilized in the literature, were applied to build the series of side chains. In these methods, triethylamine (TEA) was used as the sole solvent and base, but the coupling resulted in only moderate yields. However, when THF was added as a cosolvent, based on work conducted by the Tour group<sup>74, 97, 101-103</sup>, yields improved substantially.

We learned that a simple change in protecting groups can have a considerable impact on the solvent required for successful couplings. The synthetic route for building the side chains was redesigned to include TMS as the only protecting group. Based on the polymer coupling procedure at the time, when bromo-arene **4** was coupled to **H-U-CN** in a toluene (PhMe) and TEA system, yields once again were quite poor. Since THF/TEA had worked so well with the triazene structures, it seemed logical that it would also work well with the TMS structures, but surprisingly the yield decreased compared to that of the PhMe/TEA system. Recognizing the apparent difference in reactivities between the triazene and TMS moieties, coupling was again attempted in TEA, but with iodo-arene **5** and **H-U-CN** and proved successful with yields greater than 84%. Whether this is a function of the difference in the protecting groups or simply due to the transition to iodine as the aryl-halide is unclear.

We determined that a change in the base used for the polymer-side chain couplings drastically reduced reaction times and polymer cleavage. Sonogashira couplings are commonly performed using TEA as the sole solvent; however, **p-B-Br/I** was not sufficiently soluble, therefore a 1:1 mixture of PhMe:TEA was used (Figure 24). This large excess of base did not sequester the hydroiodic (or hydrobromic) acid byproduct, but instead the PhMe:TEA mixture likely caused some aggregation of the chains, thereby excluding the base from the site of HI (or HBr) formation. It was determined that the acid byproduct cleaved the polymer backbone at the  $sp^3$  CH<sub>2</sub>-O bonds, and with the exceedingly long reaction times, this cleavage greatly reduced the

molecular weight of the polymers. A search of the literature revealed piperidine as an alternative, and when utilized as the base and cosolvent, the reaction rate increased more than 10-fold; however, the cleavage was still substantial. It was established, through a timed experiment, that cleavage could be minimized by stopping the reaction after about 30 minutes, a nearly 400-fold increase in rate, and substitution remained near-quantitative.

### 2.5.2 Polymer Properties

The molecular weights observed in the SEC traces (Figure 27) of the substituted polymers were not in agreement with the theoretical expectation for the coupling reactions. While the molecular weights for **p-BSU-CN** and **p-BSSU-CN** did increase, the increases were modest, despite the sizeable increase in their repeat unit molecular weight ( $M_{RU}$ ) compared to that of **p-B-I**. In contrast, the  $M_{RU}$  for **p-BU-CN** was identical to that of **p-B-I** yet its  $M_n$  decreased after coupling. Although contrary to what was expected, these reduced  $M_n$ s, and corresponding DPs, were in congruence with the polymer cleavage observed during the coupling process. However, the apparent dramatic drop in DP for **p-BSU-CN** and **p-BSSU-CN** can be attributed to the use of a different batch of **p-B-I** as the backbone, whose DP was 42 instead of 54.

Based on the detected cleavage, it would also be expected to find increased polymer dispersities. Although small, this was the result seen for **p-BU-CN** and **p-BSU-CN**. However surprisingly, the  $\bar{D}$  of **p-BSSU-CN** exhibited a slight decrease, which could simply be an indication that this polymer was better purified.

The  $T_g$ s exhibited by **p-B-Br** and **p-B-I** (Figure 28) are congruent with polymers whose compositions are mainly aliphatic and lack a significant side chain structure<sup>92</sup>. The increase observed for each of the substituted polymers is in contradiction to the well-known trend in which

an increase in the side chain length has a plasticizing effect and leads to a decrease in  $T_g$ . However, Bonardd<sup>87</sup>, et al. reported a trend similar to that seen here, where their polyitaconates and polymethacrylates, bearing polar end groups on the side chains, showed an increase in  $T_g$  over variants without polar end groups. Additionally, they saw an increase in  $T_g$  when the end groups were changed from a nitrile to a sulfonyl, an effect also reported by Zhu, et.al.<sup>92</sup>. Bonardd surmised that, as the polarity of a side group increased, there was an increase in dipolar interactions, which would require more energy to disrupt and thereby increase  $T_g$ . Therefore, the contribution of the nitriles to an increase in intermolecular forces could account for the increase in  $T_g$  for the substituted polymers.

With the addition of a side chain, all substituted polymers have extended conjugation which could promote inter- and intramolecular  $\pi$ - $\pi$  stacking. The resulting increase in interactions would require more energy to disrupt and thereby contribute to the increase seen in the  $T_g$ s. Although shortest in length, the side chain of **p-BU-CN** is unique in that it does not contain freely moving alkoxy substituents. Without the hinderance of additional aliphatic material on the side chain,  $\pi$ - $\pi$  stacking may occur more readily and contribute to the large increase in its  $T_g$ .

Despite having an increased conjugation length, which could lead to stronger  $\pi$ - $\pi$  stacking and an increase in  $T_g$ , **p-BSU-CN**, with an additional PhE in the side chain, exhibited a slight decrease in  $T_g$ . There are a few possible competing effects, one of which is the large increase in chain ends with the added alkoxy-substituted PhE segment, which would decrease the  $T_g$ . These freely moving alkoxy chains may inhibit additional  $\pi$ - $\pi$  stacking, thereby preventing a significant increase in intermolecular interactions. As a result of the rigid nature of conjugated aromatic species, chain movement is likely to be more hindered and would cause an increase in  $T_g$ . These factors are also at play with **p-BSSU-CN**, and it was seen that its  $T_g$  was virtually unchanged. It is

likely that the longer rigid side chain has a larger effect on chain entanglement, thereby increasing the  $T_g$  value more than the plasticizing effect from the added length and chain ends.

### 2.5.3 Broadband Dielectric Spectroscopy

All of the polymers achieved high permittivities and aligned in response to poling. These polymers were successfully synthesized with a high coupling rate and reached good molecular weights. Their dielectric properties were investigated by frequency and temperature dependent broadband dielectric spectroscopy. The results are quite promising, as even the unpoled variants exhibited higher permittivities,  $\epsilon' \geq 4.3$  (Appendix Table 1), than the average organic polymer,  $\epsilon' \approx 2-4$ . All the polymers attained improved permittivities through poling, and the top performer, **p-BU-CN**, achieved the highest permittivity of approximately 12.4.

It was established that the mobility of the side chain was the crucial factor in eliciting a polarization response for these polymers. Initial broadband experiments with polymer **p-B-Br** demonstrated that this system exhibited a distinct polarization process in response to the different frequencies applied (Appendix Figure 1: Permittivity, as a function of frequency, of all the vacuum dried samples (blue curves), measured at 20 °C, and the average of each (orange dashed curves); unpoled **p-B-Br** (top), unpoled **p-BU-CN** (bottom left) and poled **p-BU-CN** (bottom right) ). However, surprisingly, when experiments with polymer **p-BU-CN** began, no polarization responses were observed (Figure 37), and the obtained permittivity was lower than that observed with polymer **p-B-Br**. It was thought that plasticization may address the lack of mobility in the side chains, and the DSC experiments revealed that the  $T_g$  of polymer **p-BU-CN** decreased by as much as 85 °C (Figure 29). Additional BDS experiments showed that plasticized **p-BU-CN** exhibited a distinct polarization response and the permittivity increased by  $\Delta\epsilon' \sim 1.5$ , at 20 °C and

1 kHz, compared to the vacuum dried sample (Figure 30 and Appendix Figure 5 ). This demonstrated that plasticization improved the mobility of the side chain thereby allowing observation of the polarization processes of the substituted polymers.

Of all the polymers, **p-BU-CN** exhibited the most desirable properties. The unpoled variant exhibited the greatest increase in permittivity, a  $\Delta\epsilon'$  of approximately 4, in the measured frequency range (Figure 30). Once poled, it outperformed all the polymers studied, with a  $\epsilon'$  of about 12.4 and a  $\Delta\epsilon'$  around 7.8, at 20 °C and 1 kHz. The side chain length clearly represented an optimization of the factors that affect alignment. As it was the shortest side chain, it required the least amount of free volume to rotate; even small movements of the backbone may 'free' a hindered side chain to rotate. Its side chain also lacked the additional alkoxy chains present in the other substituted polymers, which may facilitate  $\pi$ - $\pi$  interactions and therefore increased cooperative motions of the dipoles. These combined effects could be expected to allow the side chain of **p-BU-CN** to align more easily with an applied field, thus improving the  $\epsilon'$  of the system.

It is generally known that, when a side chain is added to a polymer and when the side chain length is increased, there is a corresponding increase in free volume. The observed decrease in the polarization response as the side chain length increased suggested that the increase in free volume was insufficient for the mobility of the longer side chains. Polymer **p-BU-CN** had the smallest side chain; therefore it would have the smallest increase in free volume and would require the least free volume for side chain mobility. There was a large increase in its unpoled and poled permittivity, in the measured frequency range (Figure 30), a  $\Delta\epsilon'$  of approximately 4.0 and 7.0, respectively. This frequency dependent polarization response provides evidence that the increased free volume for **p-BU-CN** was sufficient for the mobility of its side chain. While there was an additional increase in the free volume for **p-BSU-CN** and **p-BSSU-CN**, this increase was likely not proportional to

the amount required for free mobility of the longer side chains. This is evident in the decreasing change in the polarization response with longer side chains. For the unpoled materials, the  $\Delta\epsilon'$  was approximately 3.2 for **p-BSU-CN** and 1.6 for **p-BSSU-CN**, and for the poled materials the  $\Delta\epsilon'$  was approximately 4.0 and 2.4, respectively.

The frequency dependent polarization process displayed by the unpoled substituted polymers may be influenced by aggregation. As noted above, the response of the shortest side chain, **p-BU-CN**, was the largest, but as the side chain length increased, the magnitude of the polarization process decreased. This trend in  $\Delta\epsilon'$  suggested that there is some aggregation of the side chains that decreases with increasing length, which seems counterintuitive. It is generally understood that with a longer conjugated system there is a tendency for more aggregation through  $\pi$ - $\pi$  interactions. However, for **p-BSU-CN** and **p-BSSU-CN**, the phenyl groups employed introduce additional alkoxy side chains. The sequential increase in the aliphatic material connected directly to the conjugated system may incrementally inhibit the aggregation of the side chains. Stronger interactions, such as that suggested for **p-BU-CN**, could induce additional dipole response leading to the large  $\Delta\epsilon'$  observed.

Aggregation may have an impact on the effectiveness of poling the substituted polymers. On the surface, aggregation may appear to hinder the ability of a dipole to orient under the influence of a static field, as it would be expected that an aggregate would need more free volume to orient. However, it is important to note that the static field has a large, applied potential, 15 V, and is applied for an extended period of time, upward of  $7 \times 10^5$  s or more. While the broadband measurements were obtained at a 1 V potential and the slowest frequency measured had a 10 s oscillation. It is also important to bear in mind that these films are poled at RT, which is well above the plasticized  $T_g$ . With the large force applied, the extended time for poling and large segmental

motions possible, aggregated dipoles could be oriented with a static field. As suggested, with increasing side chain length, the amount of aggregation likely decreased, which was correlated with the decreased  $\Delta\epsilon'$  observed for poled polymers. For example, the polymer **p-BU-CN**, with the most aggregation, showed the greatest  $\Delta\epsilon'$ , which may be the result of dipole interactions that facilitate the alignment of nearby dipoles combined with the smaller size of its side chain and overall greater mobility in the polymer. Whereas polymer **p-BSSU-CN**, with the least aggregation and a comparatively reduced overall polymer mobility, showed the smallest  $\Delta\epsilon'$  after poling.

The design goals of high permittivity, easy modification, scalability, and solubility were achieved for this polymer system. The method developed for post-polymerization coupling of the side chains allows for ease of modification and tuning with high fidelity, and the syntheses are easily scalable. The polymer backbone itself is easily modifiable; for example, altering its length or possibly a modification of the alkene provides an avenue for improvement. The film deposition process is simple, and the employment of an aliphatic backbone, instead of a fully conjugated one, provides solubility and improves processability. The high permittivities achieved with this design provides a promising new route toward high dielectric materials.

### 3.0 Phenylene Vinylene Based Polymers.

#### 3.1 Introduction

The original monomer design and synthetic method for these side chain dielectric polymers targeted the well-studied and characterized phenylene vinylene (**PV**) system as the initial side chain components.<sup>56</sup> The bulk properties of a polymer have been shown to be affected by sequence as much as the identities and ratios of monomers. Norris et al. showed that by rigorously controlling their sequence, the bulk optoelectronic properties of the resulting oligomers can be tuned.<sup>54</sup> Furthermore, Zhang et al. reported that sequence plays a key role in inter/intrachain interactions and short-range order. The presence of  $\pi$ -stacking was demonstrated by a different absorption pattern in the solid state for trimers and their corresponding polymers, as well as longer sequences.<sup>55, 57</sup> This project employs these discoveries in the monomer design and incorporates sequences for a tailorable side chain that should aid with orientation.

This work was discontinued after extensive attempts to synthesize these series of polymers in which several different routes were pursued. These methods include polymerizations of monomers with fully synthesized side chains that resulted in short oligomeric species or significant crosslinking, causing them to be insoluble and, therefore, not viable for film preparation. Post polymerization coupling was also attempted; however, as the nitrile monomer was the only species that did not crosslink, conversion of the nitrile to the aldehyde caused significant cleavage of the polymer and incomplete conversion. It was subsequently determined that these **PV** based side



chain polymers were incapable of providing the desired set of polymers, and therefore a new synthetic route was devised.

### **3.2 Project Goals**

The goal of this project is to identify influential monomer parameters, through side chain engineering, for rationally tuning the dielectric properties of this new class of polymers. These studies will address three factors hypothesized to influence the dielectric behavior of the polymers. First, what length of the side chain is required to induce a measurable effect on the dielectric constant? Second, will the sequence of the side chain successfully control the alignment of the side chains, and which sequence produces the greatest dielectric constant? Finally, by varying the substituents incorporated in the side chain, can we tune the dielectric constant of the polymer?

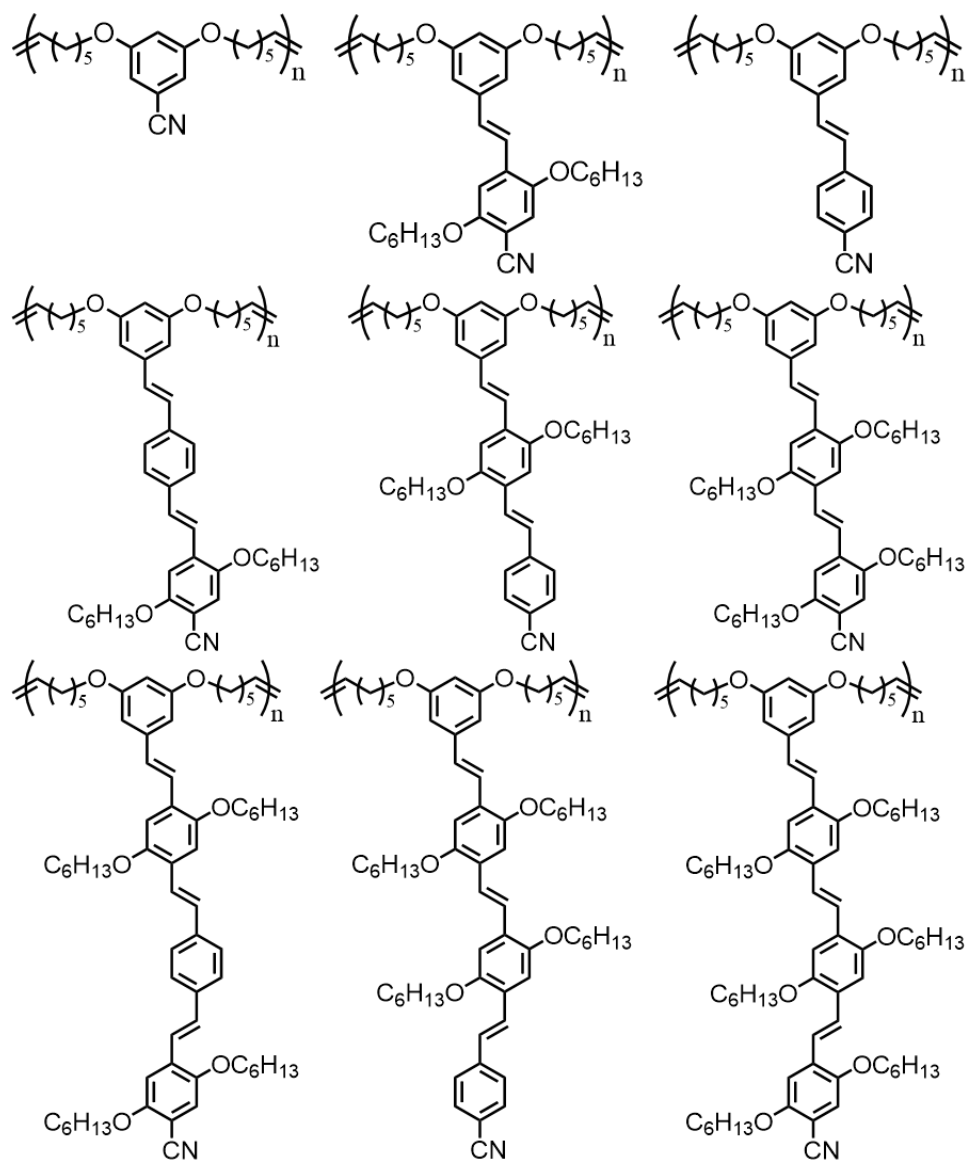


Figure 42: Proposed polymer sequences. Starting from the top left is the base structure, i.e. the backbone or mono-phenylene, continuing with dimers, trimers, and tetramers. The trimers and tetramers have one unsequenced chain and two sequenced chains with the same composition. (note on nomenclature, a dimer, trimer, etc. refers to the number of phenyl groups in the monomer)

A series of systematically sequenced monomers will be synthesized and polymerized based on the well-established phenylene vinylene system. The macromonomers and polymers will be described by the number of phenyl groups in the side chain where the term dimer will refer to a unit bearing two phenyl groups and a trimer with three. The dimer, trimer, tetramer, and pentamer series', depicted in Figure 42 and Figure 43, will each contain one homo-oligomeric side chain as

well as two or three compositionally equivalent side chains. Each of these polymers will also bear a terminal nitrile (or other electron acceptor) functional group to increase the side chain's dipole. This series of polymers will establish what length side chain is required to produce a measurable effect on the dielectric constant, and the isomeric substrates will provide insight into the effect of sequence on the polymeric dielectric properties.

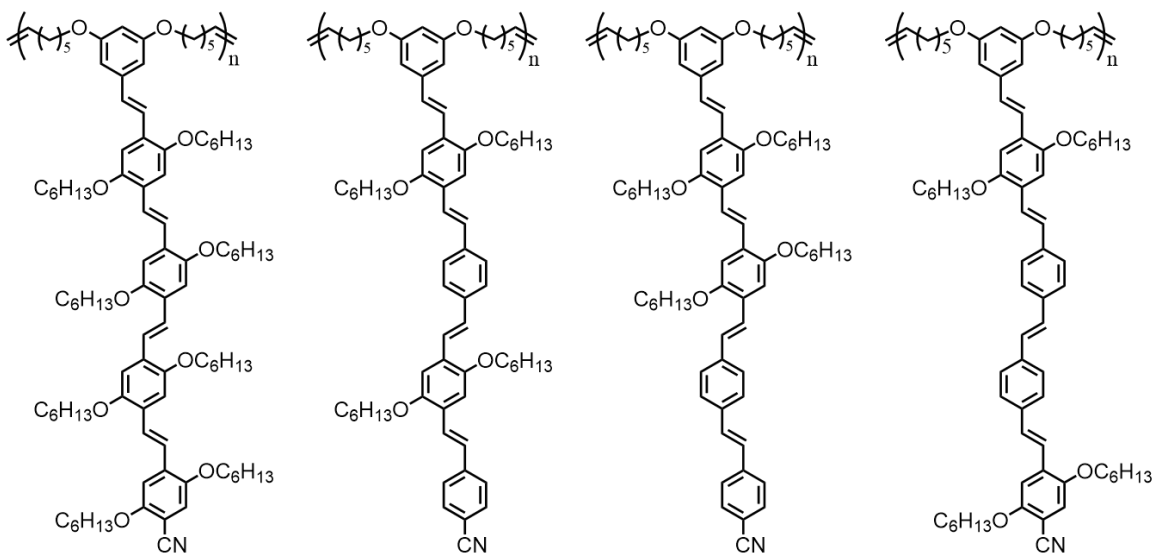


Figure 43: Proposed pentamer sequences have one unsequenced chain and three sequenced chains with the same composition. (note on nomenclature, pentamer refers to the number of phenyl groups in the monomer)

The Meyer and Hutchison collaboration reported the terminal group dramatically changed the optoelectronic properties of the oligomers, accordingly replacement of the terminal nitrile with highly polarizable end groups, depicted in Figure 44 a and b, should increase the side chain's dipole, and provide evidence toward how influential the terminal group is on the dielectric constant. In another study, the collaborators reported the oligomers sequenced with benzothiadiazole showed measurable differences in optoelectronic properties, thus alternative electron donating units (EDU) are being investigated to optimize dielectric properties.<sup>55</sup> Integration of EDUs (Figure 44 c and d) should increase the polarizability of the side chains and demonstrate how the identity of the side chain substituents affect their behavior.

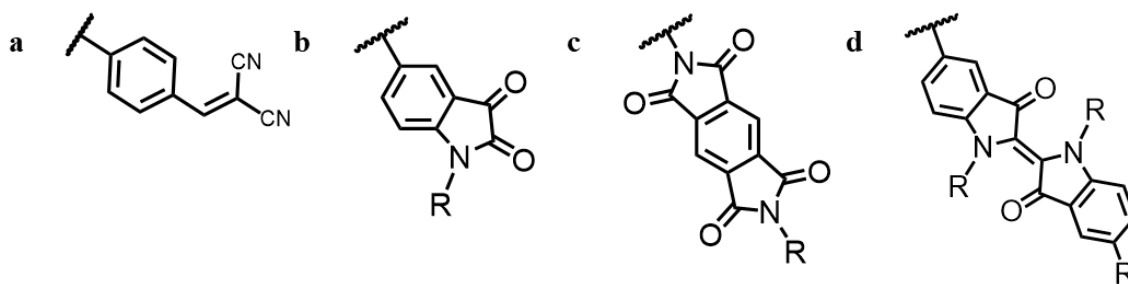


Figure 44: Alternative monomers for increased polarizability of the polymer side chains. (a) and (b) are polarizable end groups; (c) and (d) are electron deficient moieties.

### 3.3 Results

#### 3.3.1 Naming Convention

The following conventions will be employed for naming the prepared compounds (Table 5). The monomers' names consist of the side chain sequence in order from the backbone arene to the terminal functional group in the phenylene side chains.

Table 5: Abbreviations used in naming prepared phenylene vinylene compounds

Symbol	Definition
N	Terminal nitrile group
A	Terminal aldehyde group
O	Dialkoxy-substituted phenylenevinylene
P	Unsubstituted p-phenylenevinylene
B	Backbone moiety, 3,5-bis(hexyloxy)benzene
mono-	Monomer
poly-	Polymer
oligo-	Oligomer

### 3.3.2 Synthesis of Monomers and Their Building Blocks

Macromonomer **mono-B-A**, bearing a single functional aryl group, was synthesized using a modified version of the Williamson ether synthesis (WES) reported by Eggers, et al. (Figure 45).<sup>104</sup> 3,5-Dihydroxybenzonitrile was coupled after deprotonation to 2 equivalents of 7-bromohept-1-ene to give  $\alpha,\omega$ -diene **mono-B-N** in a 94% yield after purification by distillation. Disubstitution of the arene's hydroxyl groups was verified by the integration of the protons on the carbon  $\alpha$  to the oxygen and the absence of hydroxyl protons in the <sup>1</sup>H NMR spectrum. The GCMS chromatogram showed a single peak present, whose parent ion matched the expected molecular weight. The isolated **mono-B-N** was subjected to diisobutylaluminum hydride (DIBAL-H) reduction to give aldehyde-derivative **mono-B-A** in an 87% yield.

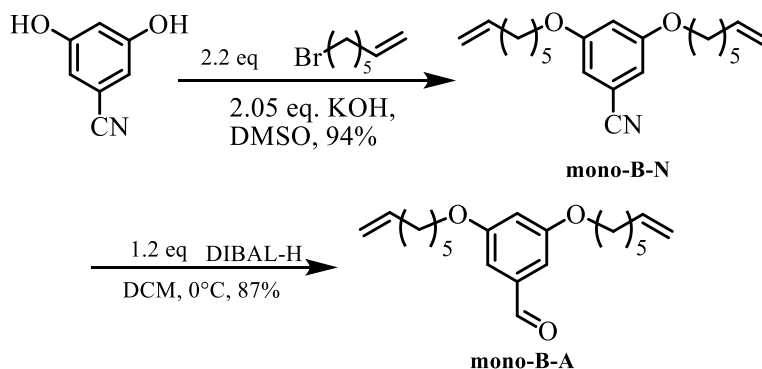


Figure 45: Synthesis of **mono-B-A**.

The greatest yields were obtained when deprotonation of the dihydroxy-arene was allowed to run for 15 h, rather than simultaneous addition of the alkyl halide and phenolic moiety, and vacuum distillation was performed before extraction and washing. In contrast, when Eggers' reported procedure and purification was implemented some mono-substitution occurred, extraction took more than twelve h, and significant losses were seen.

The precursors of the **P** and **O** units, for side chain extension and sequencing, were prepared using the Meyer group's previously reported methodology (Figure 46 and Figure 47, respectively).<sup>54, 56</sup> *p*-Tolunitrile was brominated with N-bromosuccinimide (NBS) and benzoylperoxide (BPO) in dichloroethane (DCE) to give brominated-arene **3** in 97% yield. The brominated-arene was treated with trimethyl phosphite in toluene, and phosphonate **4** was obtained in 64% yield.

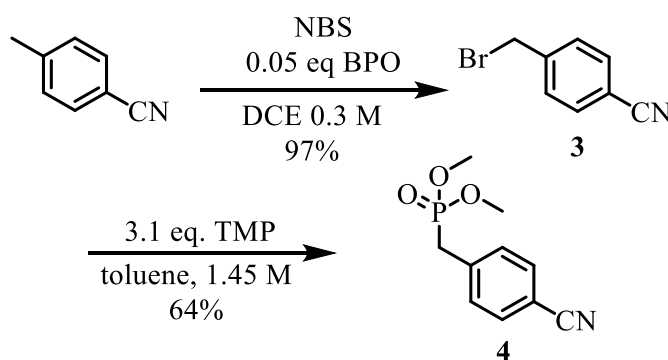


Figure 46: Synthesis of phosphonate **4**.

Dialkoxy-substituted arene **5** was prepared, in 92% yield, from 2-methylhydroquinone with 2 equivalents of 1-bromohexane in the presence of sodium thiosulfate (Figure 47). The isolated material was treated with NBS/BPO in DCE, and after recrystallization from methanol (MeOH), brominated-arene **6** was obtained in 84% yield. Lithium-halogen exchange was performed on brominated-arene **6** using *n*-butyl lithium (<sup>n</sup>BuLi). Formylation with dimethylformamide (DMF) gave aldehyde **7** with yields as high as 99%. The aldehyde-derivative **7** was converted to nitrile **8**, in 84% yield, using hydroxylamine hydrochloride in formic acid. Phosphonate **9** was formed in two steps: 1) the benzylic carbon of the nitrile-derivative **8** was brominated with NBS/BPO in DCE and 2) the isolated intermediate was treated with trimethyl phosphite in toluene, to give the phosphonate **9** in 52% yield.

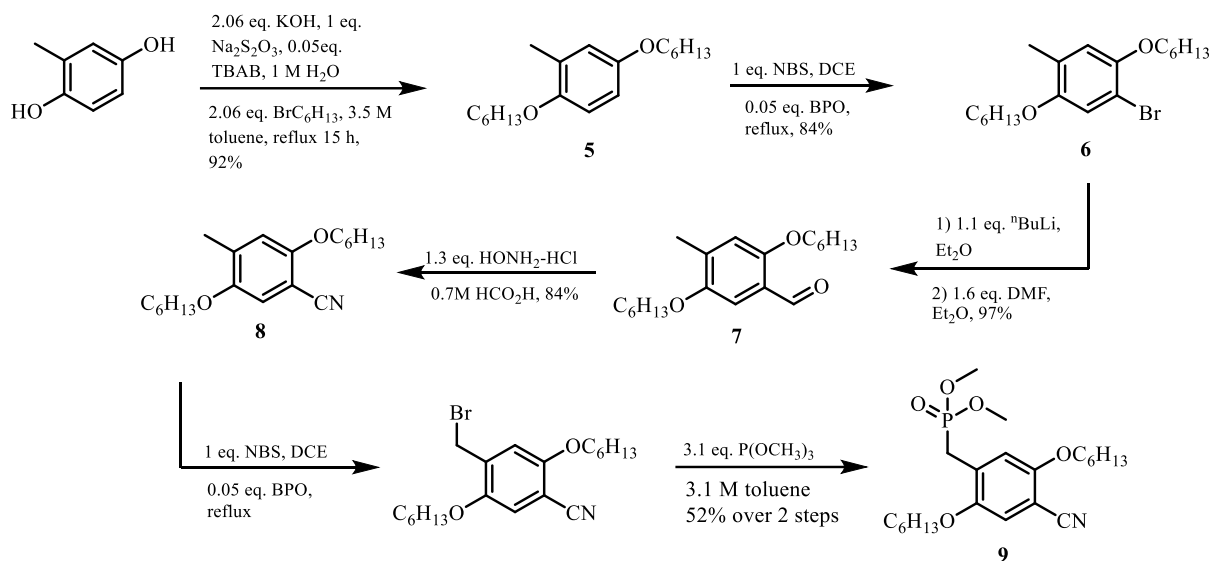


Figure 47: Synthesis of phosphonate **9**.

Successful formation of phosphonate **9** was determined by  $^1\text{H}$  NMR analysis (Figure 48). Bromination of nitrile-derivative **8** deshields the benzylic protons resulting in a downfield shift of the peak from 2.25 ppm, with an integration of 3 (Figure 48 a), to 4.50 ppm, with an integration of 2 (Figure 48 b). Conversion to the phosphonate (Figure 48 c), shifts the benzylic protons upfield from 4.50 ppm to 3.26 ppm, which appear as a doublet, and the new methoxy protons  $\beta$  to the phosphorus, also a doublet, are observed at 3.69 ppm with an integration of 6.

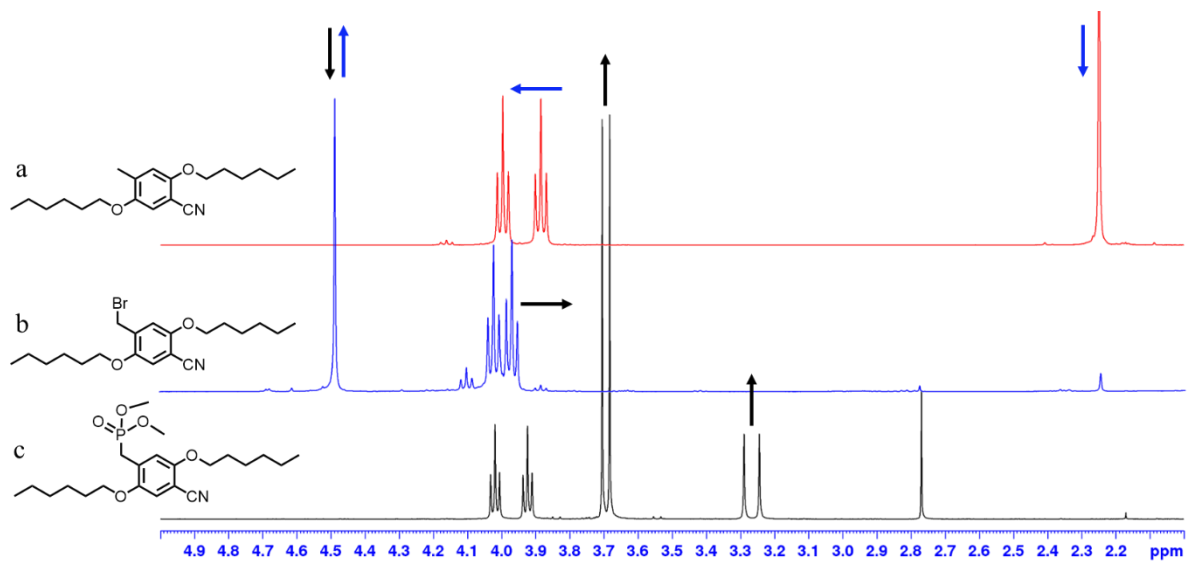


Figure 48:  $^1\text{H}$  NMR for the transformation of nitrile-derivative **8** to phosphonate-derivative **9**. (a) nitrile **8**; (b) intermediate; (c) phosphonate **9**. The arrow colors correspond product spectrum color and indicate the peak changes that occur from the starting material to the product.

Improved yields were obtained, and over-bromination was eliminated, for brominated-arene **6** when the reflux time was reduced. The yields of aldehyde **7** were drastically increased when a new bottle of extra-dry DMF was used. After the impurity in the crude for aldehyde **7** was identified as the dialkoxy-substituted arene **5** (based on  $^1\text{H}$  NMR analysis), it was deduced that water was present in the DMF, since water reacts faster with the lithiated intermediate than DMF. The overall yield for phosphonate **9** was improved when all residual formic acid was removed from the isolated nitrile-derivative **8**.



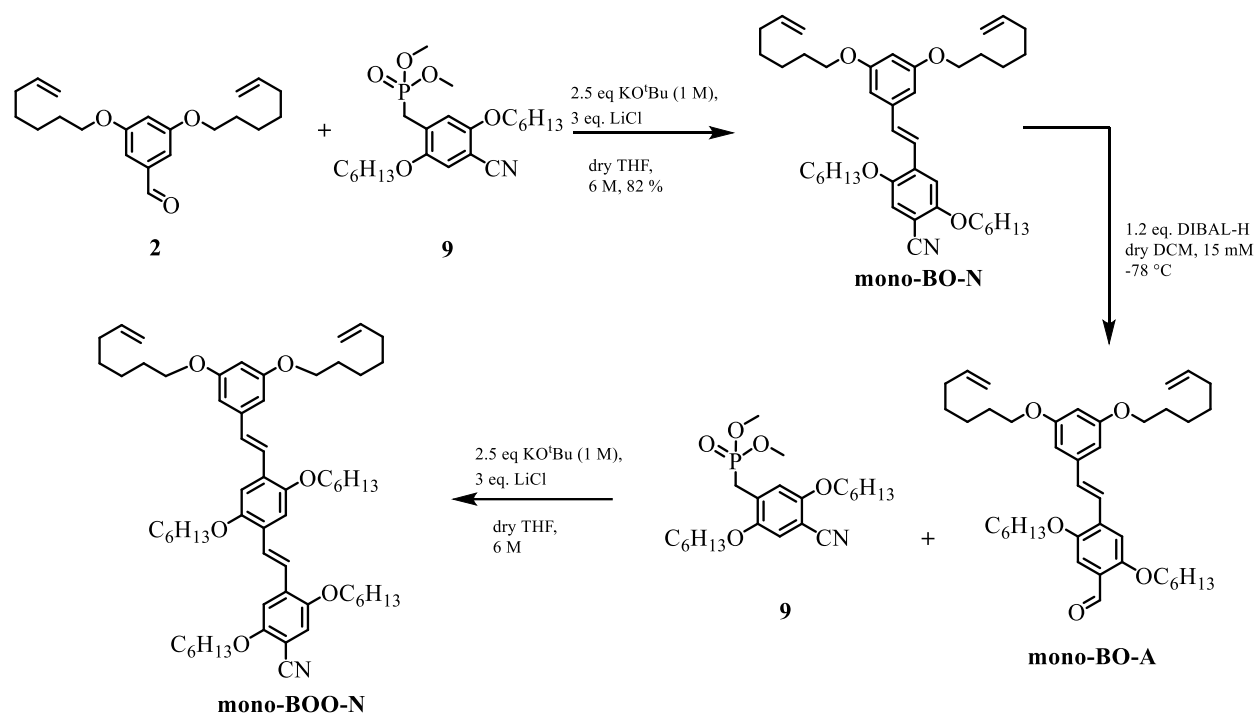


Figure 49: Representative iterative HWE coupling sequence.

Once all the building blocks were prepared, monomer side chains were sequenced via successive Horner Wadsworth Emmons (HWE) couplings of an aldehyde and a phosphonate, yielding, for example, **mono-BO-N** or **mono-BOO-N** (Figure 49). In preparation for the next HWE coupling, **mono-BO-N** or **mono-BOO-N** was converted to an aldehyde, **mono-BO-A** or **mono-BOO-A**, respectively, via DIBAL-H reduction of the nitrile at -78 °C. The use of potassium tert-butoxide (KO<sup>t</sup>Bu), a milder base, produced the highest yields from the HWE couplings, with the yield for **mono-P-N** > 80% and **mono-O-N** ~68%, whereas with sodium hydride the yield for **mono-P-N** was moderate, ~70%, but the yield for **mono-O-N** was only 27%.

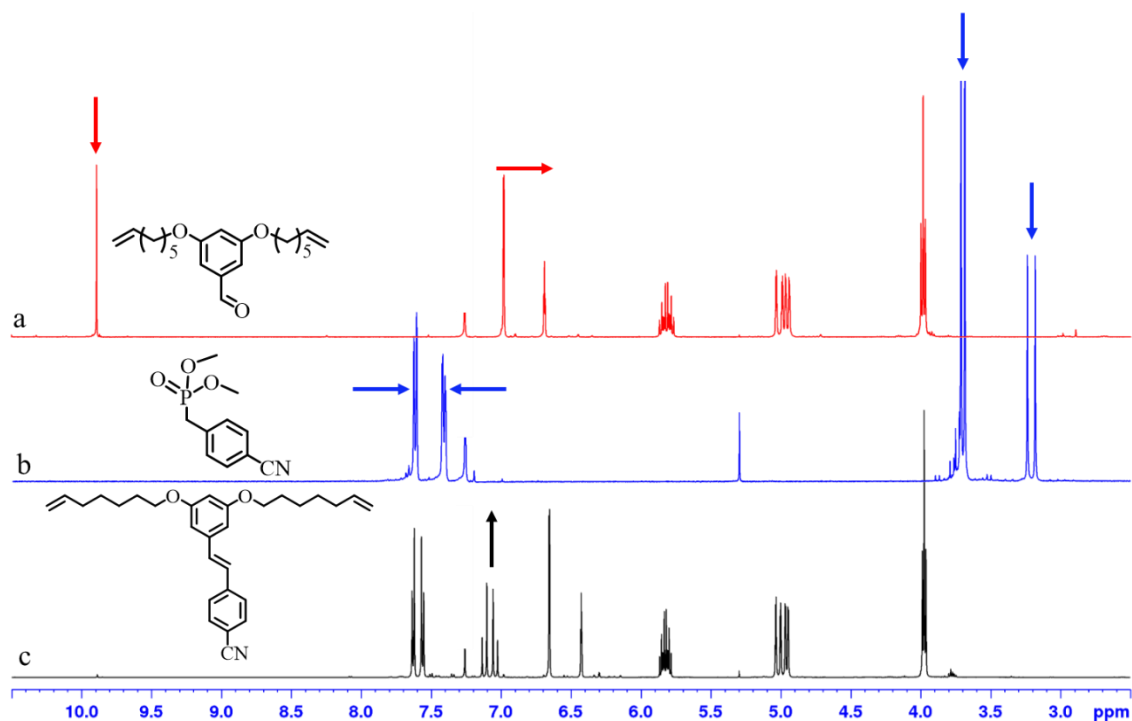


Figure 50:  $^1\text{H}$  NMR for the synthesis of **mono-BP-N**. (a) **mono-B-A**; (b) phosphonate **4**; (c) **mono-BP-N**. The arrow colors correspond to the respective spectrum color and indicate the peak changes that occur from the starting materials to the product.

The success of these couplings was verified by  $^1\text{H}$  NMR analysis (Figure 50). As the oxaphosphetane intermediate is being formed from **mono-B-A** (Figure 50 a) and phosphonate **4** (Figure 50 b), the aldehyde is consumed, resulting in the absence of the aldehyde peak in Figure 50 c. After the oxaphosphetane collapses to form the new carbon-carbon double bond, and kicks off the dimethyl phosphate anion, the protons associated with the phosphonate group are no longer observed. The product spectrum (Figure 50 c) shows the new alkene formed, as two doublets at 7.1 ppm, the aromatic peaks from mono-B-A shifted upfield, and the aromatic peaks from phosphonate 4 converged.

### 3.3.3 Metathesis of Polymers and Ring-Closed Monomers

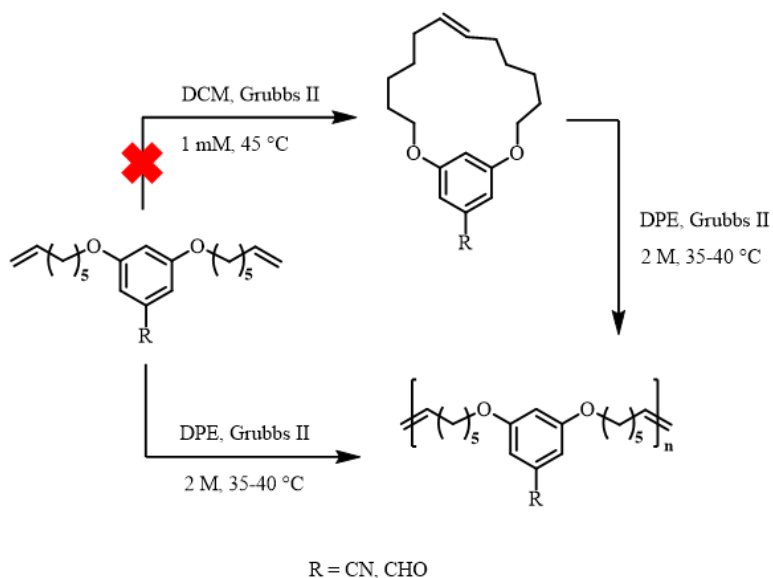


Figure 51: ADMET proved a more viable route for polymerization than RCM.

Polymerization via metathesis can be accomplished through two methods, acyclic diene metathesis (ADMET) and ring opening metathesis polymerization (ROMP). The Meyer group has shown that better molecular weights can be obtained via entropy driven ROMP (ED-ROMP)<sup>105, 106</sup>, thus in the early stages of this project, ring closing of **mono-B-N** was attempted, via ring closing metathesis (RCM) with second generation Grubbs catalyst (GII) at 1 mM (Figure 51). These trials resulted in very low yields, 11-26%, and some dimer formation was seen, as shown in the slight downfield shift of the internal alkene peak from Figure 51 b left to Figure 51 a left (teal arrow). Consequently, the polymerizations were conducted via ADMET with GII at 2 M (Figure 51). Metathesis was confirmed for both RCM and ADMET by the absence of the terminal alkene protons at ~5.8 ppm and ~4.9 ppm, red arrows, and the presence of the internal olefin protons at

~5.4 ppm, teal arrows, (Figure 52). The distinguishing feature for polymerization is broadening of the other proton peaks, purple arrows (Figure 52 a right).

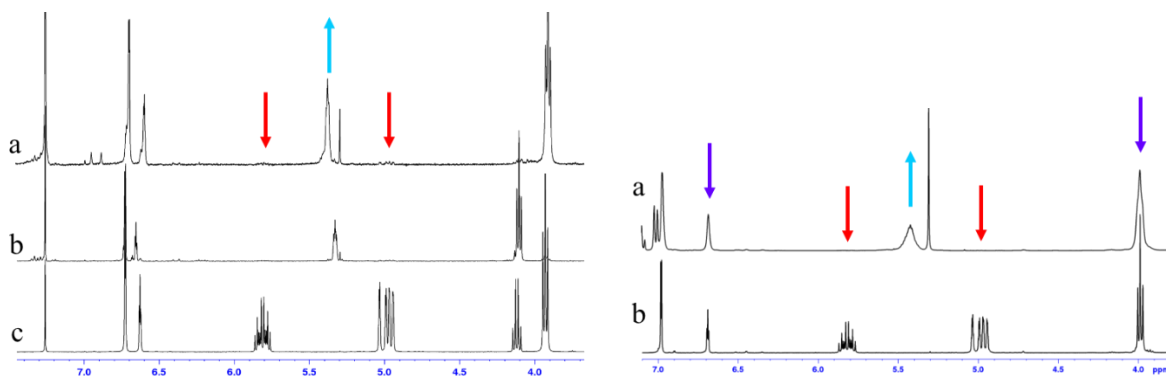


Figure 52: Left- RCM of mono-B-N; (a) dimer; (b) monomer; (c) starting material. Right - ADMET of mono-B-N; (a) polymer; (b) starting material. Red arrows - terminal olefin; teal arrow - internal olefin; purple arrows – broadened peaks.

The size exclusion chromatography (SEC) curves in Figure 53 and Figure 54 were acquired before precipitation, except one each for a nitrile and an aldehyde sample, as noted. The number average molecular weights ( $M_n$ ) were calculated relative to polystyrene standards and the values are presented in Table 6. For the samples that have not been precipitated, the region selected for the calculation of  $M_n$  was based upon an estimation of the range of elution times the precipitated curve would extend across. For example, trial one of **poly-P-N** has a clear envelope, when the troughs of the peaks on the right-hand side are envisioned as the second half of the curve, with its peak at approximately 16 min and the region selected was approximately 14-18 min.

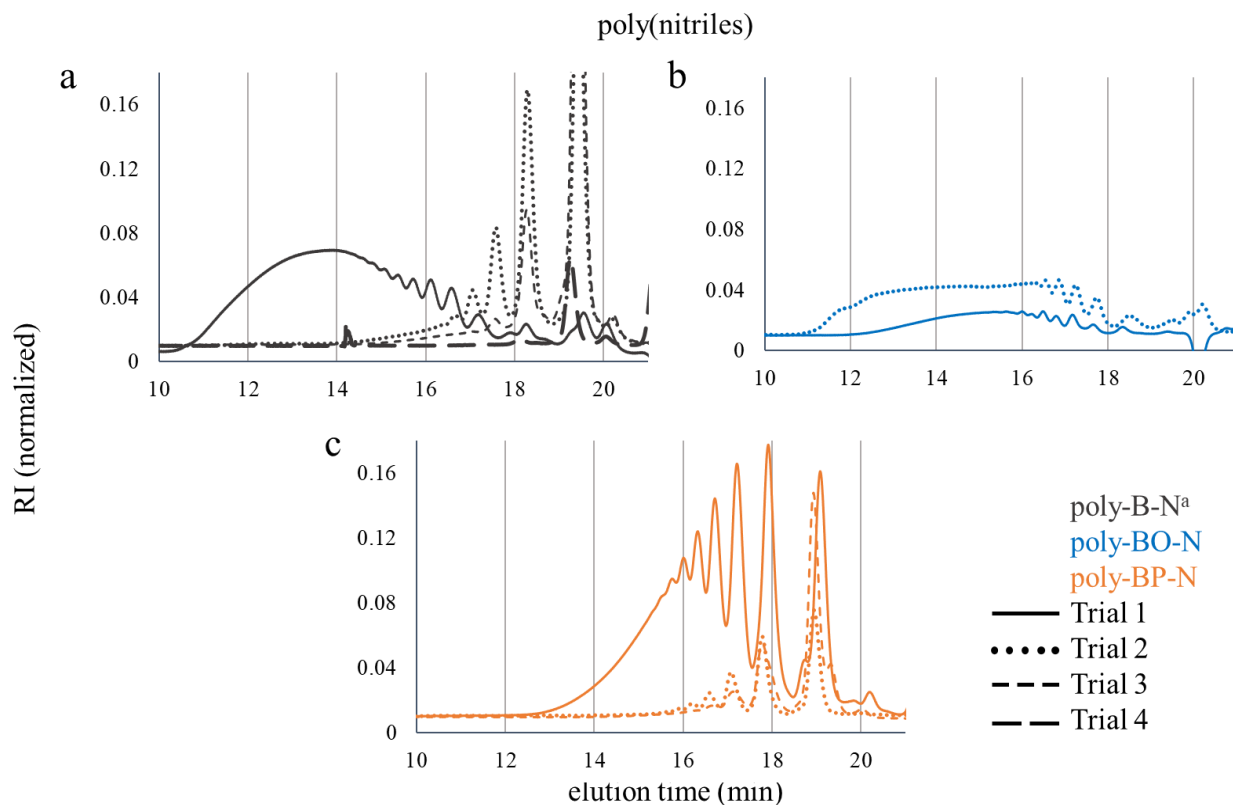


Figure 53: SEC curves for poly(nitriles). <sup>a</sup>Trial one for **poly-B-N** was precipitated.

The SEC curve for trial one of **poly-B-N** (Figure 53 a) suggests the monomer does form moderately high  $M_n$  species however, in the three subsequent trials sample elution times are greater than 17 min, indicating only small oligomer formation. The broad peaks in Figure 53 b reveal the polymerizations of **mono-BO-N** are disperse, i.e. contain a wide range of  $M_n$ , and suggests, though there is some high  $M_n$  species formed, there is a preference for oligomerization. In general, the SEC traces in Figure 54 shows sharp peaks at longer elution times, indicating that the nitrile derivatives tend toward oligomerization; consequently, all further polymerizations were carried out with the aldehyde derivatives.

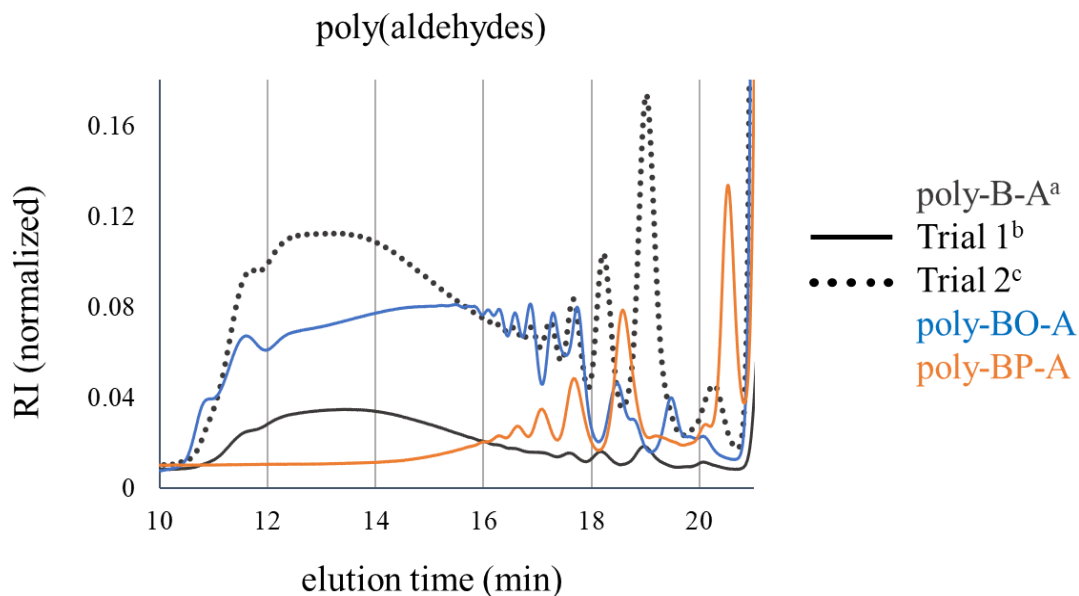


Figure 54: SEC curves for poly(aldehydes). <sup>a</sup>Trial one for **poly-B-A** was precipitated. <sup>b</sup>Trial one ran for 19 h. <sup>c</sup>Trial two ran for 35 h.

The increased intensity of the peaks at shorter elution times in Figure 54 clearly demonstrate the monomers with aldehyde-terminated side chains resulted in higher concentrations of larger molecular weight species, i.e. favor polymerization. Based on the significant increase in intensity from trial one of **poly-B-A** to trial two, it can be inferred that, for poly(aldehyde)s, increasing the polymerization time can yield significantly larger proportions of high molecular weight chains.

The degree of polymerization ( $n$ ), which is the average number of repeat units per chain, for the poly(aldehyde)s approached the target value of  $n = 34$  (Table 6) which is the  $n$  when the backbone moiety has a molecular weight of  $M_n \approx 10$  kDa. However, Oligo-**P-A** exhibited significant crystalline character identified by formation of a precipitate. We hypothesize that the rapid precipitation may be interfering with chain growth which would explain the very low degree of polymerization observed.

Table 6: Polymerization results for phenylene vinylene substrates

Monomer	Terminating Group	M <sub>repeatunit</sub> (g/mol)	M <sub>n</sub> (kDa) <sup>a</sup>	D	n
B-N	-CN	299.41	7.1	2.4	24
			0.5	1.7	2
			1.0	1.3	3
			0.5	1.1	2
BO-N	-CN	601.87	5.6	2.4	9
			7.8	2.7	13
BP-N	-CN	401.55	2.2	1.9	6
			1.6	1.3	4
			1.4	1.4	3
B-A	-CHO	302.41	8.0 <sup>b</sup>	4.4 <sup>b</sup>	27 <sup>b</sup>
			11.0 <sup>c</sup>	2.5 <sup>c</sup>	36 <sup>c</sup>
			13.3	2.3	44
BO-A	-CHO	604.87	10.4	2.9	17
BP-A	-CHO	404.55	1.3	2.9	3

<sup>a</sup>Molecular weight measured by SEC relative to polystyrene standards; <sup>b</sup>before precipitation; <sup>c</sup>after one precipitation

To date, the three initial building blocks have been completed, four nitrile- and three aldehyde-terminated monomers have been synthesized, and six of the monomers have been polymerized. SEC analysis shows, of the nitrile-terminated species two formed somewhat high M<sub>n</sub> oligomers and the third, on average, only formed tetramers. Whereas **poly-B-A** exceeds the minimum criteria for polymerization, and **poly-BO-A** should meet these criteria after precipitation, leading to the conclusion that aldehyde-terminated monomers afford a more viable synthetic route for polymerization.

## 4.0 Future directions

The framework for side chain dielectric polymers is outlined in chapters 2 and 3, and it is easy to envision many directions that could be pursued. A method for plasticization that is more in accordance with manufacturing processes is highly desirable. One possible means to fulfill this need would be to dope the films. Several options that would preclude the need to have residual solvent present in the films include the backbone monomer or the side chain segment, both of which could be added in a precise quantity. Another option would be the oligomeric species obtained from the purification of the polymer backbone or the coupled polymer. Perhaps these options would allow the samples to be vacuum dried yet maintain their mobility.

One of the original goals of this project was to investigate whether the sequence of aromatic species in the side chain would improve permittivity and aid in alignment. This work indicates that the side chain length limits mobility more than theorized, which seemingly makes sequence immaterial. However, there are still possibilities that can be developed to promote alignment. For instance, if one of the plasticizers mentioned above was employed with an added solvent, rather than to eliminate the solvent, this may provide enough free volume and mobility for the poly-trimer and poly-tetramer side chains to move with an oscillating field and align when the static field is applied. Once an effective method is devised to improve the mobility of the longer side chains, it would then be possible to investigate sequence.

The system designed here utilized a flexible backbone in which the aliphatic region was 14 atoms long between the aromatic moieties. This constrains the number of dipoles in the polymer film. Decreasing the length of the side chains by even 2 atoms would significantly increase the



number of dipoles in a film. It seems feasible that even a decrease by 4 atoms would still allow for the short side chains to rotate with an applied field. Here, two important questions must be considered. How short can these aliphatic tie-chains be to: 1) still get alignment of the dipoles? 2) still allow for near quantitative substitution?

Qiao et al. reported that their polymer with oligothiophene side chains showed a higher permittivity for the sample with a lower molecular weight. This may be due to mobility since there would be more end groups in the same size film, which would increase plasticization.<sup>83, 107, 108</sup> Perhaps there is an optimal  $M_n$  for this system that would increase the  $\epsilon'$ . Utilizing the polymer cleavage seen for the side chain coupling by controlling the reaction time is one route to varied  $M_n$  for this system.

Ring closing metathesis (RCM) followed by entropy-driven ring-opening metathesis polymerization (ED-ROMP) is a well-known method for molecular weight control. The difficulties observed with this method for the monomers with a nitrile may be similar to those that caused significant cross-linking with the phenylene vinylene system. Perhaps RCM of the bromo or iodo monomer would not encounter the same problems. It was observed that there was no apparent cleavage of the side chain alkoxys when the coupling procedure was used to build the side chains. It seems feasible that side chain coupling with a ring closed material might not cause cleavage of the phenyl ether rings. Therefore, RCM followed by side chain coupling and then ED-ROMP could be an alternative route to control  $M_n$ . This potentially could lead to the incorporation of different side chains into the polymer, fairly easily forming a random copolymer, and with some additional effort this could lead to some sequenced variants.

There are a number of possibilities that could be pursued with the alkene in the backbone. One option might be alkylation, which would provide the plasticization needed and might remove

the need for an added plasticizer. Another option would be the hydration of the alkene, which would incorporate additional polarizable components to the system, perhaps even aiding with alignment through hydrogen bonding.

One final area to investigate would be to use alternate aromatic species in the side chains. By varying the substituents, it may be possible to tune the dielectric constant of the polymer. For instance, an aromatic heterocycle, such as thiophene, would be interesting to investigate, since they would provide additional polarizability in the side chains.

## Appendix A Supporting Data and Spectra for Chapter 2

### Appendix A.1 Synthesis and Characterization Data

#### Appendix A.1.1 General Procedures

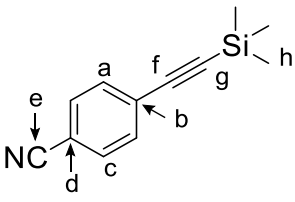
Unless specified otherwise, the polymers were synthesized by the following typical coupling procedure.

**Typical Coupling of Side Chains with the Polymer Backbone:** The reaction was maintained under a nitrogen atmosphere, and air free techniques were used to perform all steps. Without stirring, toluene (0.03 M) was used to transfer **p-B-I** (1 eq) to a dried Schlenk flask, piperidine (0.03 M) was added and the solution was degassed. To this solution the coupling reagents: Pd(dba)<sub>2</sub> (0.15 eq), PPh<sub>3</sub> (2.1 eq), and CuI (0.3 eq) were added, and the mixture was degassed again. The terminal alkyne was added (1.25-1.40 eq), and the reaction mixture was stirred for about 30 minutes. Saturated ammonium chloride solution was added and allowed to stir for 5 minutes, and the mixture was extracted with tetrahydrofuran. The combined organic layers were washed with brine and filtered through a plug of celite with a thin layer of silica on top. The filtrate was concentrated *in vacuo*, and the crude was purified by precipitation from DCM into methanol, 8-15 times, to obtain the title polymer.

Unless specified otherwise, the side chain moieties were deprotected by the following typical procedure.

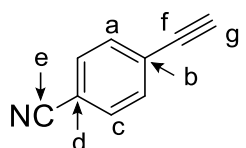
**Typical TMS Deprotection:** The protected alkyne was dissolved in either methanol, or a 1:1 mixture of MeOH:THF for the longer conjugated materials. To this solution  $\text{K}_2\text{CO}_3$  (1.9 eq) was added and the reaction was stirred for 45 minutes to an hour. The reaction mixture was concentrated *in vacuo*, dissolved in DCM and filtered through a plug of silica. The filtrate was concentrated *in vacuo*, and the material was used without further purification.

## Appendix A.1.2 Synthesis of Side Chain Moieties

4-((trimethylsilyl)ethynyl)benzonitrile ( <b>1</b> )						
				<sup>13</sup> C-NMR (400 MHz, CDCl <sub>3</sub> )	HRMS (ESI)	
				δ (ppm) + Assignment	Calc. Mass	
				-0.15	h	199.05 amu
				99.71	g	
				103.11	e	Calc.
				111.91	b	[M + H] <sup>+</sup>
				118.55	d	200.09 amu
				128.15	f	
				132.05	c	Found
				132.57	a	[M + H] <sup>+</sup>
						200.09 amu
						Composition
						C <sub>12</sub> H <sub>13</sub> NSi
				<sup>1</sup> H-NMR (400 MHz, CDCl <sub>3</sub> )		
δ (ppm)	Mult.	Int.	Assignment			
0.26	s	9	h			
7.53	d	2	a			
7.58	d	2	c			

p-Bromobenzonitrile (6.0 g, 33 mmol), PdCl<sub>2</sub>(PPh<sub>3</sub>)<sub>2</sub> (0.44 g, 0.63 mmol, 0.02 eq), and CuI (0.25 g, 1.3 mmol, 0.04 eq) were added to a round bottom flask under N<sub>2</sub> and dissolved in THF (157 mL) and distilled TEA (10.5 mL). TMSA (5.5 mL, 40 mmol) was added to and mixture was degassed. An inert atmosphere was maintained, and a reflux condenser was installed, and the reaction was stirred at 50 °C for about 20 hours. Once cooled, saturated ammonium chloride solution was added, stirred for 5 minutes, and the mixture was extracted with diethyl ether. The combined organic layers were washed with brine and filtered through a plug of celite with a thin layer of silica on top. The filtrate was concentrated *in vacuo*, and the material was used without further purification. The title compound was an off white solid (6.5 g, 99%).

4-ethynylbenzonitrile (**H-U-CN**)

				<sup>13</sup> C-NMR (400 MHz, CDCl <sub>3</sub> )	HRMS (ESI)	
				δ (ppm) + Assignment	Calc. Mass	
				81.67	g	127.04 amu
				82.01	e	
				112.50	b	Calc.
				118.38	d	[M + H] <sup>+</sup>
				127.15	f	128.05 amu
				132.17	c	
132.82	a	Found				
				[M + H] <sup>+</sup>	128.05 amu	
<sup>1</sup> H-NMR (400 MHz, CDCl <sub>3</sub> )					Composition	
δ (ppm)	Mult.	Int.	Assignment		C <sub>9</sub> H <sub>6</sub> N	
3.30	s	1	g			
7.57	d	2	a			
7.62	d	2	c			

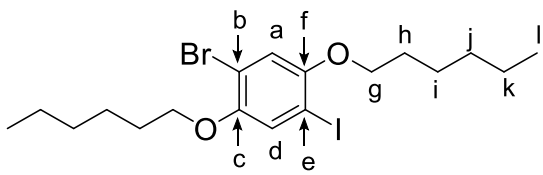
See the typical procedure for TMS deprotection. The compounds used were 4-((trimethylsilyl)ethynyl)benzonitrile (**1**) (2.0 g, 10 mmol), MeOH (20 mL), and K<sub>2</sub>CO<sub>3</sub> (0.31 g, 2.3 mmol). The reaction gave the title compound as an off white solid (1.0 g, 81%)

2-bromo-1,4-bis(hexyloxy)benzene (2)

				<sup>13</sup> C-NMR (500 MHz, CDCl <sub>3</sub> )	HRMS (ESI)
				δ (ppm) + Assignment	Calc. Mass
				14.17 l	356.14 amu
				22.74 k	
				25.83 i	Calc.
				29.39 h	[M + H] <sup>+</sup>
				31.71 j	357.14 amu
				68.99 g'	Found
				70.41 g	[M + H] <sup>+</sup>
				112.96 b	357.14 amu
				114.56 e	
				114.91 d	Composition
				119.65 a	C <sub>18</sub> H <sub>29</sub> BrO <sub>2</sub>
				149.94 f	
				153.75 c	
<sup>1</sup> H-NMR (500 MHz, CDCl <sub>3</sub> )					
δ (ppm)	Mult.	Int.	Assignment		
0.91	t	6	l		
1.34	m	8	j,k		
1.44	m	2	i'		
1.49	m	2	i		
1.74	m	2	h'		
1.80	m	2	h		
3.88	t	2	g'		
3.95	t	2	g		
6.78	dd	1	e		
6.82	d	1	d		
7.11	d	1	a		

To a round bottom flask, KOH (7.5 g, 114 mmol), and Na<sub>2</sub>S<sub>2</sub>O<sub>3</sub>·5H<sub>2</sub>O (21.6 g, 87 mmol) were dissolved in water (16 mL) with stirring. The flask was cooled on an ice bath then, bromohydroquinone (10.4 g, 55 mmol) and TBAB (0.72 g, 2.2 mmol) were added. The mixture was stirred until most of the solid had dissolved, and then the ice bath was removed. To the stirring mixture, 1-bromohexane (16.4 mL, 113 mmol) and toluene (32 mL) were added, and the flask was equipped with a water-cooled condenser. The mixture was refluxed with vigorous stirring for 24 – 48 h. Once complete, the mixture was allowed to cool to RT, the aqueous layer was extracted once with toluene. The combined organic layers were washed with water and brine and dried over MgSO<sub>4</sub>. The solvent was removed *in vacuo*, and the crude was purified by column chromatography (silica, 20% DCM:hexanes) to give the title compound (17.6 g, 89%). Note, to remove possible monosubstituted product, and ensure good M<sub>n</sub>s from subsequent polymerizations, the product was purified a second time, by column chromatography (silica, 10% DCM:hexanes).

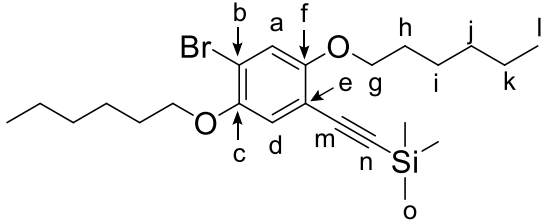
1-bromo-2,5-bis(hexyloxy)-4-iodobenzene (**3**)

				<sup>13</sup> C-NMR (500 MHz, CDCl <sub>3</sub> )	HRMS (ESI)	
				δ (ppm) + Assignment	Calc. Mass	
				14.16	l	482.03 amu
				22.72	k	
				25.81	i	Calc.
				29.26	h	[M + H] <sup>+</sup>
				31.62	j	483.04 amu
				70.52	g	Found
				84.94	b	[M] <sup>+</sup>
				112.70	e	482.03 amu
				117.27	a	
				124.45	d	Composition
				150.60	f	C <sub>18</sub> H <sub>28</sub> BrIO <sub>2</sub>
				152.73	c	
<sup>1</sup> H-NMR (500 MHz, CDCl <sub>3</sub> )						
δ (ppm)	Mult.	Int.	Assignment			
0.91	t	6	l			
1.35	m	8	j, k			
1.49	m	4	i			
1.80	m	4	h			
3.94	t	4	g			
6.98	s	1	a			
7.28	s	1	d			

2-bromo-1,4-bis(hexyloxy)benzene (**2**) (5.5 g, 15.5 mmol) was dissolved in acetic acid (20 mL) and chloroform (5.1 ml). To this solution iodine (3.9 g, 15.5 mmol), conc. H<sub>2</sub>SO<sub>4</sub> (1.3 mL), water (0.64 ml) and finally potassium iodate (1.37 g, 6.38 mmol) were added. The reaction mixture was refluxed for 5 hr. To remove excess iodine, Na<sub>2</sub>S<sub>2</sub>O<sub>3</sub> was added until the violet color of the iodine disappeared. Ice/water was added, and the mixture was extracted with DCM. The organic phase was neutralized with a saturated NaHCO<sub>3</sub>-solution and dried over MgSO<sub>4</sub>. The solvent was concentrated *in vacuo*, and the residue was recrystallized from MeOH to obtain a white solid (5.1 g, 68%).

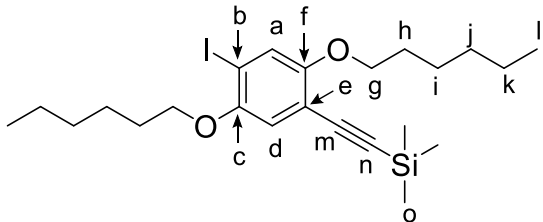


**((4-bromo-2,5-bis(hexyloxy)phenyl)ethynyl)trimethylsilane (4)**

				<sup>13</sup> C-NMR (500 MHz, CDCl <sub>3</sub> )	HRMS (ESI)
				δ (ppm) + Assignment	Calc. Mass
				0.08 o	452.17 amu
				14.15, l	Calc. [M + H] <sup>+</sup>
				14.20 l'	
				22.72 k	453.18 amu
				22.76 k'	
				25.78 i	Found [M + H] <sup>+</sup>
				25.80 i'	
				29.28 h	453.18 amu
				29.39 h'	
				31.64 j	Composition C <sub>23</sub> H <sub>37</sub> BrO <sub>2</sub> Si
				31.73 j'	
				69.89 g	
				70.25 g'	
				99.35 n	
				100.77 b	
				112.59 m	
				113.73 e	
				118.10 a, d	
				118.12 a, d	
				149.46 c	
				154.87 f	
<sup>1</sup> H-NMR (500 MHz, CDCl <sub>3</sub> )					
δ (ppm)	Mult.	Int.	Assignment		
0.25	s	9	o		
0.91	t	6	l		
1.34	m	8	j, k		
1.49	m	4	i		
1.79	m	4	h		
3.94	t	4	g		
6.94	s	1	a		
7.04	s	1	d		

The reaction was maintained under a nitrogen atmosphere, and air free techniques were used to perform all steps., To a dried Schlenk flask, the coupling reagents were added without stirring: PdCl<sub>2</sub>(PPh<sub>3</sub>)<sub>2</sub> (0.14 g, 0.20 mmol, 0.02 eq), CuI (0.08 g, 0.40 mmol, 0.04 eq), and distilled TEA (20.1 mL). To this mixture 1-bromo-2,5-bis(hexyloxy)-4-iodobenzene (5.0 g, 10 mmol, 1 eq) (**3**), and the mixture was degassed. TMSA (1.4 mL, 10 mmol, 1 eq) was added to the mixture, and the reaction was stirred for about 2 hours. Saturated ammonium chloride solution was added, stirred for 5 minutes, and the mixture was extracted with diethyl ether. The combined organic layers were washed with brine and concentrated *in vacuo*. The crude material was purified by column chromatography (silica, 10% DCM:hexanes) to give the title compound (3.9 g, 83%).

**((2,5-bis(hexyloxy)-4-iodophenyl)ethynyl)trimethylsilane (5)**

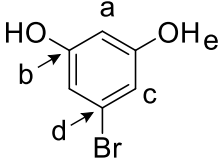
				<sup>13</sup> C-NMR (500 MHz, CDCl <sub>3</sub> )	HRMS (ESI)	
				δ (ppm) + Assignment	Calc. Mass	
				0.09	o	500.16 amu
				14.16	l	
				14.19	l'	Calc.
				22.73	k	[M + H] <sup>+</sup>
				22.77	k'	501.17 amu
				25.82	i	Found
				25.89	i'	[M + H] <sup>+</sup>
				29.31	h	501.16
				29.45	h'	amu
				31.64	j	
				31.74	j'	Composition
				70.02	g	C <sub>23</sub> H <sub>37</sub> IO <sub>2</sub> Si
				70.31	g'	
				88.07	e	
				99.58	n	
				100.97	m	
				113.70	b	
				116.58	d	
				124.14	a	
				151.92	f	
				155.09	c	

<sup>1</sup> H-NMR (500 MHz, CDCl <sub>3</sub> )			
δ (ppm)	Mult.	Int.	Assignment
0.25	s	9	o
0.91	t	6	l
1.34	m	8	j, k
1.50	m	4	i
1.79	m	4	h
3.94	t	4	g
6.83	s	1	d
7.25	s	1	a

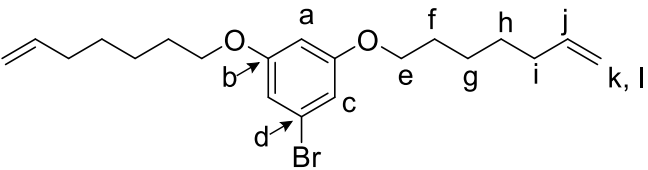
Two Schlenk flasks were set up side by side and cooled with a dry ice bath to -78 °C. To one Schlenk flask was added (4-bromo-2,5-bis(hexyloxy)phenyl)ethynyl)trimethylsilane (4) (3.0 g, 6.7 mmol) and THF (37 mL). Once cooled, <sup>n</sup>BuLi (3.7 mL, 10 mmol, 2.7 M in toluene) was added dropwise and the mixture was stirred for about an hour. To the second Schlenk flask was added iodine (2.3 g, 9.0 mmol) and THF (37 mL), and cooled while the bromo-lithium exchange was reacting. Once complete, the lithiated solution was transferred via cannula to the cold iodine mixture. The reaction was allowed to warm to RT and stirred overnight. Concentrated bisulfite solution was added to remove the excess iodine. This mixture was extracted with diethyl ether, washed with brine, dried over MgSO<sub>4</sub>, and concentrated *in vacuo*. The crude material was purified by column chromatography (silica, 15% DCM:hexanes) to give the title compound (2.7 g, 80%).

5-bromobenzene-1,3-diol (**6**)

				<sup>13</sup> C-NMR (500 MHz, DMSO)	HRMS (ESI)	
				$\delta$ (ppm) + Assignment	Calc. Mass	
				101.74	b	187.95 amu
				109.34	c	
				121.73	d	Calc.
				159.37	a	[M + H] <sup>+</sup>
					186.94 amu	
					Found	
					[M + H] <sup>+</sup>	
					186.94 amu	
					Composition	
					C <sub>6</sub> H <sub>5</sub> BrO <sub>2</sub>	
<sup>1</sup> H-NMR (500 MHz, DMSO)						
$\delta$ (ppm)	Mult.	Int.	Assignment			
6.18	t	1	a			
6.37	d	2	c			
9.66	s	1	e			

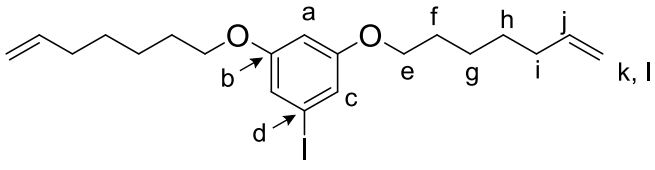
1-bromo-3,5-dimethoxybenzene, as purchased, (7.4 g, 33.9 mmol) and 225 mL dry DCM were added to a dried three neck round bottom flask fitted with a dried ground glass addition funnel. The reaction was cooled to -78 °C using a dry ice/IPA bath. Once cooled, boron tri-bromide (100 mL, 100 mmol (1 M in DCM)) was added dropwise while stirring. The reaction was allowed to warm slowly to RT and stirred overnight. The reaction was followed by NMR. If needed, the reaction was again cooled to -78 °C before more BBr<sub>3</sub> was added. Once complete, the reaction was cooled to 0 °C and 30 mL of cold water was added slowly. The reaction mixture was extracted 3 x with 50 mL diethyl ether and the combined organic layers were washed with bisulfite solution. The organic layer was dried with MgSO<sub>4</sub> and concentrated in vacuo. The crude material was recrystallized from chloroform, with a few drops of ethanol, to give the title compound as an off-white fibrous solid (5.1 g, 80% yield).

1-bromo-3,5-bis(hept-6-en-1-yloxy)benzene (**7**)

				<sup>13</sup> C-NMR (500 MHz, CDCl <sub>3</sub> )	HRMS (ESI)	
				δ (ppm) + Assignment	Calc. Mass	
				25.62	h	380.14 amu
				28.73	g	
				29.11	f	Calc.
				33.80	i	[M + H] <sup>+</sup>
				68.35	e	381.14 amu
				100.78	a	Found
				110.41	c	[M + H] <sup>+</sup>
				114.64	k/l	381.14 amu
				122.97	d	
<sup>1</sup> H-NMR (500 MHz, CDCl <sub>3</sub> )				138.90	j	Composition
δ (ppm)	Mult.	Int.	Assignment	160.87	b	C <sub>20</sub> H <sub>29</sub> BrO <sub>2</sub>
1.45	m	8	g, h			
1.76	m	4	f			
2.08	m	4	i			
3.90	t	4	e			
4.99	m	4	k, l			
5.81	m	2	j			
6.36	t	1	a			
6.63	d	2	c			

To a round bottom flask, KOH (1.7 g, 26 mmol), and Na<sub>2</sub>S<sub>2</sub>O<sub>3</sub>·5H<sub>2</sub>O (4.9 g, 20 mmol) were dissolved in water (3.6 mL) with stirring. The flask was cooled on an ice bath then, 5-bromobenzene-1,3-diol (2.4 g, 12 mmol) and TBAB (0.16 g, 0.5 mmol) were added. The mixture was stirred until most of the solid had dissolved, and then the ice bath was removed. To the stirring mixture, 7-bromo-1-heptene (3.7 mL, 26 mmol) and toluene (7.2 mL) were added, and the flask was equipped with a water-cooled condenser. The mixture was refluxed with vigorous stirring for 24 – 48 h. Once complete, the mixture was allowed to cool to RT, the aqueous layer was extracted once with toluene. The combined organic layers were washed with water and brine and dried over MgSO<sub>4</sub>. The solvent was removed *in vacuo*, and the crude was purified by column chromatography (silica, 20% DCM:hexanes) to give the title compound (4.0 g, 85%).

1-iodo-3,5-bis(hept-6-en-1-yloxy)benzene (**8**)

				<sup>13</sup> C-NMR (500 MHz, CDCl <sub>3</sub> )	HRMS (ESI)
				δ (ppm) + Assignment	Calc. Mass
				25.62 h	428.12 amu
				28.73 g	
				29.13 f	Calc.
				33.80 i	[M + H] <sup>+</sup>
				68.29 e	429.13 amu
				94.18 d	
				101.63 a	Found
				114.64 k/l	[M + H] <sup>+</sup>
				116.40 c	429.13 amu
				138.91 j	Composition
				160.74 b	C <sub>20</sub> H <sub>29</sub> IO <sub>2</sub>
<sup>1</sup> H-NMR (500 MHz, CDCl <sub>3</sub> )					
δ (ppm)	Mult.	Int.	Assignment		
1.45	m	8	g, h		
1.76	m	4	f		
2.08	m	4	i		
3.89	t	4	e		
4.99	m	4	k, l		
5.81	m	2	j		
6.38	t	1	a		
6.83	d	2	c		

Two Schlenk flasks were set up side by side and cooled with a dry ice bath to -78 °C. To one Schlenk flask was added 1-bromo-3,5-bis(hept-6-en-1-yloxy)benzene (**7**) (1.1 g, 3.0 mmol) and THF (16 mL). Once cooled, <sup>n</sup>BuLi (1.6 mL, 4.4 mmol, 2.7 M in toluene) was added dropwise and the mixture was stirred for about an hour. To the second Schlenk flask was added iodine (1.0 g, 4.0 mmol) and THF (37 mL), and cooled while the bromo-lithium exchange was reacting. Once complete, the lithiated solution was transferred via cannula to the cold iodine mixture. The reaction was allowed to warm to RT and stirred overnight. Concentrated bisulfite solution was added to remove the excess iodine. This mixture was extracted with diethyl ether, washed with brine, dried over MgSO<sub>4</sub>, and concentrated *in vacuo*. The crude material was purified by column chromatography (silica, 7.5% DCM:hexanes) to give the title compound (0.67 g, 60%). Note this yield only reflects the product obtained that was pure enough for polymerization.

### Appendix A.1.3 Polymerizations and Side Chain Couplings

4-((2,5-bis(hexyloxy)-4-((trimethylsilyl)ethynyl)phenyl)ethynyl)benzonitrile ( <b>TMS-SU-CN</b> )				
			<sup>13</sup> C-NMR (500 MHz, CDCl <sub>3</sub> )	HRMS (ESI)
			δ (ppm) + Assignment	Calc. Mass 499.29 amu
			0.07 o	
			14.15 l	
			14.21 l'	Calc.
			22.77 k	[M + H] <sup>+</sup>
			25.85 i	500.30 amu
			29.38 h	Found
			29.44 h'	[M + H] <sup>+</sup>
			31.69 j	500.30 amu
			31.75 j'	
			69.65 g	Composition
			69.73 g'	C <sub>32</sub> H <sub>42</sub> NO <sub>2</sub> Si
			90.65 m	
			93.12 n	
			100.95 p	
			101.01 q	
			111.53 r	
			113.05 e	
			115.03 b	
			117.06 a	
			117.31 d	
			118.70 v	
			128.58 u	
			132.09 s	
			132.16 t	
			153.93 f	
			154.27 c	
<sup>1</sup> H-NMR (500 MHz, CDCl <sub>3</sub> )				
δ (ppm)	Mult.	Int.	Assignment	
0.27	s	9	o	
0.90	m	6	l	
1.35	m	8	j, k	
1.53	m	4	i	
1.82	m	4	h	
3.99	t	4	g	
6.95	s (overlap)	2	a, d	
7.58	d	2	s	
7.63	d	2	t	

((2,5-bis(hexyloxy)-4-iodophenyl)ethynyl)trimethylsilane (**5**) (0.53 g, 1.1 mmol), and distilled TEA (7.4 mL) were added to a Schlenk flask under N<sub>2</sub> and the mixture was degassed. An inert atmosphere was maintained and PdCl<sub>2</sub>(PPh<sub>3</sub>)<sub>2</sub> (0.59 g, 0.08 mmol, 0.08 eq), CuI (0.20 g, 0.11 mmol, 0.10 eq), and **H-U-CN** (0.16 g, 1.3 mmol, 1.2 eq) were added. The reaction was degassed again and stirred at RT for about an hour. Saturated ammonium chloride solution was added, stirred for 5 minutes, and the mixture was extracted with diethyl ether. The combined organic layers were washed with brine and filtered through a plug of celite with a thin layer of silica on top. The filtrate was concentrated *in vacuo*, and the material was purified by column chromatography (silica, 40% DCM:hexanes), to give the title compound (0.45 g, 85%).

4-((4-ethynyl-2,5-bis(hexyloxy)phenyl)ethynyl)benzonitrile (**H-SU-CN**)

				<sup>13</sup> C-NMR (500 MHz, CDCl <sub>3</sub> )	HRMS (ESI)	
				δ (ppm) + Assignment	Calc. Mass	
				14.15	l	427.25 amu
				22.72	k	
				22.77	k'	Calc.
				25.74	i	[M + H] <sup>+</sup>
				25.85	i'	428.26 amu
				29.25	h	Found
				29.36	h'	[M + H] <sup>+</sup>
				31.66	j	428.26 amu
				31.69	j'	
				69.70	g	Composition
				69.88	g'	C <sub>29</sub> H <sub>33</sub> NO <sub>2</sub>
				79.93	m	
				82.96	n	
				90.42	p	
				93.16	q	
				111.62	r	
				113.48	e	
				113.89	b	
				117.07	a	
				117.80	d	
				118.68	v	
				128.50	u	
				132.13	s	
				132.17	t	
				153.90	c	
				154.26	f	

<sup>1</sup> H-NMR (500 MHz, CDCl <sub>3</sub> )			
δ (ppm)	Mult. (J)	Int.	Assignment
0.90	m	6	l
1.35	m	8	j, k
1.50	m	4	i
1.82	m	4	h
3.36	s	1	n
4.00	t	4	g
6.98	s (overlap)	2	a, d
7.58	d	2	s
7.63	d	2	t

See the typical procedure for TMS deprotection. The compounds used were 4-((2,5-bis(hexyloxy)-4-((trimethylsilyl)ethynyl)phenyl)ethynyl)benzonitrile (**TMS-SU-CN**) (0.91 g, 1.8 mmol), MeOH (25 mL), THF (25 mL), and K<sub>2</sub>CO<sub>3</sub> (0.47 g, 3.4 mmol). The reaction gave the title compound as an off white solid (0.75 g, 96%)

4-((2,5-bis(hexyloxy)-4-((trimethylsilyl)ethynyl)phenyl)ethynyl)benzonitrile ( <b>TMS-SSU-CN</b> )				<sup>13</sup> C-NMR (500 MHz, CDCl <sub>3</sub> )	HRMS (ESI)
				δ (ppm) + Assignment	Calc. Mass
				0.10	ak
				14.15	l, ah
				14.17	"
				14.21	"
				22.78	ag
				25.80	k
				25.81	k'
				25.86	i
				25.88	i'
				29.41	h
				29.49	"
				31.71	j, af
				31.75	"
				31.77	"
				69.64	ee, g
				69.81	"
				69.95	"
				90.81	m, n, ai, ak
				91.35	"
				92.14	"
				93.17	"
				100.39	p
				101.28	q
				111.50	r
				112.79	e
				114.10	d, aa
				114.47	s
				115.61	w
				115.61	b
				117.11	a
				117.25	x
				117.27	aa
				117.57	d
				118.72	v
				128.63	u
				132.09	s, t
				132.17	"
				153.56	y
				153.60	ab
				154.08	f
				154.32	c
<sup>1</sup> H-NMR (500 MHz, CDCl <sub>3</sub> )					
δ (ppm)	Mult. (J)	Int.	Assignment		
0.26	s	9	ak		
0.88	m	12	l, ah		
1.34	m	16	j, k, ag, af		
1.52	m	8	i, ae		
1.83	m	8	h, ad		
4.01	m	8	g, ac		
6.95	s	2	a, x		
7.00	s	2	d, aa		
7.59	d	2	s		
7.63	d	2	t		
					<u>Composition</u>
					C <sub>52</sub> H <sub>69</sub> NO <sub>4</sub>

((2,5-bis(hexyloxy)-4-iodophenyl)ethynyl)trimethylsilane (**5**) (0.88 g, 1.8 mmol), **H-SU-CN** (0.75 g, 1.8 mmol), toluene (10 mL) and piperidine (10 mL) were added to a dried Schlenk flask under N<sub>2</sub> and the mixture was degassed. An inert atmosphere was maintained and PdCl<sub>2</sub>(PPh<sub>3</sub>)<sub>2</sub> (0.99 g, 0.14 mmol, 0.08 eq), CuI (0.33 g, 0.18 mmol, 0.10 eq) were added. The reaction was stirred at RT for about an hour. Saturated ammonium chloride solution was added, stirred for 5 minutes, and the mixture was extracted with ethyl acetate. The combined organic



layers were washed with brine and filtered through a plug of celite with a thin layer of silica on top. The filtrate was concentrated *in vacuo*, and the material was purified by column chromatography (silica, 40% DCM:hexanes), to give the title compound as a yellow solid (0.45 g, 85%).

4-((4-ethynyl-2,5-bis(hexyloxy)phenyl)ethynyl)benzonitrile ( <b>H-SSU-CN</b> )				<sup>13</sup> C-NMR (500 MHz, CDCl <sub>3</sub> )	HRMS (ESI)
				δ (ppm) + Assignment	Calc. Mass
				14.15	l, ah
				14.16	"
				22.72	k, ag
				22.77	"
				25.75	i, ae
				25.79	"
				25.88	"
				29.29	h, ad
				29.39	"
				29.40	"
				29.41	"
				31.67	j, af
				31.71	"
				31.74	"
<sup>1</sup> H-NMR (500 MHz, CDCl <sub>3</sub> )				69.65	g, ac
				69.80	"
				69.86	"
				69.93	"
				80.14	m, n, aj, ai
				82.53	"
				90.77	"
				91.40	"
				91.91	p
				93.19	q
				111.51	r
				112.87	e
				112.97	z
				114.89	w
				115.51	b
				117.11	a
				117.25	x, aa
				118.09	d
				118.70	v
				128.60	u
				132.09	s, t
				132.17	"
				153.53	y
				153.62	ab
				154.08	f
				154.31	c
δ (ppm)	Mult. (J)	Int.	Assignment		
0.89	m	12	l, ah		
1.34	m	16	j, k, af, ag		
1.52	m	8	i, ae		
1.83	m	8	h, ad		
3.35	s	1	aj		
4.01	m	8	g, ac		
7.00	s	4	a, d, x, aa		
7.60	d	2	t		
7.63	d	2	s		
				<u>Composition</u> C <sub>49</sub> H <sub>61</sub> NO <sub>4</sub>	

See the typical procedure for TMS deprotection. The compounds used 4-((2,5-bis(hexyloxy)-4-((trimethylsilyl)ethynyl)phenyl)ethynyl)benzonitrile (**TMS-SSU-CN**) (0.62 g, 0.77 mmol), MeOH (20 mL), THF (20 mL), and K<sub>2</sub>CO<sub>3</sub> (0.20 g, 1.5 mmol). The reaction gave the title compound (0.55 g, 99%)

p-B-Br					
				<sup>13</sup> C-NMR (500 MHz, CDCl <sub>3</sub> )	
				δ (ppm) + Assignment	<u>M<sub>n</sub></u>
				18.7 kDa	
				<u>D</u>	
				1.6	
				<u>Repeat Unit</u>	
				<u>Mass</u>	
				352.1 amu	
<sup>1</sup> H-NMR (500 MHz, CDCl <sub>3</sub> )				<u>Repeat Unit</u>	
δ (ppm)	Mult. (J)	Int.	Assignment	<u>Composition</u>	
1.42	m	8	h, i	C <sub>18</sub> H <sub>25</sub> BrO <sub>2</sub>	
1.75	m	4	g		
2.00	m	4	j		
3.89	t	4	f		
5.40	m	2	k		
6.35	d	1	a		
6.63	t	2	c		

1-bromo-3,5-bis(hept-6-en-1-yloxy)benzene (**7**) (1.2 g, 3.1 mmol) was dissolved in diphenyl ether (1.6 mL) and GII was added (0.95 g, 0.11 mmol) was added. The mixture was stirred and heated gently under vacuum until SEC analysis indicated polymerization had reached steady state. The reaction was quenched with ethyl vinyl ether and precipitated with MeOH. (0.83 g, 75%)

<b>p-B-I</b>			
			<sup>13</sup> C-NMR (500 MHz, CDCl <sub>3</sub> )
			δ (ppm) + Assignment
			21.6 kDa
			<u>D</u>
			1.6
			<u>Repeat Unit</u>
			<u>Mass</u>
			400.1 amu
<sup>1</sup> H-NMR (500 MHz, CDCl <sub>3</sub> )			
δ (ppm)	Mult. (J)	Int.	Assignment
1.42	t	8	g, h
1.75	m	4	f
2.00	m	4	i
3.89	t	4	e
5.40	m	2	j
6.35	d	1	a
6.63	t	2	c
			<u>Repeat Unit</u>
			<u>Composition</u>
			C <sub>18</sub> H <sub>25</sub> IO <sub>2</sub>

1-iodo-3,5-bis(hept-6-en-1-yloxy)benzene (**8**) (0.38 g, 0.90 mmol) was dissolved in diphenyl ether (0.45 μL) and GII was added (0.02 g, 0.03 mmol) was added. The mixture was stirred and heated gently under vacuum until SEC analysis indicated polymerization had reached steady state. The reaction was quenched with ethyl vinyl ether and precipitated with MeOH. (0.35 g, 97%)

p-BU-CN						
				<sup>13</sup> C-NMR (500 MHz, CDCl <sub>3</sub> )		
				δ (ppm) + Assignment	<u>M<sub>n</sub></u>	
				25.68	g	19.1 kDa
				28.78	f	
				29.30	h	<u>D</u>
				32.62	i	1.8
				68.21	e	
				87.21	m	<u>Repeat Unit</u>
				94.09	k	<u>Mass</u>
				103.58	a	399.2 amu
				110.15	c	
				111.65	q	<u>Repeat Unit</u>
				118.62	r	<u>Composition</u>
				123.43	d	C <sub>27</sub> H <sub>29</sub> NO <sub>2</sub>
				128.28	n	
				130.46	j	
				132.17	o	
				132.21	p	
				160.28	b	
<sup>1</sup> H-NMR (500 MHz, CDCl <sub>3</sub> )						
δ (ppm)	Mult. (J)	Int.	Assignment			
1.35	t	8	g, h			
1.76	m	4	f			
2.00	m	4	i			
3.92	t	4	e			
5.40	m	2	j			
6.47	t	1	a			
6.65	d	2	c			
7.57	d	2	p			
7.61	d	2	o			

See the typical procedure for side chain coupling with polymer backbone. The compounds used 4-ethynylbenzonitrile (**H-U-CN**) (0.08 g, 0.66 mmol), **p-B-I** (0.21 g, 0.53 mmol), piperidine (16 mL), toluene (16 mL), Pd(dba)<sub>2</sub> (0.05 g, 0.08 mmol), PPh<sub>3</sub> (0.29 g, 1.1 mmol), and CuI (0.03 g, 0.16 mmol). The reaction gave the title compound (0.20 g, 95%)

p-BSU-CN

				<sup>13</sup> C-NMR (500 MHz, CDCl <sub>3</sub> )		
				δ (ppm) + Assignment		<u>M<sub>n</sub></u>
				14.17	y	24.4 kDa
				14.20	y'	
				22.78	x	<u>D</u>
				25.89	v, g	1.7
				29.43	f, h, u	
				31.73	w	<u>Repeat Unit</u>
				32.67	i	<u>Mass</u>
				68.21	e	699.4 amu
				69.74	t	
				85.27	m	<u>Repeat Unit</u>
				90.74	z	<u>Composition</u>
				93.16	aa	C <sub>47</sub> H <sub>57</sub> NO <sub>4</sub>
				95.76	k	
				103.01	a	
				110.01	c	
				111.51	ae	
				112.79	q	
				115.27	n	
				116.95	r, o	
				117.14	"	
118.69	af					
124.53	d					
128.59	ab					
130.46	j					
132.08	ac, ad					
132.16	"					
153.77	s, p					
154.09	"					
160.18	b					
<sup>1</sup> H-NMR (500 MHz, CDCl <sub>3</sub> )						
δ (ppm)	Mult. (J)	Int.	Assignment			
0.88	t	6	y			
1.34	m		w, x			
1.43	m	20	g, h			
1.52	m		v			
1.79	m	8	f, u			
2.03	m	4	i			
3.92	t	4	e			
4.01	t	4	t			
5.40	m	2	j			
6.44	t	1	a			
6.66	d	2	c			
6.99	s	2	r, o			
7.58	d	2	ad			
7.62	d	2	ac			

See the typical procedure for side chain coupling with polymer backbone. The compounds used 4-((4-ethynyl-2,5-bis(hexyloxy)phenyl)ethynyl)benzotrile (**H-SU-CN**) (0.15 g, 0.36 mmol), **p-B-I** (0.12 g, 0.29 mmol), piperidine (9 mL), toluene (9 mL), Pd(dba)<sub>2</sub> (0.02 g, 0.04 mmol), PPh<sub>3</sub> (0.16 g, 0.61 mmol), and CuI (0.02 g, 0.09 mmol). The reaction gave the title compound (0.15 g, 76%)

**p-BSSU-CN**

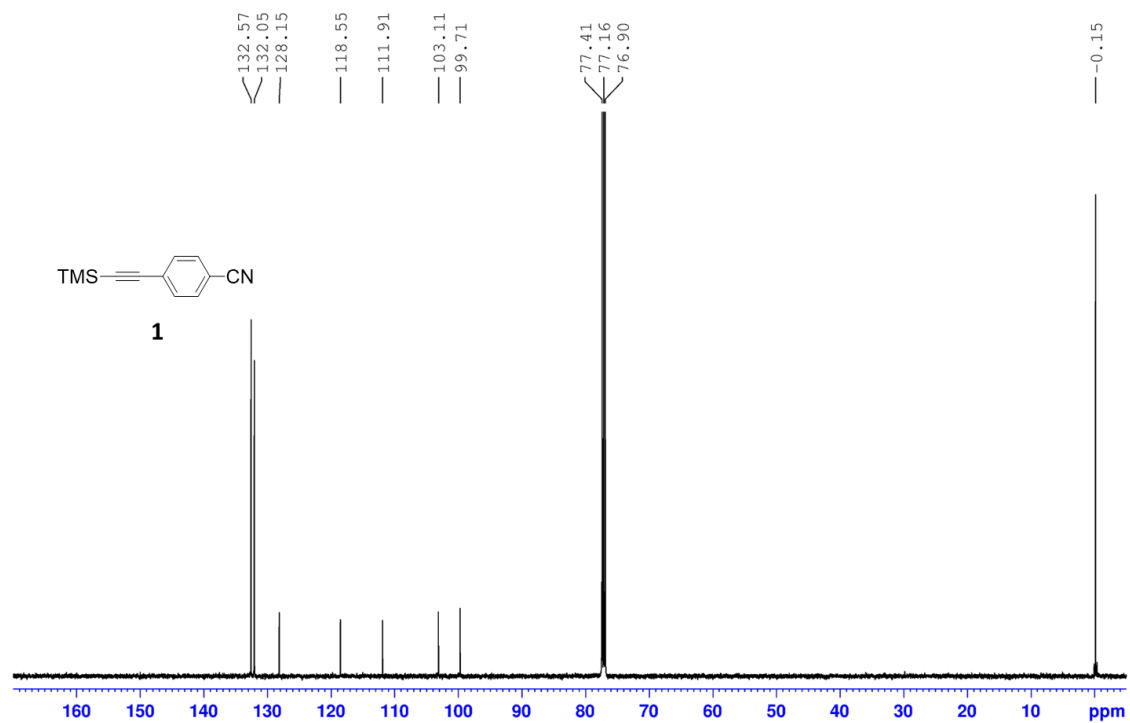
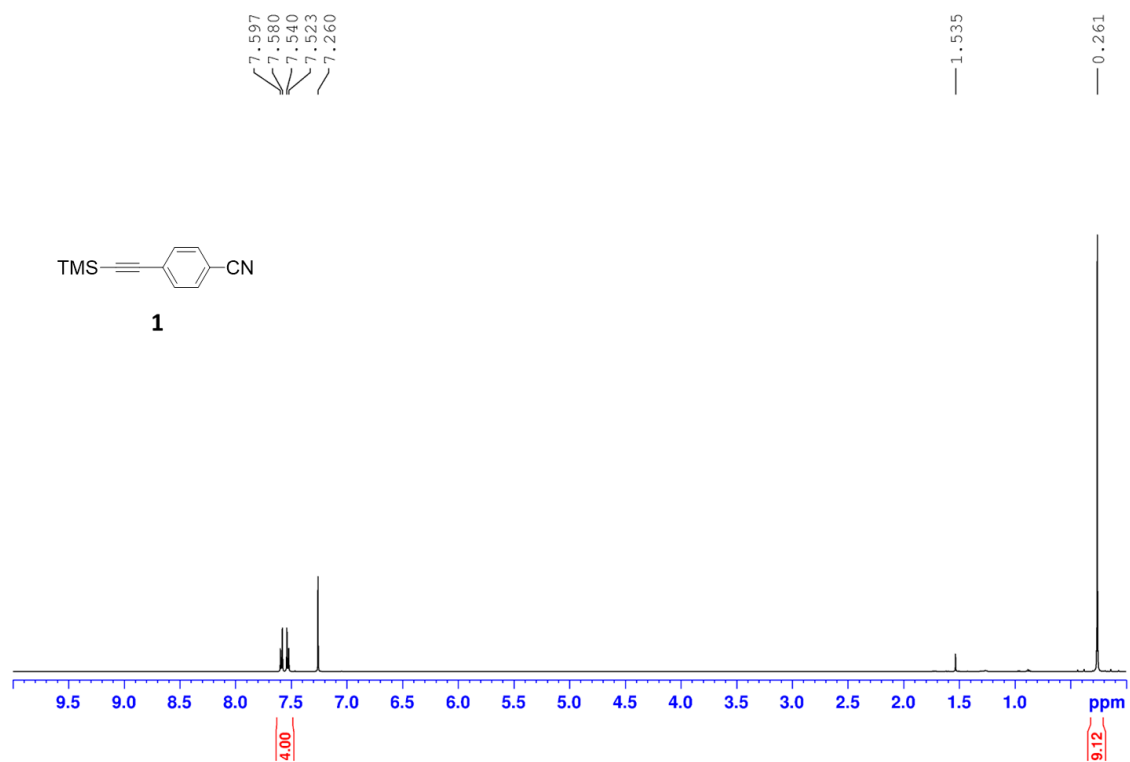
				<sup>13</sup> C-NMR (500 MHz, CDCl <sub>3</sub> )		
				δ (ppm)	Assignment	<u>M<sub>n</sub></u>
				14.17	y, am	31.3 kDa
				22.77	x, al	<u>D</u>
				25.87	g, v, aj	1.4
				29.44	f, h, u, ai	
				31.72	w, ak	
				32.52	i	<u>Repeat Unit</u>
				68.13	e	<u>Mass</u>
				69.79	t, ah	999.6 amu
				85.48	m	
				90.80	z	<u>Repeat Unit</u>
				91.37	an	<u>Composition</u>
				92.22	ao	C <sub>67</sub> H <sub>85</sub> NO <sub>6</sub>
				93.17	aa	
				95.34	k	
				102.92	a	
				109.97	c	
				111.49	as	
				112.77	q	
				114.22	ae	
				114.34	ab	
115.63	n					
117.08	o, r					
117.24	ac, af					
117.34	"					
118.69	at					
124.67	d					
128.60	ap					
130.42	j					
132.07	aq, ar					
132.15	"					
153.59	p, s, ad, ag					
153.71	"					
153.82	"					
154.08	"					
160.16	b					

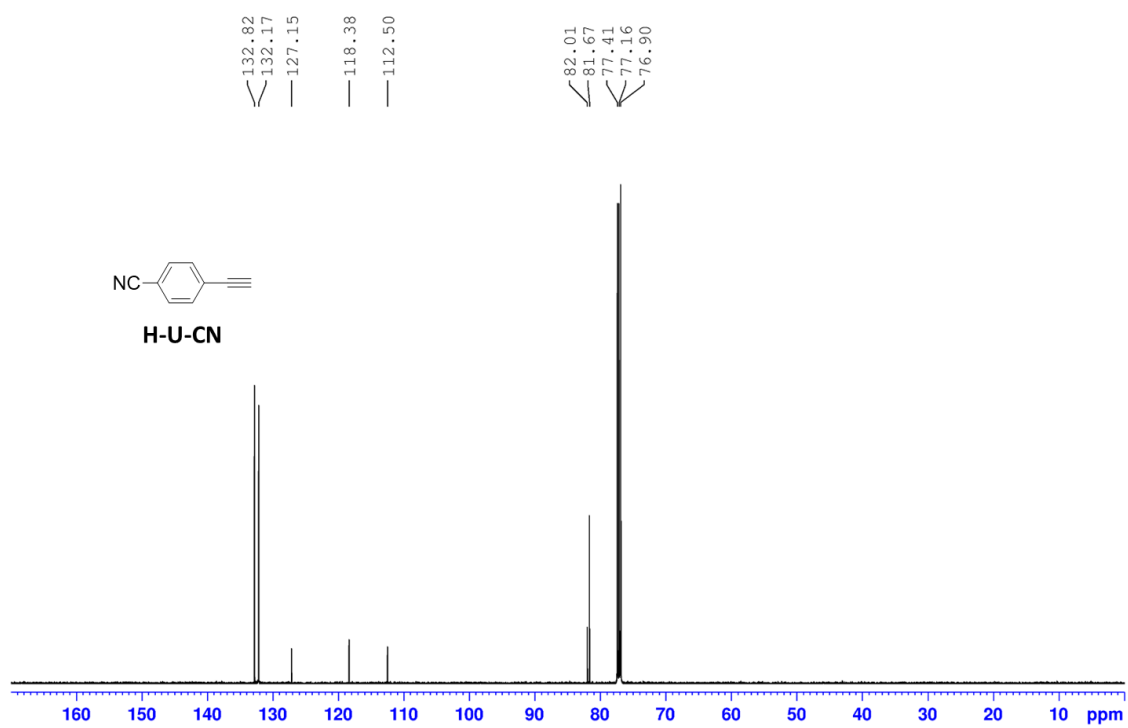
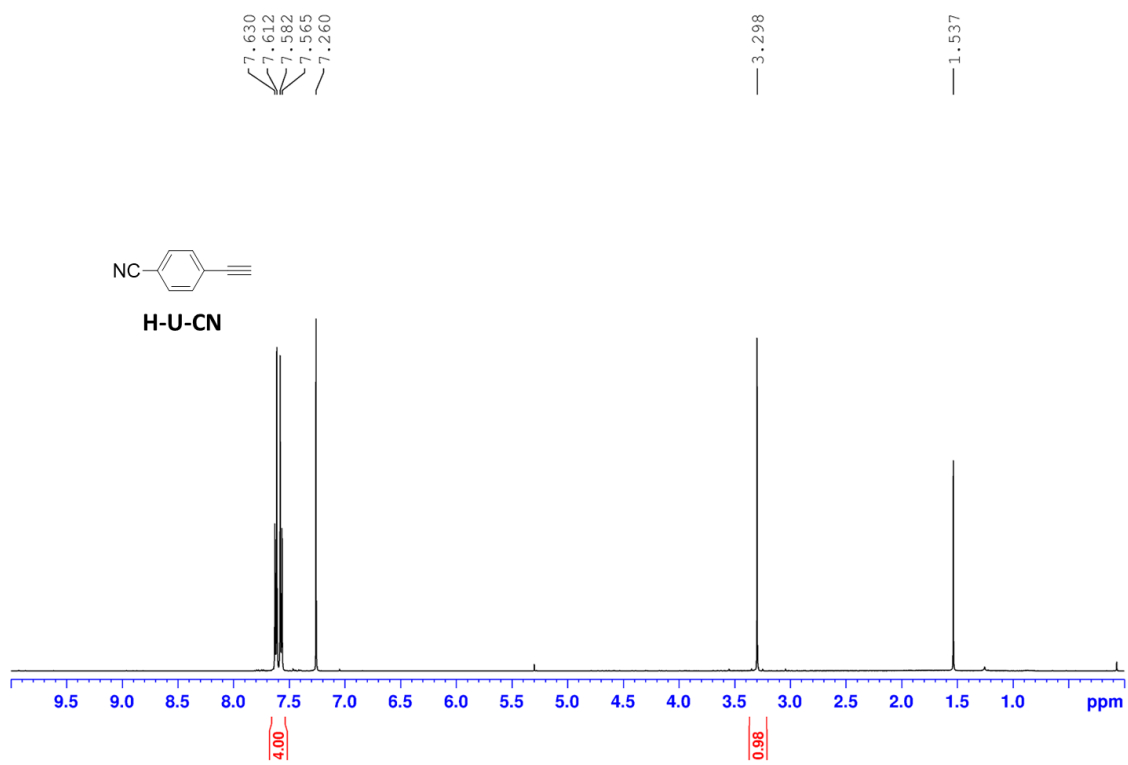
<sup>1</sup> H-NMR (500 MHz, CDCl <sub>3</sub> )			
δ (ppm)	Mult. (J)	Int.	Assignment
0.89	t	12	y, ak
1.35	m		w, x, ai, aj
1.44	m	34	g, h
1.52	m		v, ah
1.77	m		f, u
1.84	m	12	ag
2.08	m	4	i
3.93	t	4	af
4.03	t	8	e, t
5.41	m	2	j
6.45	t	1	a
6.67	d	2	c
7.01	m	4	ac, ad, o, r
7.59	d	2	ap
7.63	d	2	ao

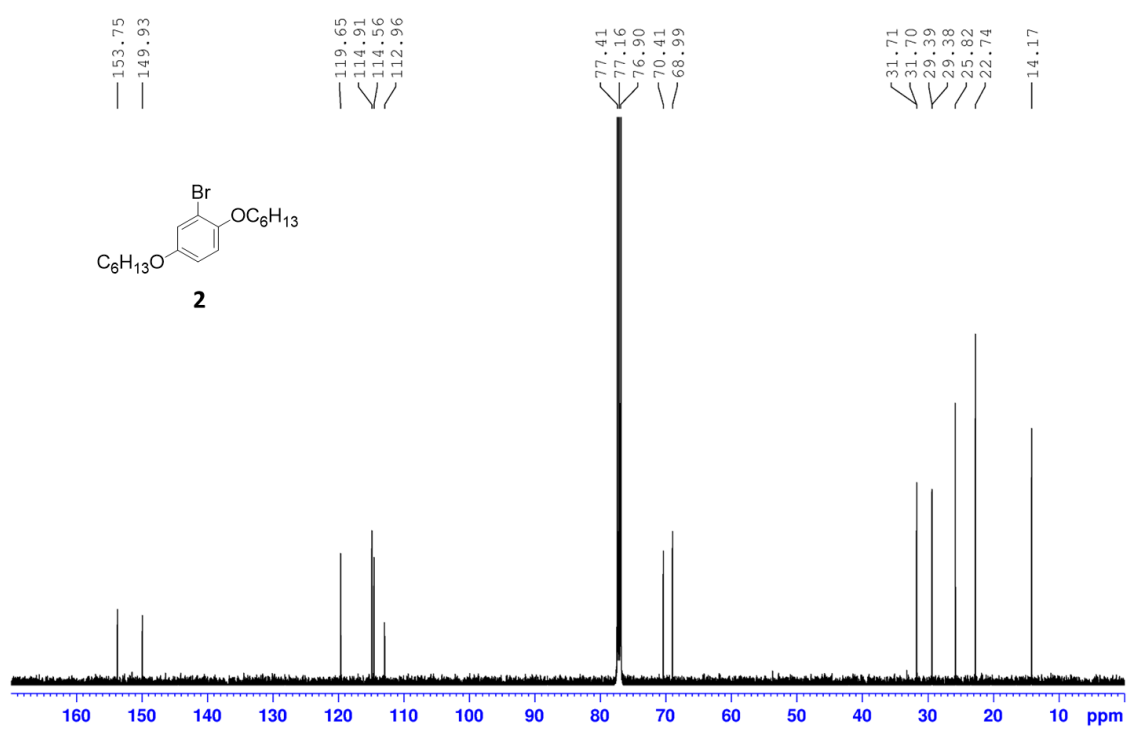
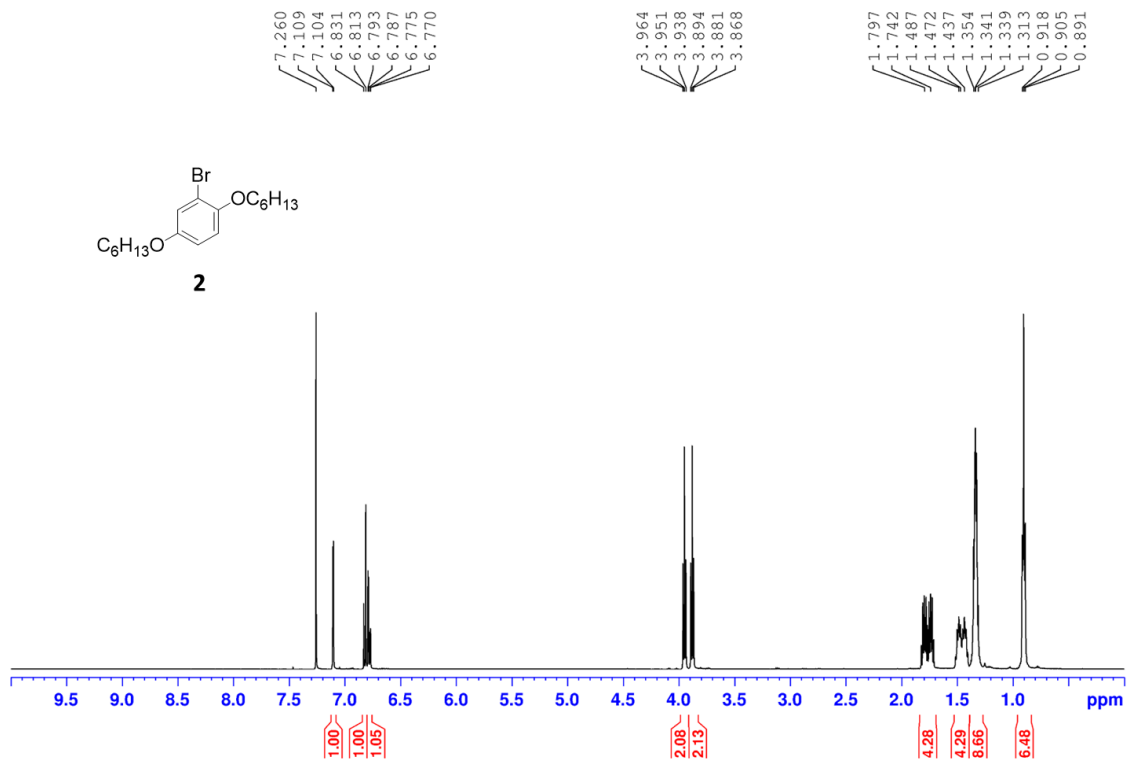
See the typical procedure for side chain coupling with polymer backbone. The compounds used 4-((4-ethynyl-2,5-bis(hexyloxy)phenyl)ethynyl)benzonitrile (**H-SSU-CN**) (0.22 g, 0.31 mmol), **p-B-I** (0.09 g, 0.22 mmol), piperidine (9 mL), toluene (9 mL), Pd(dba)<sub>2</sub> (0.02 g, 0.03 mmol), PPh<sub>3</sub> (0.12 g, 0.46 mmol), and CuI (0.01 g, 0.07 mmol). The reaction gave the title compound (0.17 g, 78%)

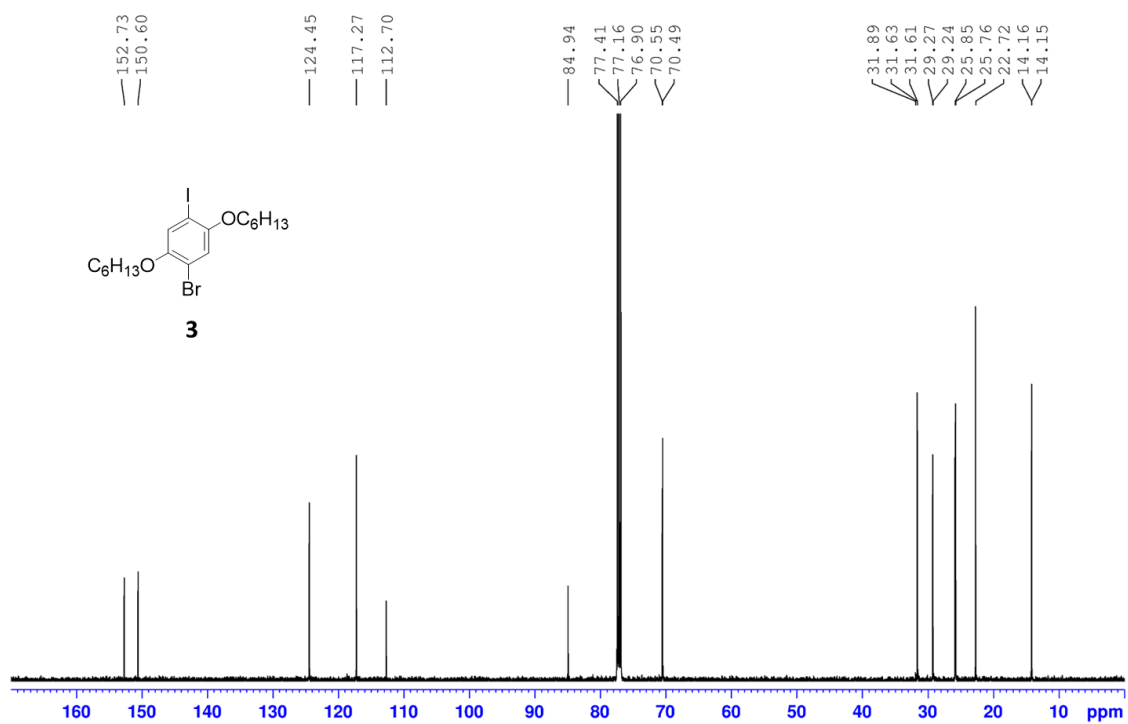
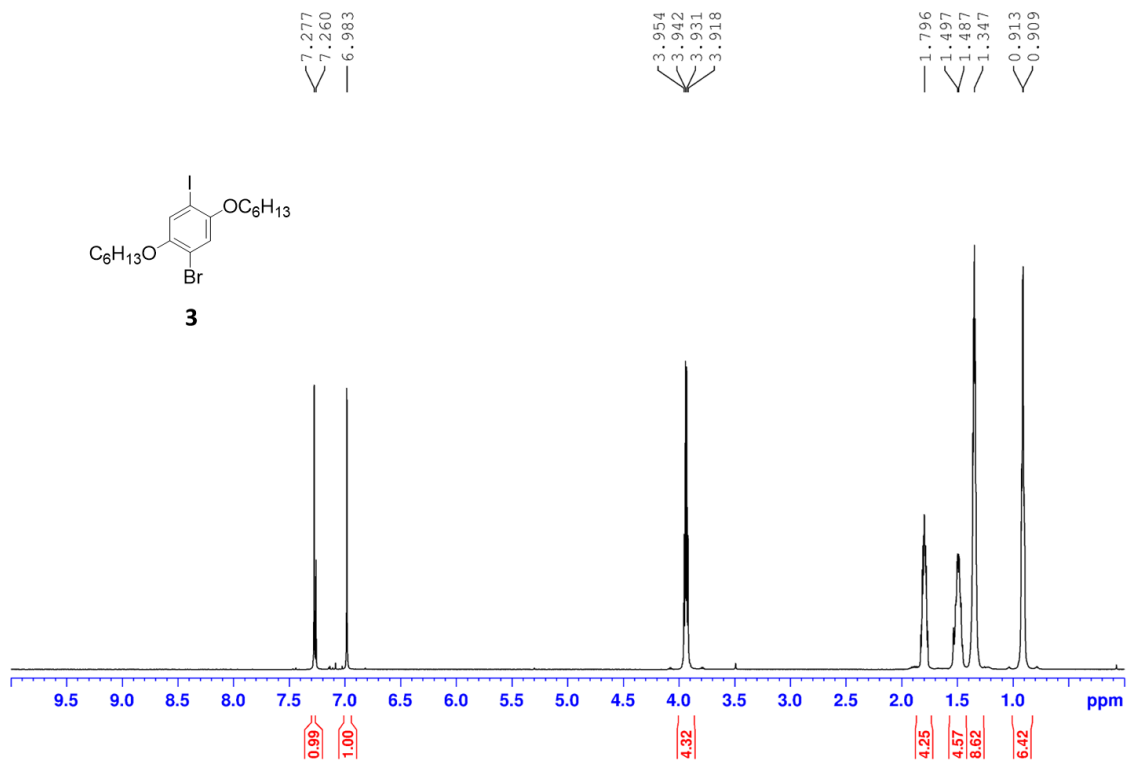
## Appendix A.1.4 NMR

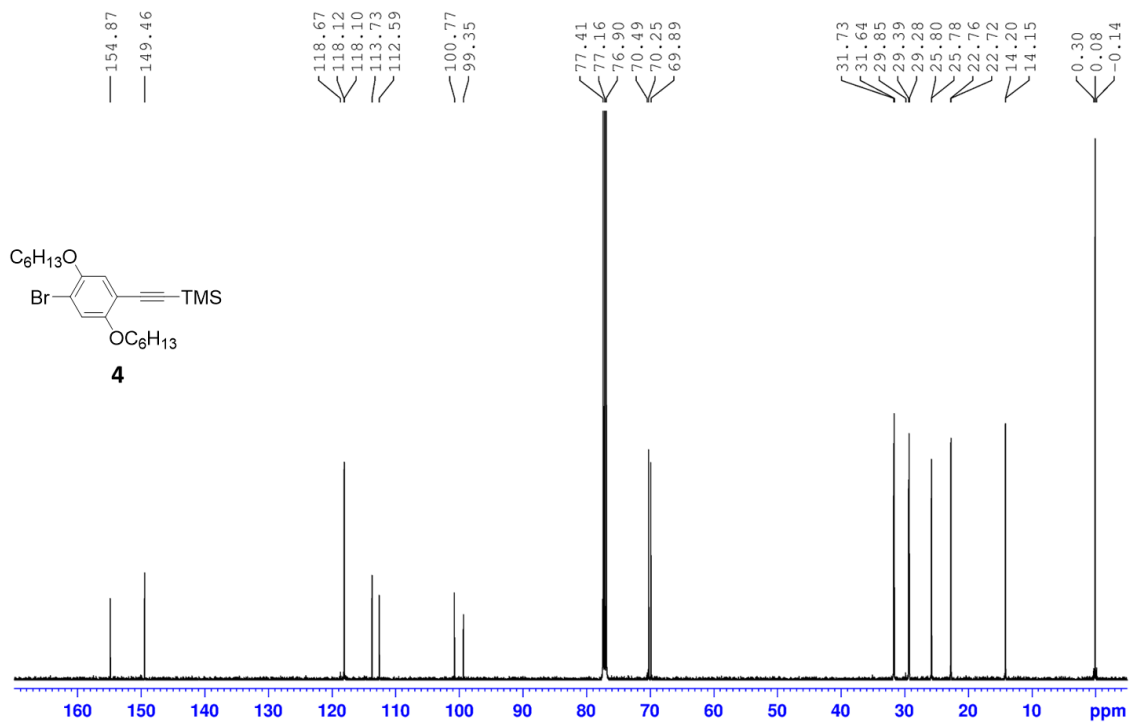
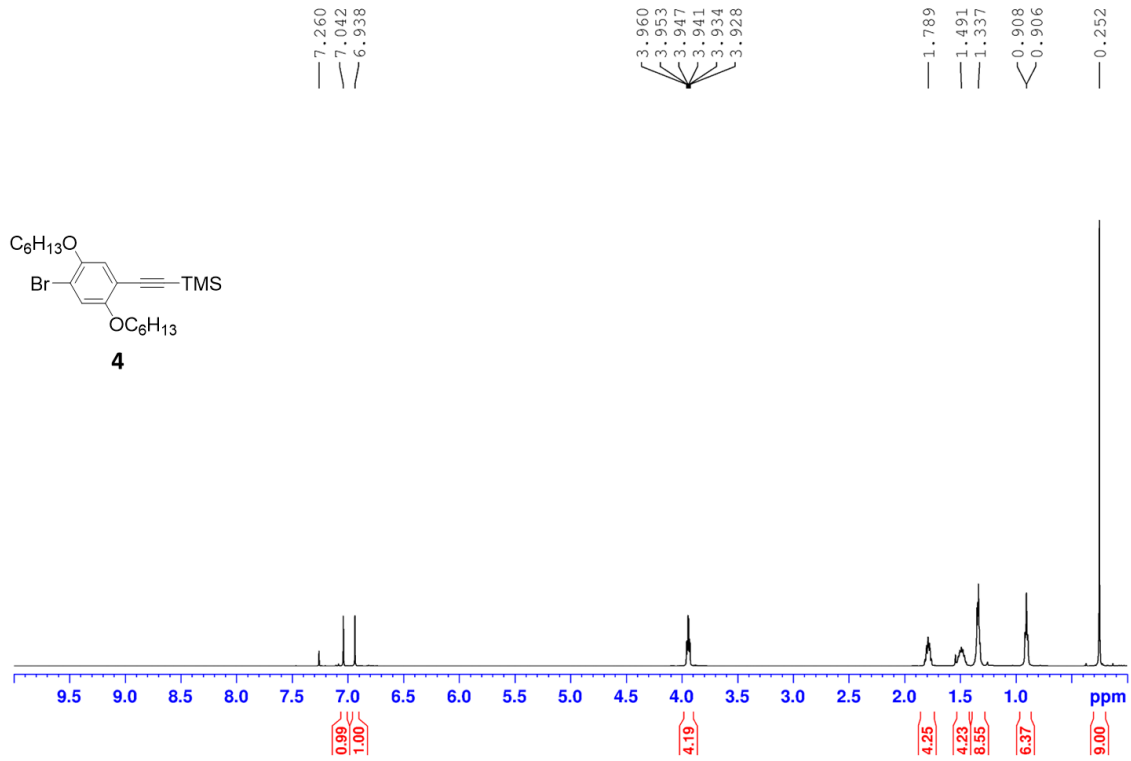


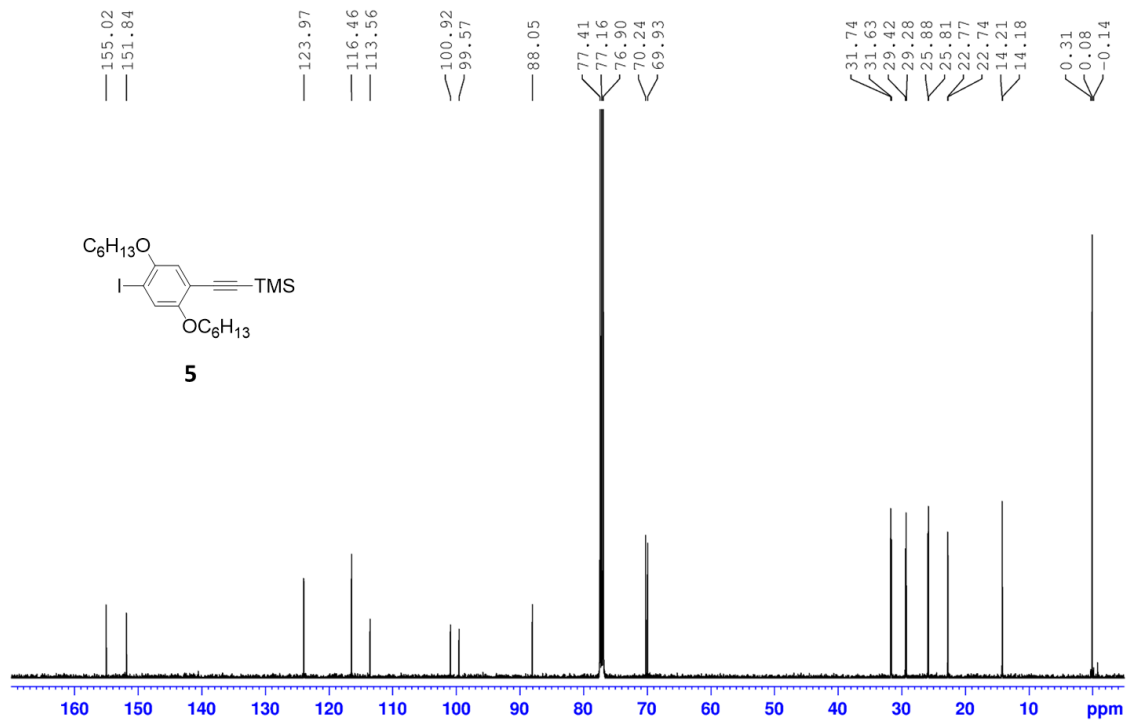
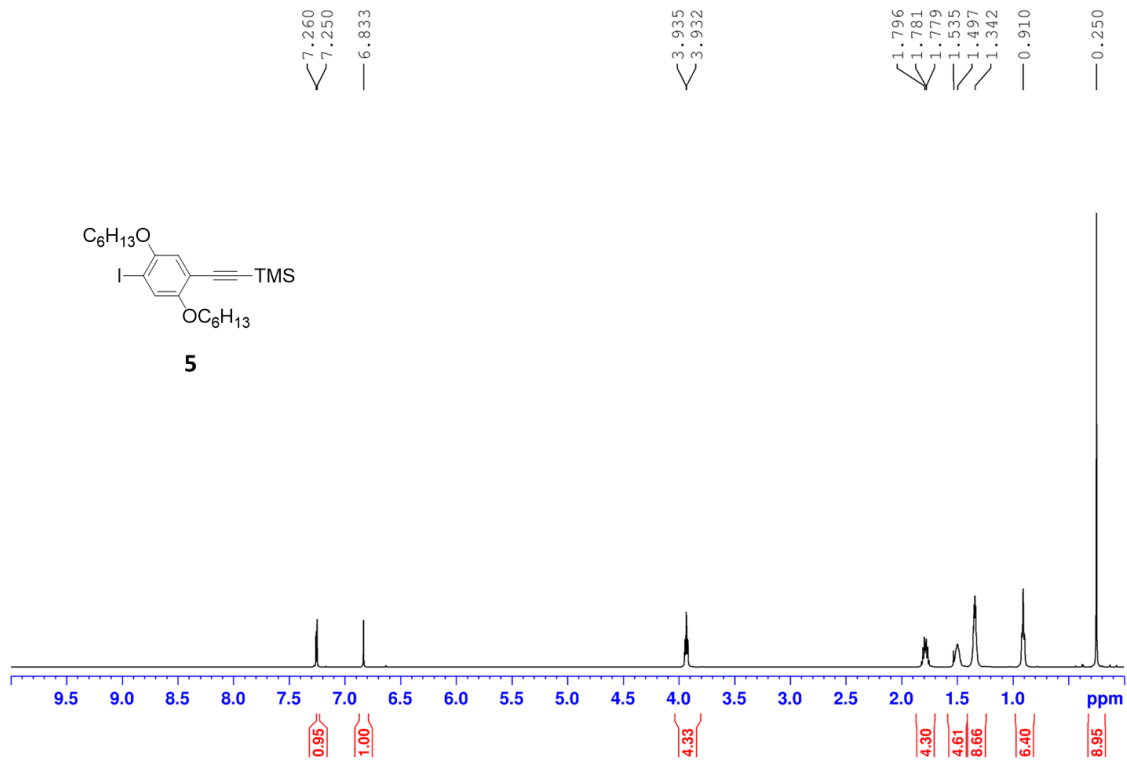


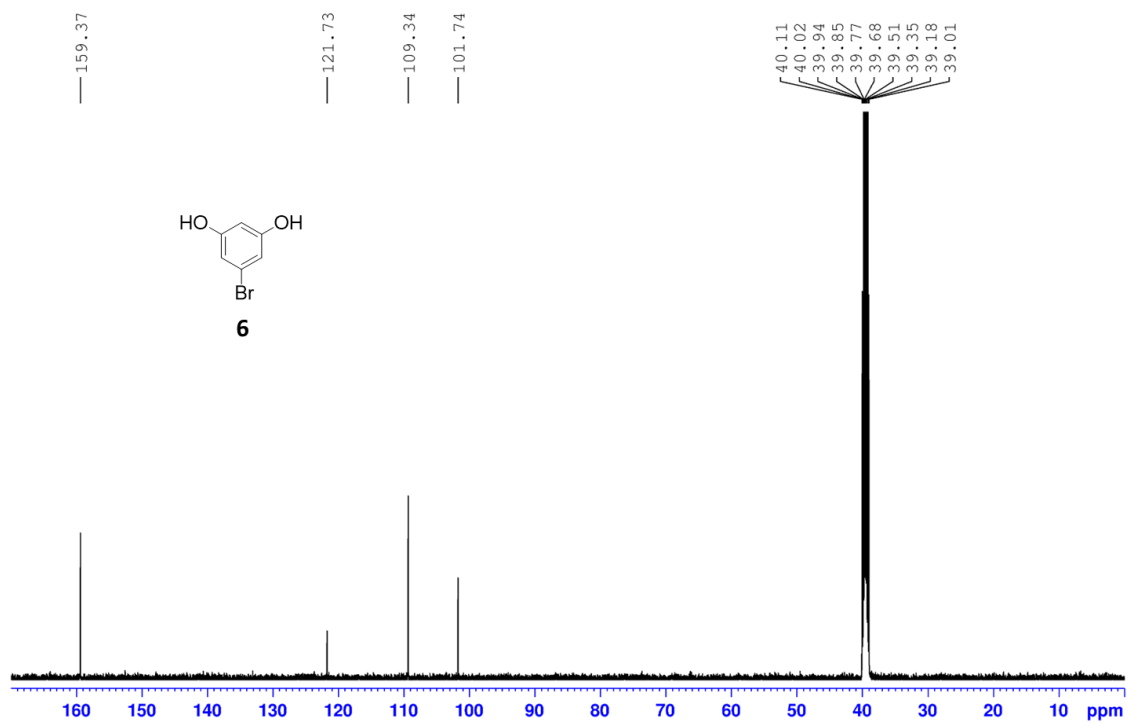
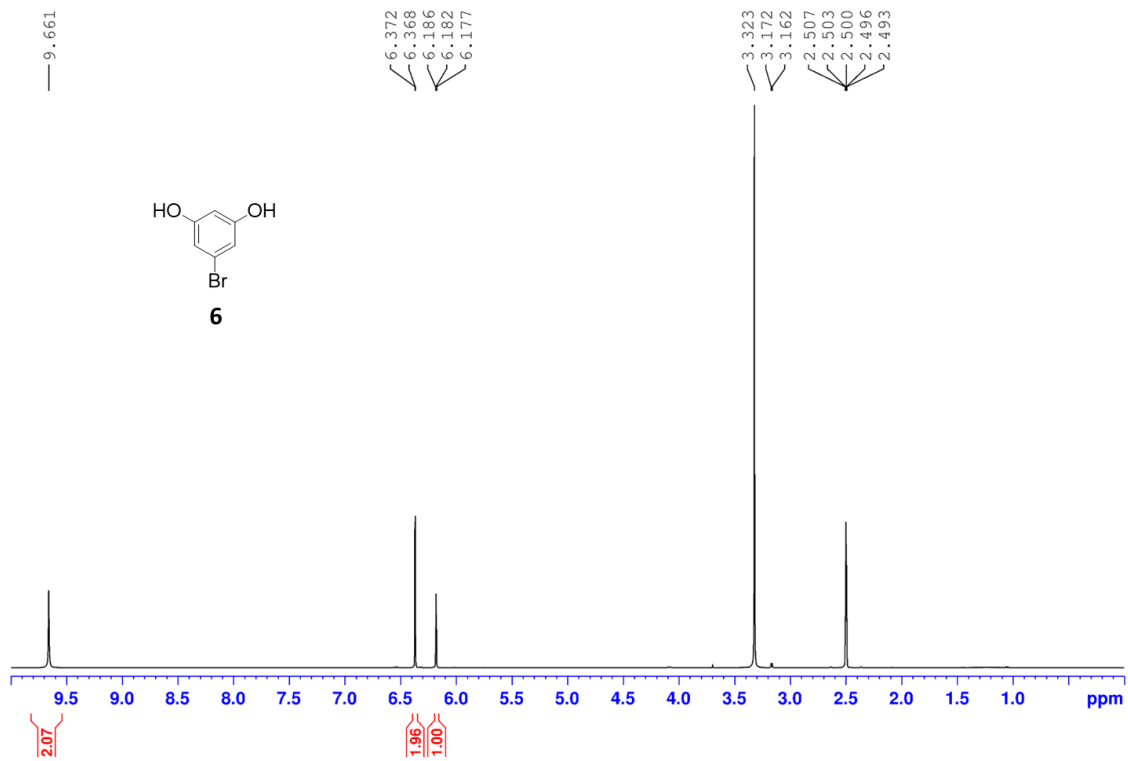


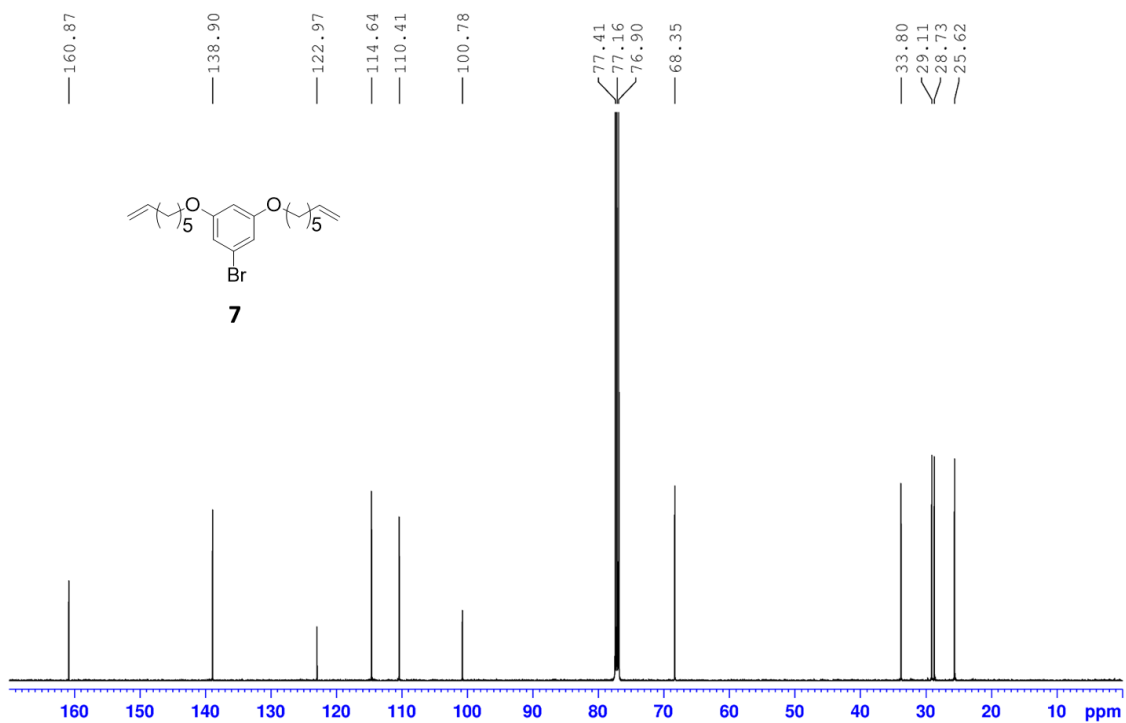
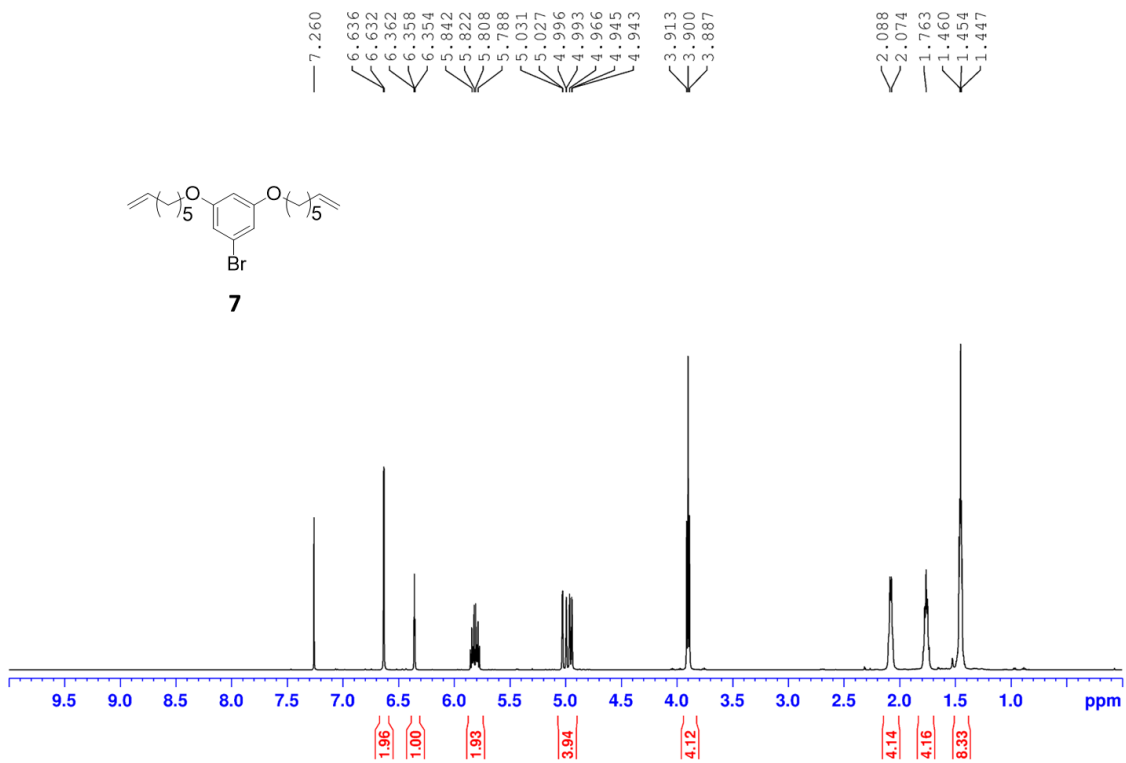
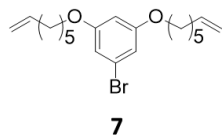


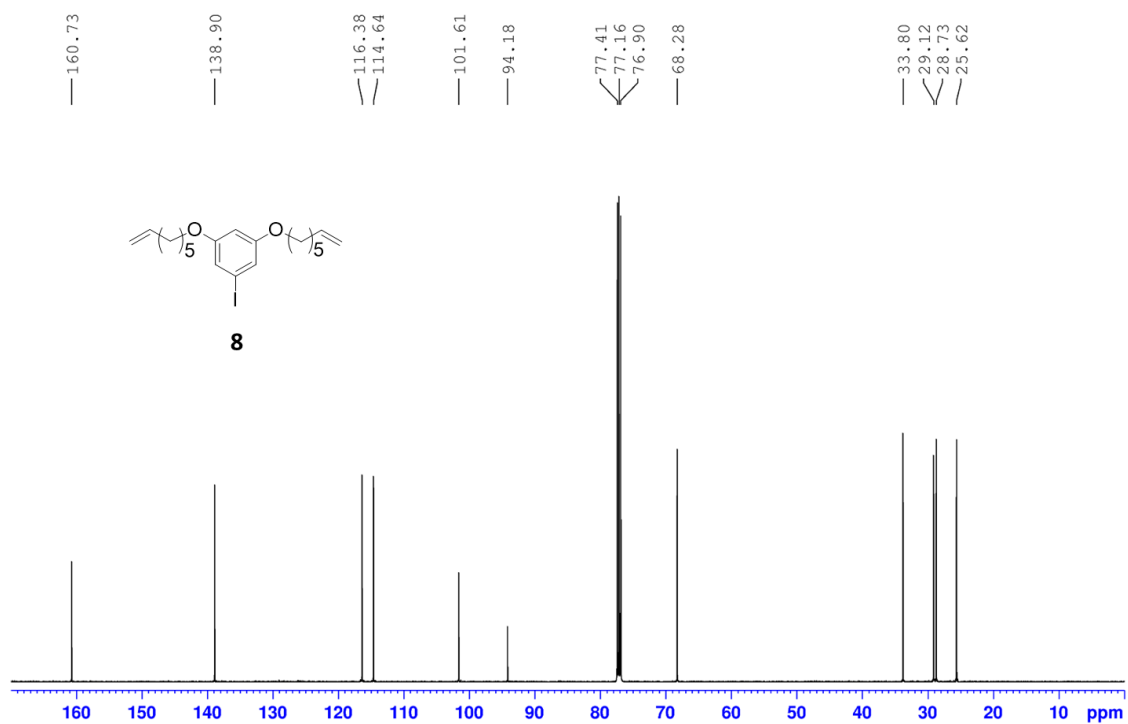
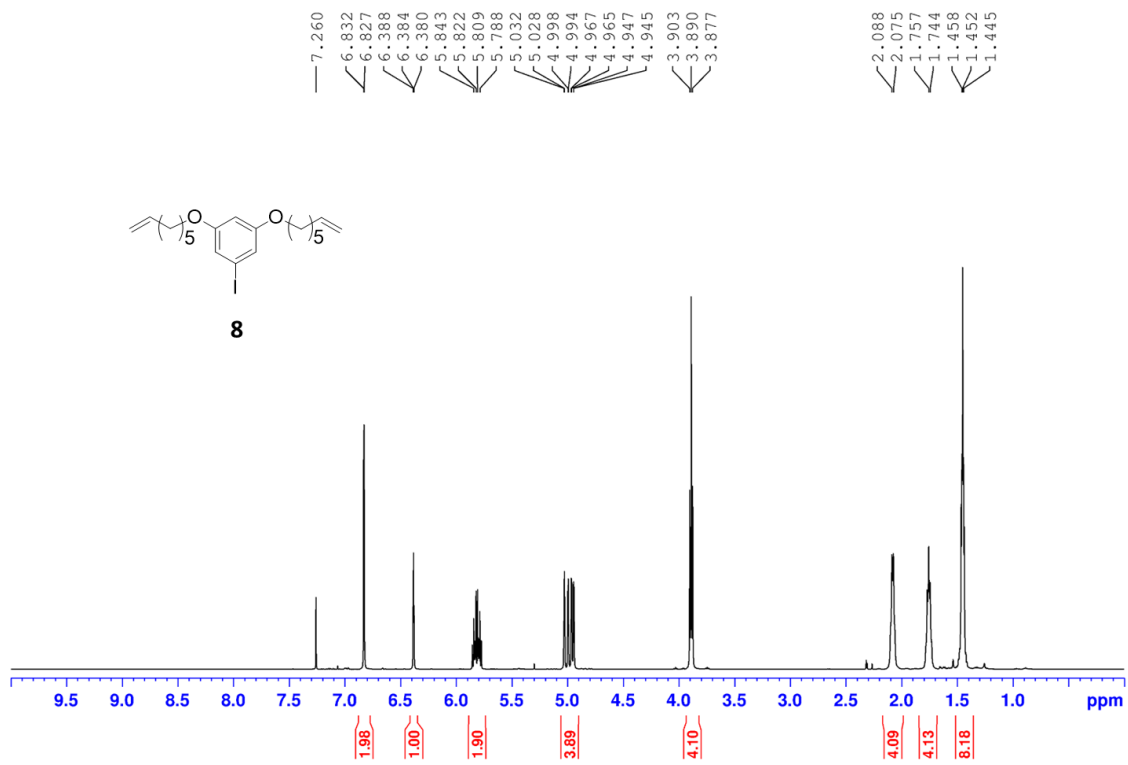




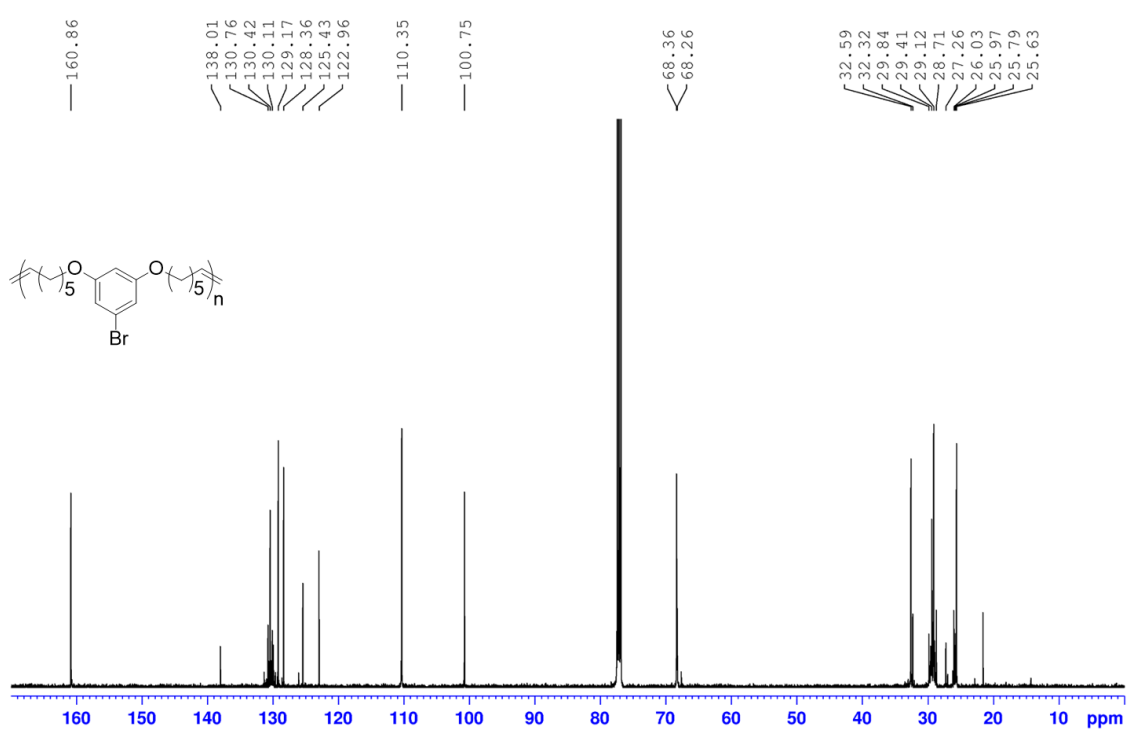
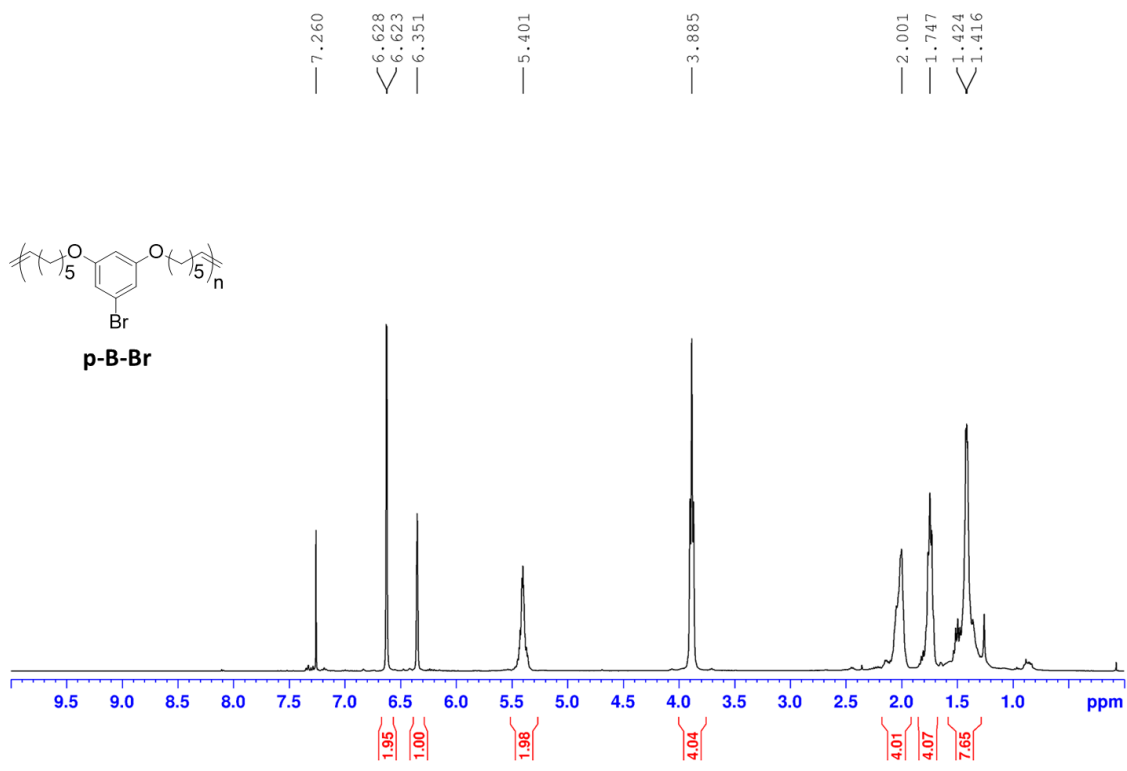


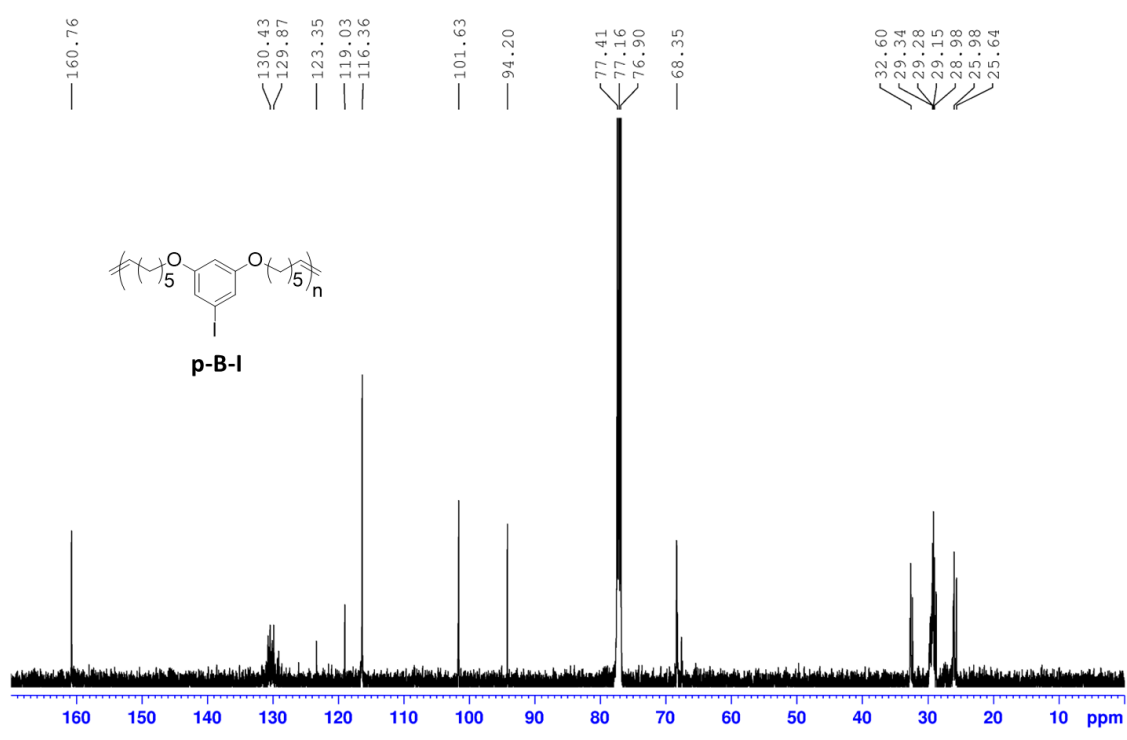
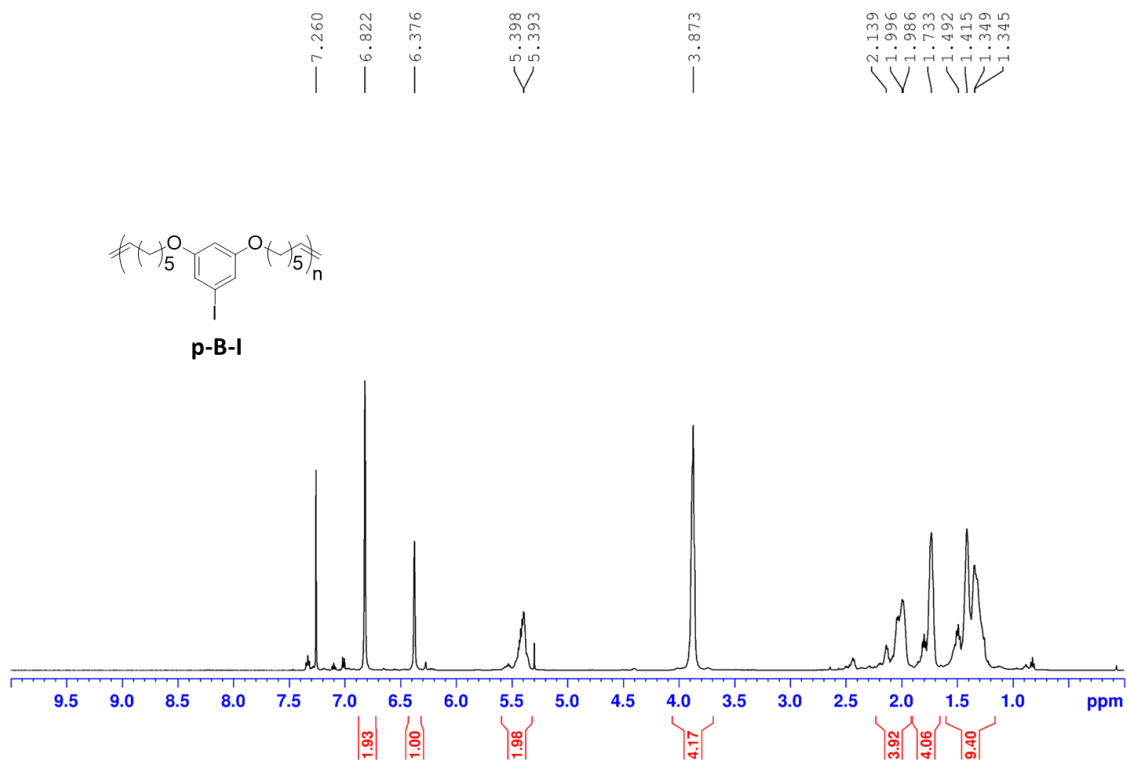


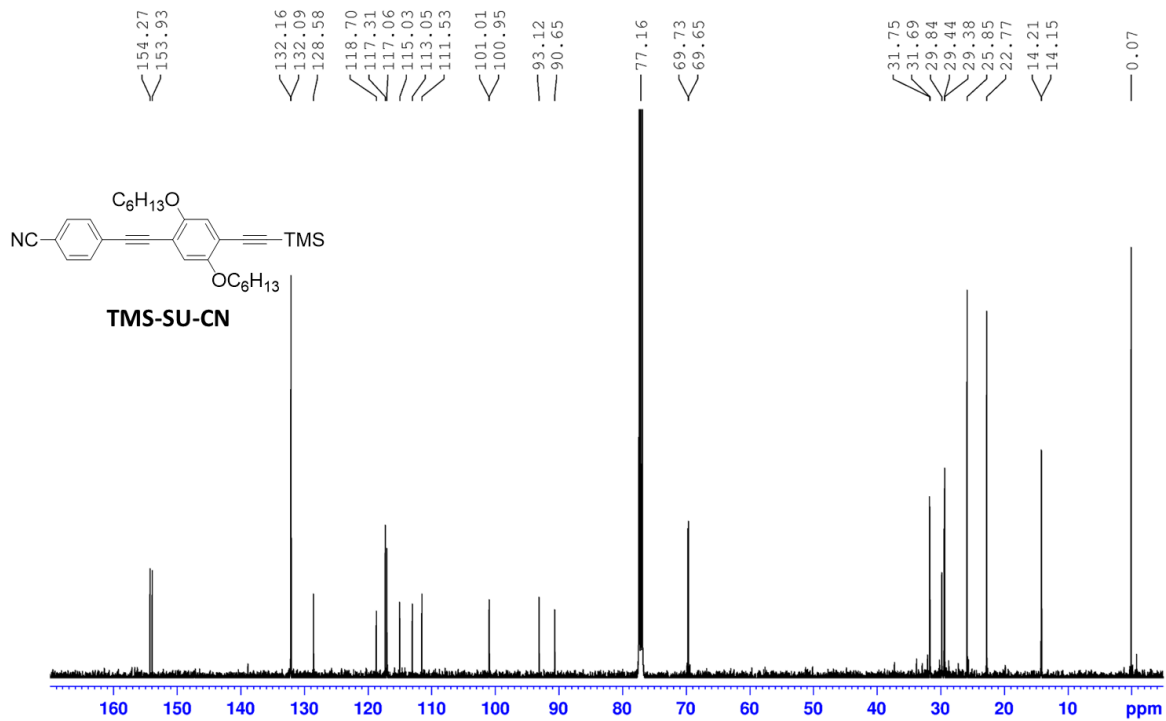
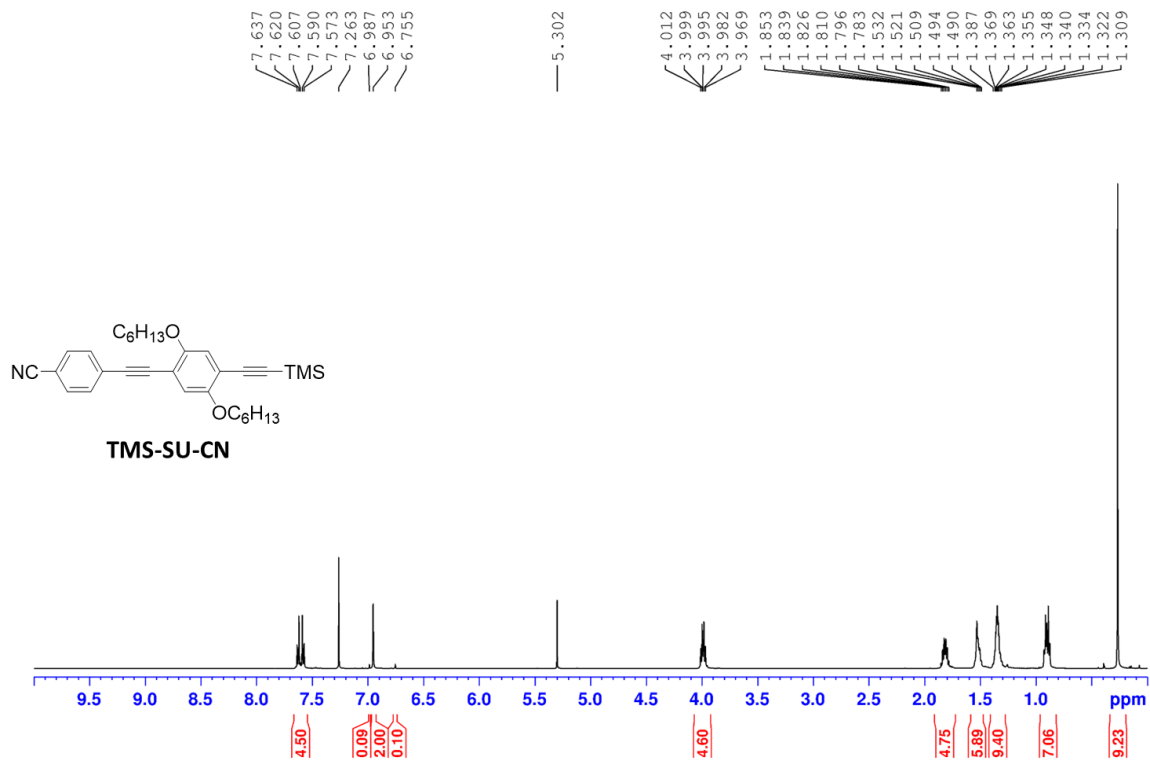


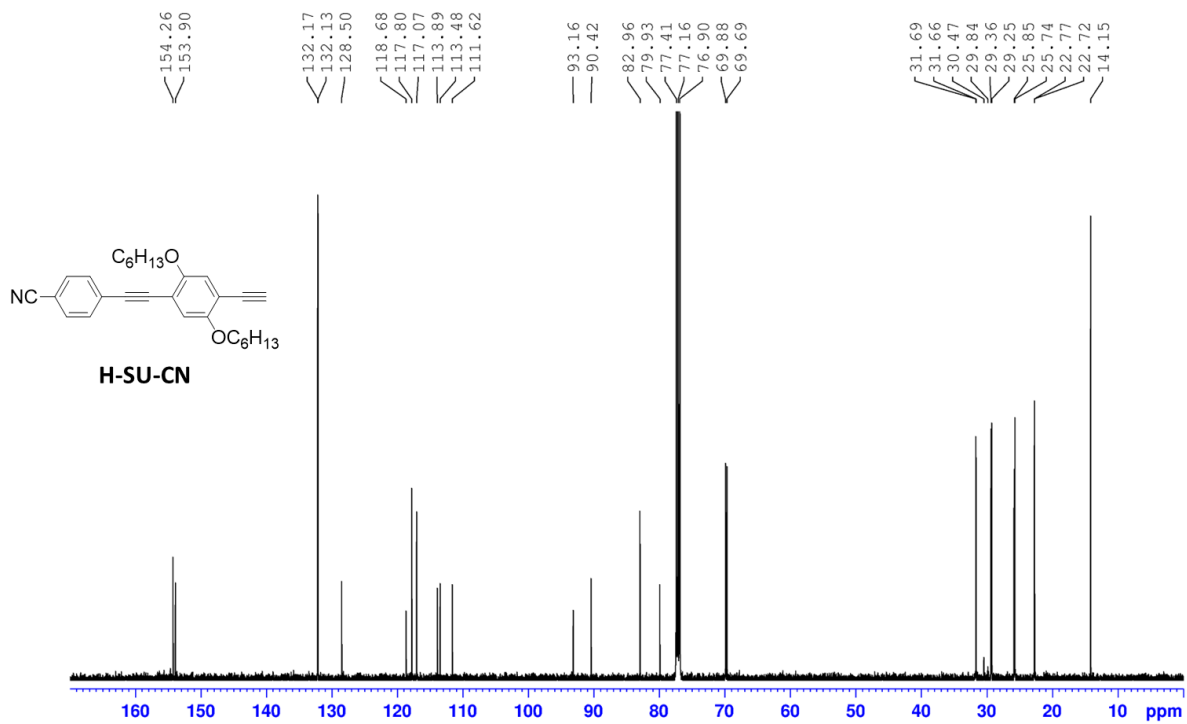
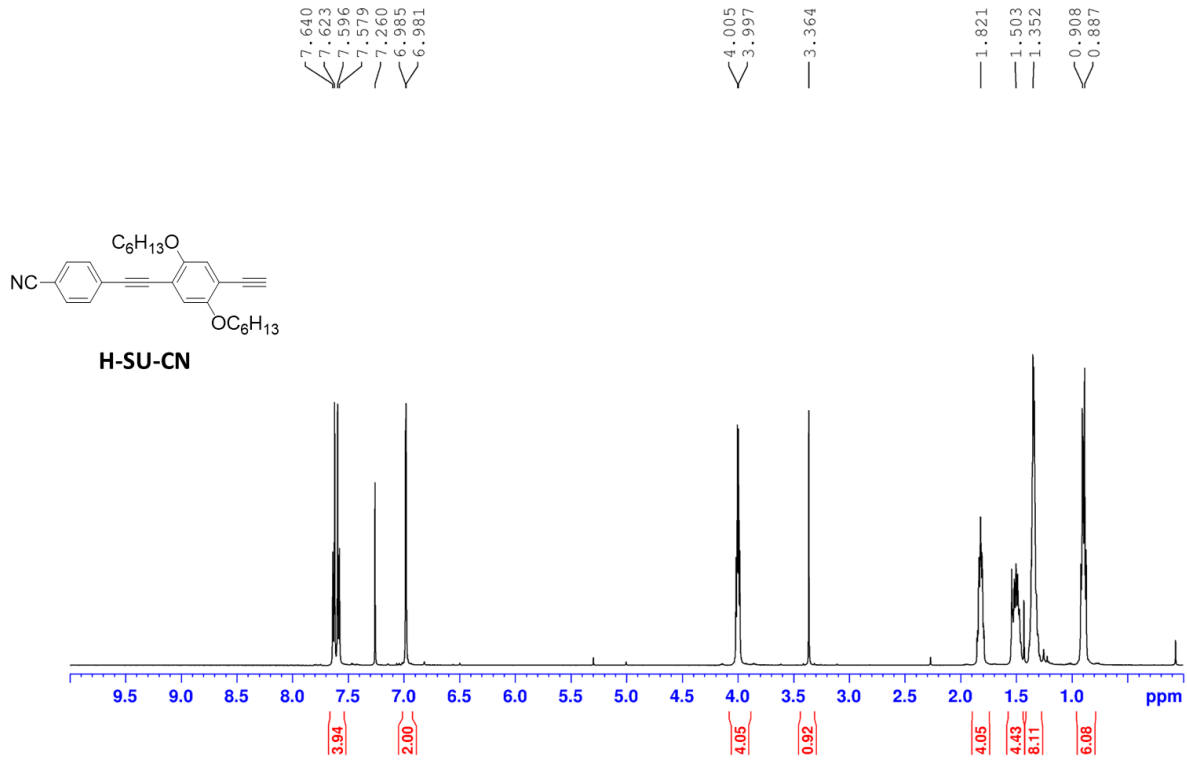


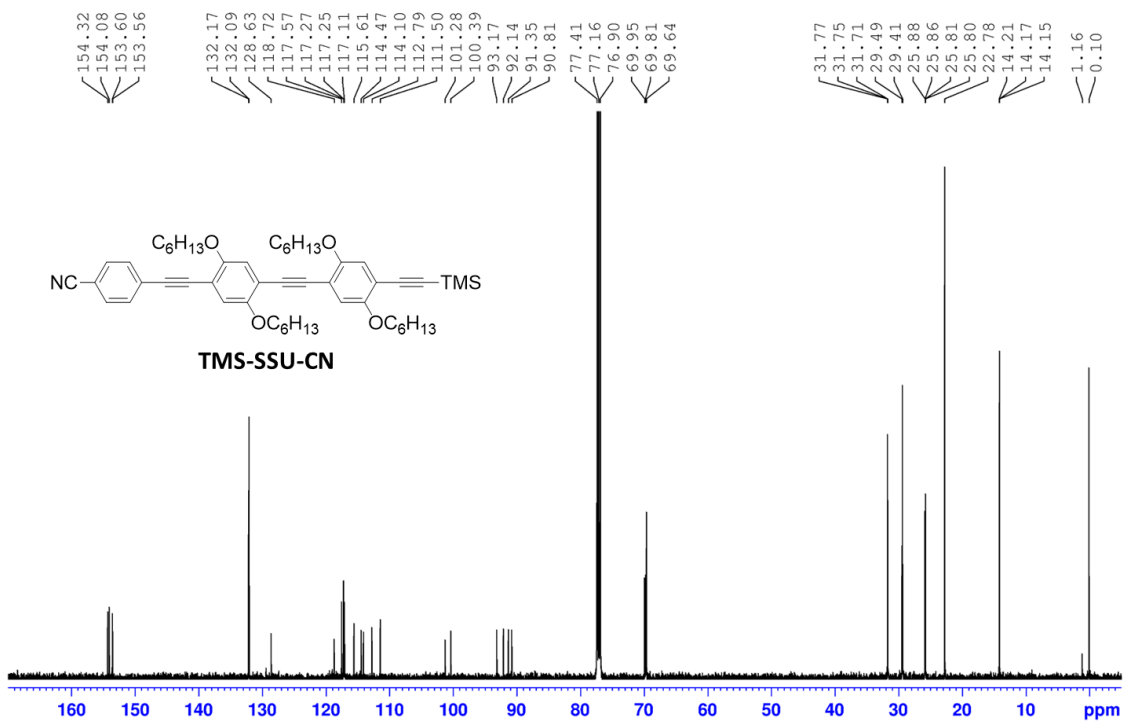
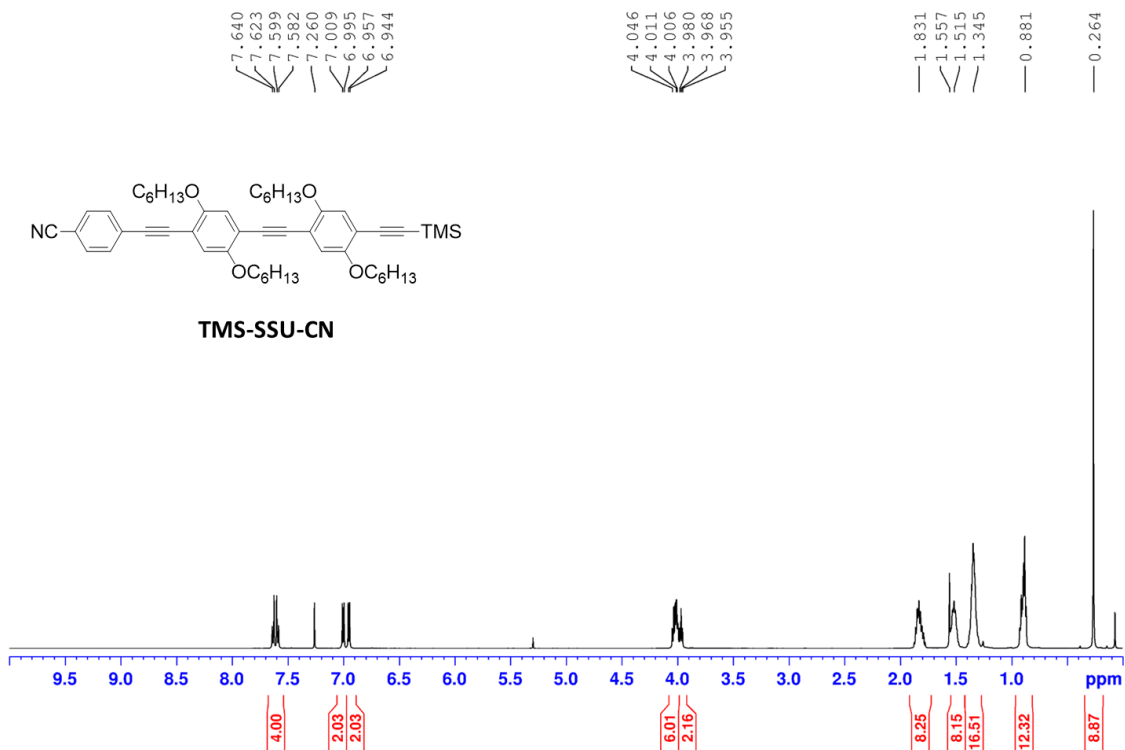


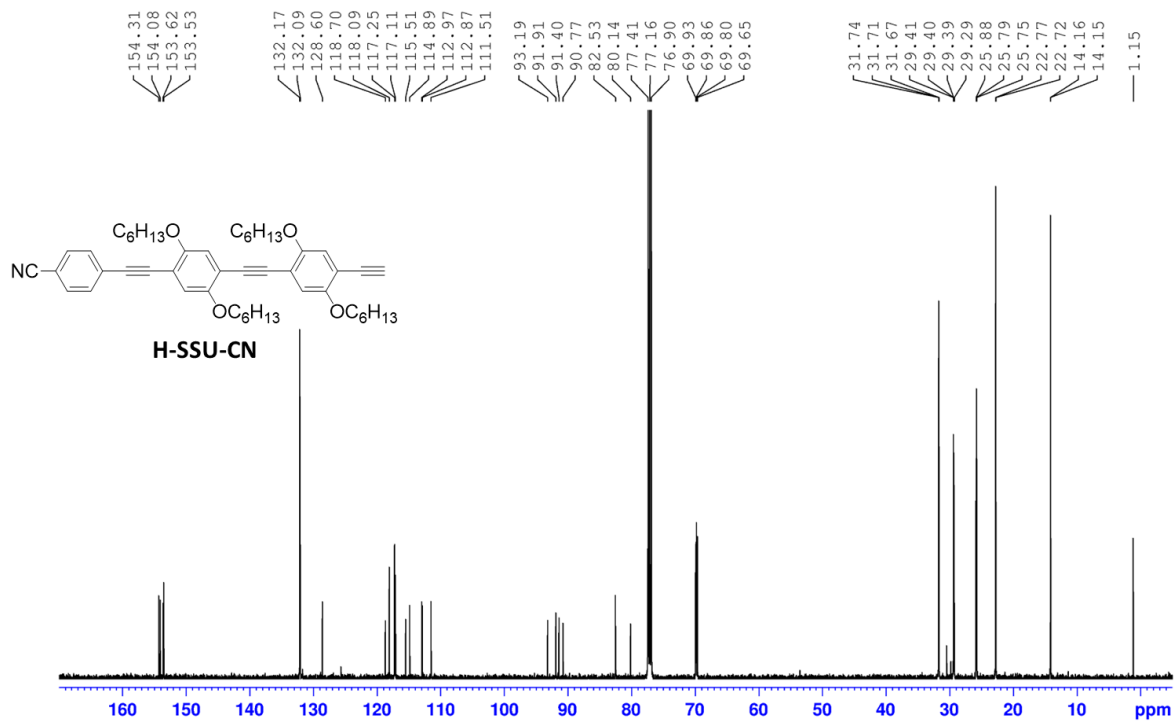
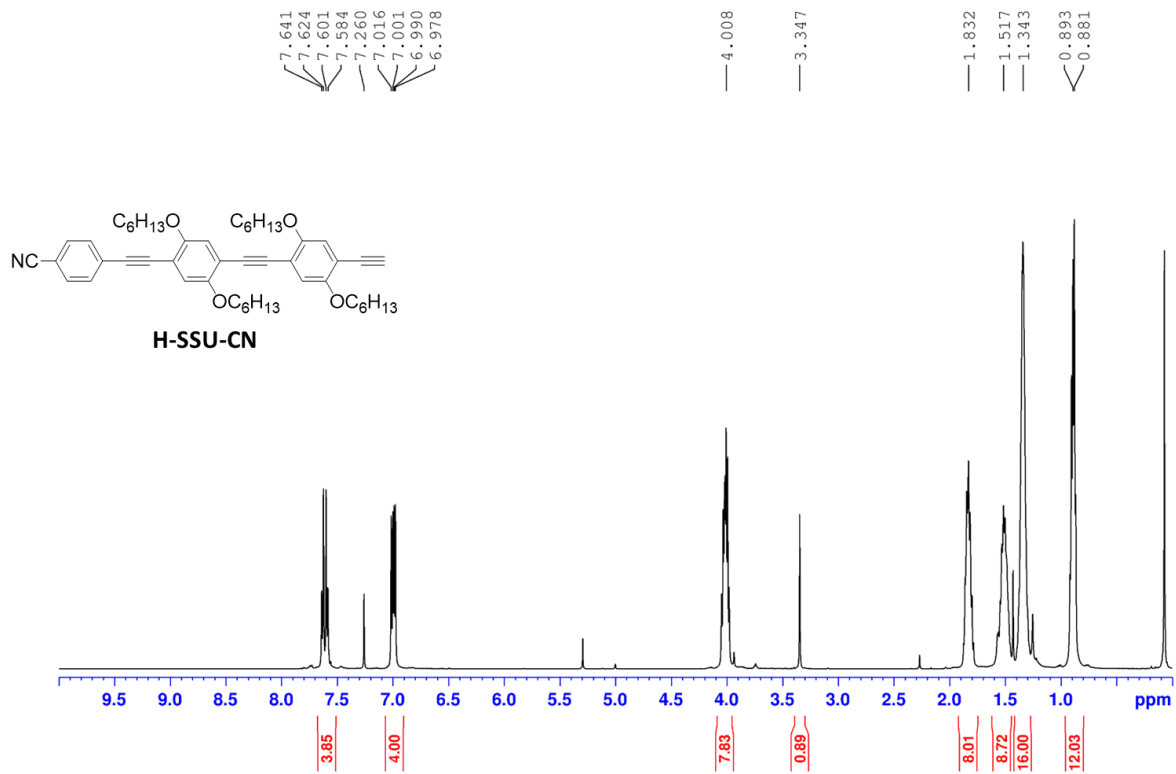


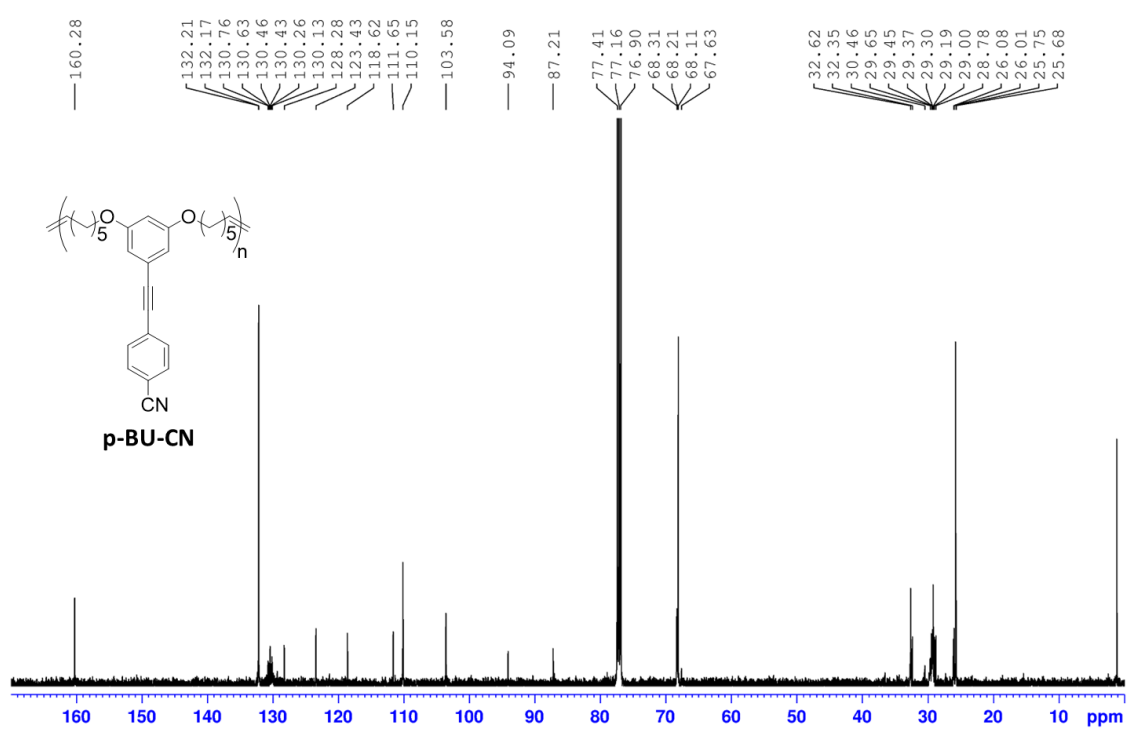
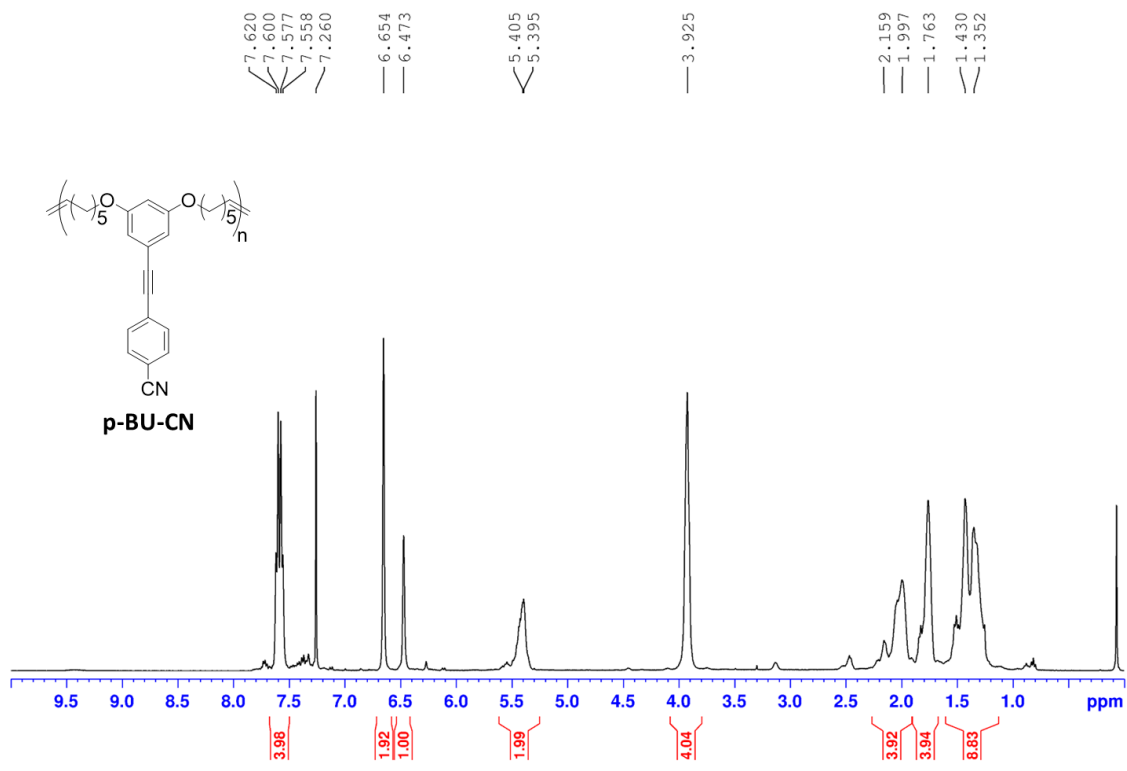


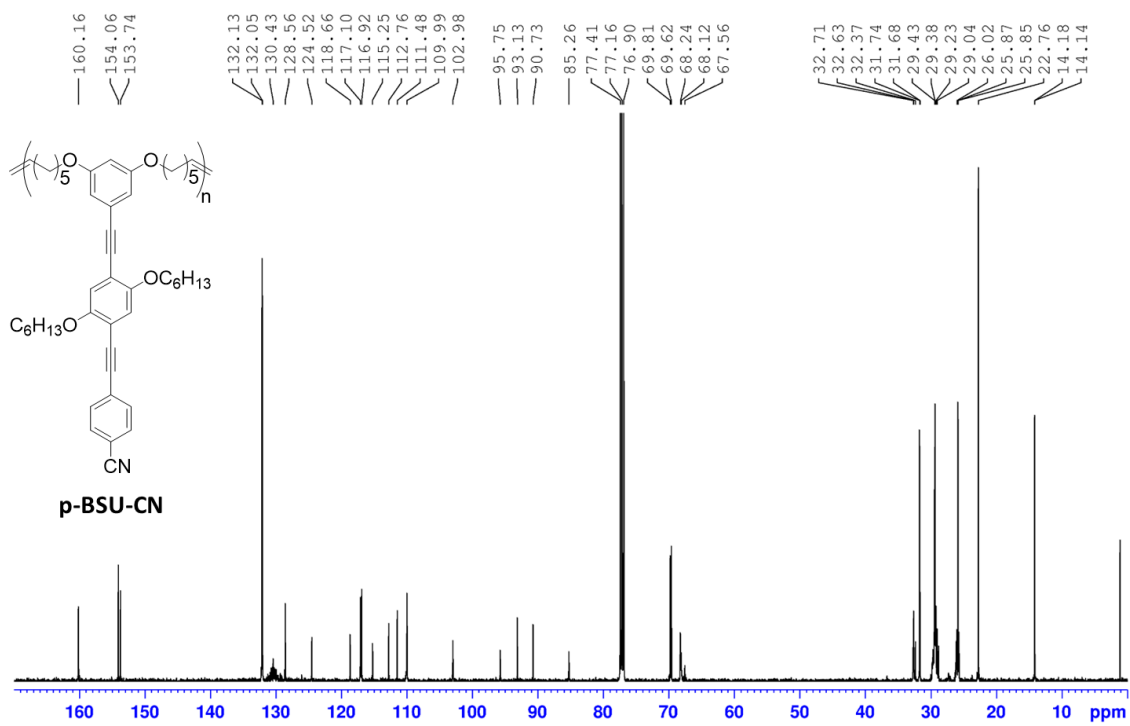
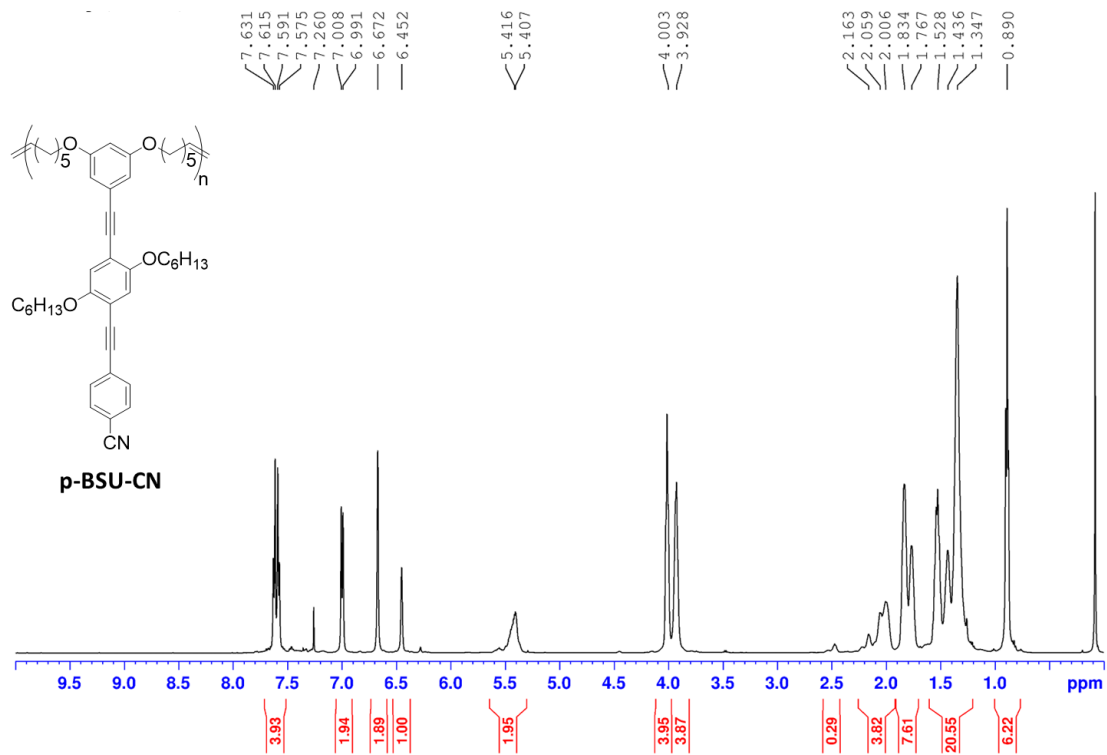




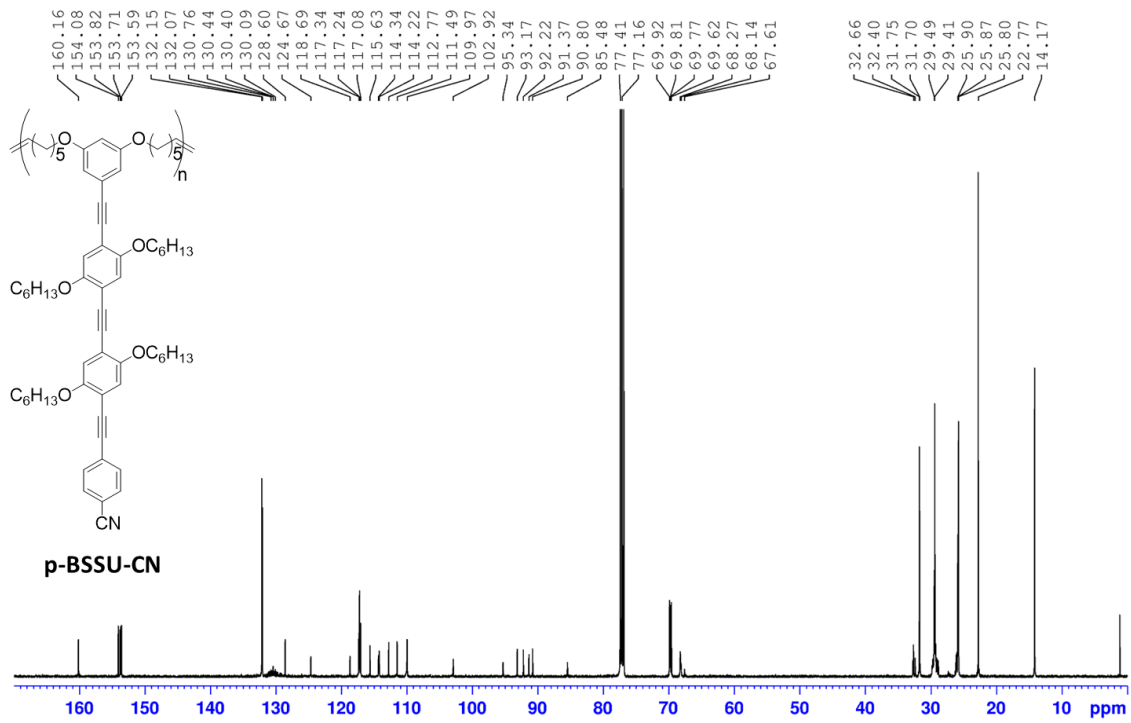
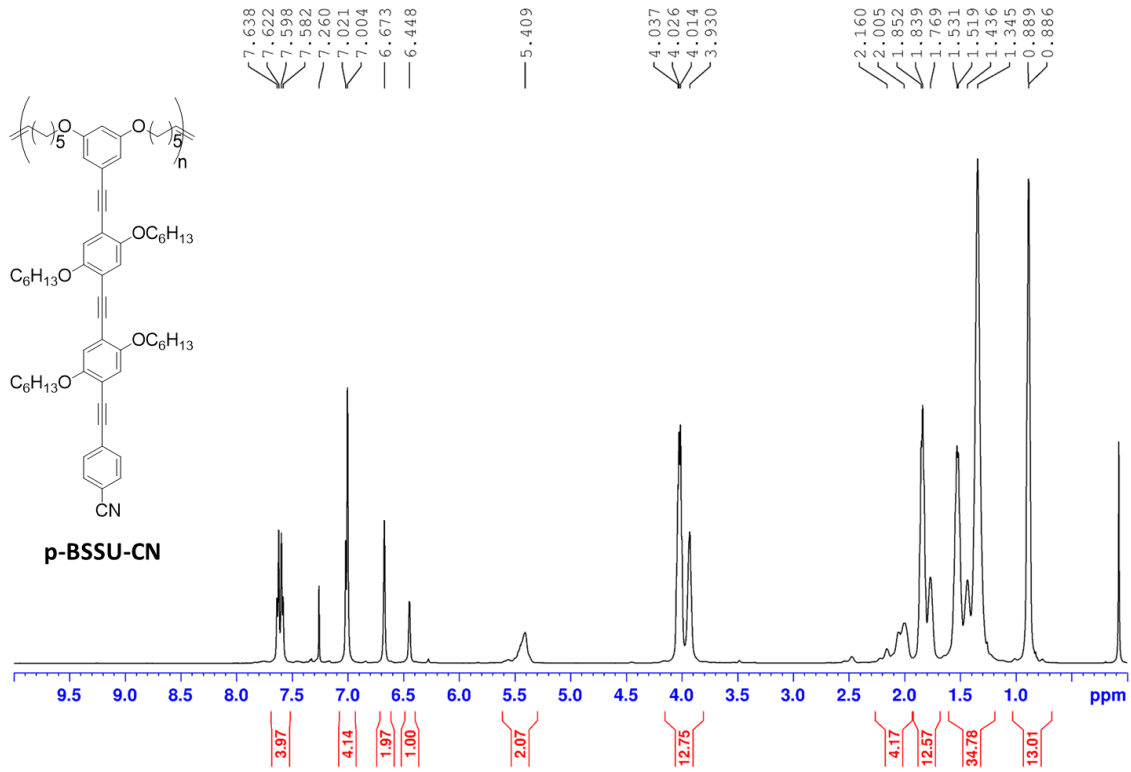




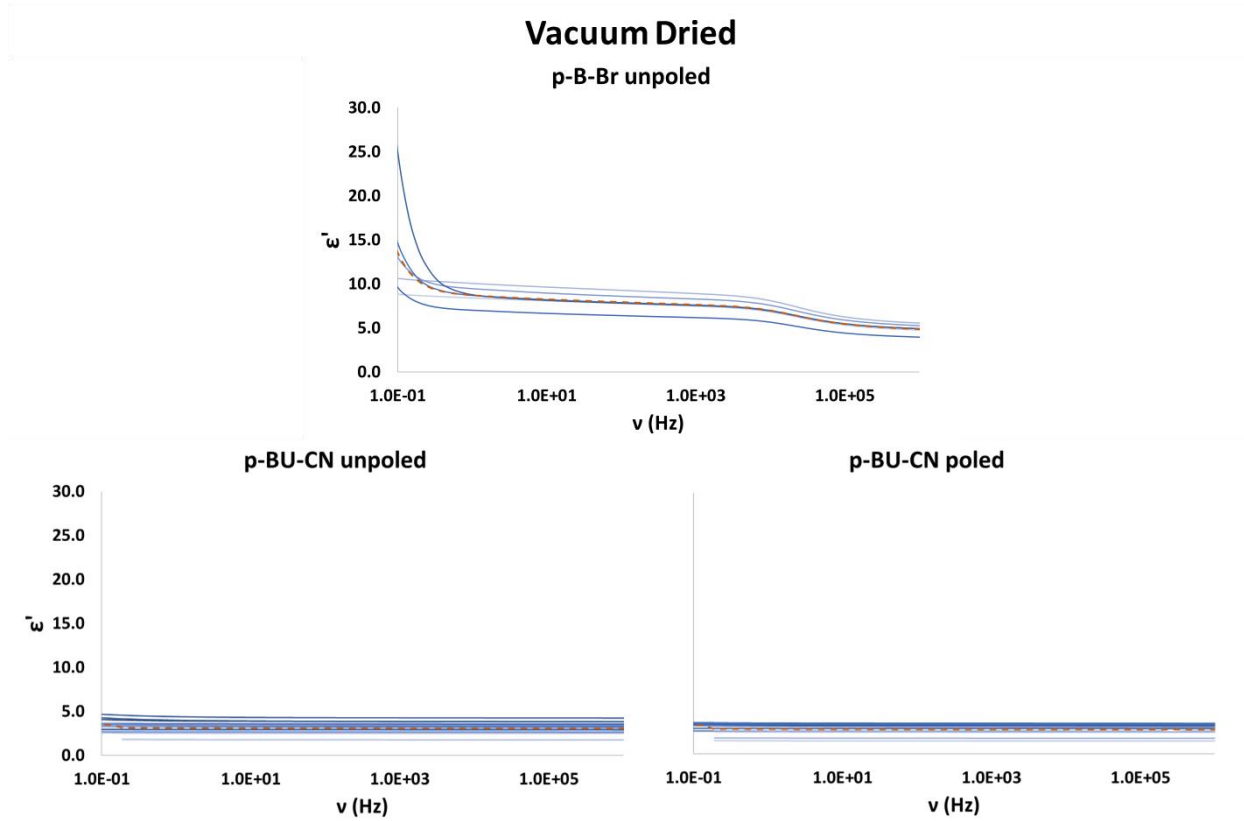








## Appendix A.2 Broadband Dielectric Spectroscopic Data



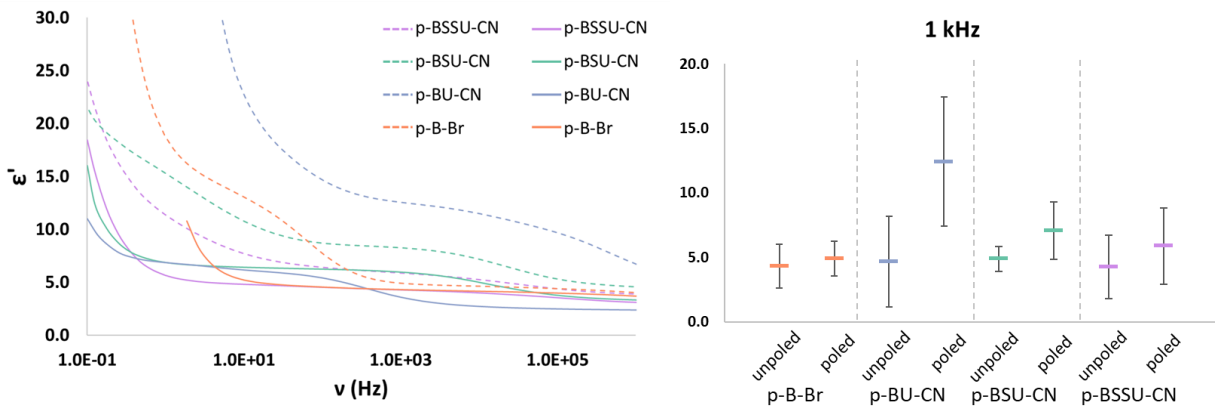
Appendix Figure 1: Permittivity, as a function of frequency, of all the vacuum dried samples (blue curves), measured at 20 °C, and the average of each (orange dashed curves); unpoled **p-B-Br** (top), unpoled **p-BU-CN** (bottom left) and poled **p-BU-CN** (bottom right)

Appendix Table 1: Average permittivities for all of the poled and unpoled polymers at 1 kHz and 20 °C

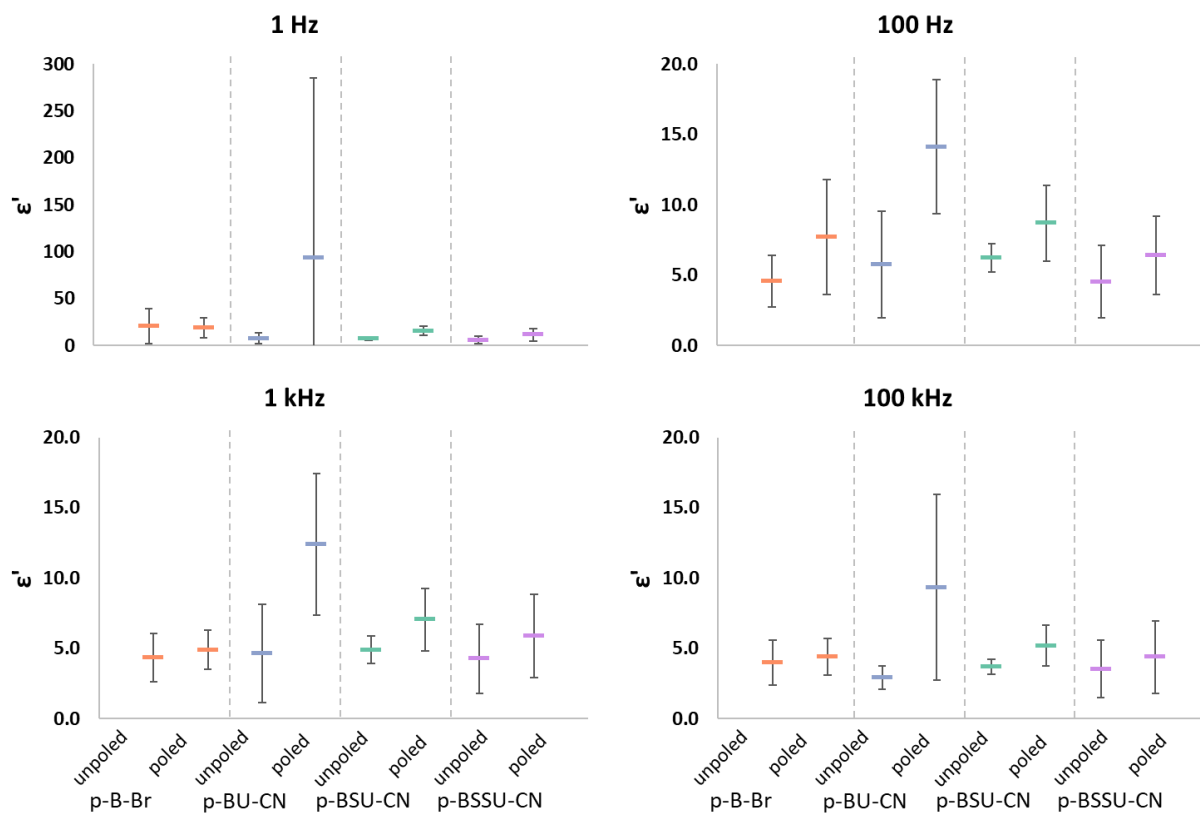
		$\epsilon'$ (1 kHz and 20 °C)							
		<b>p-B-I</b>		<b>p-BU-CN</b>		<b>p-BSU-CN</b>		<b>p-BSSU-CN</b>	
		<b>unpoled</b>	<b>poled</b>	<b>unpoled</b>	<b>poled</b>	<b>unpoled</b>	<b>poled</b>	<b>unpoled</b>	<b>poled</b>
<b>average</b>		4.31	4.90	4.64	12.42	4.89	7.05	4.28	5.89
<b>2<math>\sigma</math></b>		$\pm 1.72$	$\pm 1.37$	$\pm 3.51$	$\pm 5.03$	$\pm 9.6$	$\pm 2.22$	$\pm 2.46$	$\pm 2.96$

Appendix Table 2: Average dielectric loss for all of the poled and unpoled polymers at 1 kHz and 20 °C

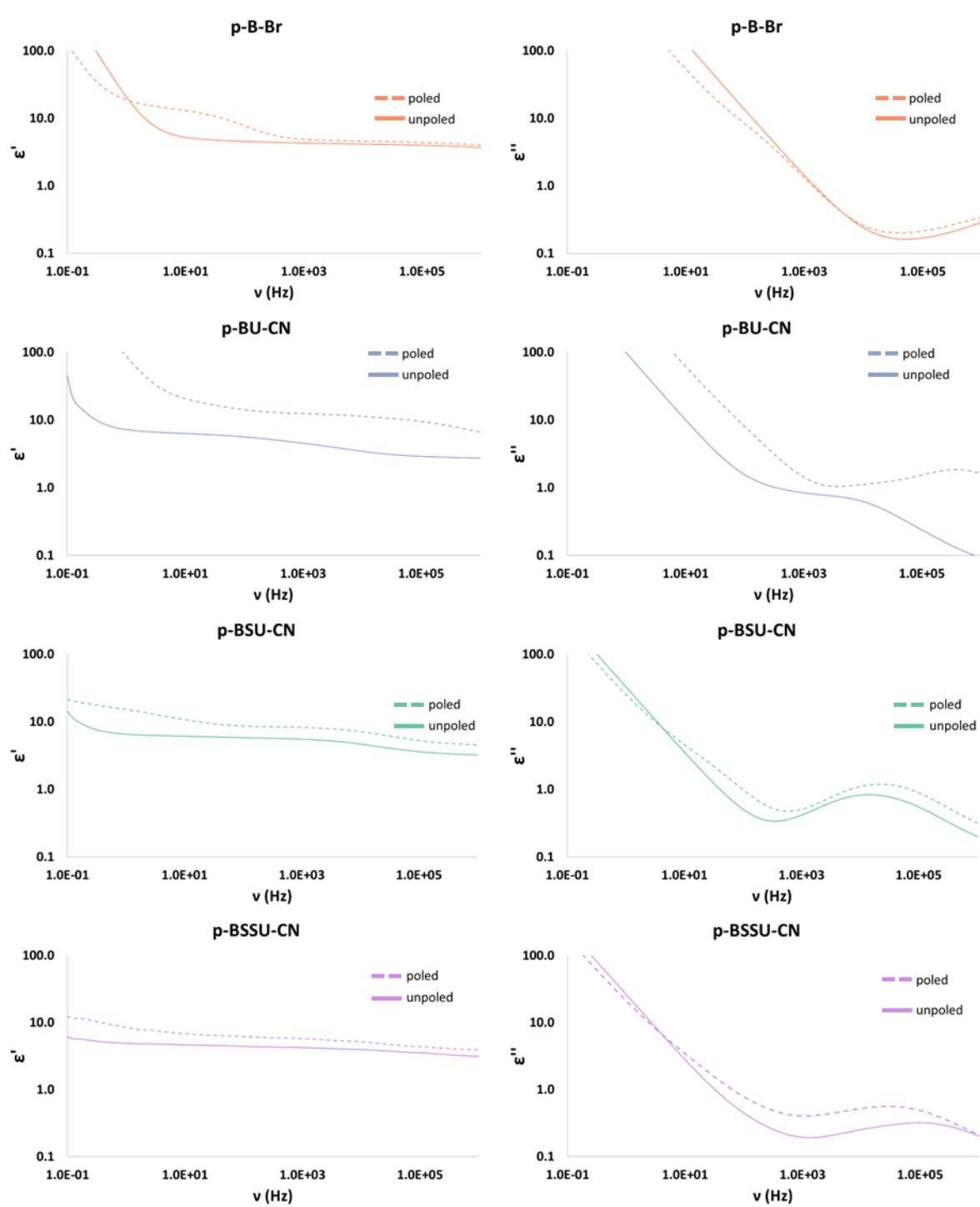
$\epsilon''$ (1 kHz and 20 °C)								
	p-B-I		p-BU-CN		p-BSU-CN		p-BSSU-CN	
	unpoled	poled	unpoled	poled	unpoled	poled	unpoled	poled
average	1.42	1.31	0.84	1.44	0.43	0.52	0.19	0.40
$2\sigma$	$\pm 0.91$	$\pm 0.88$	$\pm 0.47$	$\pm 0.71$	$\pm 0.11$	$\pm 0.12$	$\pm 0.13$	$\pm 0.16$



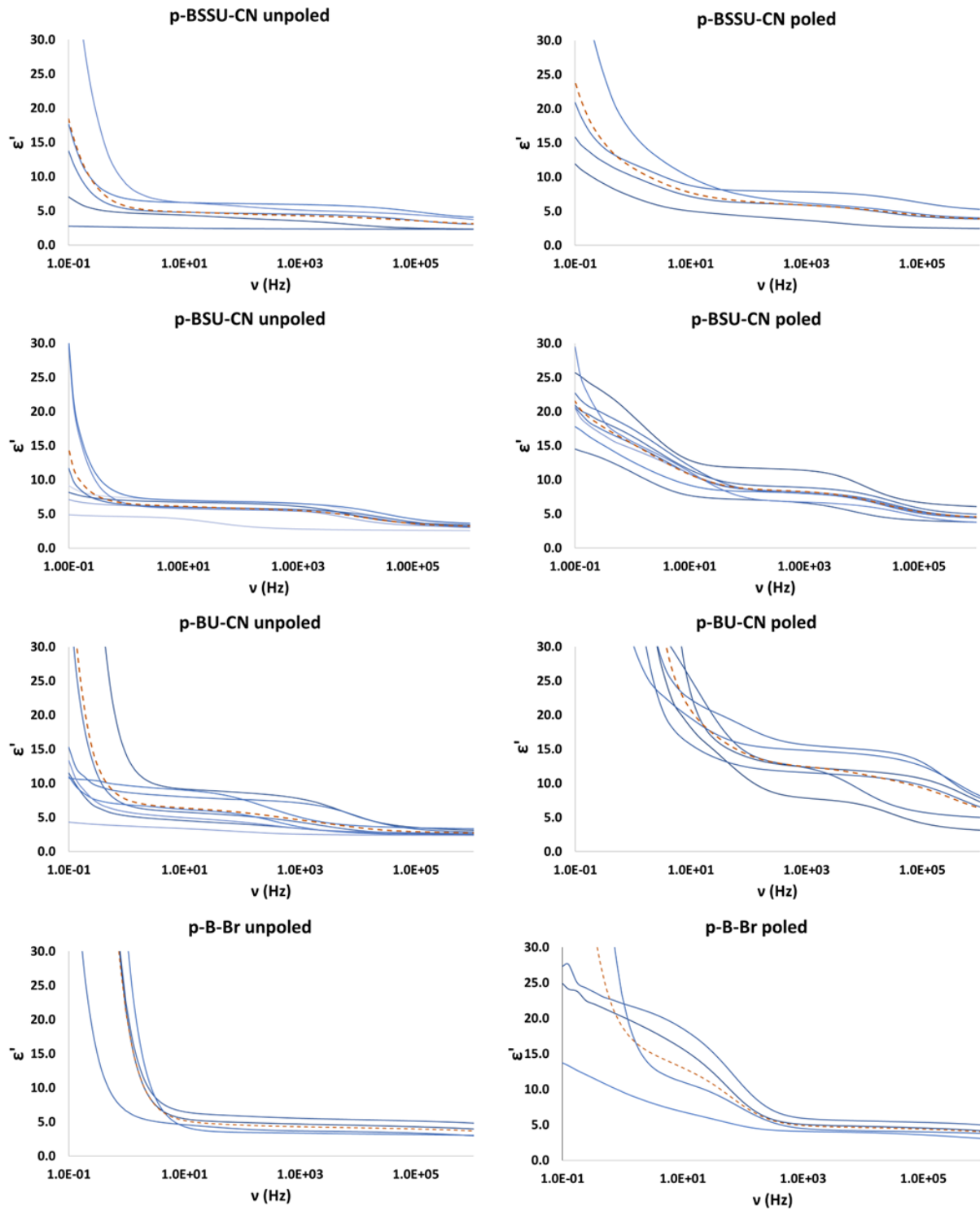
Appendix Figure 2: Comparison of the average permittivity for all of the poled (dashed curves) and unpoled (solid curves) samples for all polymers types (left) and the range of their measurements (right) at 1 kHz and 20 °C.



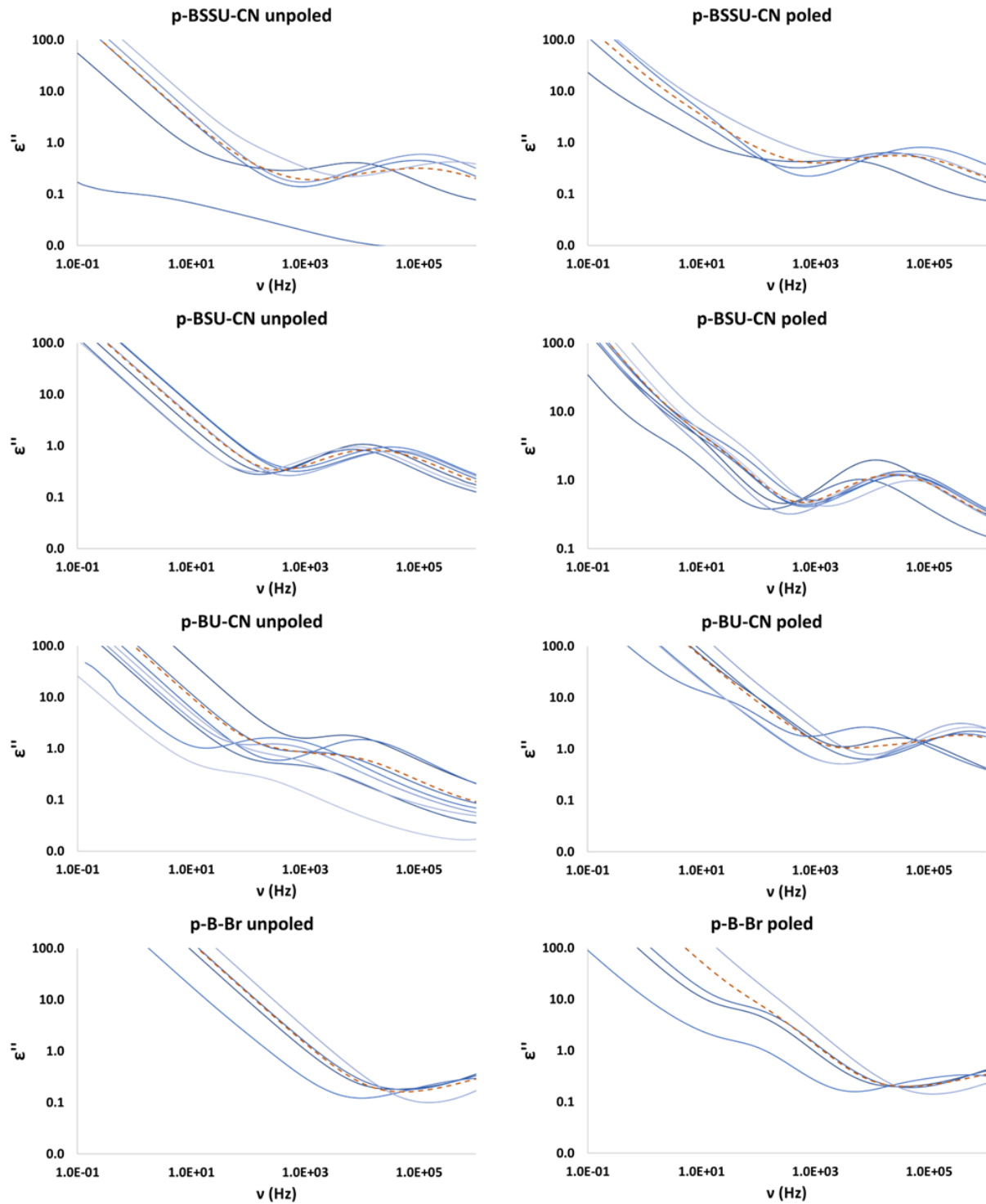
Appendix Figure 3: Average permittivity and the range of permittivities for all of the unpoled and poled polymers at specified frequencies, measured at 20 °C.



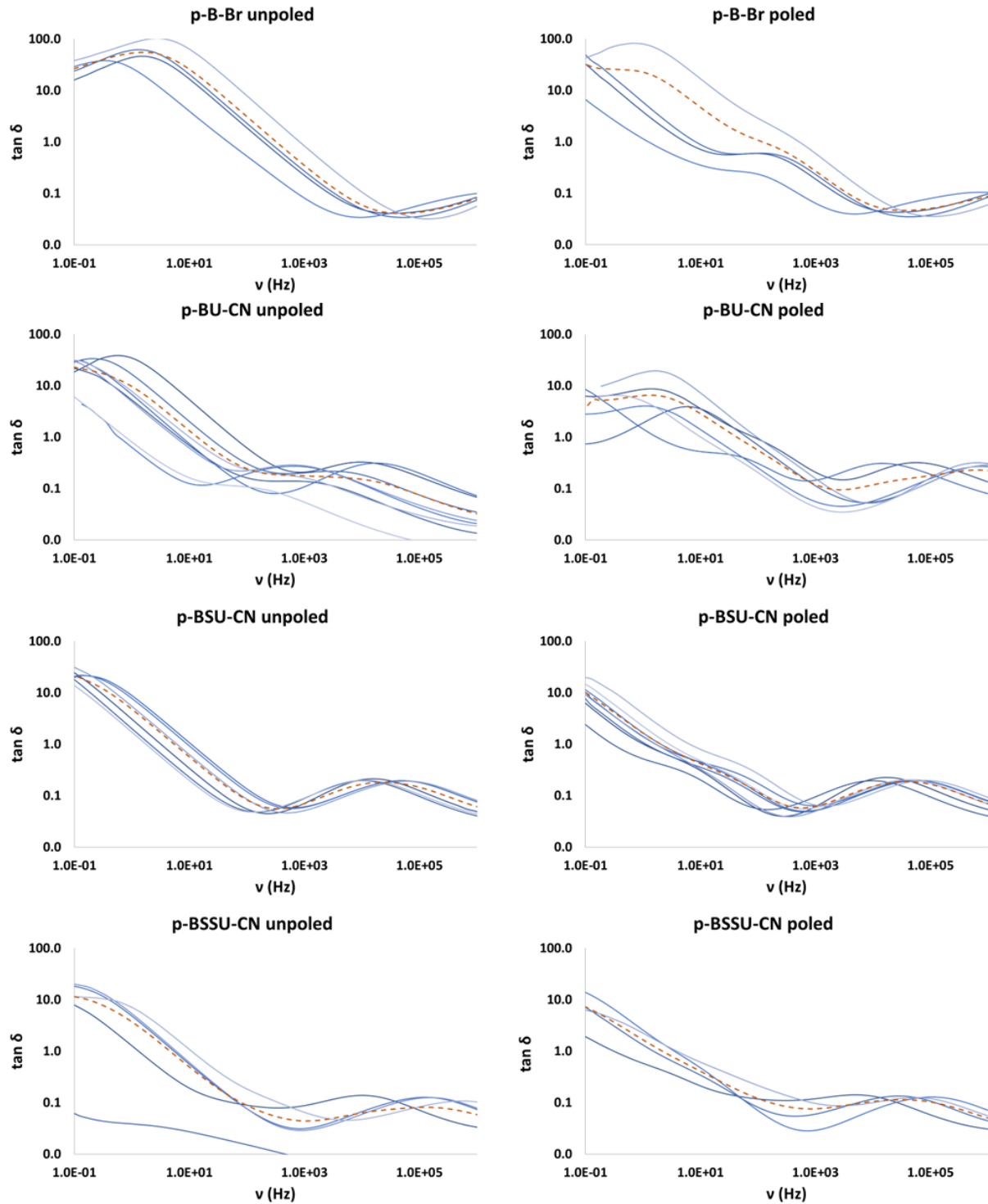
Appendix Figure 4: Permittivity and dielectric loss as a function of frequency for all of the unpoled and poled polymers, measured at 20 °C.



Appendix Figure 5: Permittivity (blue curves), as a function of frequency, for all of the samples of each polymer type and their averages (dashed orange curves), measured at 20 °C.

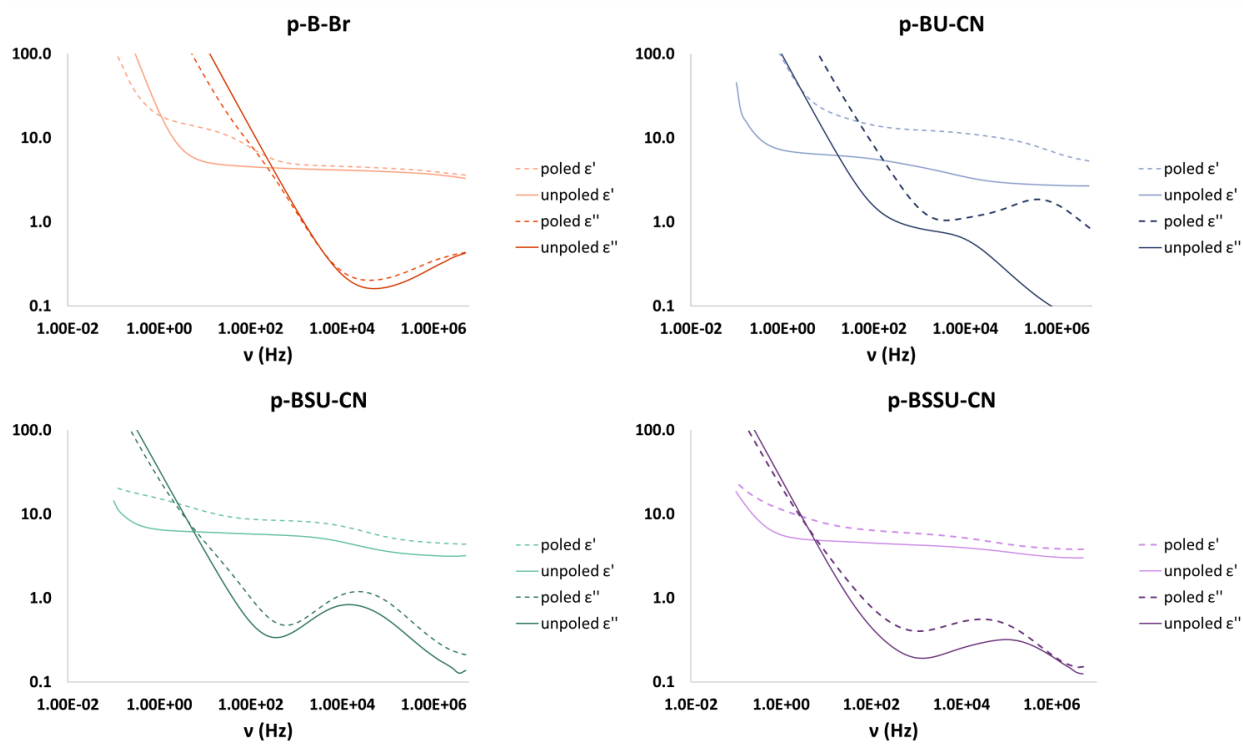


Appendix Figure 6: Dielectric loss (blue curves), as a function of frequency, for all of the samples of each polymer type and their averages (dashed orange curves), measured at 20 °C.

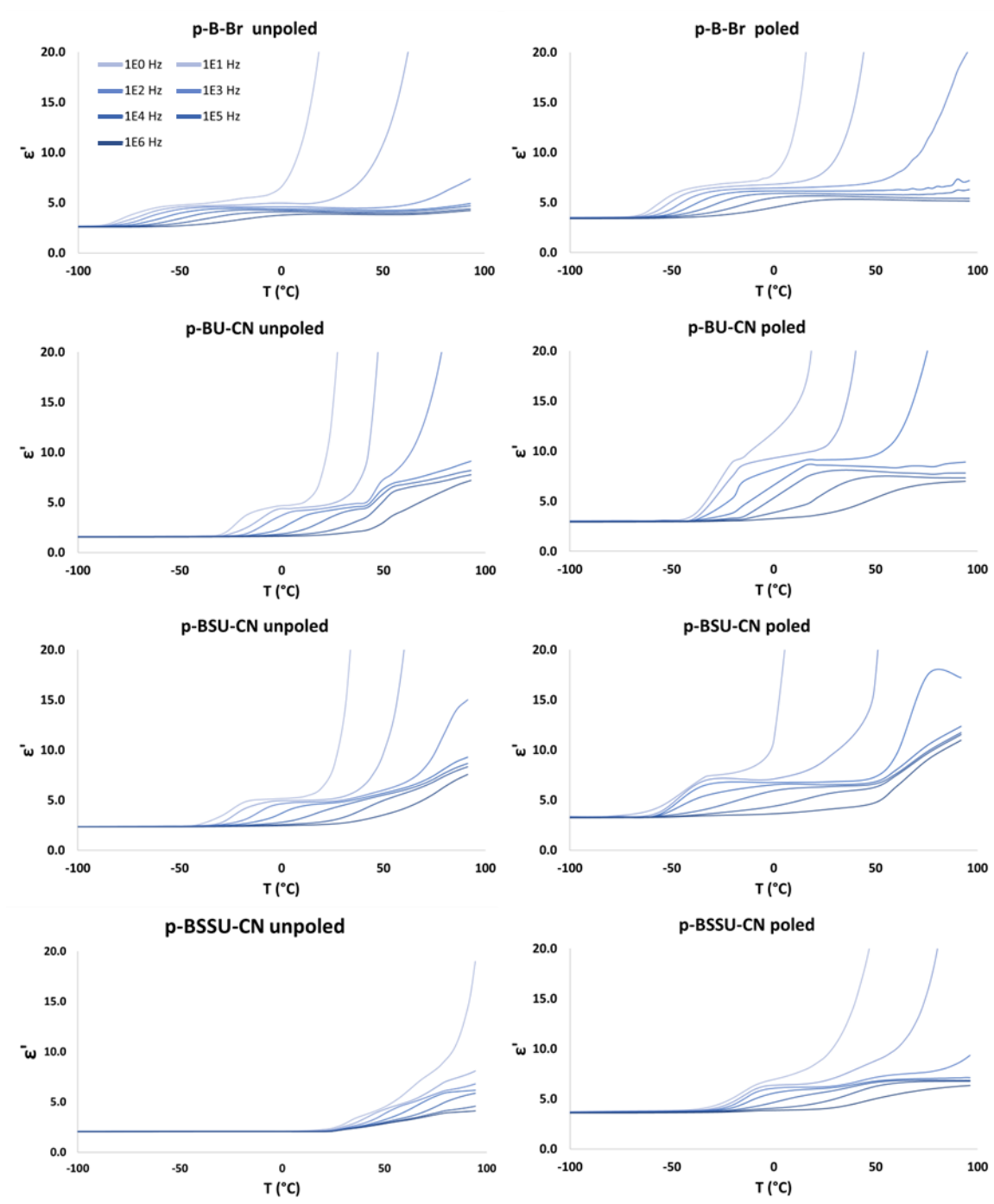


Appendix Figure 7: Dissipation factor (blue curves), as a function of frequency, for all of the samples of each polymer type and their averages (dashed orange curves), at 20°C.

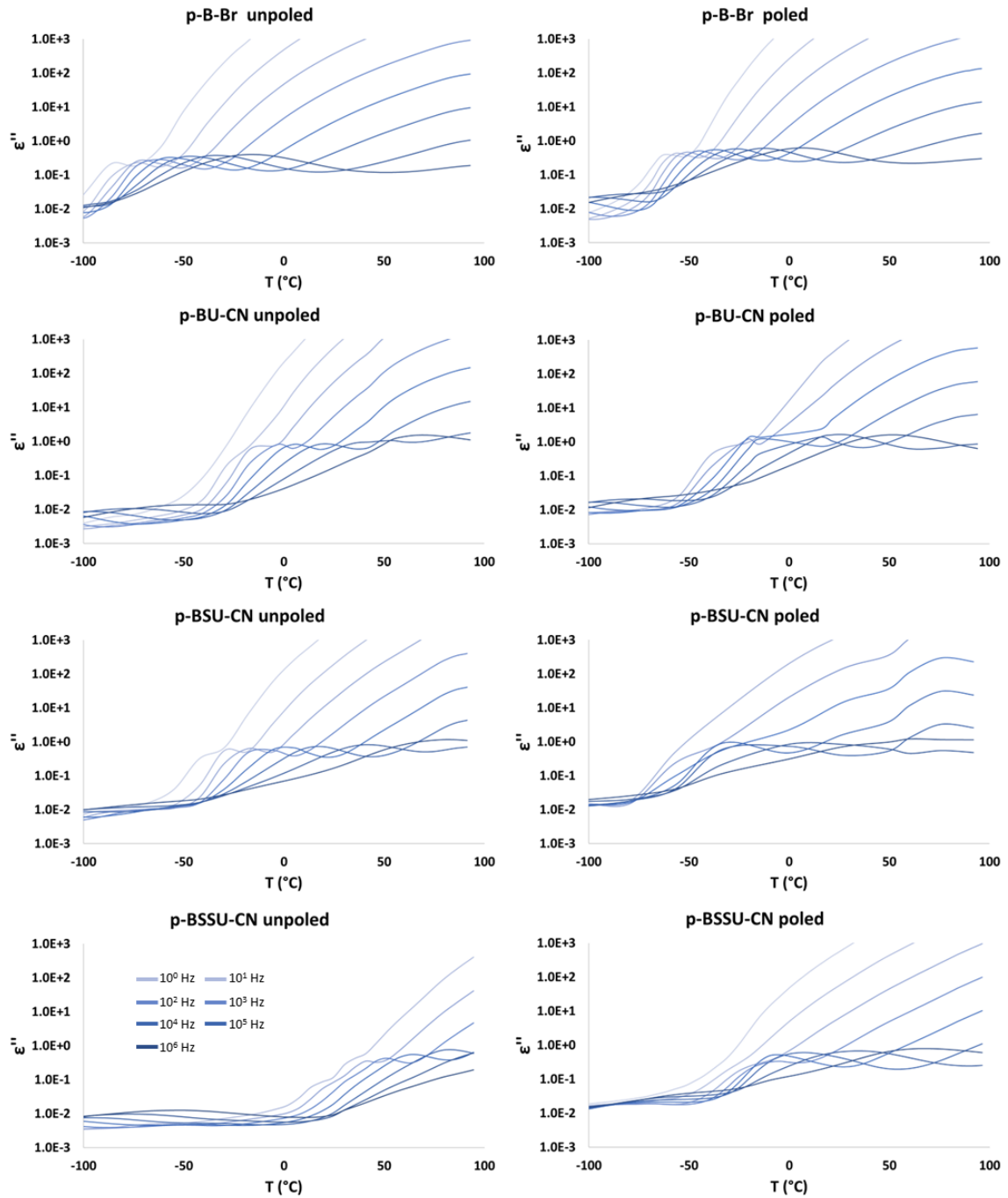




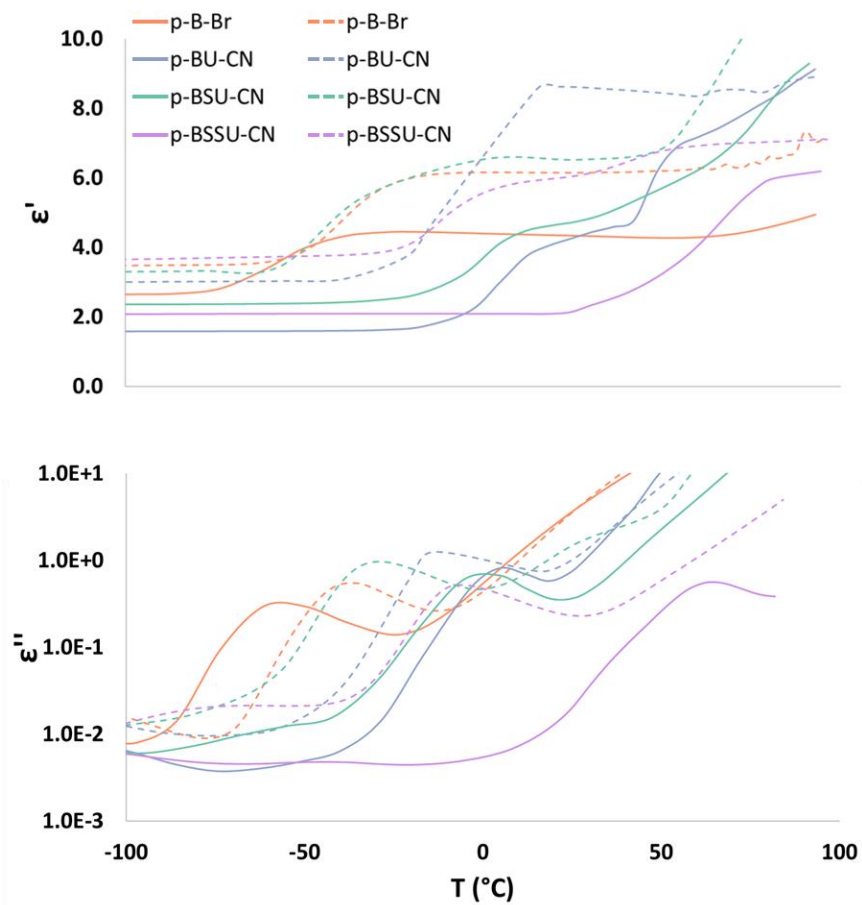
Appendix Figure 8: Overlaid view of permittivity and dielectric loss as a function of frequency for all of the unpoled and poled polymers, measured at 20 °C.



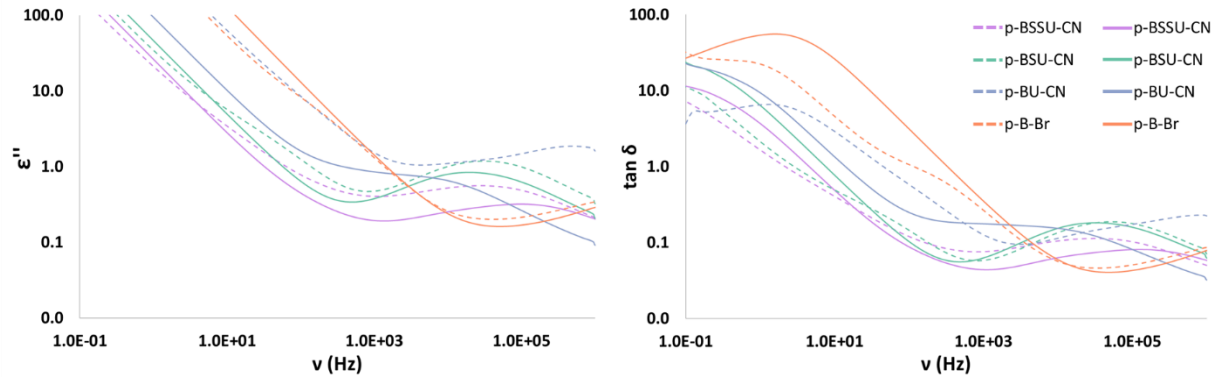
Appendix Figure 9: Permittivity as a function of temperature for all of the poled and unpoled polymers at specified frequencies from 1 Hz to 1 MHz.



Appendix Figure 10: Dielectric loss as a function of temperature for all of the poled and unpoled polymers at specified frequencies from 1 Hz to 1 MHz.



Appendix Figure 11: Permittivity and dielectric loss as a function of temperature at 1 kHz for all of the unpoled (solid curves) and poled (dashed curves) polymers.

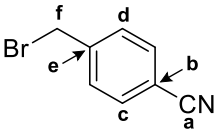


Appendix Figure 12: Dielectric loss and dissipation factor for all of the unpoled (solid curves) and poled (dashed curves) polymers, measured at 20 °C.

## **Appendix B Supporting Data and Spectra for Chapter 3**

### **Appendix B.1 Synthesis and Characterization Data**

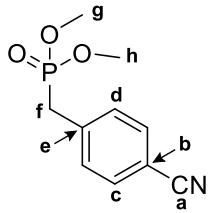
#### **Appendix B.1.1 Synthesis of Monomer Building Blocks**

3					
				$^{13}\text{C}$ -NMR (400 MHz, $\text{CDCl}_3$ )	HRMS (ESI)
				$\delta$ (ppm)	Assignment
				<u>Calc.</u> [M + H] <sup>+</sup> 195.97 amu	
				<u>Found</u> [M + H] <sup>+</sup> 195.97594 amu	
$^1\text{H}$ -NMR (400 MHz, $\text{CDCl}_3$ )					
$\delta$ (ppm)	Mult. (J)	Int.	Assignment	<u>Composition</u> $\text{C}_8\text{H}_6\text{BrN}$	
4.48	s	2	f		
7.50	d	2	d		
7.64	d	2	c		

### 3

p-Tolunitrile (3.05 g, 25.5 mmol), BPO (0.31 g, 1.28 mmol), and NBS (4.54 g, 25.5 mmol) were dissolved in DCE (75 mL) and the mixture was refluxed for 10 h. Succinimide was precipitated with hexanes (20 mL) and removed by filtration. The filtrate was washed with deionized water (3 x 20 mL), sat. aq.  $\text{NaHCO}_3$  (2 x 20 mL), and brine (2 x 20 mL). The organic layer was dried over  $\text{MgSO}_4$  and concentrated *in vacuo*. The crude product, an off-white solid, (4.80 g, 96% yield and 97% purity) was used in subsequent reactions without further purification.

## 4

				<sup>13</sup> C-NMR (400 MHz, CDCl <sub>3</sub> )			HRMS (ESI)
				δ (ppm)	J (Hz)	Assignment	Calc. Mass
	33.06	<sup>1</sup> J <sub>CP</sub> = 548	f	225.06 amu			
	52.94	<sup>2</sup> J <sub>CP</sub> = 27	g				
	110.88		a	<u>Calc.</u>			
	118.59		b	[M + H] <sup>+</sup>			
	130.46	<sup>3</sup> J <sub>CP</sub> = 24	d	226.06 amu			
	132.28	<sup>4</sup> J <sub>CP</sub> = 12	c				
	137.18	<sup>2</sup> J <sub>CP</sub> = 40	e	<u>Found</u>			
				[M + H] <sup>+</sup>			
				226.06318 amu			
				<u>Composition</u>			
				C <sub>10</sub> H <sub>12</sub> NO <sub>3</sub> P			
<sup>1</sup> H-NMR (400 MHz, CDCl <sub>3</sub> )							
δ (ppm)	Mult. (J Hz)	Int.	Assignment				
3.21	d <sup>2</sup> J <sub>PH</sub> = 22	2	f				
3.70	d <sup>1</sup> J <sub>PH</sub> = 8	6	g, h				
7.41	dd	2	d				
7.62	d	2	c				

## 4

4-(Bromomethyl)benzonitrile (1,195 mg, 5.10 mmol) was dissolved in toluene (3.5 mL). Trimethyl phosphite (TMP) (1.9 mL, 16.0 mmol) was added via cannula transfer, and the reaction was refluxed overnight. The solvent was removed via vacuum distillation, and the crude product was purified by column chromatography (silica gel, 1% EtOAc:Hexanes) to give the title compound as a yellow solid (904 mg, 79%).



				<sup>13</sup> C-NMR (500 MHz, CDCl <sub>3</sub> )		HRMS (ESI)
				δ (ppm)	Assignment	Calc. Mass
				14.16	l	292.24 amu
				16.50	m	Calc. [M + H] <sup>+</sup>
				22.76	k	
				25.93	i	293.24 amu
				29.63	h	Found [M + H] <sup>+</sup>
				31.77	j	
				68.74	g'	293.24896
				69.03	g	amu
				111.81	c	Composition C <sub>19</sub> H <sub>32</sub> O <sub>2</sub>
				112.53	d	
				117.82	a	
				128.31	f	
				151.64	e	
153.03	b					

<sup>1</sup> H-NMR (500 MHz, CDCl <sub>3</sub> )			
δ (ppm)	Mult. (J)	Int.	Assignment
0.91	t	6	l
1.34	m	8	j, k
1.46	m	4	i
1.76	m	4	h
2.21	s	3	m
3.89	dt	4	g
6.65	dd	1	c
6.73	d, s	2	a, d

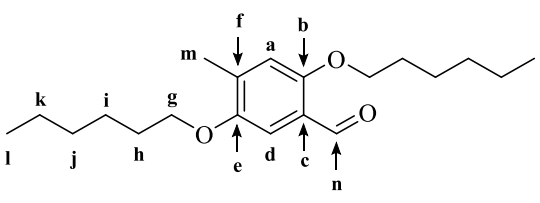
## 5

Based on our previous methods, KOH (46.5 g, 704.9 mmol) and Na<sub>2</sub>SO<sub>3</sub> (84.9 g, 342.2 mmol) were dissolved in deionized water (196 mL) and cooled with an ice bath. 2-methylhydroquinone, tetrabutylammonium bromide (TBAB), 1-bromohexane, and toluene were added to the round bottom flask (RBF), in the order listed. The mixture was allowed to reflux with vigorous stirring for 26 h. The aqueous layer was extracted with toluene (2 x 100 mL). The organic layers were combined, washed with water, followed by brine, and dried over MgSO<sub>4</sub>. The solvent was removed via vacuum distillation, to give the title compound as a brown liquid (99.8 g, 99.8%)

				<sup>13</sup> C-NMR (500 MHz, CDCl <sub>3</sub> )		HRMS (ESI)
				δ (ppm)	Assignment	Calc. Mass
				14.14	l	370.15 amu
				16.35	m	
				22.84	k	<u>Calc.</u>
				25.89	i	[M + H] <sup>+</sup>
				29.51	h	371.15 amu
				31.72	j	
				69.22	g	<u>Found</u>
				70.66	g'	[M + H] <sup>+</sup>
				109.28	c	371.15795 amu
				116.75	d	<u>Composition</u>
				117.37	a	C <sub>19</sub> H <sub>31</sub> BrO <sub>2</sub>
				127.28	f	
				149.51	e	
152.05	b					
<sup>1</sup> H-NMR (400 MHz, CDCl <sub>3</sub> )						
δ (ppm)	Mult. (J)	Int.	Assignment			
0.90	t	6	l			
1.34	m	8	j, k			
1.47	m	4	i			
1.78	m	4	h			
2.17	s	3	m			
3.88	t	2	g			
3.94	t	2	g'			
6.73	s	1	a			
6.97	s	1	d			

## 6

1,4-Bis(hexyloxy)-2-methylbenzene (31.5 g, 107.7 mmol), BPO (1.3 g, 5.4 mmol), and NBS (19.2 g, 107.7 mmol) were dissolved in DCE (320 mL) and the mixture was refluxed for 2 h. Succinimide was precipitated with hexanes (200 mL) and removed by filtration. The filtrate was washed with deionized water (2 x 100 mL), sat. aq. NaHCO<sub>3</sub> (2 x 50 mL), and brine (2 x 50 mL). The organic layer was dried over MgSO<sub>4</sub> and concentrated *in vacuo*. The crude material was recrystallized from MeOH to give the title compound as an off-white solid (33.8 g, 84.4%).

				<sup>13</sup> C-NMR (500 MHz, CDCl <sub>3</sub> )	HRMS (ESI)
				δ (ppm)	Assignment
<sup>1</sup> H-NMR (500 MHz, CDCl <sub>3</sub> )					
δ (ppm)	Mult. (J)	Int.	Assignment		
0.90	t	6	l	14.15	l
1.34	m	8	j,k	17.40	m
1.46	m	4	i	22.74	k
1.79	m	4	h	25.92	i
2.27	s	3	m	29.40	h
3.95	t	2	g	31.70	j
4.02	t	2	g'	68.74	g
6.79	s	1	a	69.47	g'
7.22	s	1	d	108.52	d
10.41	s	1	n	115.94	a
				123.34	f
				136.96	c
				151.73	e
				156.38	b
				189.57	n

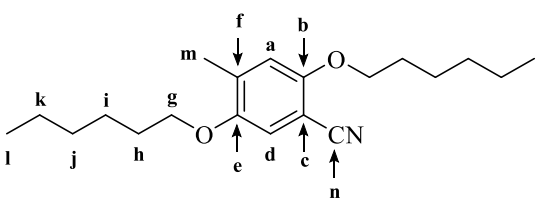
320.24 amu  
 Calc.  
 [M + H]<sup>+</sup>  
 321.24 amu

Found  
 [M + H]<sup>+</sup>  
 321.24401  
 amu

Composition  
 C<sub>20</sub>H<sub>32</sub>O<sub>3</sub>

## 7

1-Bromo-2,5-bis(hexyloxy)-4-methylbenzene (5.0 g, 13.5 mmol) was dissolved in dry Et<sub>2</sub>O (25 mL) and cooled to 0 °C under N<sub>2</sub>. <sup>n</sup>BuLi (9.24 mL, 14.8 mmol) was diluted with dry Et<sub>2</sub>O (16.8 mL) was added dropwise and allowed to stir for 30 min. DMF (1.7 mL, 21.8 mmol) was diluted with dry Et<sub>2</sub>O (5.8 mL) was added. The ice bath was removed, and the reaction was allowed to stir at RT for ~2 h. Cold water was added to quench the reaction, and the aqueous layer was extracted with Et<sub>2</sub>O (3 x 50 mL). The organic layers were combined, washed with brine (100 mL), dried over MgSO<sub>4</sub>, and the solvent was removed *in vacuo*. The crude material was purified via column chromatography (silica gel, 1% EtOAc:Hexanes) to give the title compound as an off-white solid (4.25 g, 98.6%).

				<sup>13</sup> C-NMR (400 MHz, CDCl <sub>3</sub> )	HRMS (ESI)	
				δ (ppm)	Assignment	<u>Calc. Mass</u>
				14.14	l	317.47 amu
				17.30	m	
				22.70	k	<u>Calc.</u>
				25.78	i	[M + H] <sup>+</sup>
				29.27	h	318.47 amu
				31.64	j	
				68.96	g	<u>Found</u>
				69.78	g'	[M + H] <sup>+</sup>
				98.87	n	318.24430
				114.82	d	amu
				115.66	a	<u>Composition</u>
				117.14	c	C <sub>20</sub> H <sub>31</sub> NO <sub>2</sub>
				134.93	f	
				151.05	e	
				155.27	b	
<sup>1</sup> H-NMR (400 MHz, CDCl <sub>3</sub> )						
δ (ppm)	Mult. (J)	Int.	Assignment			
0.90	t	6	l			
1.34	m	8	j,k			
1.47	m	4	i			
1.79	m	4	h			
2.25	s	3	m			
3.89	t	2	g			
4.00	t	2	g'			
6.75	s	1	a			
6.90	s	1	d			

## 8

2,5-Bis(hexyloxy)-4-methylbenzaldehyde (1.46 g, 4.56 mmol) and hydroxylamine hydrochloride (410.6 mg, 5.85 mmol) were added to formic acid (6.2 mL), and the mixture was refluxed overnight. The reaction was quenched with iced deionized water (12.4 mL). The aqueous mixture was extracted with Et<sub>2</sub>O (3 x 10 mL), the combined organic layers were washed with brine (2 x 10 mL) and dried over MgSO<sub>4</sub>. The solvent was removed *in vacuo*, and the crude material was purified by column chromatography (silica gel, 1% EtOAc:Hexanes) to give the title compound (1.23 g, 84.8%).

				<sup>13</sup> C-NMR (400 MHz, CDCl <sub>3</sub> )			HRMS (ESI)
				δ (ppm)	J (Hz)	Assignment	Calc. Mass
				14.14		l	425.23 amu
				22.70		k	
				25.79		i	Calc.
				27.18		h	[M + H] <sup>+</sup>
				29.20	<sup>1</sup> J <sub>CP</sub> = 76	m	426.23 amu
				31.65		j	Found
				52.99	<sup>2</sup> J <sub>CP</sub> = 28	o	[M + H] <sup>+</sup>
				69.63		g	426.24190
				100.62	<sup>2</sup> J <sub>CP</sub> = 16	f	amu
				115.72	<sup>3</sup> J <sub>CP</sub> = 12	a	Composition
				115.97		d	C <sub>22</sub> H <sub>36</sub> NO <sub>5</sub> P
				116.65		n	
				127.67		c	
				150.38	<sup>3</sup> J <sub>CP</sub> = 12	e	
155.10		b					
<sup>1</sup> H-NMR (500 MHz, CDCl <sub>3</sub> )							
δ (ppm)	Mult. (J)	Int.	Assignment				
0.91	m	6	l				
1.33	m	8	j,k				
1.47	m	4	i				
1.80	m	4	h				
3.27	d <sup>1</sup> J <sub>PH</sub> = 23	2	m				
3.69	d <sup>2</sup> J <sub>PH</sub> = 11	6	o				
3.92	t	2	g'				
4.02	t	2	g				
6.98	m	2	a, d				

## 9

2,5-Bis(hexyloxy)-4-methylbenzonitrile (5.02 g, 15.8 mmol), BPO (306 mg, 1.3 mmol), and NBS (2.87 g, 16.1 mmol) were dissolved in DCE (46 mL) and the mixture was refluxed for 2 h. The mixture was filtered through a plug of silica, and the filtrate was concentrated *in vacuo*. The intermediate was dissolved in toluene (11 mL). TMP (5.8 mL, 49.4 mmol) was added via cannula transfer, and the reaction was refluxed overnight. The solvent was removed via vacuum distillation, and the crude product was purified by column chromatography (silica gel, 1% EtOAc:Hexanes) to give the title compound as viscous liquid (3.44 g, 51.1%).

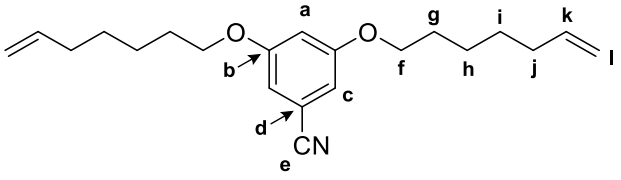
### Appendix B.1.2 Synthesis of Monomers

Unless specified otherwise, the monomers were synthesized by the following typical coupling and reduction procedures.

**Typical Horner Wadsworth Emmons Coupling:** The aldehyde (1 equiv) and the phosphonate (1.2-1.5 equiv) were dissolved in dry THF under N<sub>2</sub>, cooled to 0 °C, and KO<sup>t</sup>Bu (2.5 equiv) was added semi-dropwise. The mixture was allowed to warm to RT and stirred overnight. The reaction was quenched with saturated aq NH<sub>4</sub>Cl and extracted 3 x with ethyl acetate. The combined organic layers were washed 2 x with brine, dried over MgSO<sub>4</sub>, and the solvent was removed *in vacuo*. The crude product was purified by column chromatography.

**Typical Reduction of Monomer Nitrile:** The nitrile (1 equiv) was dissolved in dry DCM and cooled to -78 °C, under N<sub>2</sub>. DIBAL-H (1 M in hexanes, 1.2 equiv) was added semi-dropwise and the reaction was stirred at -78 °C until <sup>1</sup>H NMR analysis indicated completion. Wet silica (0.4 mL H<sub>2</sub>O and 1.5 g SiO<sub>2</sub> per mmol DIBAL-H) was added over 5 min, and stirring was continued for 1 h. A mixture of K<sub>2</sub>CO<sub>3</sub> (0.5 mg per mmol DIBAL-H) and MgSO<sub>4</sub> (0.5 mg per mmol DIBAL-H) was added and stirring continued for an additional hour. The mixture was filtered, the solids were washed with excess DCM, and the solvent was removed *in vacuo*. The crude product was purified by column chromatography.

**mono-B-N**

				<sup>13</sup> C-NMR (500 MHz, CDCl <sub>3</sub> )		HRMS (ESI)
				δ (ppm)	Assignment	Calc. Mass
				28.55	g	
				28.87	i	<u>Calc.</u>
				33.59	j	[M + H] <sup>+</sup>
				68.45	f	328.47 amu
				106.57	a	<u>Found</u>
				110.31	c	[M + H] <sup>+</sup>
				113.30	e	328.22862
				114.55	l	amu
				118.84	d	
				138.65	k	<u>Composition</u>
				160.49	b	C <sub>21</sub> H <sub>29</sub> NO <sub>2</sub>
<sup>1</sup> H-NMR (400 MHz, CDCl <sub>3</sub> )						
δ (ppm)	Mult. (J)	Int.	Assignment			
1.46	m	8	h, i			
1.78	m	4	g			
2.09	m	4	j			
3.93	t	4	f			
4.99	m	4	l			
5.81	m	2	k			
6.63	t	1	a			
6.73	d	2	c			

**mono-B-N**

3,5-Dihydroxybenzonnitrile (1.68 g, 12.2 mmol) and KOH (1.65 g, 25.0 mmol) were stirred at RT overnight in DMSO (160 mL). 7-Bromo-1-heptene (4.22 mL, 26.9 mmol) was added and the reaction was stirred for an additional 6 h. The reaction was cooled with an ice bath and cold deionized water (10 mL, 556 mmol) was added slowly. The solvent was removed via vacuum distillation, and the resulting mixture was extracted with ethyl acetate (3 x 20 mL) and washed with brine (2 x 20 mL). The organic layer was dried over MgSO<sub>4</sub> and the solvent was removed *in vacuo* to give **mono-B-N** as a brown viscous liquid (3.36 g, 84%).

**mono-B-A**

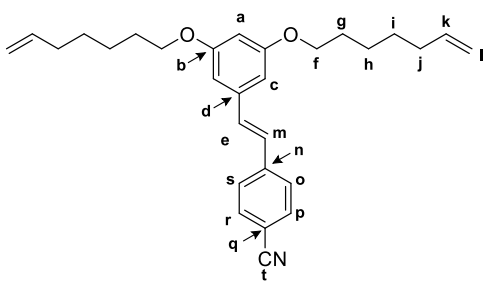
				<sup>13</sup> C-NMR (500 MHz, CDCl <sub>3</sub> )	HRMS (ESI)	
				<sup>δ</sup> (ppm)	Assignment	<u>Calc. Mass</u>
				25.76	h	330.22 amu
			28.86	g		
			29.24	i	<u>Calc.</u>	
			33.93	j	[M + H] <sup>+</sup>	
			68.56	f	331.22 amu	
			107.84	c		
			108.25	a	<u>Found</u>	
			114.81	l	[M + H] <sup>+</sup>	
			138.58	d	331.22967	
			138.98	k	amu	
			160.98	b	<u>Composition</u>	
			192.30	e	C <sub>21</sub> H <sub>30</sub> O <sub>3</sub>	
<sup>1</sup> H-NMR (400 MHz, CDCl <sub>3</sub> )						
<sup>δ</sup> (ppm)	Mult. (J)	Int.	Assignment			
1.47	m	8	h, i			
1.80	m	4	g			
2.09	m	4	j			
3.99	t	4	f			
4.98	m	4	l			
5.82	m	2	k			
6.69	t	1	a			
6.98	d	2	c			
9.89	s	1	e			

**mono-B-A**

3,5-Bis(hexyloxy)benzamide (1.7 g, 5.2 mmol) was dissolved in dry DCM (520 mL) and cooled to 0 °C. DIBAL-H (6.2 mL, 6.2 mmol, 1.0 M in hexanes) was added semi-dropwise, and the reaction was stirred at 0 °C, under N<sub>2</sub>, for 8-10 h. Wet silica (0.4 mL H<sub>2</sub>O and 1.3 g SiO<sub>2</sub> per mmol DIBAL-H) was added over 5 min and the reaction was stirred for 1 h. A mixture of K<sub>2</sub>CO<sub>3</sub> (0.5 g per mmol DIBAL-H) and MgSO<sub>4</sub> (0.5 g per mmol DIBAL-H) was added and the reaction was stirred for an additional hour. The reaction mixture was filtered, and the solids were washed with DCM. The solvent was removed *in vacuo* to give the title compound (orange viscous liquid) (1.29 g, 87%).



mono-BP-N

				<sup>13</sup> C-NMR (500 MHz, CDCl <sub>3</sub> )	HRMS (ESI)	
				δ (ppm)	Assignment	Calc. Mass
				25.56	h	429.27 amu
				28.64	g	
				29.12	i	Calc.
				33.67	j	[M + H] <sup>+</sup>
				68.08	f	430.27 amu
				101.83	a	Found
				105.58	c	[M + H] <sup>+</sup>
				110.67	t	430.27596
				114.48	l	amu
				118.98	q	
				126.89	s, o	Composition
				127.05	e	C <sub>29</sub> H <sub>35</sub> NO <sub>2</sub>
				132.48	r, p	
				132.57	m	
				138.14	d	
				138.78	k	
				141.78	n	
				160.59	b	
<sup>1</sup> H-NMR (400 MHz, CDCl <sub>3</sub> )						
δ (ppm)	Mult. (J)	Int.	Assignment			
1.48	m	8	h, i			
1.80	m	4	g			
2.09	m	4	j			
3.98	t	4	f			
4.97	m	4	l			
5.82	m	2	k			
6.43	t	1	a			
6.65	d	2	c			
7.04	d	1	e			
7.12	d	1	m			
7.56	d	2	s, o			
7.63	d	2	r, p			

mono-BP-A

				<sup>13</sup> C-NMR (500 MHz, CDCl <sub>3</sub> )	HRMS (ESI)	
				$\delta$ (ppm)	Assignment	<u>Calc. Mass</u>
				25.58	g	432.27 amu
			28.65	h		
			29.14	i	<u>Calc.</u>	
			33.68	j	[M + H] <sup>+</sup>	
			68.08	f	433.27 amu	
			101.77	a	<u>Found</u>	
			105.56	c	[M + H] <sup>+</sup>	
			114.48	l	433.27533	
			126.94	s, o	amu	
			127.66	e		
			130.22	r, p	<u>Composition</u>	
			132.35	m	C <sub>29</sub> H <sub>36</sub> O <sub>3</sub>	
			135.41	q		
			138.41	d		
			138.79	k		
			143.35	n		
			160.58	b		
			191.53	t		
<sup>1</sup> H-NMR (400 MHz, CDCl <sub>3</sub> )						
$\delta$ (ppm)	Mult. (J)	Int.	Assignment			
1.49	t	6	h, i			
1.81	m	8	g			
2.10	m	4	j			
3.98	t	4	f			
4.98	m	4	l			
5.83	m	2	k			
6.43	t	1	a			
6.68	d	2	c			
7.10	d	1	e			
7.18	d	1	m			
7.64	d	2	s, o			
7.87	d	2	r, p			
10.02	s	1	t			

mono-BO-N

				<sup>13</sup> C-NMR (500 MHz, CDCl <sub>3</sub> )		HRMS (ESI)
				δ (ppm)	Assignment	Calc. Mass
				13.99	y	629.44 amu
				22.55	x	
				22.59	w	<u>Calc.</u>
				25.57	v	[M + H] <sup>+</sup>
				25.83	v'	630.44 amu
				28.64	i	<u>Found</u>
				29.08	g	[M + H] <sup>+</sup>
				29.14	g'	630.45439
				31.50	u	amu
				31.55	u'	
				33.66	h	<u>Composition</u>
				68.04	f	C <sub>41</sub> H <sub>59</sub> NO <sub>4</sub>
				69.59	t	
				69.77	t'	
				100.64	z	
				101.55	a	
				105.58	c	
				110.56	o	
				114.46	l	
				116.60	r	
				116.71	n	
				122.83	e	
				132.48	m	
				132.83	q	
				138.77	k	
				138.91	d	
				150.26	s	
				155.27	p	
				160.54	b	
<sup>1</sup> H-NMR (400 MHz, CDCl <sub>3</sub> )						
δ (ppm)	Mult. (J)	Int.	Assignment			
0.92	m	6	y			
1.36	m	8	h, x			
1.48	m	12	i, w, v			
1.81	m	8	g, u			
2.10	m	4	j			
3.98	m	6	f, t			
4.08	t	2	t'			
4.98	m	4	l			
5.82	m	2	k			
6.42	t	1	a			
6.66	d	2	c			
7.01	s	1	o			
7.10	s	1	r			
7.11	d	1	e			
7.36	d	1	m			

mono-BO-A

				<sup>13</sup> C-NMR (500 MHz, CDCl <sub>3</sub> )	HRMS (ESI)	
				$\delta$ (ppm)	Assignment	<u>Calc. Mass</u>
				14.00	y	632.44 amu
			22.58	x		
			25.58	w	<u>Calc.</u>	
			25.77	v	[M + H] <sup>+</sup>	
			25.89	v'	633.44 amu	
			28.65	i		
			29.15	g	<u>Found</u>	
			29.22	g'	[M + H] <sup>+</sup>	
			31.53	u	633.45333	
			31.58	u'	amu	
			33.67	h	<u>Composition</u>	
			68.02	f	C <sub>41</sub> H <sub>60</sub> NO <sub>5</sub>	
			69.16	t		
			69.29	t'		
			101.49	a		
			105.55	c		
			110.22	o		
			110.83	r		
			114.46	l		
			123.40	e		
			124.34	n		
			132.48	m		
			134.24	q		
			138.78	k		
			139.13	d		
			150.82	s		
			156.21	p		
			160.51	b		
			189.12	z		
<sup>1</sup> H-NMR (400 MHz, CDCl <sub>3</sub> )						
$\delta$ (ppm)	Mult. (J)	Int.	Assignment			
0.91	m	6	y			
1.36	m	8	h, x			
1.48	m	12	i, w, v			
1.81	m	8	g, u			
2.09	m	4	j			
3.98	t	4	f			
4.03	t	2	t			
4.10	t	2	t'			
4.99	m	4	l			
5.82	m	2	k			
6.41	t	1	a			
6.68	d	2	c			
7.14	s	1	e			
7.15	d	1	o			
7.32	s	1	r			
7.42	d	1	m			
10.44	s	1	z			

mono-BPO-N

				<sup>13</sup> C-NMR (400 MHz, CDCl <sub>3</sub> )	HRMS (ESI)	
				δ (ppm)	Assignment	Calc. Mass
				13.99	ag	731.49 amu
22.58	af					
25.58	ae	Calc.				
25.82	h	[M + H] <sup>+</sup>				
28.66	g	732.49 amu				
29.16	i					
31.52	j	Found				
33.68	ad	[M + H] <sup>+</sup>				
68.03	f	732.49510				
69.61	ac	amu				
69.78	ab	Composition				
100.59	ah	C <sub>49</sub> H <sub>65</sub> NO <sub>4</sub>				
101.13	a					
105.26	c					
110.32	w					
114.46	l					
116.59	z					
116.75	y					
122.26	u					
126.95	s, o					
127.24	r, p					
128.44	m					
129.21	e					
131.83	t					
132.89	q					
136.43	v					
137.35	d					
138.81	k					
139.10	n					
150.24	x					
155.29	aa					
160.53	b					
<sup>1</sup> H-NMR (500 MHz, CDCl <sub>3</sub> )						
δ (ppm)	Mult. (J)	Int.	Assignment			
0.92	t	6	ag			
1.37	m	8	j, af			
1.49	m	12	h, i, ae			
1.84	m	8	g, ad			
2.10	m	4	ac			
3.98	m	6	f, ab			
4.10	t	2	ab'			
5.00	m	4	l			
5.83	m	2	k			
6.40	s	1	a			
6.67	s	1	c			
7.02	s	1	w			
7.06	d	2	E, m			
7.14	s	1	z			
7.19	d	1	t			
7.43	d	1	u			
7.52	s	4	o, p, r, s			

### Appendix B.1.3 Polymerizations

Unless specified otherwise, the polymers were synthesized by the following typical procedures.

**Typical Polymerization:** The diene (1 equiv) was dissolved in diphenyl ether (2 M) and GII dissolved in DCM (0.1-0.12 g/mL at 1-2 mol%) was added. The mixture was stirred and heated gently under vacuum until SEC analysis indicated polymerization had reached steady state. The reaction was quenched with ethyl vinyl ether and precipitated with MeOH.

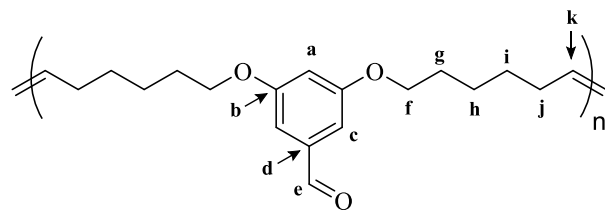
poly-B-N				
			<sup>13</sup> C-NMR (500 MHz, CDCl <sub>3</sub> )	
			δ (ppm)    Assignment	<u>M<sub>n</sub></u>
			25.58    h	2,271 Da
			28.70    g	
			29.02    i	<u>D</u>
			33.76    j	1.61
			68.59    f	
			106.71    a	<u>Repeat Unit</u>
			110.45    c	<u>.Mass</u>
			113.45    e	299.19 amu
			114.71    l	
			119.01    d	<u>Repeat Unit</u>
			138.81    k	<u>Composition</u>
			160.64    b	C <sub>19</sub> H <sub>25</sub> NO <sub>2</sub>
<sup>1</sup> H-NMR (400 MHz, CDCl <sub>3</sub> )				
δ (ppm)	Mult. (J)	Int.	Assignment	
1.46	m	8	h, i	
1.78	m	4	g	
2.09	m	4	j	
3.93	t	4	f	
4.99	m	4	l <sup>a</sup>	
5.41	m	0.34	k <sup>b</sup>	
5.81	m	2	k <sup>a</sup>	
6.63	t	1	a	
6.73	d	2	c	

<sup>a</sup>terminal olefin peaks, indicating end groups or unreacted monomer

<sup>b</sup>internal olefin peak

**poly-B-A**

<sup>1</sup> H-NMR (400 MHz, CDCl <sub>3</sub> )				<sup>13</sup> C-NMR (400 MHz, CDCl <sub>3</sub> )		<u>M<sub>n</sub><sup>a</sup></u> 10,680 Da
δ (ppm)	Mult. (J)	Int.	Assignment	δ (ppm)	Assignment	
1.44	m	8	h, i	25.64	h	<u>D<sup>a</sup></u> 3.40
1.78	m	4	g	29.11	g	
2.01	m	4	j	29.43	i	<u>Repeat Unit</u> <u>Mass</u> 302.19 amu
3.97	t	4	f	32.60	j	
5.41	m	2	k	68.48	f	<u>Repeat Unit</u> <u>Composition</u> C <sub>19</sub> H <sub>16</sub> O <sub>3</sub>
6.68	s	1	a	107.68	a	
6.97	s	2	c	108.13	c	
9.87	s	1	e	130.42	k	
				138.43	d	
				160.84	b	
				192.18	e	



<sup>a</sup>average of two unprecipitated trials

**poly-BP-N**

				<sup>13</sup> C-NMR (400 MHz, CDCl <sub>3</sub> )		
				δ (ppm)	Assignment	
				25.56	h	M <sub>n</sub> 1,722 Da
				28.64	g	
				29.12	i	D 1.51
				33.67	j	
				68.08	f	Repeat Unit Mass 403.24 amu
				101.83	a	
				105.58	c	
				110.67	t	Repeat Unit Composition C <sub>27</sub> H <sub>31</sub> NO <sub>2</sub>
				114.48	l	
				118.98	q	
				126.89	s, o	
				127.05	e	
				132.48	r, p	
				132.57	m	
				138.14	d	
				138.78	k	
141.78	n					
160.59	b					

<sup>1</sup> H-NMR (400 MHz, CDCl <sub>3</sub> )			
dδ (ppm)	Mult. (J)	Int.	Assignment
1.48	m	8	h, i
1.79	m	4	g
2.05	m	4	j
3.97	t	4	f
4.98	m	1.12	l <sup>a</sup>
5.44	m	2	k <sup>b</sup>
5.82	m	0.53	k <sup>a</sup>
6.42	t	1	a
6.65	d	2	c
7.04	d	1	e
7.12	d	1	m
7.56	d	2	s, o
7.63	d	2	r, p

<sup>a</sup>terminal olefin peaks, indicating end groups or unreacted monomer

<sup>b</sup>internal olefin peak



**poly-BP-A**

$^{13}\text{C-NMR}$ (500 MHz, $\text{CDCl}_3$ )			
	$\delta$ (ppm)	Assignment	
	25.73	g	1,306 Da
	28.80	h	
	29.29	i	$\bar{D}$
	33.83	j	2.56
	68.23	f	<u>Repeat Unit</u>
	101.93	a	
	105.72	c	
	114.63	l	404.24 amu
	127.09	s, o	<u>Repeat Unit</u>
	127.82	e	
	130.37	r, p	<u>Composition</u>
	132.51	m	$\text{C}_{27}\text{H}_{32}\text{O}_3$
	135.57	q	
	138.57	d	
	138.95	k	
143.51	n		
160.74	b		
191.68	t		

$^1\text{H-NMR}$ (400 MHz, $\text{CDCl}_3$ )			
$\delta$ (ppm)	Mult. (J)	Int.	Assignment
1.49	t	6	i, j
1.81	m	8	h
2.10	m	4	g
3.98	t	4	f
4.98	m	4	l
5.83	m	2	k
6.43	t	1	a
6.68	d	2	c
7.10	d	1	e
7.18	d	1	m
7.64	d	2	s, o
7.87	d	2	r, p
10.02	s	1	t

## poly-BO-N

				<sup>13</sup> C-NMR (500 MHz, CDCl <sub>3</sub> )		
				δ (ppm)	Assignment	<u>M<sub>n</sub></u>
				13.99	y	6,676 Da
				22.55	x	<u>D</u>
				22.59	w	2.53
				25.57	v	
				25.83	v'	
				28.64	i	<u>Repeat Unit</u>
				29.08	g	<u>Mass</u>
				29.14	g'	601.41 amu
				31.50	u	
				31.55	u'	<u>Repeat Unit</u>
				33.66	h	<u>Composition</u>
				68.04	f	C <sub>39</sub> H <sub>55</sub> NO <sub>4</sub>
				69.59	t	
				69.77	t'	
				100.64	z	
				101.55	a	
				105.58	c	
				110.56	o	
				114.46	l	
				116.60	r	
				116.71	n	
				122.83	e	
				132.48	m	
				132.83	q	
				138.77	k	
				138.91	d	
				150.26	s	
				155.27	p	
				160.54	b	
				<sup>1</sup> H-NMR (400 MHz, CDCl <sub>3</sub> )		
δ (ppm)	Mult. (J)	Int.	Assignment			
0.92	m	6	y			
1.35	m	8	w, x			
1.48	m	12	v, h, i			
1.81	m	8	u, g			
2.05	m	4	j			
3.96	m	6	f, t			
4.07	t	2	t'			
4.98	m	0.88	l <sup>a</sup>			
5.42	m	2	k <sup>b</sup>			
5.82	m	0.39	k <sup>a</sup>			
6.40	t	1	a			
6.65	d	2	c			
7.00	s	1	o			
7.10	s	1	r			
7.11	d	1	e			
7.31	d	1	m			

<sup>a</sup>terminal olefin peaks, indicating end groups or unreacted monomer

<sup>b</sup>internal olefin peak

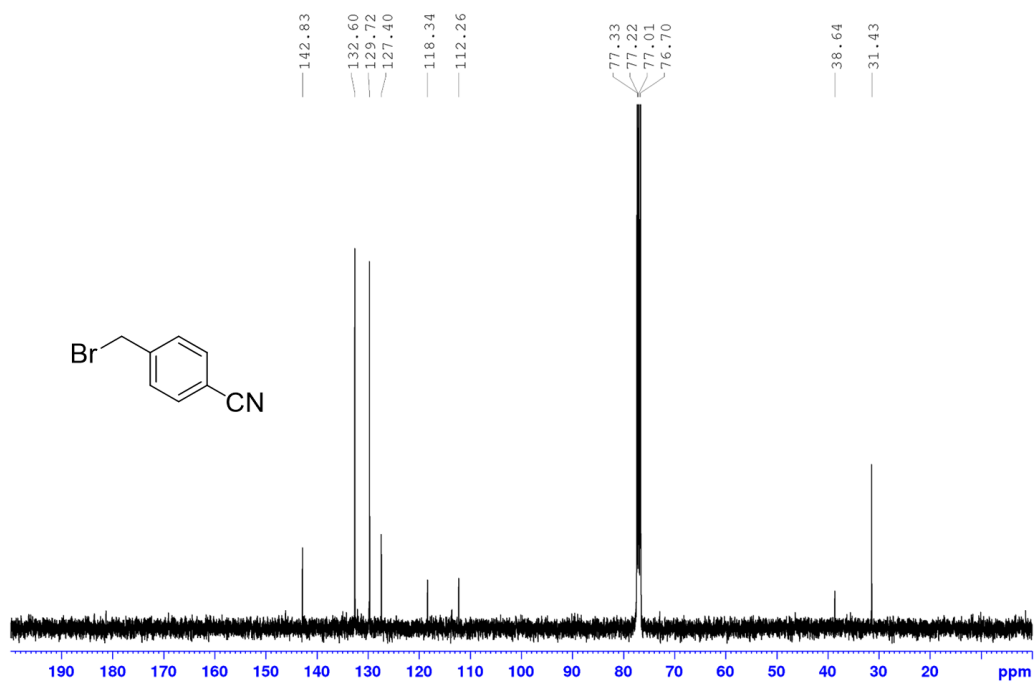
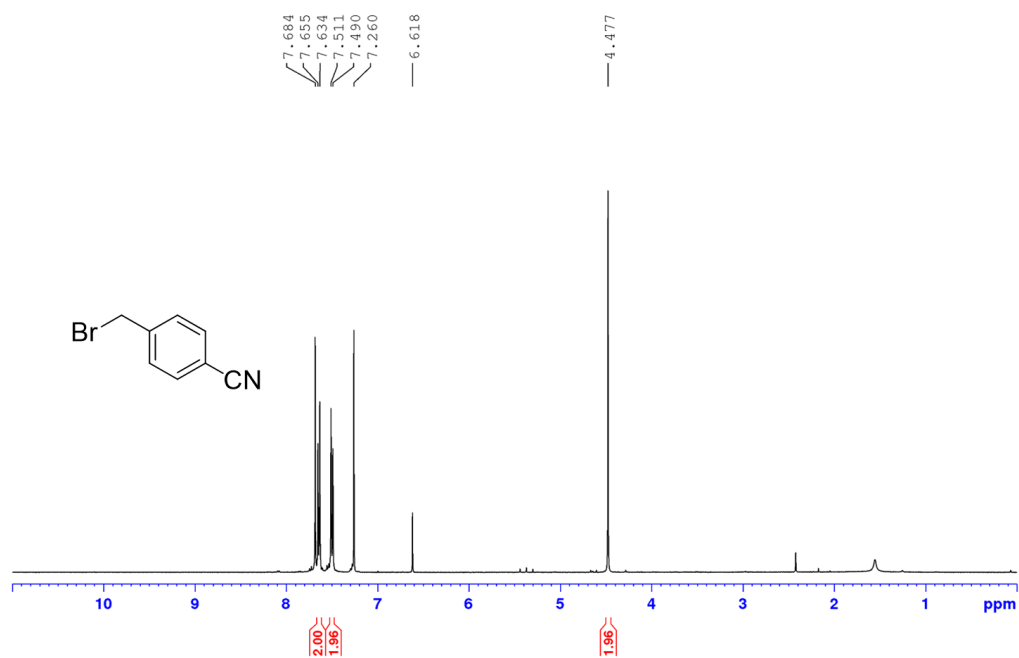
poly-BO-A

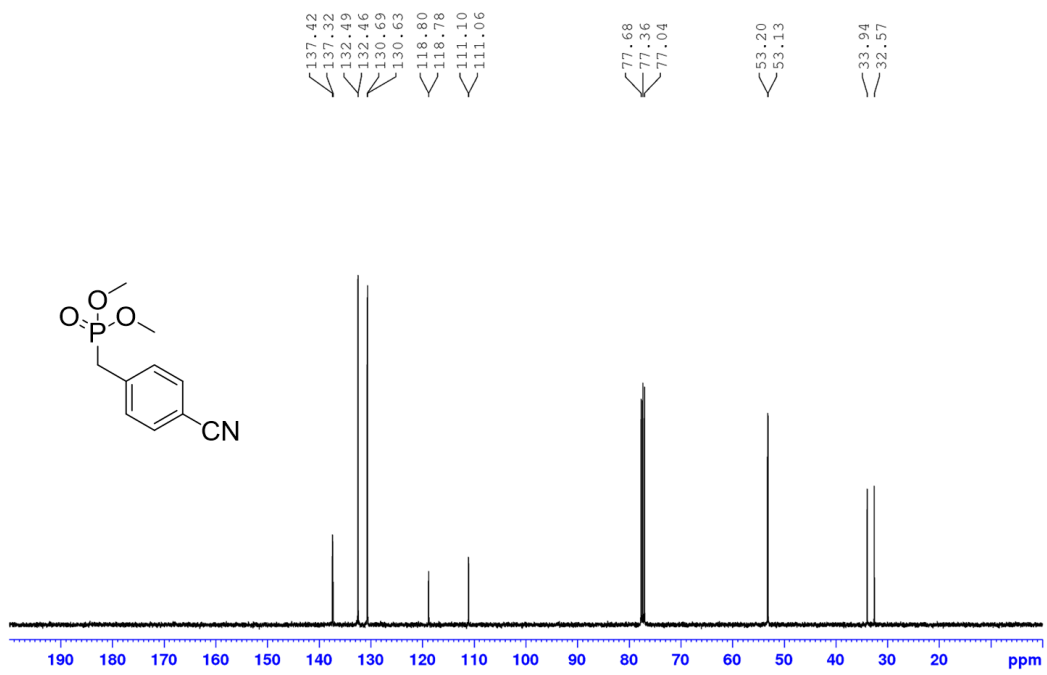
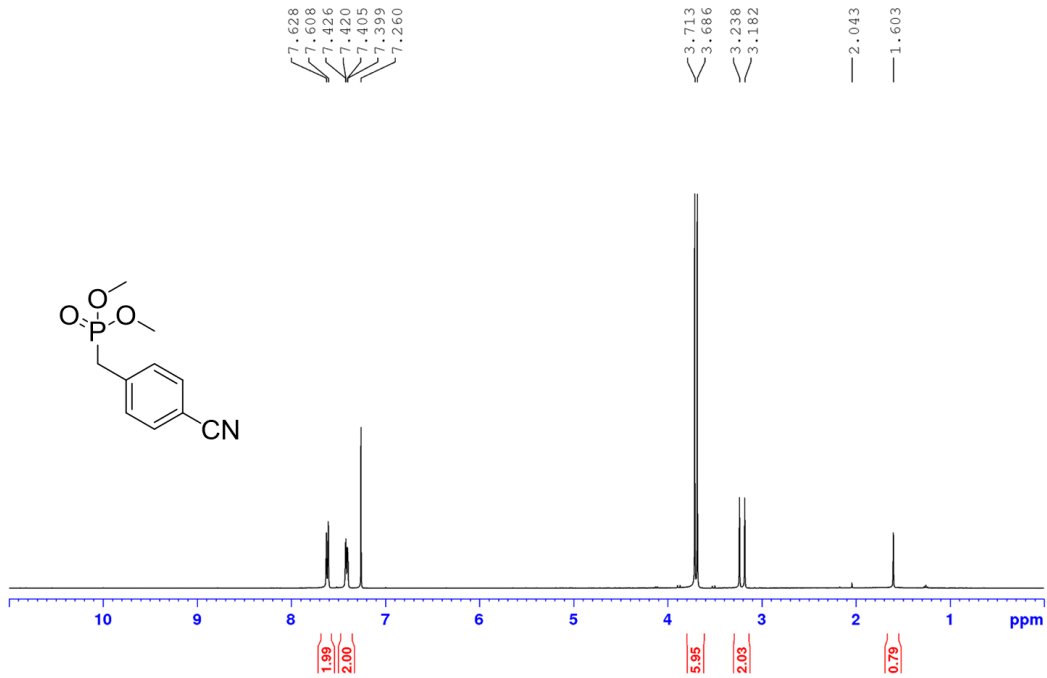
<sup>1</sup> H-NMR (400 MHz, CDCl <sub>3</sub> )				<sup>13</sup> C-NMR (400 MHz, CDCl <sub>3</sub> )	<u>M<sub>n</sub></u> 10,350 Da
δ (ppm)	Mult. (J)	Int.	Assignment	δ (ppm) Assignment	
0.90	t	6	y	14.18 y	<u>D</u> 2.93
1.35	m	8	w, x	22.74 x	
1.46	m	12	h, i, v	22.78 w	<u>Repeat Unit</u> <u>Mass</u> 604.41 amu
1.81	m	8	g, u	25.92 g	
2.01	s	4	j	26.04 h	<u>Repeat Unit</u> <u>Composition</u> C <sub>39</sub> H <sub>56</sub> O <sub>5</sub>
4.00	t	6	t, f	29.35 i	
4.08	t	4	t'	31.69 j	
4.99	m	.37	l <sup>a</sup>	31.73 v	
5.41	m	2	k <sup>b</sup>	32.68 u	
5.80	m	.17	k <sup>a</sup>	68.18 f	
6.40	s	1	a	69.29 t	
6.67	s	2	c	101.60 a	
7.12	s	1	o	105.62 c	
7.14	d	1	e	110.30 o	
7.31	s	1	r	110.89 r	
7.41	d	1	m	114.63 l	
				119.03 e	
				123.35 k	
				129.87 n	
				130.44 m	
				132.57 q	
				139.25 d	
				150.91 s	
				156.33 p	
				160.65 b	
				189.27 z	

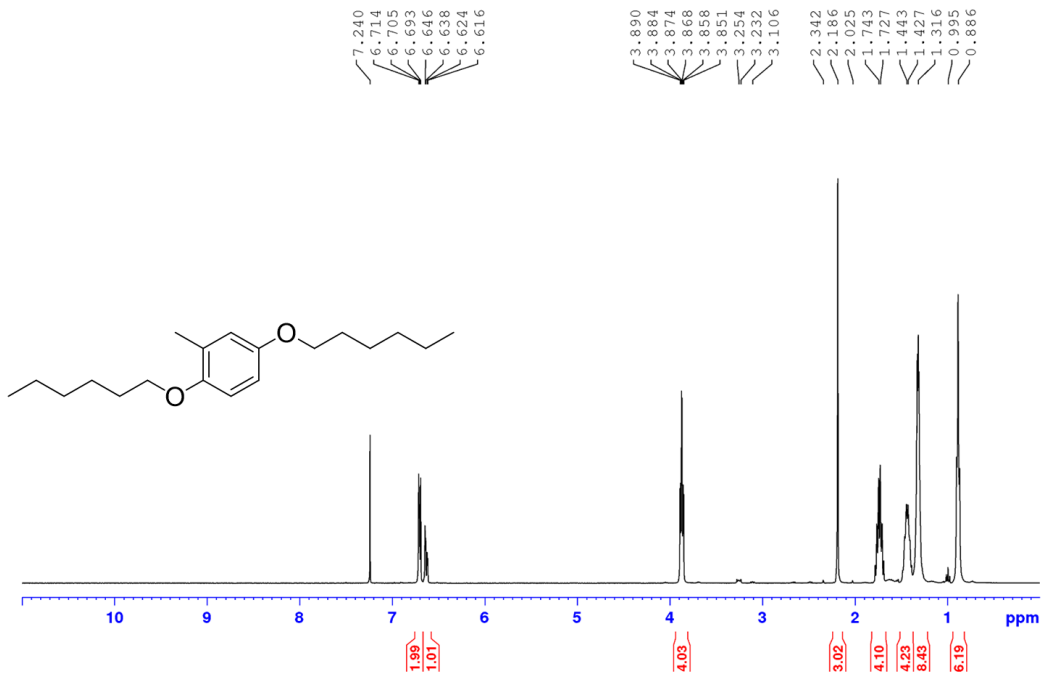
<sup>a</sup>terminal olefin peaks, indicating end groups or unreacted monomer

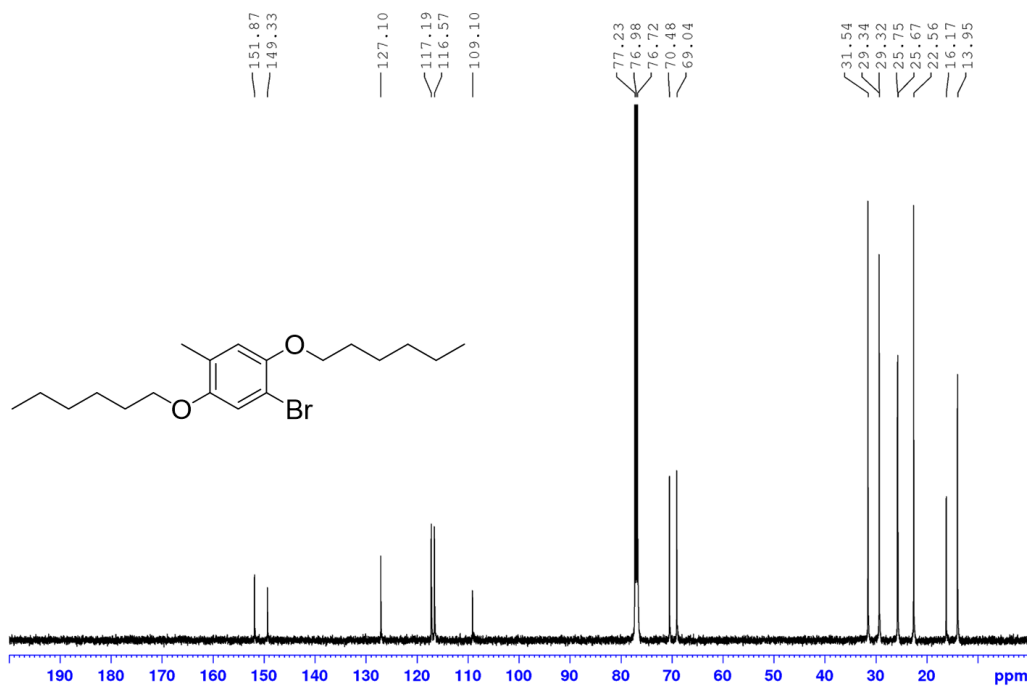
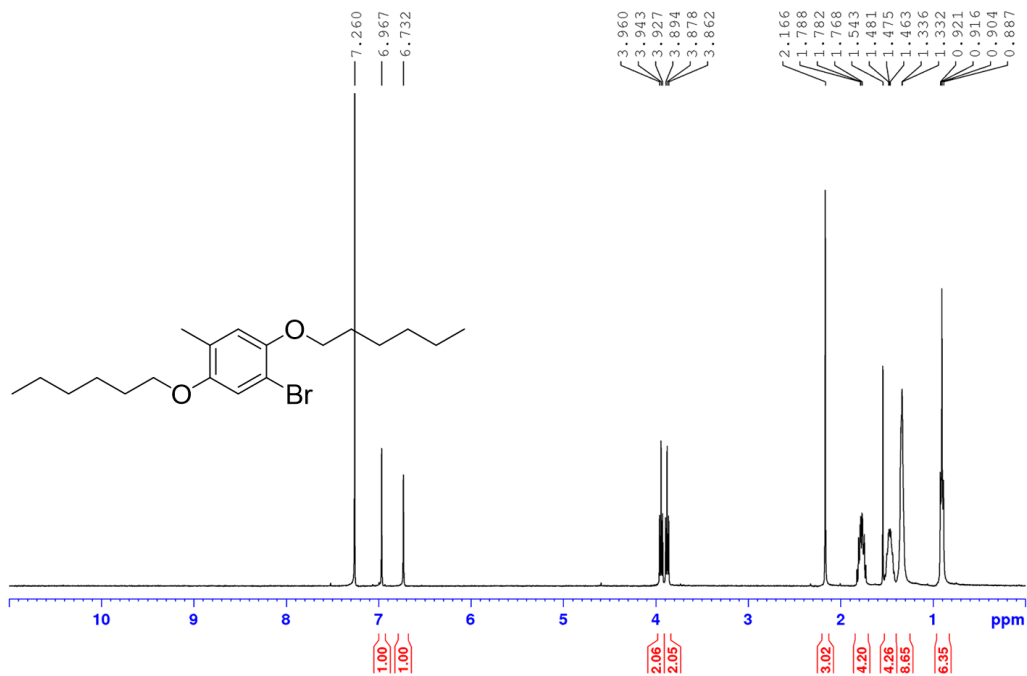
<sup>b</sup>internal olefin peak

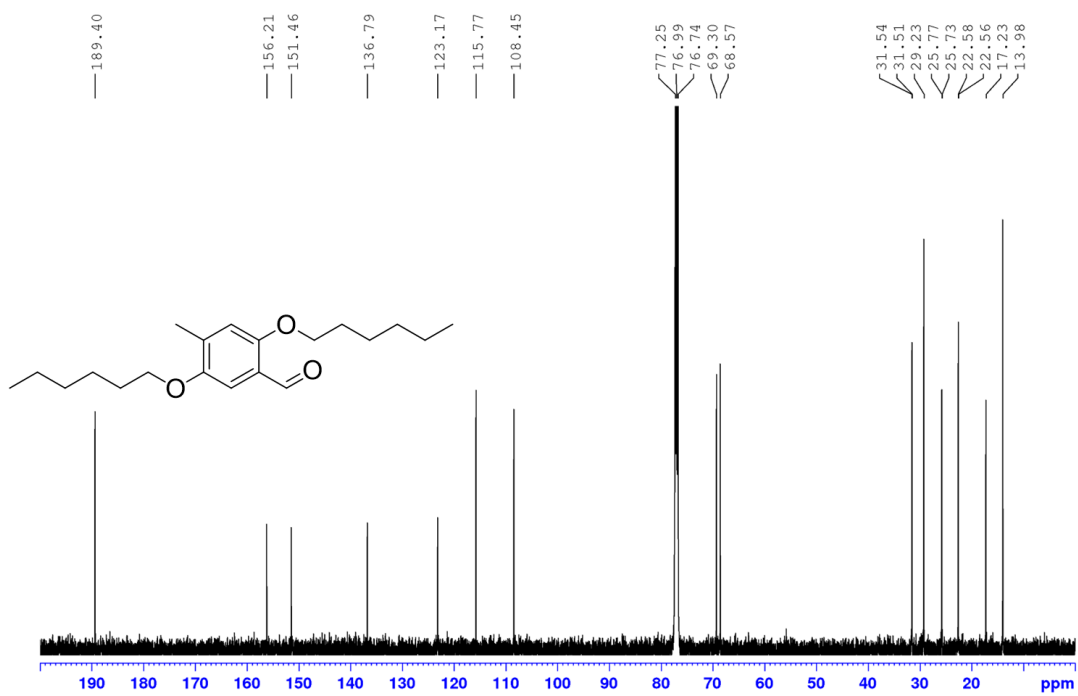
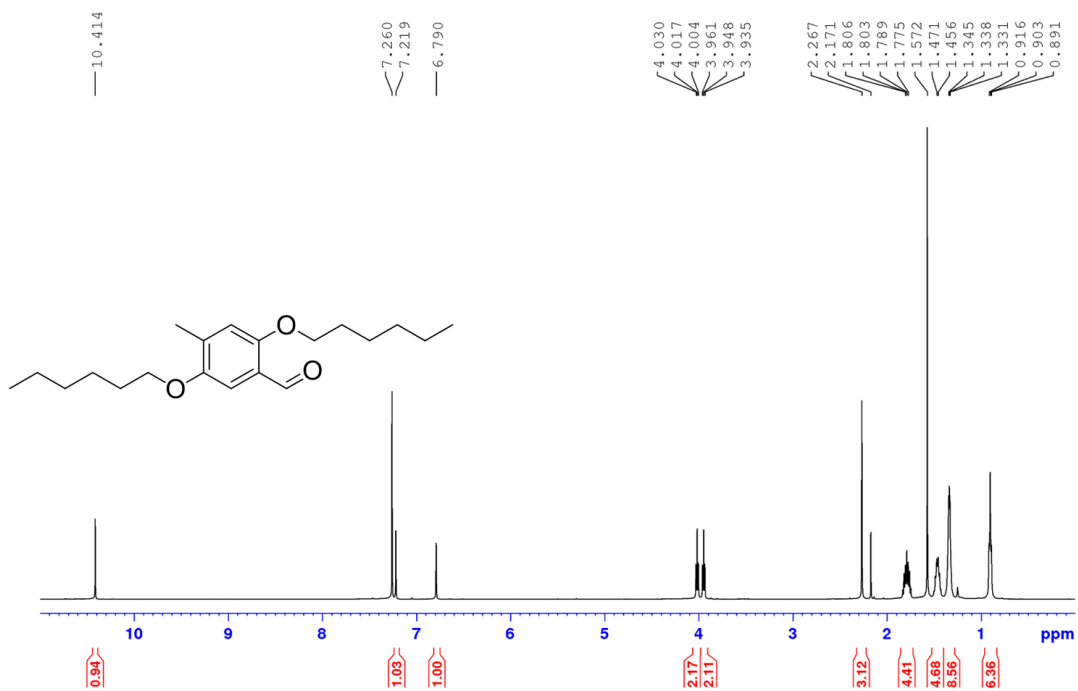
## Appendix B.1.4 NMR



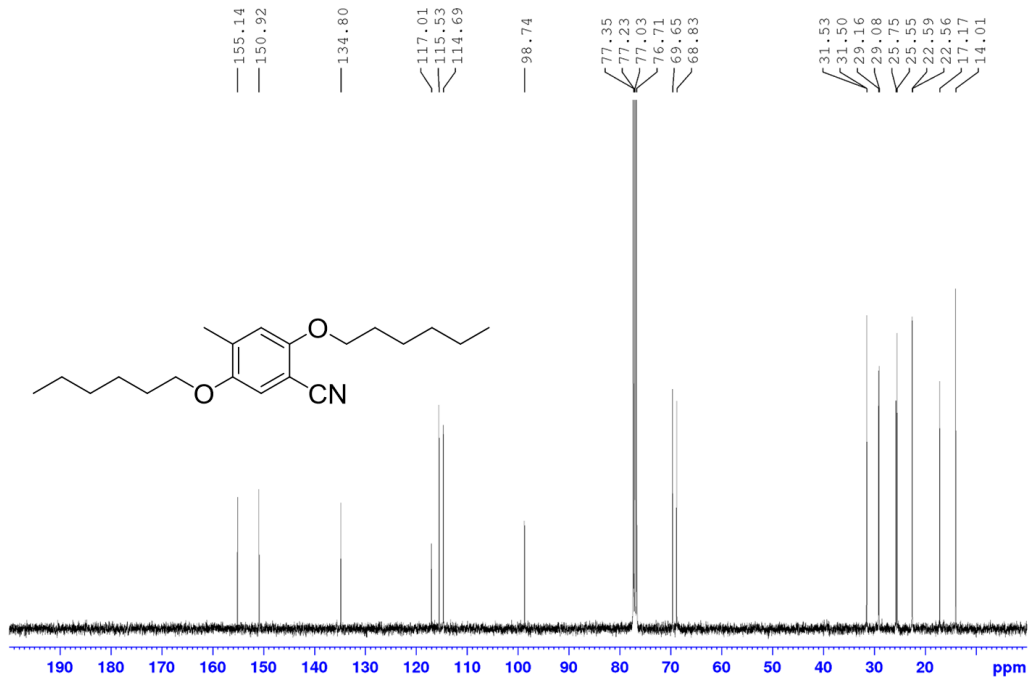
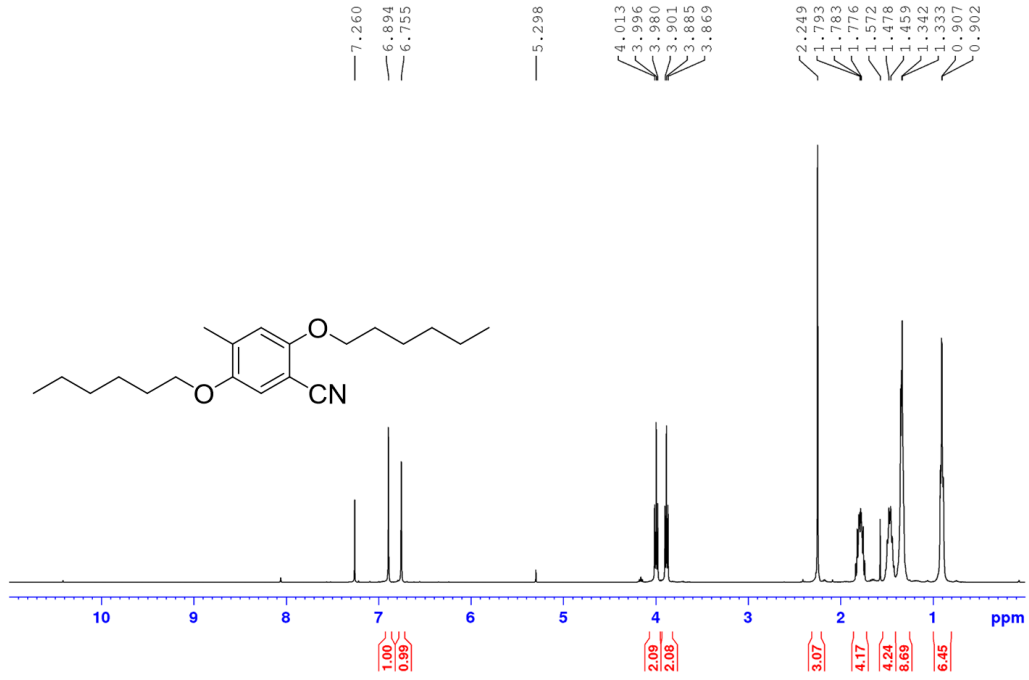


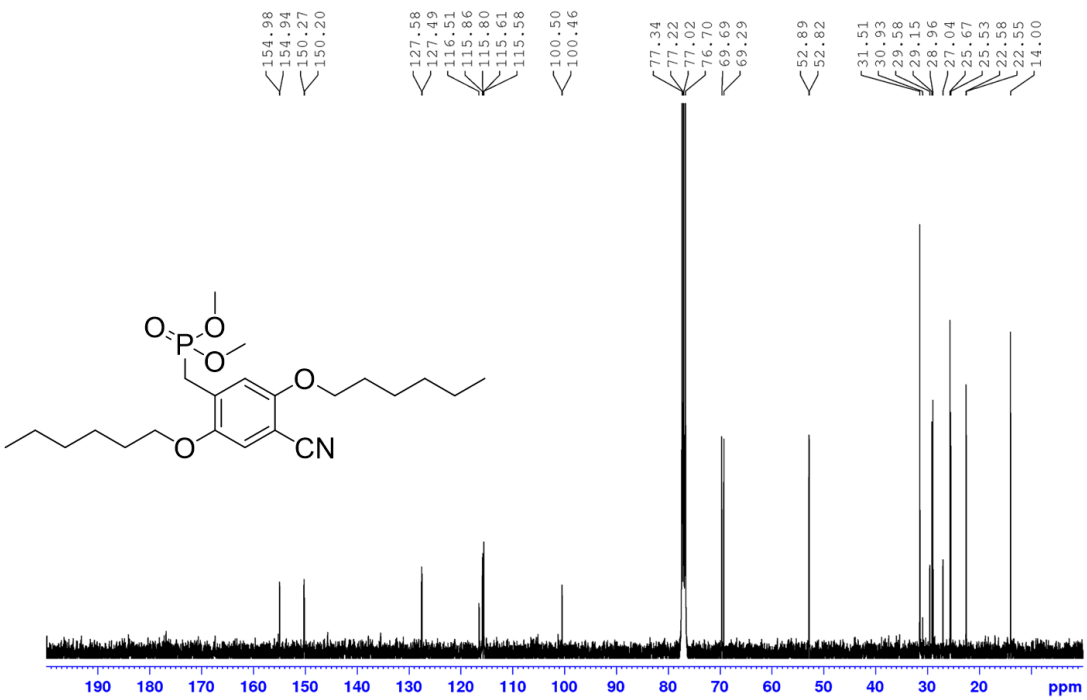
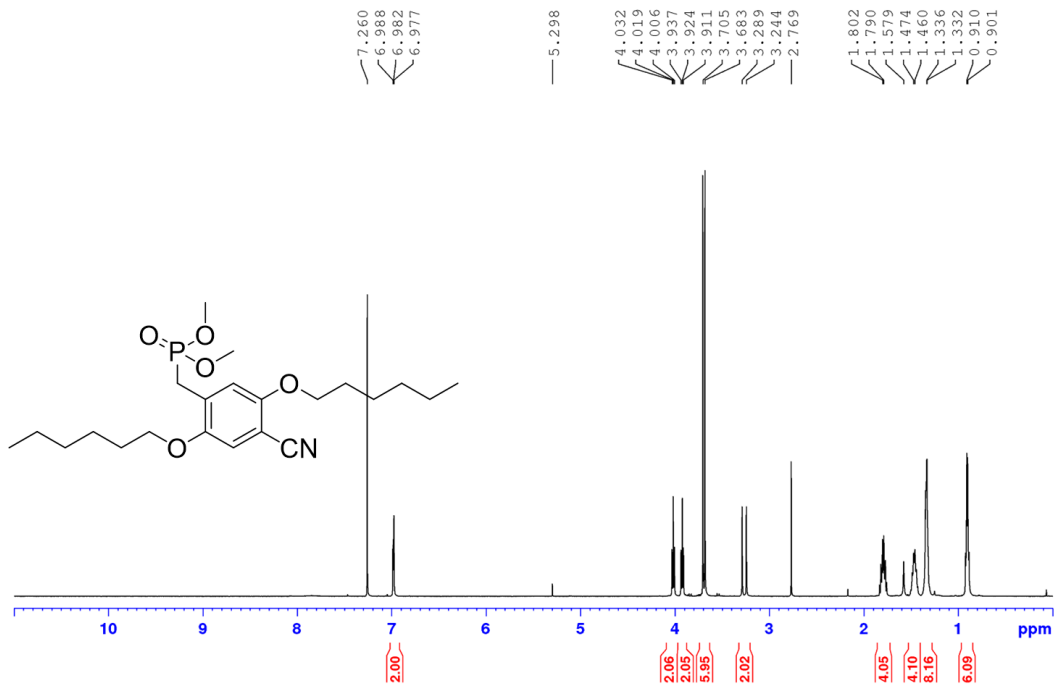


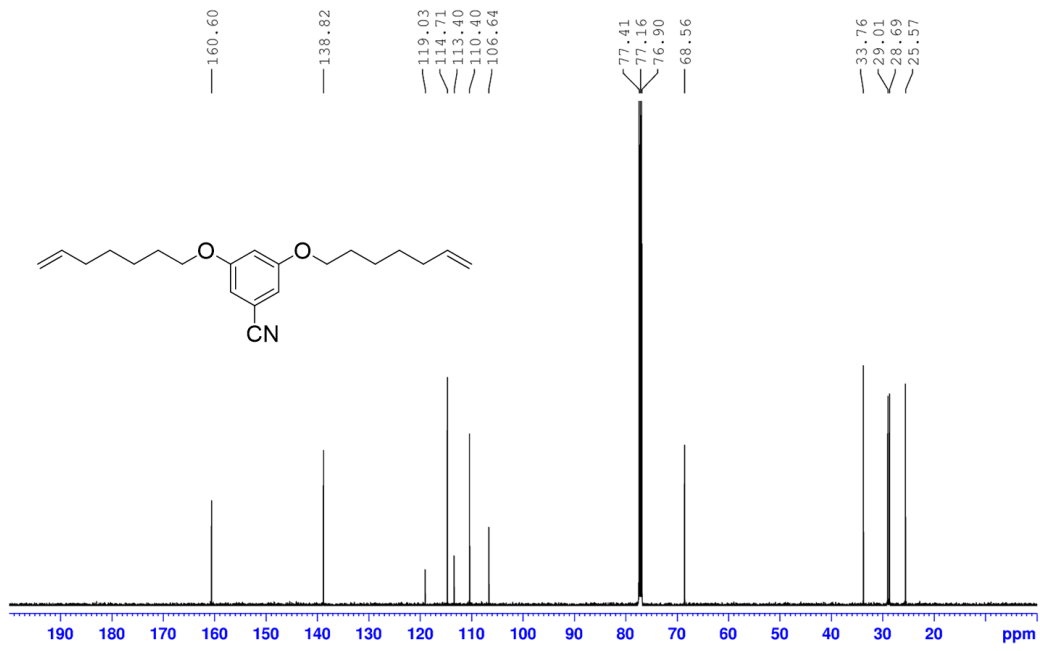
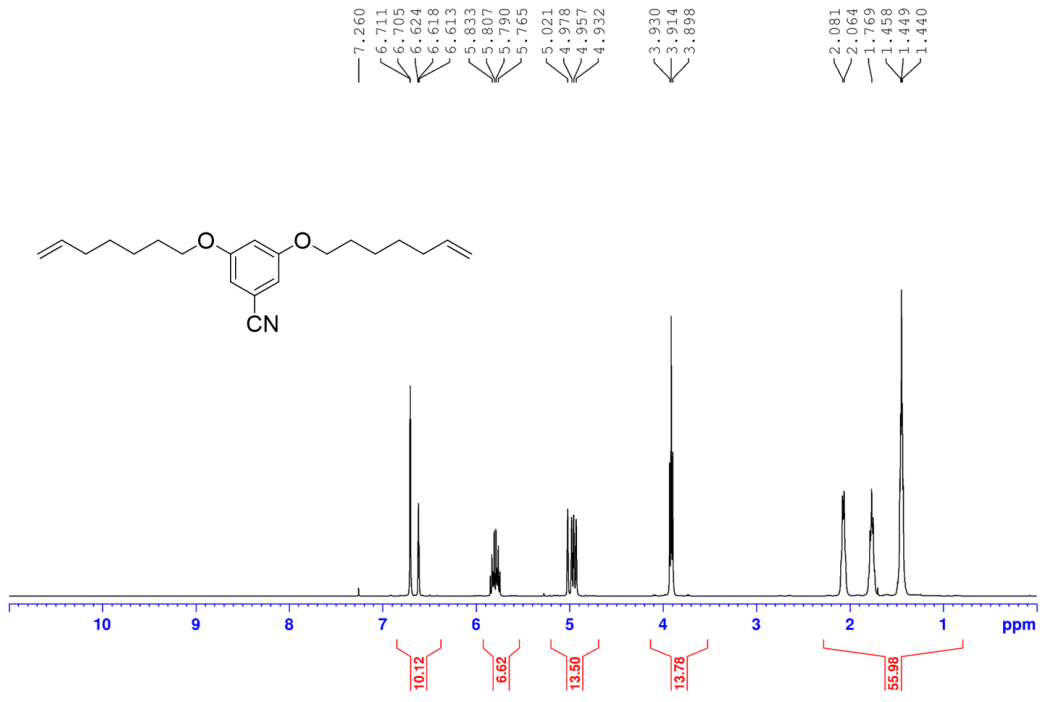


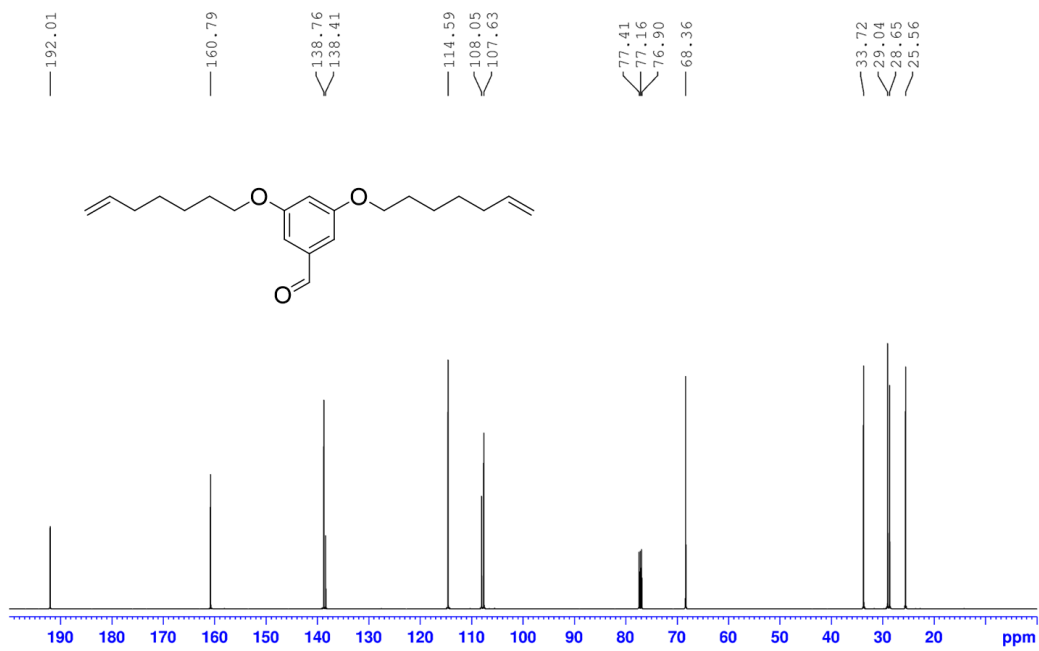
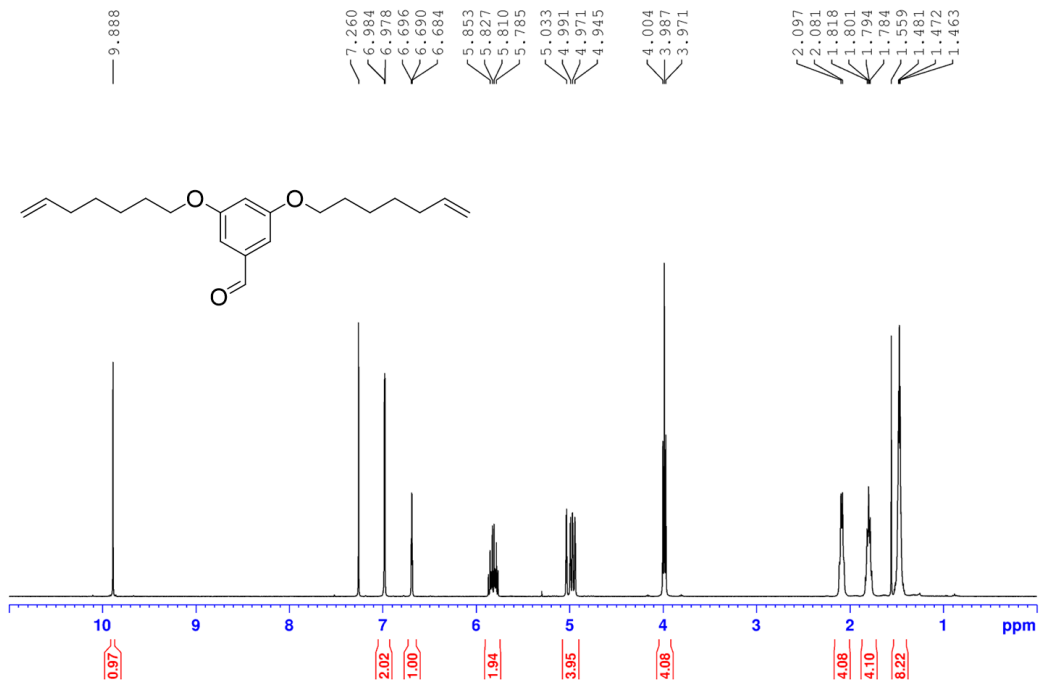


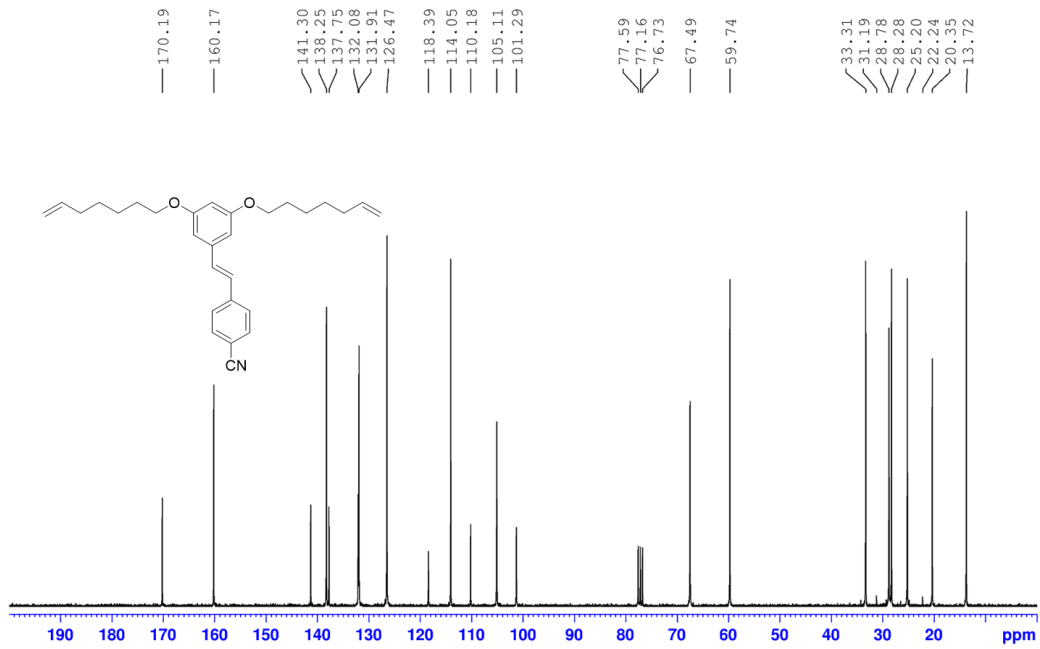
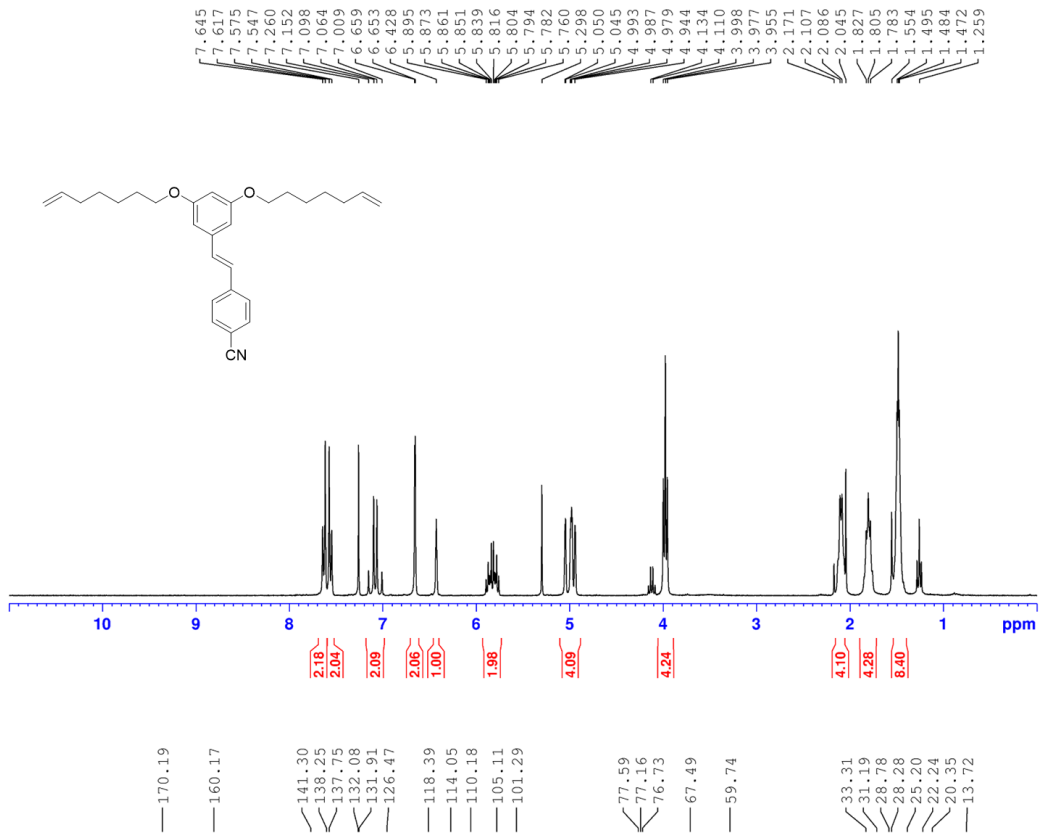


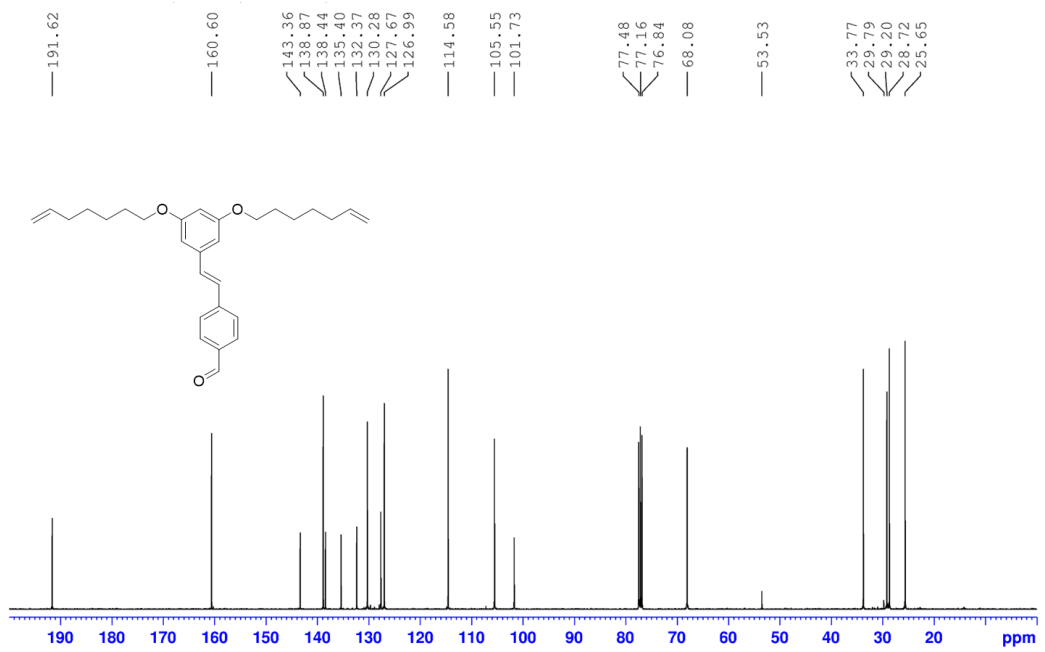
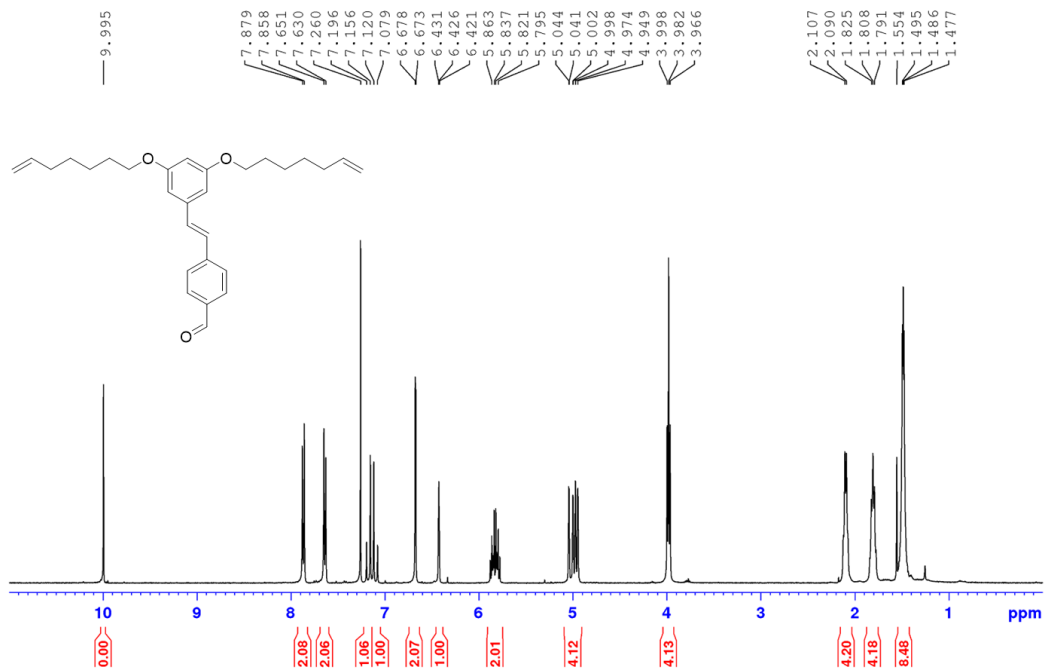


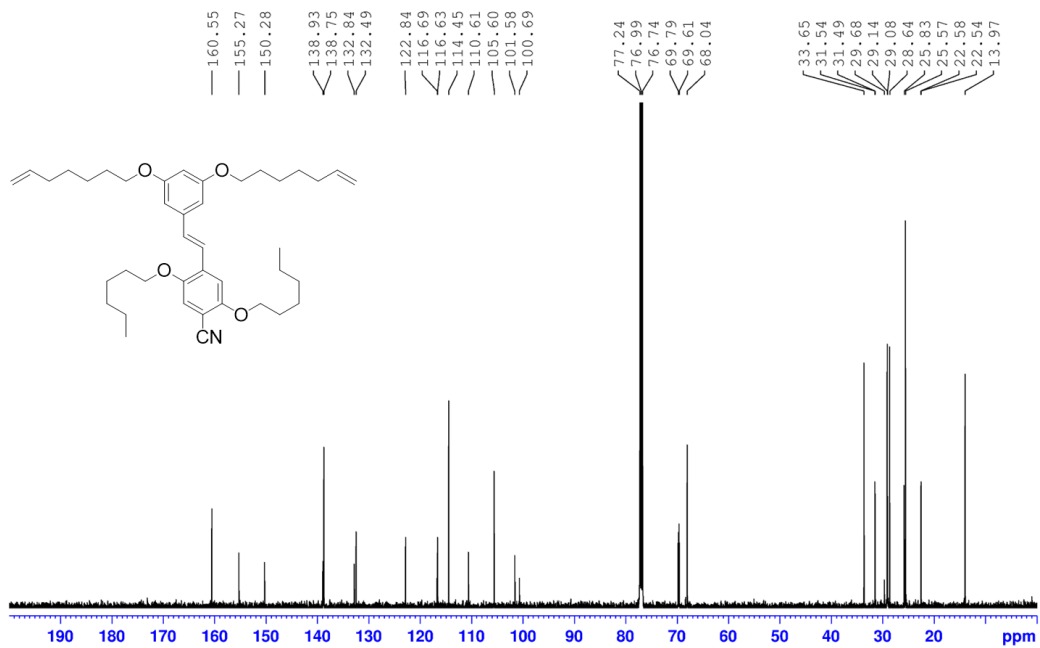
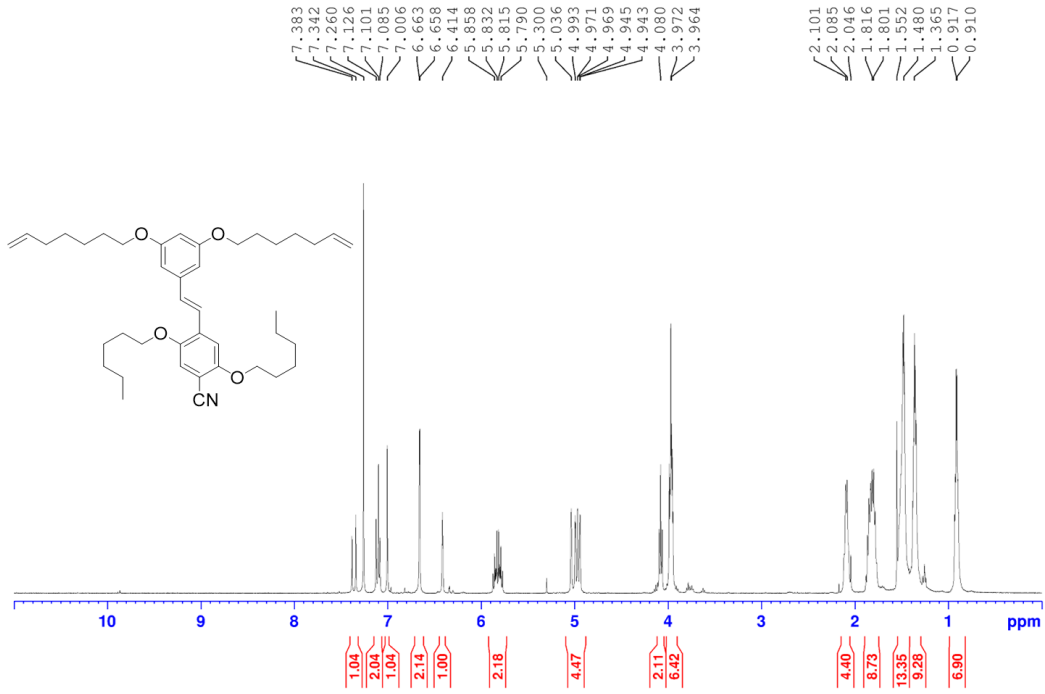


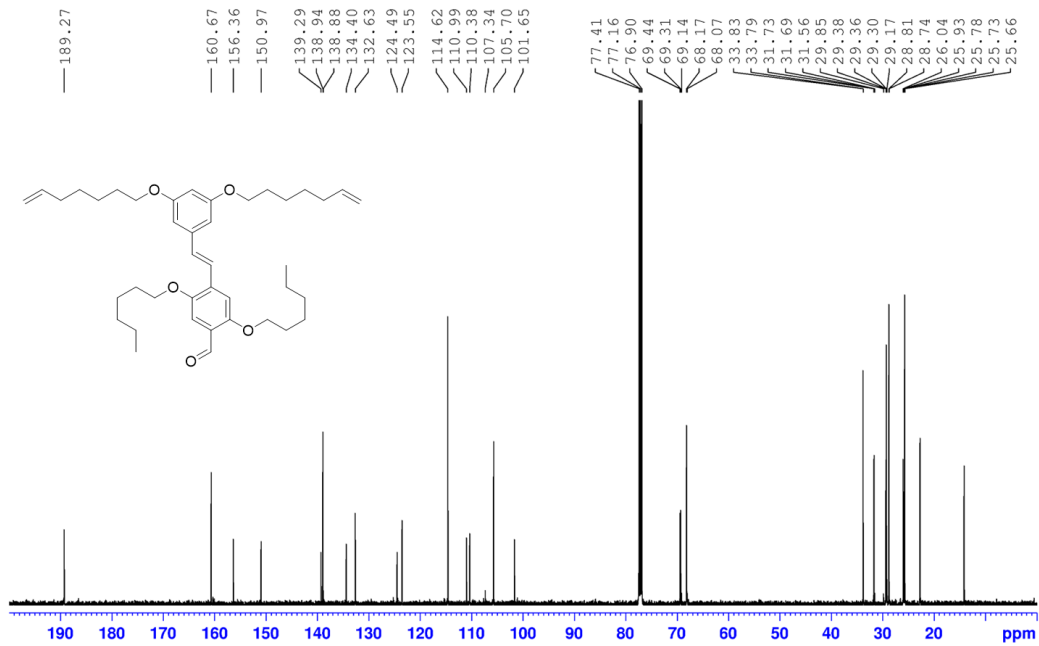
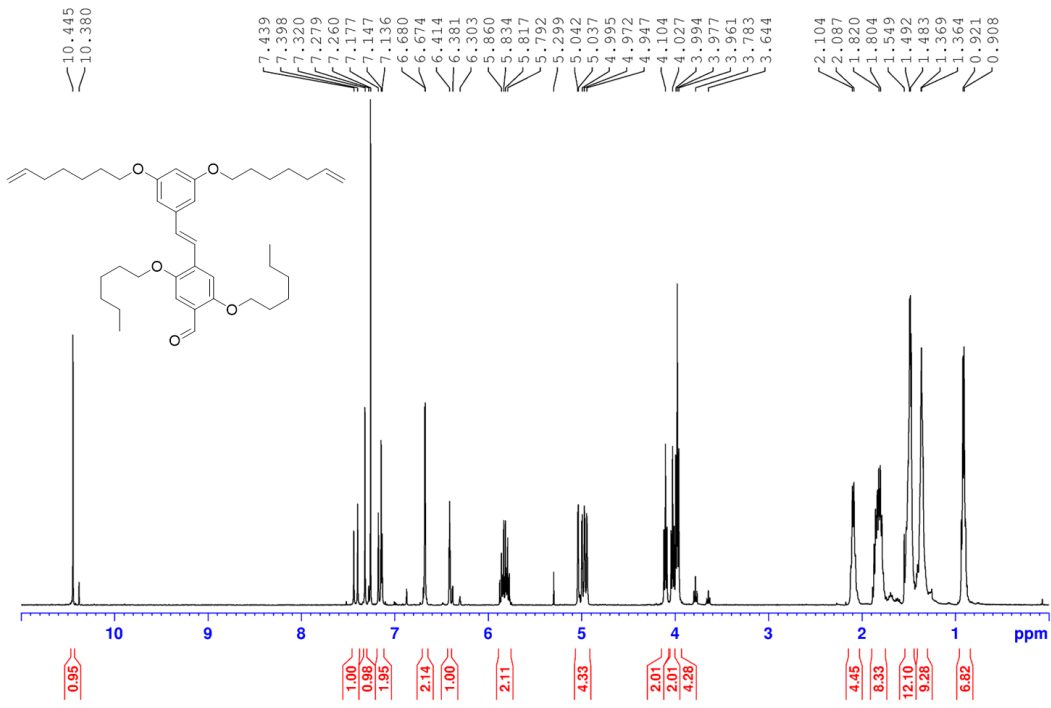




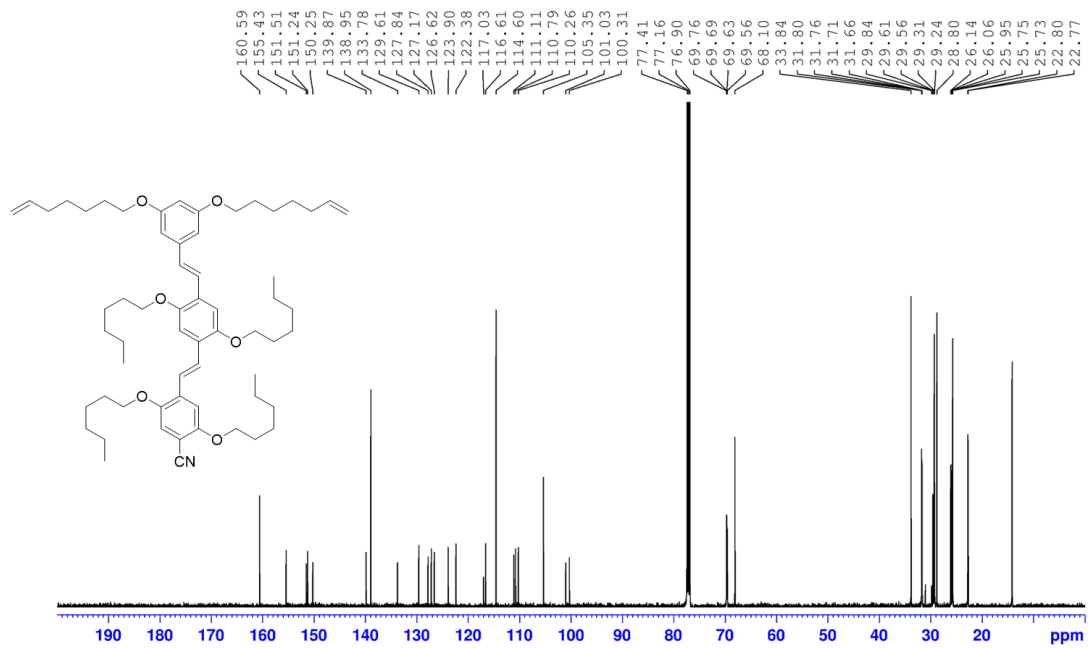
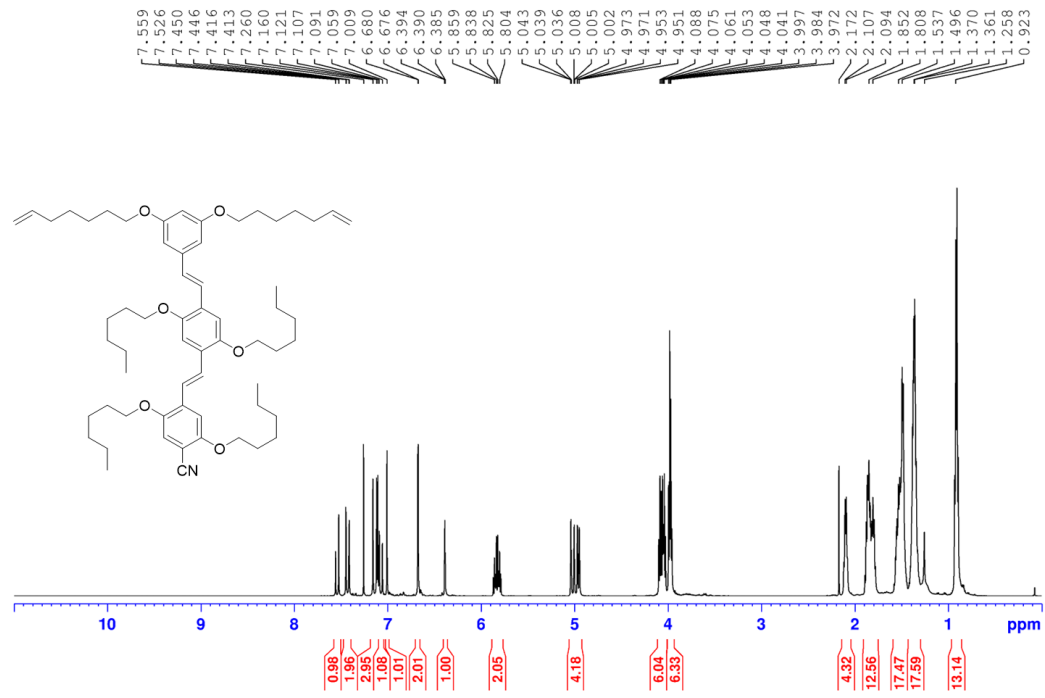


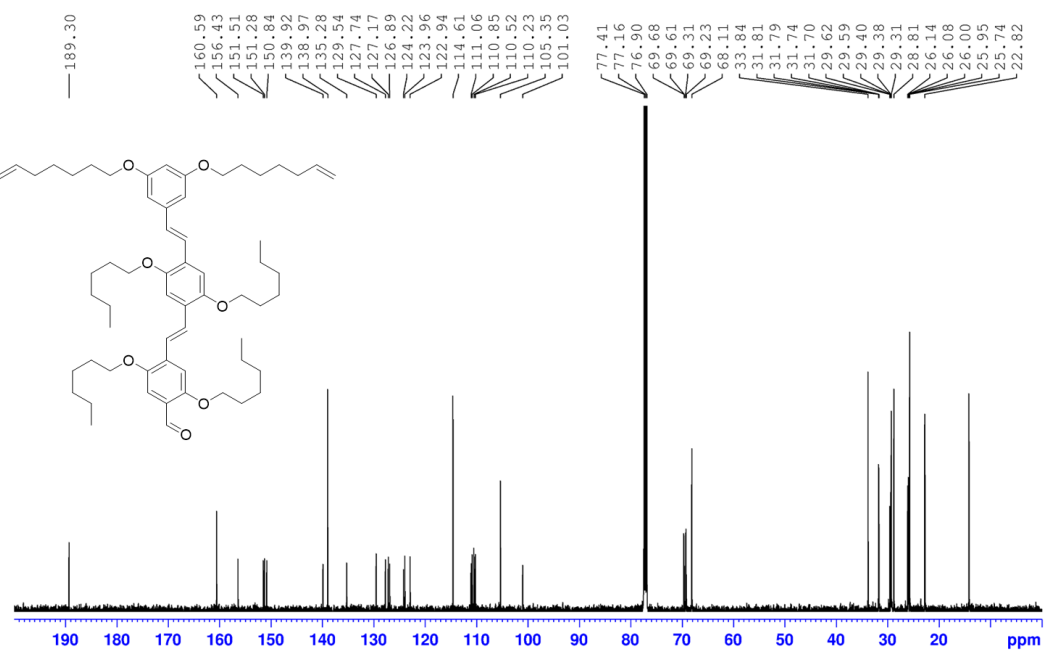
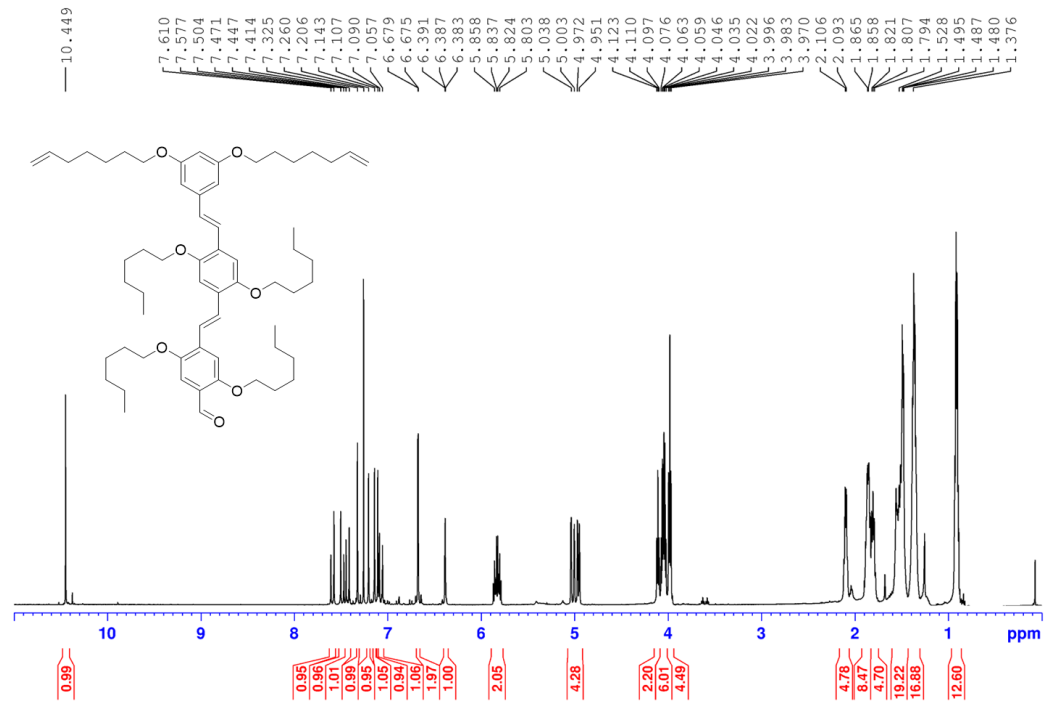


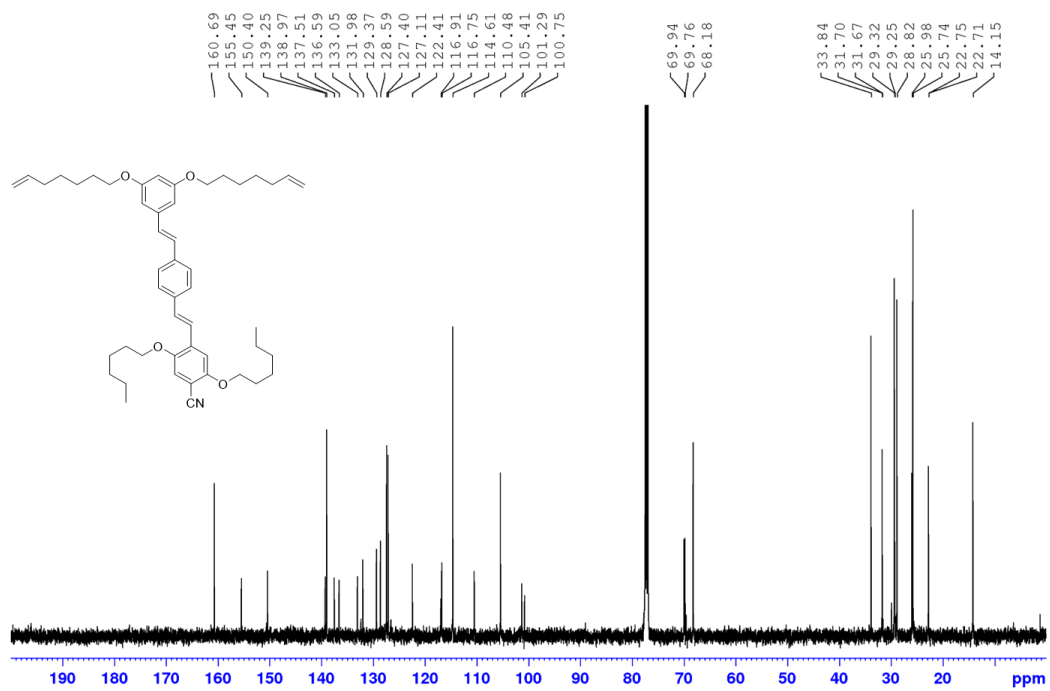
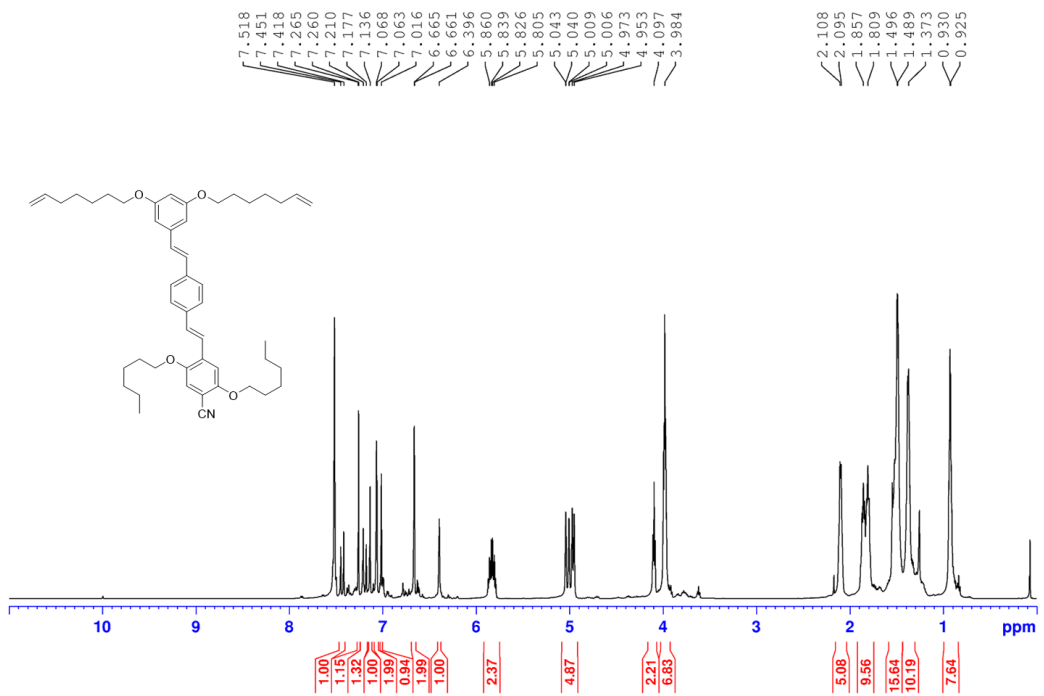


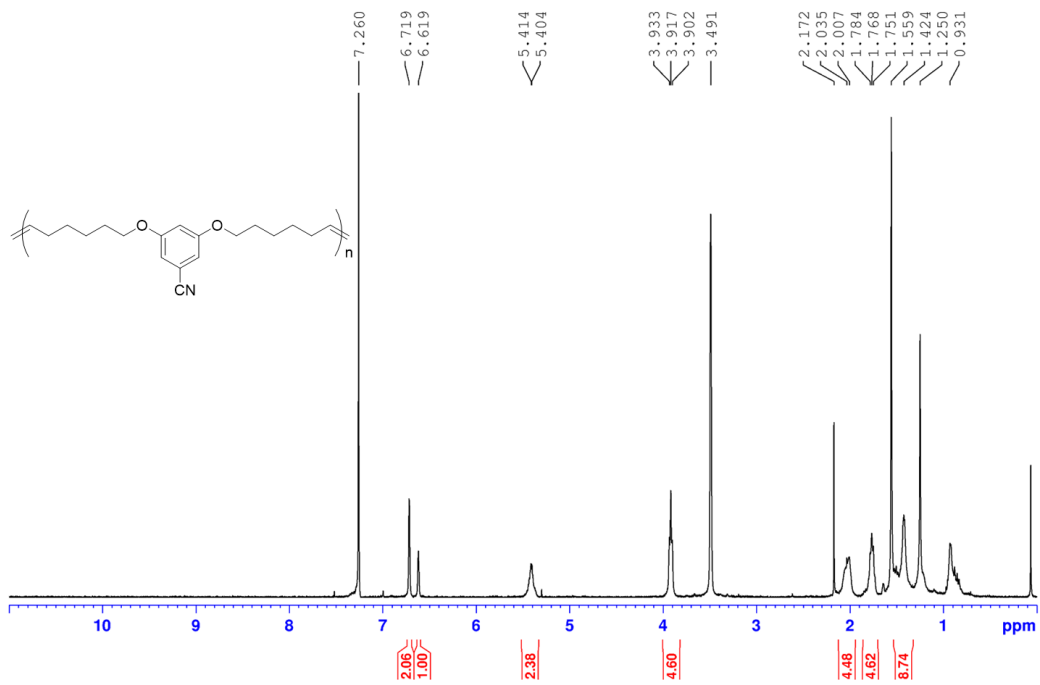


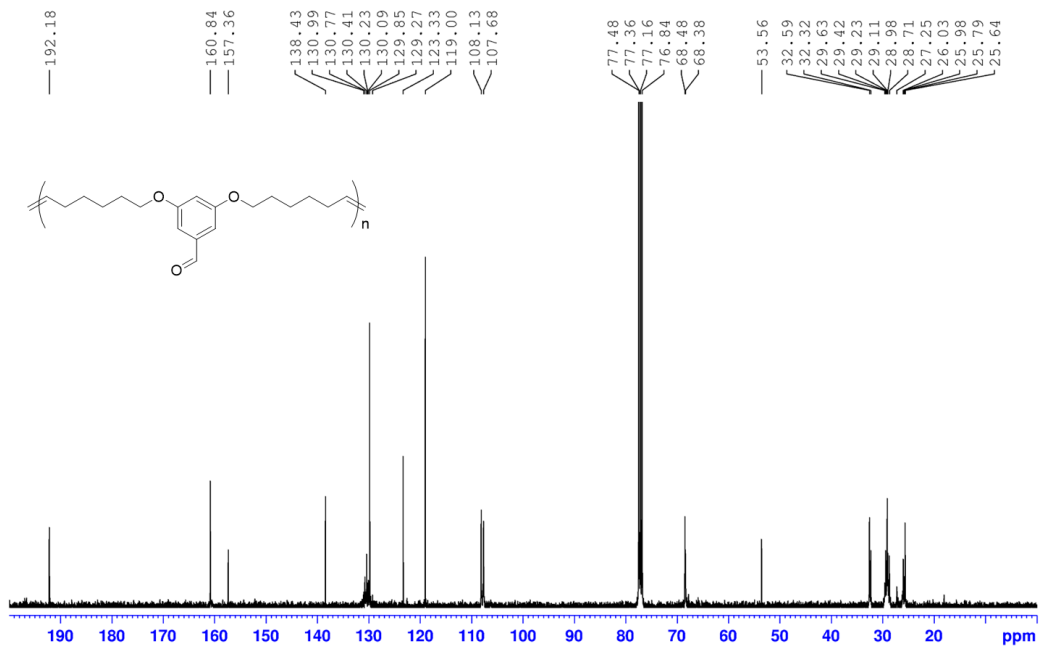
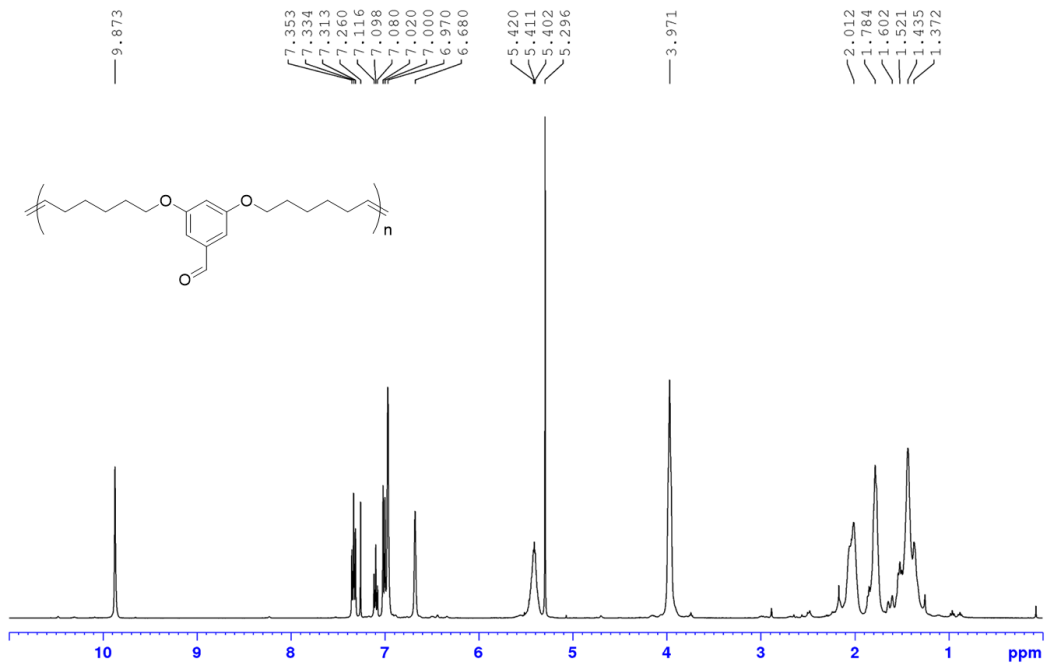


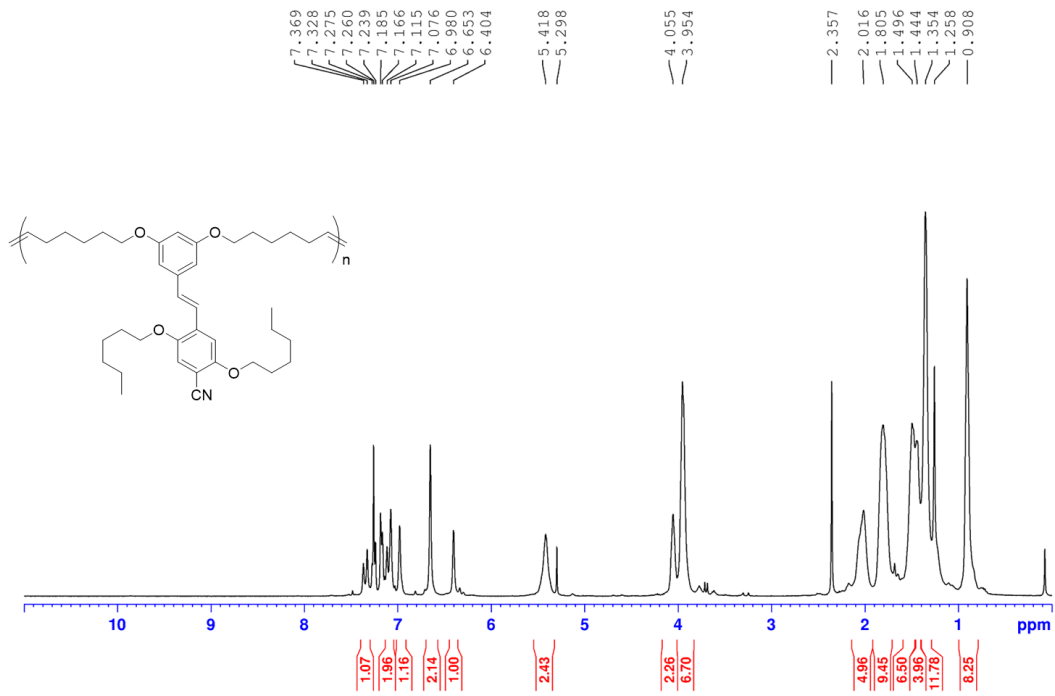


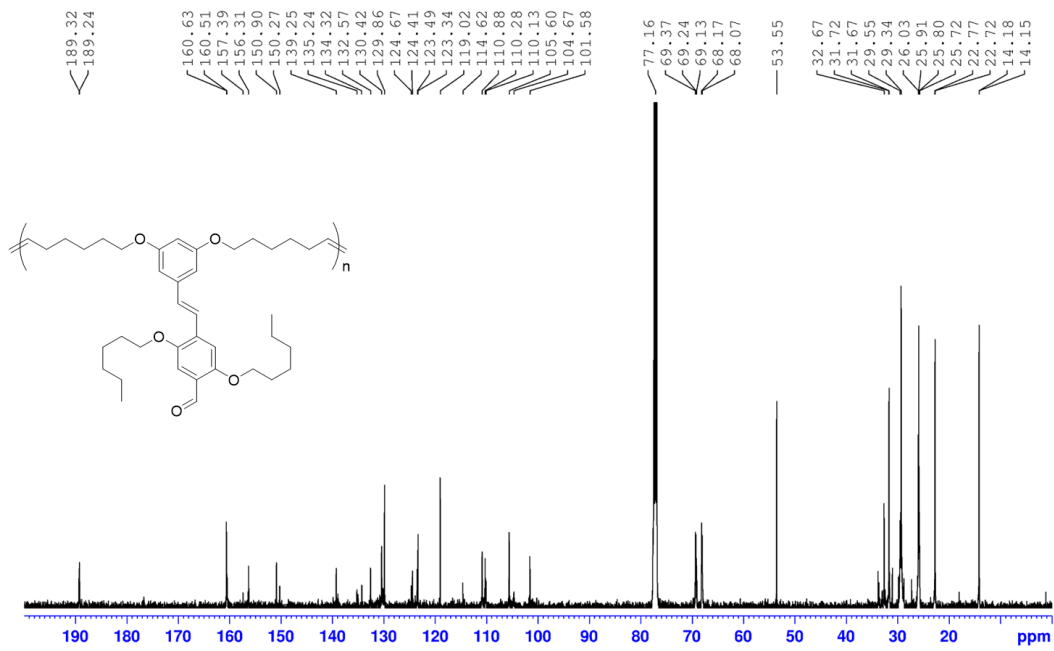
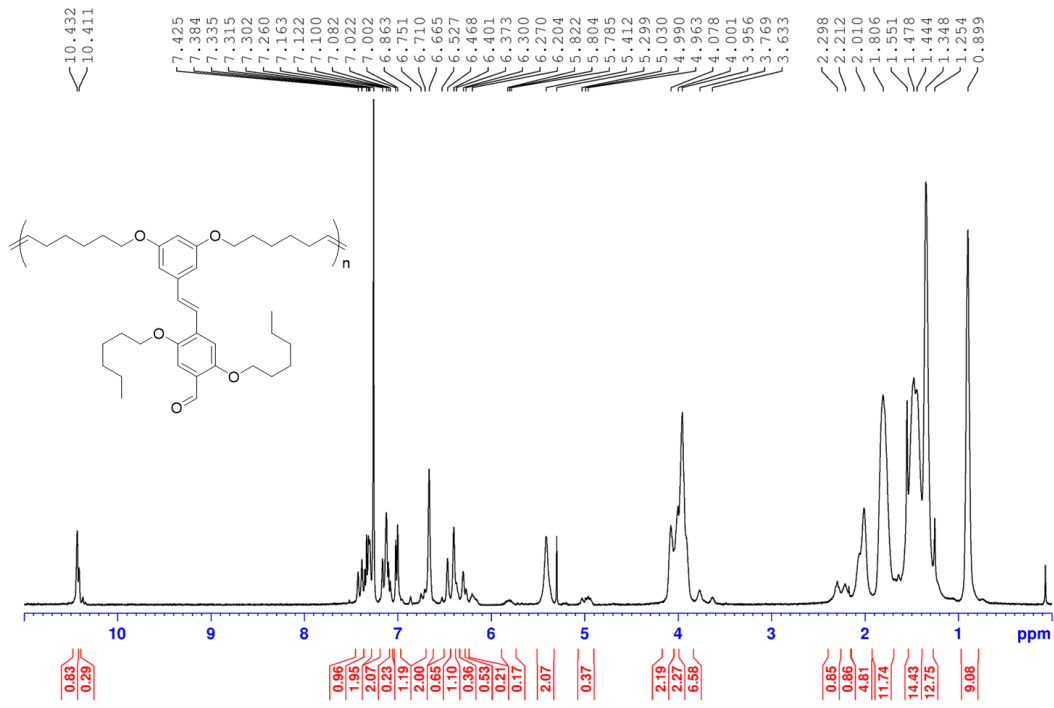












## Bibliography

- (1) Feng, Q. K.; Zhong, S. L.; Pei, J. Y.; Zhao, Y.; Zhang, D. L.; Liu, D. F.; Zhang, Y. X.; Dang, Z. M. Recent Progress and Future Prospects on All-Organic Polymer Dielectrics for Energy Storage Capacitors. *Chem Rev* **2022**, *122* (3), 3820-3878. DOI: 10.1021/acs.chemrev.1c00793 From NLM PubMed-not-MEDLINE.
- (2) Ahmad, Z. Polymeric Dielectric Materials. In *Dielectric Material*, Silaghi, M. A. Ed.; IntechOpen, 2012.
- (3) Guo, M.; Hayakawa, T.; Kakimoto, M.-a.; Goodson, T. Organic Macromolecular High Dielectric Constant Materials: Synthesis, Characterization, and Applications. *The Journal of Physical Chemistry B* **2011**, *115* (46), 13419-13432. DOI: 10.1021/jp205428j.
- (4) Li, Y.; Wang, H.; Shi, Z.; Mei, J.; Wang, X.; Yan, D.; Cui, Z. Novel high-k polymers as dielectric layers for organic thin-film transistors. *Polymer Chemistry* **2015**, *6* (37), 6651-6658, 10.1039/C5PY00891C. DOI: 10.1039/C5PY00891C.
- (5) Baer, E.; Zhu, L. 50th Anniversary Perspective: Dielectric Phenomena in Polymers and Multilayered Dielectric Films. *Macromolecules* **2017**, *50* (6), 2239-2256. DOI: 10.1021/acs.macromol.6b02669.
- (6) Sarjeant, W. J.; Zirnheld, J.; MacDougall, F. W. Capacitors. *IEEE Transactions on Plasma Science* **1998**, *26* (5), 1368-1392. DOI: 10.1109/27.736020.
- (7) Yoon, M.-H.; Facchetti, A.; Marks, T. J.  $\sigma$ - $\pi$  Molecular Dielectric Multilayers for Low-Voltage Organic Thin-Film Transistors. *Proceedings of the National Academy of Sciences of the United States of America* **2005**, *102* (13), 4678-4682.
- (8) Zeng, L.; Turrisi, R.; Fu, B.; Emery, J. D.; Walker, A. R.; Ratner, M. A.; Hersam, M. C.; Facchetti, A. F.; Marks, T. J.; Bedzyk, M. J. Measuring Dipole Inversion in Self-Assembled Nano-Dielectric Molecular Layers. *ACS Applied Materials & Interfaces* **2018**, *10* (7), 6484-6490. DOI: 10.1021/acsami.7b16160.
- (9) Zhu, L. Exploring Strategies for High Dielectric Constant and Low Loss Polymer Dielectrics. *The Journal of Physical Chemistry Letters* **2014**, *5* (21), 3677-3687. DOI: 10.1021/jz501831q.
- (10) Zhang, G.; Li, Q.; Allahyarov, E.; Li, Y.; Zhu, L. Challenges and Opportunities of Polymer Nanodielectrics for Capacitive Energy Storage. *ACS Applied Materials & Interfaces* **2021**, *13* (32), 37939-37960. DOI: 10.1021/acsami.1c04991.
- (11) Heitzer, H. M.; Marks, T. J.; Ratner, M. A. Maximizing the Dielectric Response of Molecular Thin Films via Quantum Chemical Design. *ACS Nano* **2014**, *8* (12), 12587-12600. DOI: 10.1021/nn505431p.
- (12) Evaristo Riande, R. D.-C. *Electrical Properties of Polymers*; CRC Press, 2004. DOI: 10.1201/9780367801304.
- (13) Dissado, L. Dielectric Response. In *Springer Handbook of Electronic and Photonic Materials*, Kasap, S., Capper, P. Eds.; Springer US, 2007; pp 187-212.
- (14) Schönhals, A.; Kremer, F. Theory of Dielectric Relaxation. In *Broadband Dielectric Spectroscopy*, Kremer, F., Schönhals, A. Eds.; Springer Berlin Heidelberg, 2003; pp 1-33.
- (15) Feldman, Y.; Ishai, P. B.; Puzenko, A.; Raicu, V. 3233Elementary Theory of the Interaction of Electromagnetic Fields with Dielectric Materials. In *Dielectric Relaxation in Biological*



*Systems: Physical Principles, Methods, and Applications*; Oxford University Press, 2015; p 0. DOI: 10.1093/acprof:oso/9780199686513.003.0002.

(16) Poplavko, Y. M. Chapter 7 - Dielectrics. In *Electronic Materials*, Poplavko, Y. M. Ed.; Elsevier, 2019; pp 287-408.

(17) Zhu, L.; Wang, Q. Novel Ferroelectric Polymers for High Energy Density and Low Loss Dielectrics. *Macromolecules* **2012**, *45* (7), 2937-2954. DOI: 10.1021/ma2024057.

(18) Wang, B.; Huang, W.; Chi, L.; Al-Hashimi, M.; Marks, T. J.; Facchetti, A. High-k Gate Dielectrics for Emerging Flexible and Stretchable Electronics. *Chemical Reviews* **2018**, *118* (11), 5690-5754. DOI: 10.1021/acs.chemrev.8b00045.

(19) Team, T. I. [https://imagine.gsfc.nasa.gov/science/toolbox/spectrum\\_chart.html](https://imagine.gsfc.nasa.gov/science/toolbox/spectrum_chart.html) (accessed).

(20) Wei, J.; Zhu, L. Intrinsic polymer dielectrics for high energy density and low loss electric energy storage. *Progress in Polymer Science* **2020**, *106*. DOI: 10.1016/j.progpolymsci.2020.101254.

(21) *LiebreTexts* libraries. Phys.liebretexts.org, [https://phys.libretexts.org/Bookshelves/University\\_Physics/Book%3A\\_Physics\\_\(Boundless\)/18%3A\\_Electric\\_Potential\\_and\\_Electric\\_Field/18.4%3A\\_Capacitors\\_and\\_Dielectrics](https://phys.libretexts.org/Bookshelves/University_Physics/Book%3A_Physics_(Boundless)/18%3A_Electric_Potential_and_Electric_Field/18.4%3A_Capacitors_and_Dielectrics) (accessed 2023 April 16).

(22) *Capacitor with voltage source*. <http://www.kshitij-iitjee.com/Capacitors-with-dielectrics/> (accessed July 15, 2018).

(23) Yin, H.; Schönhals, A. Broadband Dielectric Spectroscopy on Polymer Blends. In *Polymer Blends Handbook*, 2014; pp 1299-1356.

(24) Park, S.; Kim, C.-H.; Lee, W.-J.; Sung, S.; Yoon, M.-H. Sol-gel metal oxide dielectrics for all-solution-processed electronics. *Materials Science and Engineering: R: Reports* **2017**, *114*, 1-22. DOI: <https://doi.org/10.1016/j.mser.2017.01.003>.

(25) Xu, W.-H.; Tang, Y.-D.; Yao, H.-Y.; Zhang, Y.-H. Dipolar Glass Polymers for Capacitive Energy Storage at Room Temperatures and Elevated Temperatures. *Chinese Journal of Polymer Science* **2022**, *40* (7), 711-725. DOI: 10.1007/s10118-022-2728-y.

(26) Bonardd, S.; Moreno-Serna, V.; Kortaberria, G.; Díaz Díaz, D.; Leiva, A.; Saldías, C. Dipolar Glass Polymers Containing Polarizable Groups as Dielectric Materials for Energy Storage Applications. A Minireview. In *Polymers*, 2019; Vol. 11.

(27) Cheng, R.; Wang, Y.; Men, R.; Lei, Z.; Song, J.; Li, Y.; Guo, M. High-energy-density polymer dielectrics via compositional and structural tailoring for electrical energy storage. *iScience* **2022**, *25* (8), 104837. DOI: 10.1016/j.isci.2022.104837 From NLM PubMed-not-MEDLINE.

(28) Wei, J.; Zhang, Z.; Tseng, J.-K.; Treufeld, I.; Liu, X.; Litt, M. H.; Zhu, L. Achieving High Dielectric Constant and Low Loss Property in a Dipolar Glass Polymer Containing Strongly Dipolar and Small-Sized Sulfone Groups. *ACS Applied Materials & Interfaces* **2015**, *7* (9), 5248-5257. DOI: 10.1021/am508488w.

(29) Chen, X.; Allahyarov, E.; Li, Q.; Langhe, D.; Ponting, M.; Schuele, D. E.; Baer, E.; Zhu, L. Reducing dielectric loss by nanoconfined impurity ion transport in multilayer films under low electric fields. *Composites Part B: Engineering* **2020**, *190*, 107908. DOI: <https://doi.org/10.1016/j.compositesb.2020.107908>.

(30) Bonardd, S.; Moreno-Serna, V.; Kortaberria, G.; Diaz Diaz, D.; Leiva, A.; Saldías, C. Dipolar Glass Polymers Containing Polarizable Groups as Dielectric Materials for Energy Storage Applications. A Minireview. *Polymers (Basel)* **2019**, *11* (2). DOI: 10.3390/polym11020317 From NLM PubMed-not-MEDLINE.

- (31) Polymer Dielectrics for Capacitor Application. In *Kirk-Othmer Encyclopedia of Chemical Technology*.
- (32) Chen, J.; Wang, Y.; Li, H.; Han, H.; Liao, X.; Sun, R.; Huang, X.; Xie, M. Rational Design and Modification of High-k Bis(double-stranded) Block Copolymer for High Electrical Energy Storage Capability. *Chemistry of Materials* **2018**, *30* (3), 1102-1112. DOI: 10.1021/acs.chemmater.7b05042.
- (33) Cheng, X.-Y.; Feng, Q.-K.; Dang, Z.-M.; Du, F.-S.; Li, Z.-C. Alternating [1.1.1]Propellane-(Meth)Acrylate Copolymers: A New Class of Dielectrics with High Energy Density for Film Capacitors. *Macromolecular Rapid Communications* **2023**, *44* (6), 2200888, <https://doi.org/10.1002/marc.202200888>. DOI: <https://doi.org/10.1002/marc.202200888> (accessed 2023/04/12).
- (34) Prateek; Thakur, V. K.; Gupta, R. K. Recent Progress on Ferroelectric Polymer-Based Nanocomposites for High Energy Density Capacitors: Synthesis, Dielectric Properties, and Future Aspects. *Chemical Reviews* **2016**, *116* (7), 4260-4317. DOI: 10.1021/acs.chemrev.5b00495.
- (35) EETech Media, LLC., <https://eepower.com/capacitor-guide/fundamentals/dielectric-materials/#> (accessed).
- (36) Zulkifli, N.; Johar, M.; Marwah, O. M. F.; Ibrahim, M. Review on Advances of Functional Material for Additive Manufacturing. *IOP Conference Series: Materials Science and Engineering* **2017**, *226*, 012177. DOI: 10.1088/1757-899X/226/1/012177.
- (37) Li, Q.; Chen, L.; Gadinski, M. R.; Zhang, S.; Zhang, G.; Li, H. U.; Iagodkine, E.; Haque, A.; Chen, L.-Q.; Jackson, T. N.; et al. Flexible high-temperature dielectric materials from polymer nanocomposites. *Nature* **2015**, *523*, 576. DOI: 10.1038/nature14647 <https://www.nature.com/articles/nature14647#supplementary-information>.
- (38) Heitzer, H. M.; Marks, T. J.; Ratner, M. A. Computation of Dielectric Response in Molecular Solids for High Capacitance Organic Dielectrics. *Accounts of Chemical Research* **2016**, *49* (9), 1614-1623. DOI: 10.1021/acs.accounts.6b00173.
- (39) Qi, L.; Petersson, L.; Liu, T. Review of Recent Activities on Dielectric Films for Capacitor Applications. *Journal of International Council on Electrical Engineering* **2014**, *4* (1), 1-6. DOI: 10.5370/JICEE.2014.4.1.001.
- (40) Zhang, X.; Shen, Y.; Shen, Z.; Jiang, J.; Chen, L.; Nan, C.-W. Achieving High Energy Density in PVDF-Based Polymer Blends: Suppression of Early Polarization Saturation and Enhancement of Breakdown Strength. *ACS Applied Materials & Interfaces* **2016**, *8* (40), 27236-27242. DOI: 10.1021/acsami.6b10016.
- (41) Wu, X.; Ivry, Y.; Zheng, J.; Zhang, P.; Zheng, Z.; Tan, D. Q. Dielectric loss reduction and validation of P(VDF-HFP) films via sandwiching film fabrication for capacitive energy storage. *Materials Today Energy* **2023**, *31*, 101209. DOI: <https://doi.org/10.1016/j.mtener.2022.101209>.
- (42) Huang, H.; Chen, X.; Yin, K.; Treufeld, I.; Schuele, D. E.; Ponting, M.; Langhe, D.; Baer, E.; Zhu, L. Reduction of Ionic Conduction Loss in Multilayer Dielectric Films by Immobilizing Impurity Ions in High Glass Transition Temperature Polymer Layers. *ACS Applied Energy Materials* **2018**, *1* (2), 775-782. DOI: 10.1021/acs.aem.7b00211.
- (43) Chen, X.; Allahyarov, E.; Langhe, D.; Ponting, M.; Li, R.; Fukuto, M.; Schuele, D. E.; Baer, E.; Zhu, L. Reducing dielectric loss and enhancing electrical insulation for multilayer polymer films by nanoconfined ion transport under high poling electric fields. *Journal of Materials Chemistry C* **2020**, *8* (18), 6102-6117. DOI: 10.1039/d0tc00522c.

- (44) Ortiz, R. P.; Facchetti, A.; Marks, T. J. High-k Organic, Inorganic, and Hybrid Dielectrics for Low-Voltage Organic Field-Effect Transistors. *Chemical Reviews* **2010**, *110* (1), 205-239. DOI: 10.1021/cr9001275.
- (45) Van Dyck, C.; Marks, T. J.; Ratner, M. A. Chain Length Dependence of the Dielectric Constant and Polarizability in Conjugated Organic Thin Films. *ACS Nano* **2017**, *11* (6), 5970-5981. DOI: 10.1021/acsnano.7b01807.
- (46) Heitzer, H. M.; Marks, T. J.; Ratner, M. A. Molecular Donor–Bridge–Acceptor Strategies for High-Capacitance Organic Dielectric Materials. *Journal of the American Chemical Society* **2015**, *137* (22), 7189-7196. DOI: 10.1021/jacs.5b03301.
- (47) Ha, Y.-g.; Emery, J. D.; Bedzyk, M. J.; Usta, H.; Facchetti, A.; Marks, T. J. Solution-Deposited Organic–Inorganic Hybrid Multilayer Gate Dielectrics. Design, Synthesis, Microstructures, and Electrical Properties with Thin-Film Transistors. *Journal of the American Chemical Society* **2011**, *133* (26), 10239-10250. DOI: 10.1021/ja202755x.
- (48) Jackson, N. E.; Savoie, B. M.; Kohlstedt, K. L.; Marks, T. J.; Chen, L. X.; Ratner, M. A. Structural and Conformational Dispersion in the Rational Design of Conjugated Polymers. *Macromolecules* **2014**, *47* (3), 987-992. DOI: 10.1021/ma4023923.
- (49) Chen, Y.; Zhuang, X.; Goldfine, E. A.; Dravid, V. P.; Bedzyk, M. J.; Huang, W.; Facchetti, A.; Marks, T. J. Printable Organic-Inorganic Nanoscale Multilayer Gate Dielectrics for Thin-Film Transistors Enabled by a Polymeric Organic Interlayer. *Advanced Functional Materials* **2020**, *30* (40). DOI: 10.1002/adfm.202005069.
- (50) Stallings, K.; Turrisi, R.; Chen, Y.; Zeng, L.; Wang, B.; Smith, J.; Bedzyk, M. J.; Beverina, L.; Facchetti, A.; Marks, T. J. Systematic Analysis of Self-Assembled Nanodielectric Architecture and Organization Effects on Organic Transistor Switching. *ACS Applied Electronic Materials* **2022**, *4* (4), 2015-2025. DOI: 10.1021/acsaelm.2c00177.
- (51) Albert, I. D. L.; Marks, T. J.; Ratner, M. A. Rational Design of Molecules with Large Hyperpolarizabilities. Electric Field, Solvent Polarity, and Bond Length Alternation Effects on Merocyanine Dye Linear and Nonlinear Optical Properties. *The Journal of Physical Chemistry* **1996**, *100* (23), 9714-9725. DOI: 10.1021/jp960860v.
- (52) DiBenedetto, S. A.; Facchetti, A.; Ratner, M. A.; Marks, T. J. Molecular Self-Assembled Monolayers and Multilayers for Organic and Unconventional Inorganic Thin-Film Transistor Applications. *Advanced Materials* **2009**, *21* (14-15), 1407-1433. DOI: doi:10.1002/adma.200803267.
- (53) DiBenedetto, S.; Frattarelli, D.; Facchetti, A.; Ratner, M.; Marks, T. J. Structure-Performance Correlations in Vapor Phase Deposited Self-Assembled Nanodielectrics for Organic Field-Effect Transistors. *J Am Chem Soc* **2009**, *131* (31), 11. DOI: 10.1021/ja902751e.
- (54) Norris, B. N.; Zhang, S.; Campbell, C. M.; Auletta, J. T.; Calvo-Marzal, P.; Hutchison, G. R.; Meyer, T. Y. Sequence Matters: Modulating Electronic and Optical Properties of Conjugated Oligomers via Tailored Sequence. *Macromolecules* **2013**, *46* (4), 1384-1392. DOI: 10.1021/ma400123r.
- (55) Zhang, S.; Bauer, N. E.; Kanal, I. Y.; You, W.; Hutchison, G. R.; Meyer, T. Y. Sequence Effects in Donor–Acceptor Oligomeric Semiconductors Comprising Benzothiadiazole and Phenylenevinylene Monomers. *Macromolecules* **2017**, *50* (1), 151-161. DOI: 10.1021/acs.macromol.6b02215.
- (56) Norris, B. N.; Pan, T.; Meyer, T. Y. Iterative Synthesis of Heterotelechelic Oligo(phenylenevinylene)s by Olefin Cross-Metathesis. *Organic Letters* **2010**, *12* (23), 5514-5517. DOI: 10.1021/ol102398y.

- (57) Shaopeng, Z.; R., H. G.; Y., M. T. Sequence Effects in Conjugated Donor–Acceptor Trimers and Polymers. *Macromolecular Rapid Communications* **2016**, *37* (11), 882-887. DOI: doi:10.1002/marc.201600086.
- (58) Mannodi-Kanakkithodi, A.; Huan, T. D.; Ramprasad, R. Mining Materials Design Rules from Data: The Example of Polymer Dielectrics. *Chemistry of Materials* **2017**, *29* (21), 9001-9010. DOI: 10.1021/acs.chemmater.7b02027.
- (59) Sharma, V.; Wang, C.; Lorenzini, R. G.; Ma, R.; Zhu, Q.; Sinkovits, D. W.; Pilania, G.; Oganov, A. R.; Kumar, S.; Sotzing, G. A.; et al. Rational design of all organic polymer dielectrics. *Nature Communications* **2014**, *5*, 4845, Article. DOI: 10.1038/ncomms5845  
<https://www.nature.com/articles/ncomms5845#supplementary-information>.
- (60) Hiener, D. C.; Hutchison, G. R. Pareto Optimization of Oligomer Polarizability and Dipole Moment Using a Genetic Algorithm. *The Journal of Physical Chemistry A* **2022**, *126* (17), 2750-2760. DOI: 10.1021/acs.jpca.2c01266.
- (61) Greenstein, B. L.; Hiener, D. C.; Hutchison, G. R. Computational evolution of high-performing unfused non-fullerene acceptors for organic solar cells. *The Journal of Chemical Physics* **2022**, *156* (17), 174107. DOI: 10.1063/5.0087299 (accessed 11/20/2023).
- (62) Hiener, D. C.; Folmsbee, D. L.; Langkamp, L. A.; Hutchison, G. R. Evaluating fast methods for static polarizabilities on extended conjugated oligomers. *Physical Chemistry Chemical Physics* **2022**, *24* (38), 23173-23181, 10.1039/D2CP02375J. DOI: 10.1039/D2CP02375J.
- (63) Abarbanel, O. D.; Rozon, J.; Hutchison, G. R. Strategies for Computer-Aided Discovery of Novel Open-Shell Polymers. *The Journal of Physical Chemistry Letters* **2022**, *13* (9), 2158-2164. DOI: 10.1021/acs.jpcllett.2c00509.
- (64) Woodward, W. H. H. Broadband Dielectric Spectroscopy—A Practical Guide. In *Broadband Dielectric Spectroscopy: A Modern Analytical Technique*, ACS Symposium Series, Vol. 1375; American Chemical Society, 2021; pp 3-59.
- (65) Schönhals, A.; Kremer, F. Broadband Dielectric Measurement Techniques (10-6 Hz to 1012 Hz). In *Broadband Dielectric Spectroscopy*, Kremer, F., Schönhals, A. Eds.; Springer Berlin Heidelberg, 2003; pp 35-57.
- (66) Schultz, J. W. Dielectric Spectroscopy in Analysis of Polymers. In *Encyclopedia of Analytical Chemistry*, 2006.
- (67) Carr, J. M.; Mackey, M.; Flandin, L.; Schuele, D.; Zhu, L.; Baer, E. Effect of biaxial orientation on dielectric and breakdown properties of poly(ethylene terephthalate)/poly(vinylidene fluoride-co-tetrafluoroethylene) multilayer films. *Journal of Polymer Science Part B: Polymer Physics* **2013**, *51* (11), 882-896, <https://doi.org/10.1002/polb.23277>. DOI: <https://doi.org/10.1002/polb.23277> (accessed 2023/06/16).
- (68) Wu, X.; Song, G.; Zhang, X.; Lin, X.; Ivry, Y.; Tan, D. Q. Multilayer polyetherimide films incorporating alumina nanolayers for dielectric capacitors. *Chemical Engineering Journal* **2022**, *450*, 137940. DOI: <https://doi.org/10.1016/j.cej.2022.137940>.
- (69) Treufeld, I.; Wang, D. H.; Kurish, B. A.; Tan, L.-S.; Zhu, L. Enhancing electrical energy storage using polar polyimides with nitrile groups directly attached to the main chain. *Journal of Materials Chemistry A* **2014**, *2* (48), 20683-20696, 10.1039/C4TA03260H. DOI: 10.1039/C4TA03260H.
- (70) Stallings, K.; Smith, J.; Chen, Y.; Zeng, L.; Wang, B.; Di Carlo, G.; Bedzyk, M. J.; Facchetti, A.; Marks, T. J. Self-Assembled Nanodielectrics for Solution-Processed Top-Gate Amorphous IGZO Thin-Film Transistors. *ACS Appl Mater Interfaces* **2021**, *13* (13), 15399-15408. DOI: 10.1021/acsami.1c00249.

- (71) Huang, W.; Yu, X.; Zeng, L.; Wang, B.; Takai, A.; Di Carlo, G.; Bedzyk, M. J.; Marks, T. J.; Facchetti, A. Ultraviolet Light-Densified Oxide-Organic Self-Assembled Dielectrics: Processing Thin-Film Transistors at Room Temperature. *ACS Appl Mater Interfaces* **2021**, *13* (2), 3445-3453. DOI: 10.1021/acsami.0c20345.
- (72) Liu, J.; Hennek, J. W.; Buchholz, D. B.; Ha, Y.-g.; Xie, S.; Dravid, V. P.; Chang, R. P. H.; Facchetti, A.; Marks, T. J. Reinforced Self-Assembled Nanodielectrics for High-Performance Transparent Thin Film Transistors. *Advanced Materials* **2011**, *23* (8), 992-997. DOI: <https://doi.org/10.1002/adma.201004198> (accessed 2023/10/10).
- (73) Xu, H.; He, G.; Chen, S.; Chen, S.; Qiao, R.; Luo, H.; Zhang, D. All-Organic Polymer Dielectrics Containing Sulfonyl Dipolar Groups and  $\pi$ - $\pi$  Stacking Interaction in Side-Chain Architectures. *Macromolecules* **2021**, *54* (17), 8195-8206. DOI: 10.1021/acs.macromol.1c00778.
- (74) Shirai, Y.; Zhao, Y.; Cheng, L.; Tour, J. M. Facile Synthesis of Multifullerene-OPE Hybrids via in Situ Ethynylation. *Organic Letters* **2004**, *6* (13), 2129-2132. DOI: 10.1021/ol049447t.
- (75) Wielopolski, M.; Atienza, C.; Clark, T.; Guldi, D. M.; Martin, N. p-Phenyleneethynylene molecular wires: influence of structure on photoinduced electron-transfer properties. *Chemistry* **2008**, *14* (21), 6379-6390. DOI: 10.1002/chem.200800159 From NLM Medline.
- (76) Shellaiah, M.; Ramakrishnam Raju, M. V.; Singh, A.; Lin, H.-C.; Wei, K.-H.; Lin, H.-C. Synthesis of novel platinum complex core as a selective Ag<sup>+</sup> sensor and its H-bonded tetrads self-assembled with triarylamine dendrimers for electron/energy transfers. *J. Mater. Chem. A* **2014**, *2* (41), 17463-17476. DOI: 10.1039/c4ta04231j.
- (77) Simocko, C.; Young, T. C.; Wagener, K. B. ADMET Polymers Containing Precisely Spaced Pendant Boronic Acids and Esters. *Macromolecules* **2015**, *48* (16), 5470-5473. DOI: 10.1021/acs.macromol.5b01410.
- (78) Ellinger, S.; Graham, K. R.; Shi, P.; Farley, R. T.; Steckler, T. T.; Brookins, R. N.; Taranekar, P.; Mei, J.; Padilha, L. A.; Ensley, T. R.; et al. Donor-Acceptor-Donor-based  $\pi$ -Conjugated Oligomers for Nonlinear Optics and Near-IR Emission. *Chemistry of Materials* **2011**, *23* (17), 3805-3817. DOI: 10.1021/cm201424a.
- (79) Chaudhuri, D.; Sigmund, E.; Meyer, A.; Rock, L.; Klemm, P.; Lautenschlager, S.; Schmid, A.; Yost, S. R.; Van Voorhis, T.; Bange, S.; et al. Metal-free OLED triplet emitters by side-stepping Kasha's rule. *Angew Chem Int Ed Engl* **2013**, *52* (50), 13449-13452. DOI: 10.1002/anie.201307601.
- (80) Wen, S.; Yun, X.; Chen, W.; Liu, Q.; Zhu, D.; Gu, C.; Sun, M.; Yang, R. A triple bond side-chained 2D-conjugated benzodithiophene based photovoltaic polymer. *RSC Adv.* **2014**, *4* (102), 58426-58431. DOI: 10.1039/c4ra10154e.
- (81) Lambert, C. a. K., V. . Heterogeneous Electron Transfer Processes in Self-Assembled Monolayers of Amine Terminated Conjugated Molecular Wires. *Langmuir* **2006**, *22* (21), 8807-8812. DOI: 10.1021/la061404t.
- (82) Wang, C. C.; Pilia, G.; Boggs, S. A.; Kumar, S.; Breneman, C.; Ramprasad, R. Computational strategies for polymer dielectrics design. *Polymer* **2014**, *55* (4), 979-988. DOI: <https://doi.org/10.1016/j.polymer.2013.12.069>.
- (83) Qiao, Y.; Islam, M. S.; Han, K.; Leonhardt, E.; Zhang, J.; Wang, Q.; Ploehn, H. J.; Tang, C. Polymers Containing Highly Polarizable Conjugated Side Chains as High-Performance All-Organic Nanodielectric Materials. *Advanced Functional Materials* **2013**, *23* (45), 5638-5646, <https://doi.org/10.1002/adfm.201300736>. DOI: <https://doi.org/10.1002/adfm.201300736> (accessed 2023/06/15).

- (84) Bonarrrd, S.; Alegria, Á.; Ramirez, O.; Saldías, C.; Leiva, Á.; Kortaberria, G. New poly(itaconate)s with bulky pendant groups as candidates for “all-polymer” dielectrics. *Reactive and Functional Polymers* **2019**, *140*, 1-13. DOI: <https://doi.org/10.1016/j.reactfunctpolym.2019.04.010>.
- (85) Bonarrrd, S.; Alegria, Á.; Saldías, C.; Leiva, Á.; Kortaberria, G. Synthesis of new poly(itaconate)s containing nitrile groups as high dipolar moment entities for the development of dipolar glass polymers with increased dielectric constant. Thermal and dielectric characterization. *European Polymer Journal* **2019**, *114*, 19-31. DOI: <https://doi.org/10.1016/j.eurpolymj.2019.02.013>.
- (86) Qiao, Y.; Islam, M. S.; Wang, L.; Yan, Y.; Zhang, J.; Benicewicz, B. C.; Ploehn, H. J.; Tang, C. Thiophene Polymer-Grafted Barium Titanate Nanoparticles toward Nanodielectric Composites. *Chemistry of Materials* **2014**, *26* (18), 5319-5326. DOI: 10.1021/cm502341n.
- (87) Bonarrrd, S.; Alegria, A.; Saldias, C.; Leiva, A.; Kortaberria, G. Polyitaconates: A New Family of "All-Polymer" Dielectrics. *ACS Appl Mater Interfaces* **2018**, *10* (44), 38476-38492. DOI: 10.1021/acsami.8b14636.
- (88) Xu, H.; Chen, S.; Chen, S.; Qiao, R.; Li, H.; Luo, H.; Zhang, D. Constructing High-Performance Dielectrics via Molecular and Phase Engineering in Dipolar Polymers. *ACS Applied Energy Materials* **2021**, *4* (3), 2451-2462. DOI: 10.1021/acsae.0c02962.
- (89) Qiao, Y.; Yin, X.; Wang, L.; Islam, M. S.; Benicewicz, B. C.; Ploehn, H. J.; Tang, C. Bimodal Polymer Brush Core–Shell Barium Titanate Nanoparticles: A Strategy for High-Permittivity Polymer Nanocomposites. *Macromolecules* **2015**, *48* (24), 8998-9006. DOI: 10.1021/acs.macromol.5b02018.
- (90) Liu, Y.; Lin, Y.-T.; Haibibu, A.; Xu, W.; Zhou, Y.; Li, L.; Kim, S. H.; Wang, Q. Relaxor Ferroelectric Polymers: Insight into High Electrical Energy Storage Properties from a Molecular Perspective. *Small Science* **2021**, *1* (3), 2000061, <https://doi.org/10.1002/smsc.202000061>. DOI: <https://doi.org/10.1002/smsc.202000061> (accessed 2023/04/12).
- (91) Huang, W.; Ju, T.; Li, R.; Duan, Y.; Duan, Y.; Wei, J.; Zhu, L. High- $\kappa$  and High-Temperature Dipolar Glass Polymers Based on Sulfonylated and Cyanolated Poly(Arylene Ether)s for Capacitive Energy Storage. *Advanced Electronic Materials* **2023**, *9* (1), 2200414, <https://doi.org/10.1002/aelm.202200414>. DOI: <https://doi.org/10.1002/aelm.202200414> (accessed 2023/03/12).
- (92) Zhu, Y.-F.; Zhang, Z.; Litt, M. H.; Zhu, L. High Dielectric Constant Sulfonyl-Containing Dipolar Glass Polymers with Enhanced Orientational Polarization. *Macromolecules* **2018**, *51* (16), 6257-6266. DOI: 10.1021/acs.macromol.8b00923.
- (93) Binauld, S.; Dameron, D.; Connal, L. A.; Hawker, C. J.; Drockenmuller, E. Precise synthesis of molecularly defined oligomers and polymers by orthogonal iterative divergent/convergent approaches. *Macromol Rapid Commun* **2011**, *32* (2), 147-168. DOI: 10.1002/marc.201000548.
- (94) Zhang, J.; Pesak, D. J.; Ludwick, J. L.; Moore, J. S. Geometrically-Controlled and Site-Specifically-Functionalized Phenylacetylene Macrocycles. *Journal of the American Chemical Society* **1994**, *116* (10), 4227-4239. DOI: 10.1021/ja00089a012.
- (95) Schumm, J. S.; Pearson, D. L.; Tour, J. M. Iterative Divergent/Convergent Approach to Linear Conjugated Oligomers by Successive Doubling of the Molecular Length: A Rapid Route to a 128Å-Long Potential Molecular Wire. *Angewandte Chemie International Edition in English* **1994**, *33* (13), 1360-1363. DOI: <https://doi.org/10.1002/anie.199413601> (accessed 2023/11/17).
- (96) Kosynkin, D. V.; Tour, J. M. Phenylene Ethynylene Diazonium Salts as Potential Self-Assembling Molecular Devices. *Organic Letters* **2001**, *3* (7), 993-995. DOI: 10.1021/ol007036g.

- (97) Tour, J. M.; Rawlett, A. M.; Kozaki, M.; Yao, Y.; Jagessar, R. C.; Dirk, S. M.; Price, D. W.; Reed, M. A.; Zhou, C.-W.; Chen, J.; et al. Synthesis and Preliminary Testing of Molecular Wires and Devices. *Chemistry – A European Journal* **2001**, *7* (23), 5118-5134. DOI: [https://doi.org/10.1002/1521-3765\(20011203\)7:23<5118::AID-CHEM5118>3.0.CO;2-1](https://doi.org/10.1002/1521-3765(20011203)7:23<5118::AID-CHEM5118>3.0.CO;2-1) (accessed 2023/11/17).
- (98) Zhao, Y.; Shirai, Y.; Slepko, A. D.; Cheng, L.; Alemany, L. B.; Sasaki, T.; Hegmann, F. A.; Tour, J. M. Synthesis, Spectroscopic and Nonlinear Optical Properties of Multiple [60]Fullerene–Oligo(p-phenylene ethynylene) Hybrids. *Chemistry – A European Journal* **2005**, *11* (12), 3643-3658. DOI: <https://doi.org/10.1002/chem.200401198> (accessed 2023/11/17).
- (99) Arias-Marín, E.; González-Rojano, N.; Navarro-Rodríguez, D.; Weidner, S. Bi-Directional Synthesis of a Series of 2,5-Dodecanoxy-phenyleneethynylene Oligomers. *Synlett* **2005**, *2005* (08), 1259-1262. DOI: 10.1055/s-2005-868474.
- (100) Szymaniak, A. A.; Zhang, C.; Coombs, J. R.; Morken, J. P. Enantioselective Synthesis of Nonracemic Geminal Silylboronates by Pt-Catalyzed Hydrosilylation. *ACS Catalysis* **2018**, *8* (4), 2897-2901. DOI: 10.1021/acscatal.8b00221.
- (101) Zhao, Y.; Shirai, Y.; Slepko, A. D.; Cheng, L.; Alemany, L. B.; Sasaki, T.; Hegmann, F. A.; Tour, J. M. Synthesis, spectroscopic and nonlinear optical properties of multiple [60]fullerene-oligo(p-phenylene ethynylene) hybrids. *Chemistry* **2005**, *11* (12), 3643-3658. DOI: 10.1002/chem.200401198.
- (102) Jones, L.; Schumm, J. S.; Tour, J. M. Rapid Solution and Solid Phase Syntheses of Oligo(1,4-phenylene ethynylene)s with Thioester Termini: Molecular Scale Wires with Alligator Clips. Derivation of Iterative Reaction Efficiencies on a Polymer Support. *The Journal of Organic Chemistry* **1997**, *62* (5), 1388-1410. DOI: 10.1021/jo962336q.
- (103) Pearson, D. L.; Tour, J. M. Rapid Syntheses of Oligo(2,5-thiophene ethynylene)s with Thioester Termini: Potential Molecular Scale Wires with Alligator Clips. *The Journal of Organic Chemistry* **1997**, *62* (5), 1376-1387. DOI: 10.1021/jo962335y.
- (104) Eggers, K.; Fyles, T. M.; Montoya-Pelaez, P. J. Synthesis and Characterization of Photoswitchable Lipids Containing Hemithioindigo Chromophores. *The Journal of Organic Chemistry* **2001**, *66* (9), 2966-2977. DOI: 10.1021/jo0056848.
- (105) Short, A. L.; Fang, C.; Nowalk, J. A.; Weiss, R. M.; Liu, P.; Meyer, T. Y. Cis-Selective Metathesis to Enhance the Living Character of Ring-Opening Polymerization: An Approach to Sequenced Copolymers. *ACS Macro Letters* **2018**, *7* (7), 858-862. DOI: 10.1021/acsmacrolett.8b00460.
- (106) Weiss, R. M.; Short, A. L.; Meyer, T. Y. Sequence-Controlled Copolymers Prepared via Entropy-Driven Ring-Opening Metathesis Polymerization. *ACS Macro Letters* **2015**, *4* (9), 1039-1043. DOI: 10.1021/acsmacrolett.5b00528.
- (107) Cho, H. J.; Kang, S. J.; Lee, S. M.; Jeong, M.; Kim, G.; Noh, Y. Y.; Yang, C. Influence of Simultaneous Tuning of Molecular Weights and Alkyl Substituents of Poly(thienoisindigo-alt-naphthalene)s on Morphology and Charge Transport Properties. *ACS Appl Mater Interfaces* **2017**, *9* (36), 30755-30763. DOI: 10.1021/acsaami.7b07856.
- (108) Yang, L.; Li, X.; Allahyarov, E.; Taylor, P. L.; Zhang, Q. M.; Zhu, L. Novel polymer ferroelectric behavior via crystal isomorphism and the nanoconfinement effect. *Polymer* **2013**, *54* (7), 1709-1728. DOI: 10.1016/j.polymer.2013.01.035.